9 Geologic interpretation of the seismic profiles of the Eastern Traverse (lines E1–E3, E7–E9): eastern Swiss Alps

O. A. Pfiffner & L. Hitz

Contents

9.1 Introduction

O. A. Pfiffner

The eastern traverse was originally conceived as a continuous seismic line crosscutting the Alps in a N-S direction. The main line shot was E1 (formerly also called NRP 20-EAST) and included also the registration of wide angle fan shots. The good results obtained from line E1 encouraged subsequent registration of two additional lines, a strike line (E2) and a N-S line through the Engadine window (E3). In this chapter the single lines are first discussed separately, followed by a 3D analysis combining these lines and the fan shots.

Lines E1, E2, E3 and the fan recordings E7 through E9 extend across the thin-skinned and thick-skinned compressional structures of the Helvetic zone in the northern part of the Alps and the Penninic and Austroalpine zones in the interior of the Alps (Figure 9-1). They transect deep portions of metamorphic zones exposed due to extensive uplift and erosion that started in the Tertiary and persists today. The lines cover major Alpine structures that are constrained by geologic surface data. These Alpine structures include shallow to moderately dipping thrust faults that juxtapose rocks of very different lithologies and physical characteristics; some rocks are highly anisotropic due to extensive deformation at elevated temperatures. The longest, north-south line E1 is more or less perpendicular to the regional trend of Alpine structures, but some of these structures possess a considerable plunge toward the east. By using downdip-downplunge projection there is a direct geometric tie between exposed and seismically imaged structures. Futhermore a joint interpretation of physically crossing lines (i. e. crossing reflectors at depth) attempted to gain insight into the 3D geometry of this part of Alpine crust.

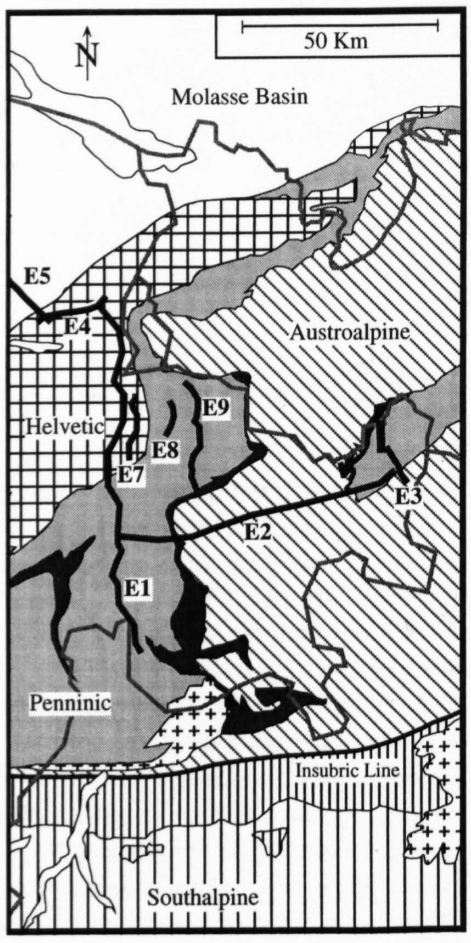

Figure 9-1
Tectonic map showing major units (nappe systems) and traces of seismic lines.

The Swiss Alps are divisible into five major geologic units defined by the pecularities of their Mesozoic-Cenozoic sedimentary sequences. From north to south they are the Molasse, the Helvetic zone (including the basement uplift of the Aar massif), the Penninic zone, the Austroalpine nappes, and the Southern Alps (Figure 9-1).

The **Molasse** comprises Oligocene to Miocene strata which were deposited on slightly tilted Mesozoic-Eocene strata that represent the autochthonous cover of the European crystalline basement; the latter outcrops in the Black Forest and Bohemian massif of southern Germany. Molasse sediments are considered to be late synorogenic. In the south they are deformed; they were tilted, detached from their substratum, and now form an imbricate fan (see Pfiffner et al., Chapter 8). In the **Helvetic zone**, Mesozoic-Oligocene sediments overlie Variscan basement. Within this basement three major units are recognized. The oldest unit consists of pre-Variscan polymetamorphic gneisses, metasediments, and schists with a steeply dipping foliation. These rocks were intruded by a series of late-Variscan, 330- to 270-Ma-old granitoids. Finally, a Permo-Carboniferous volcaniclastic sequence overlies (or is locally intruded by) the granitoids; these volcaniclastic rocks were in part tightly folded during the Variscan orogeny and now outcrop along narrow, steeply dipping zones. The cover sequence starts with thin epicontinental sediments including dolomites of Triassic age, followed by Jurassic to Eocene platform carbonates and locally Eocene-Oligocene flysch. In Eocene to Miocene times, these cover sediments were in part detached from their basement, compressed, thrust northward and now form the Helvetic cover nappes. Beneath the Helvetic nappes compression led to a thick-skinned fold-and-thrust belt, cored by the Aar massif basement uplift (see Pfiffner et al., Chapter 13.1). Alpine metamorphism is anchizonal in the north and epizonal in the south.

In the **Penninic zone**, Mesozoic-Eocene sediments overlie a Variscan basement similar to that of the Helvetic zone. Unlike in the latter, however, extensive Alpine deformation resulted in a gently dipping foliation. The cover sequence was in many instances completely detached from the crystalline basement. As a result the Penninic nappe pile consists of basement nappes on one hand, and cover nappes on the other hand. Both nappe types suffered an extensive imbrication during the early deformational history, followed by intensive post-nappe folding leading to very complex 3D geometries for many of the thrust sheets (see also schmid et al., Chapter 14).

The Mesozoic sediments of the **Austroalpine nappes** and the **Southern Alps** were deposited on the stretched passive margin of the Periadriatic promontory in the south Tethys Ocean. The cover overlies Variscan basement affected by Alpine deformation. Most of the lines of this transect pass "beneath" the Austroalpine nappes, which were eroded from the Penninic and Helvetic zones in Oligocene and Miocene times. However the strike line E2 passes through an axial depression where Austroalpine nappes are preserved between the Toce-Lepontine area and the Engadine window. Given the large recording offsets and the poor resolution of the explosion seismic experiment at shallow depth, hardly any information was gathered for the Austroalpine nappes and the former plate boundary underneath it.

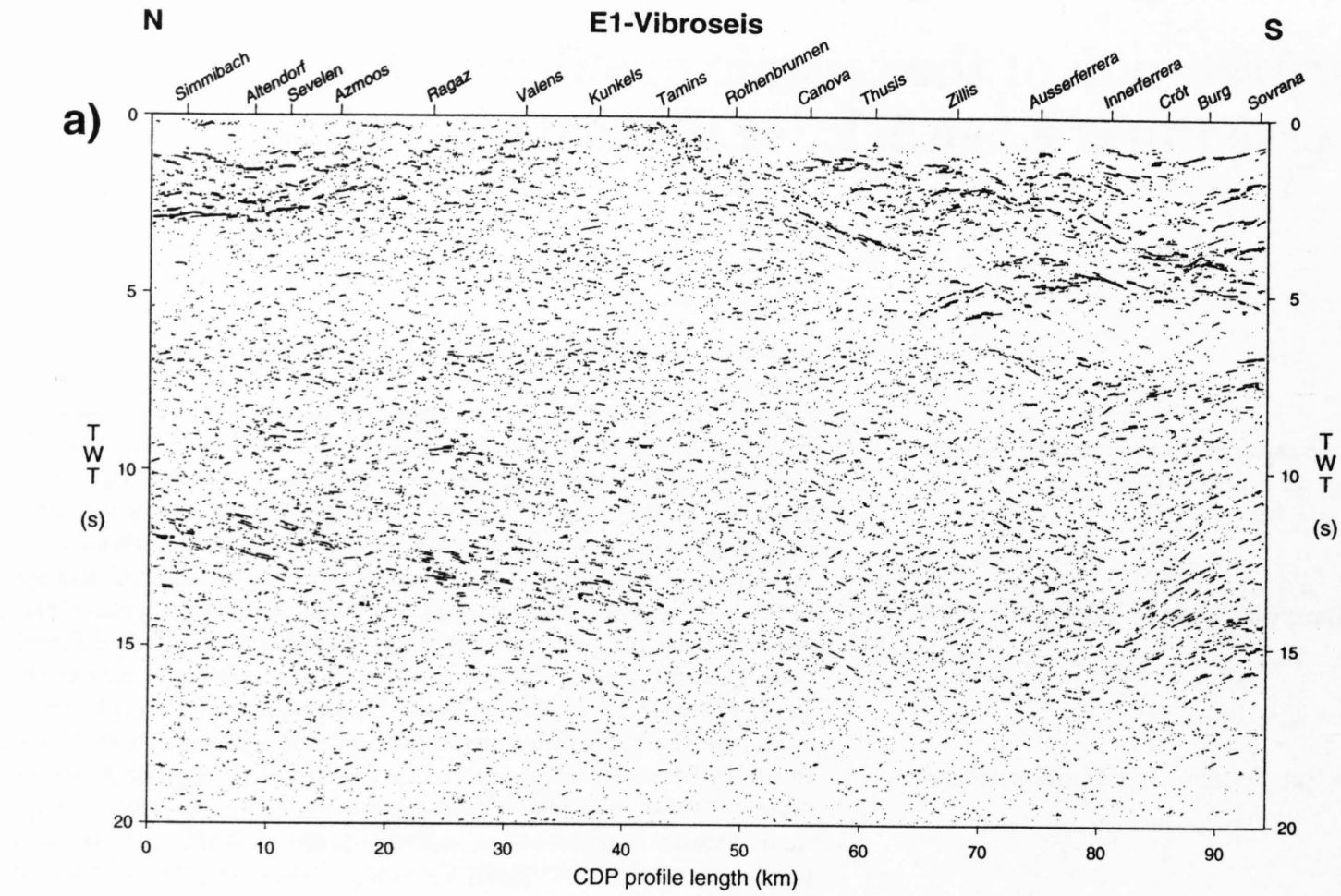

Figure 9-2
a) Unmigrated coherency enhanced Vibroseis data of line E1 (GOLD section from Valasek 1992).
b) Unmigrated coherency enhanced explosion seismic data of line E1 (GOLD section from Valasek 1992).
Names are shot points of explosion data which serve as geographic reference system throughout this Chapter.

9.2 Seismic line E1: Crustal shortening in the transect through the Helvetic and Penninic nappes and the Adriatic wedge

O. A. Pfiffner

Line E1 runs north-south across the Helvetic and Penninic nappes and intersects strike line E4 which is linked to the eastern Molasse transect (lines E5 and E6 discussed in Pfiffner et al., Chapter 8) and strike line E2 discussed below in section 9.3. In addition to the E1 vibroseis profile, which was designed to yield high resolution information on the upper crust, a deeper-penetrating explosion data set (near vertical reflection) was collected along the same line.

9.2.1 The data

The seismic data are presented in Plates 9-1 (explosion data set) and 9-2 (vibroseis data set). In Figure 9-2 coherency enhanced sections of the Vibroseis and the explosion seismic stacks are displayed. A comparison of the two stacks reveals a great similarity. The higher resolution of the Vibroseis data in the shallow part is readily explained by the low-fold coverage of the explosion seismic line. On the other hand the explosion seismic data yielded better results in the deeper part (for which they were conceived to begin with). Unmigrated line drawings for both data sets are given in Figures 9-3 and 9-4a. The computer-generated line drawings in Figure 9-3 emphasize the similarities and differences in the two seismic data sets. Comparing these computer-generated line drawings to the hand-produced line drawings shown in Figure 9-4a reveals only slight differences between the two techniques. The hand-produced line drawing appears somewhat cleaner, which is due to "filtering" of low amplitude and discontinuous signals. Although this

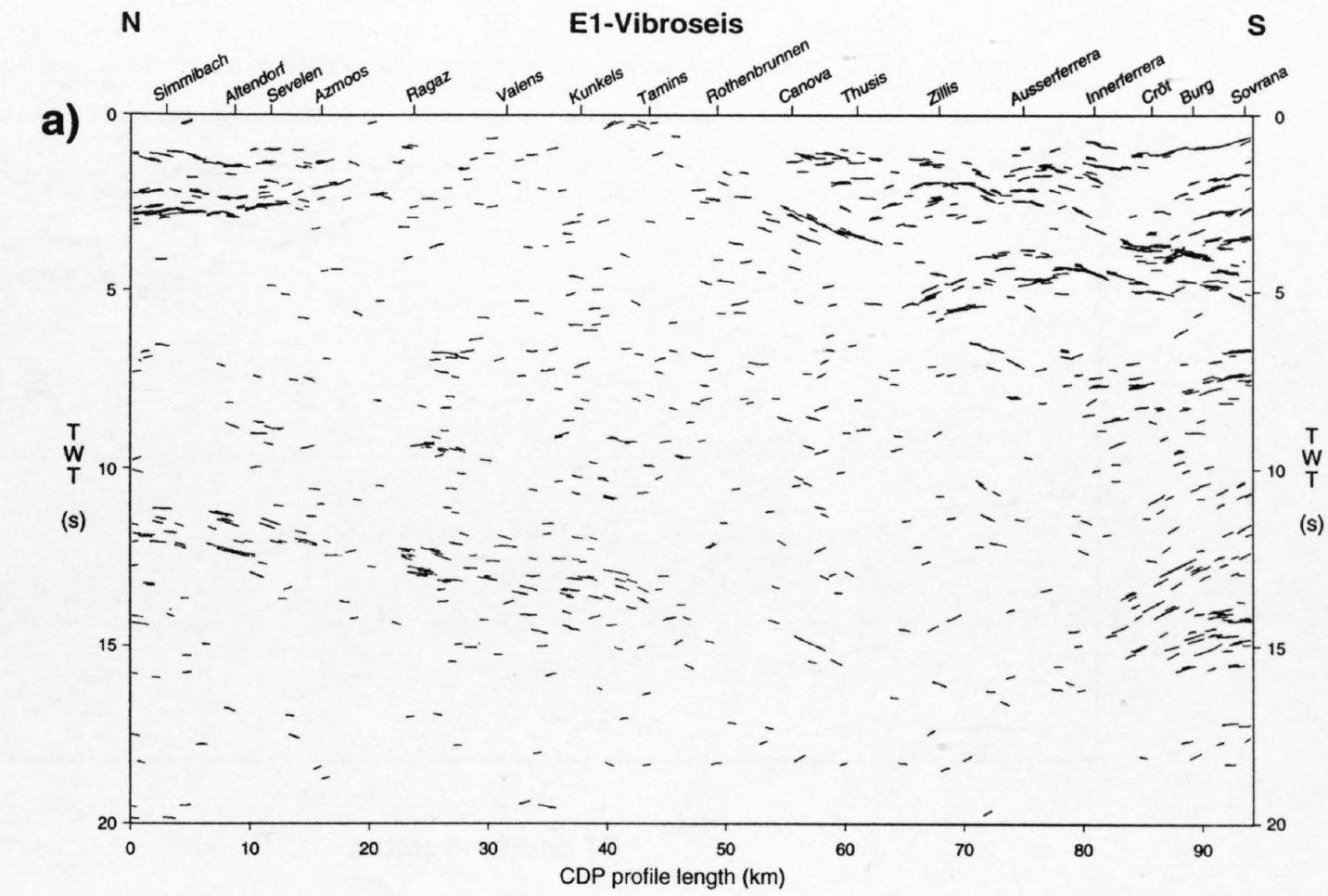

Figure 9-3
a) Computer generated line drawing of unmigrated Vibroseis data (from Valasek 1992).
b) Computer generated line drawing of explosion seismic data data (from Valasek 1992).

subjective filtering may suppress real short reflections, it also emphasizes the more obvious reflections, on which the process of geologic interpretation concentrated to begin with. The difference is most obvious beneath shot points Tamins and Kunkels and at around 5 s TWT beneath Valens-Simmibach. The numerous short reflections recognizable in this area in the computer-generated line drawings of Figure 9-3 could not be interpreted subsequently. Migration of the seismic data cleared up some of the complex patterns, but created new problems in other instances. Figure 9-4b is a migrated version of the computer-generated Vibroseis stack. Upon comparison with the non-migrated data in Figure 9-4a or 9-3 one notes that the depth-migrated reflections at 30 – 40 km depth form a rather continuous band in the northern half and are cleaned up in the southern half of line E1. On the other hand the depth-migrated shallow reflections are in places less coherent. In an area of considerable dips and cross-dips a conventional 2D migration is bound to mis-place reflections from a complex 3D structure and should thus be applied with care (Stäuble et al. 1993, Litak et al. 1993). Due to these difficulties the identification of individual reflection events will be discussed on the coherency-enhanced, unmigrated Vibroseis stack (Figures 9-5a). The geologic profile constructed on the basis of the interpreted seismic data is a vertical section through the final version obtained from 3D modeling.

Considering the entire line E1 shown in Figure 9-2 and 9-5a, crustal reflections in the shallow part (down to around 5 s TWT) are prominent in the north (Helvetic nappes) and in the south (Penninic nappes), with the Aar massif in the central part being largely transparent. At mid-crustal level (5–10 s TWT) weak, discontinuous reflections can be recognized. A prominent band of reflections finally, is distinguished at lowermost crustal level (11–15 s TWT) and can be traced across the northern half of the profile. At the southern end deep reflections are predominantly north dipping.

The **shallow reflections** in the **northern half** of the Vibroseis section, down to 3 s two-way-travel time (TWT), extend over the Helvetic zone. Coherent reflections can be seen mainly in the north; they degrade in strength toward the south. A detailed interpretation of these reflections is given by Pfiffner et al. in Chapter 13.1. The most noticeable reflection, marked *B1* in Figure 9-5a, is situated at 2.8 s at the northernmost end. It is characterized by its high amplitude, double cyclic nature. south of sevelen this strong reflection begins to dip upward and then continues as discrete panels of progressively

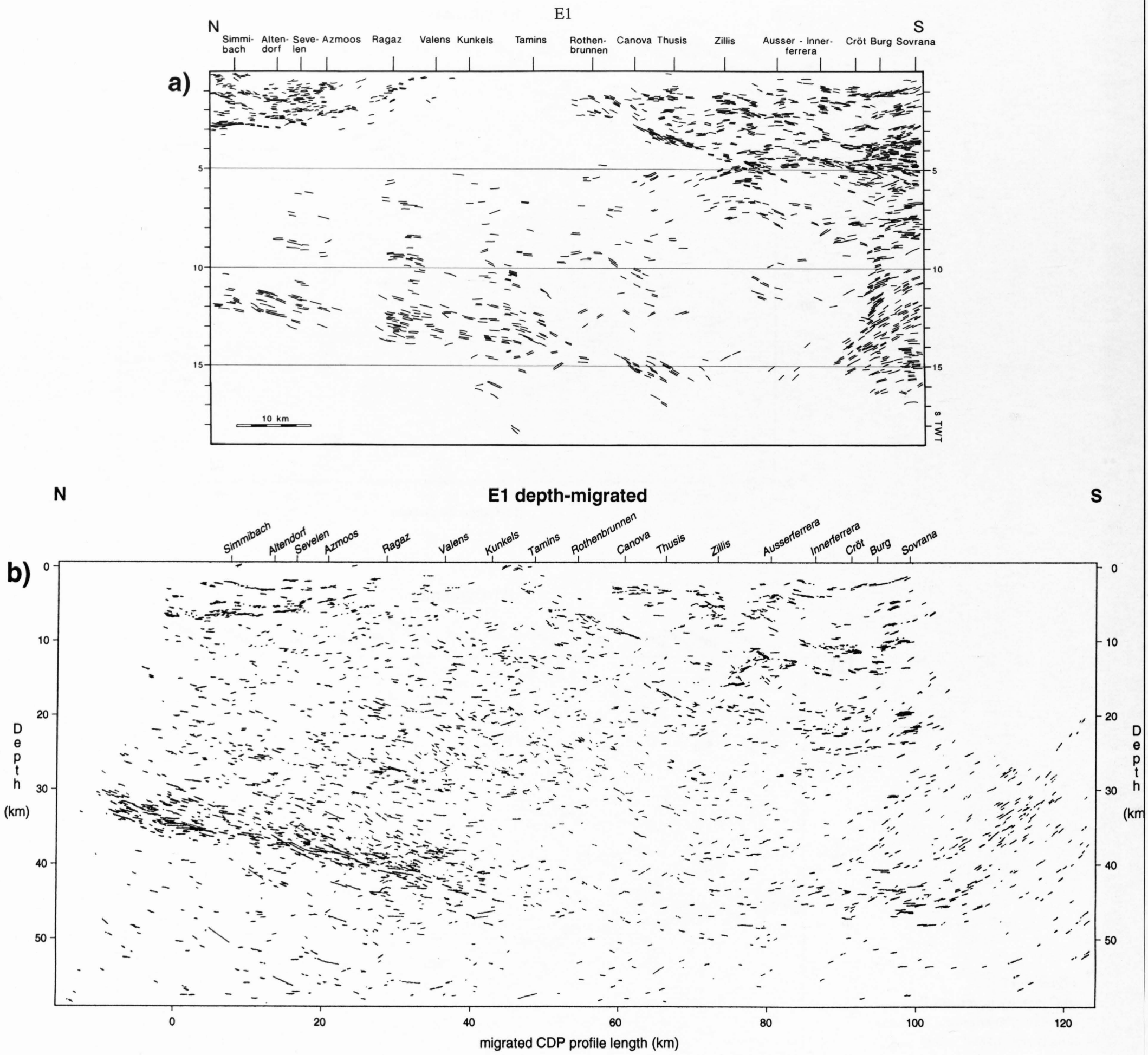

Figure 9-4
a) Hand-produced line drawing of unmigrated Vibroseis data, combining partial stacks of variable offsets (from Pfiffner et al. 1991).
b) Depth-migrated stack of the computer-generated line drawing (from Valasek 1992).

weaker reflections (*B2* in Figure 9-5a) rising stepwise toward the south. Between 1 and 1.6 s TWT north of Simmibach a pattern of several south dipping reflections is notable. These events, marked *J* in Figure 9-5a, also show a double cyclic swing and high amplitudes.

The **shallow reflections** in the **southern half** of the section, shown in Figures 9-2 and 9-5a, extend over the Penninic zone. strong reflections occur between 0 and 7 s TWT are mainly south dipping in the north (*B3* in Figure 9-5a) and north dipping in the southern portion (*sp*, *Ch*, *Ad*) with several reflections crossing each other *(B4)*.

Three **deep reflection packages** are observed on the vibroseis section of Figures 9-2 and 9-5a. These deep reflections can also be recognized in the explosion data set (Pfiffner et al., 1988). The first package, marked *C* in Figure 9-5a, comprises sparse, discontinuous, short reflections within an ill-defined zone extending from about 9 s beneath Sevelen to 10 s TWT beneath Tamins. steeply north dipping reflections at 8 to 14 s TWT *(CA)* at the southern end of the section form a second package of reflections.

The third package, m in Figure 9-5a, is a highly reflective band with a duration of 1-1.5 s. It is located at a depth of around 11 s TWT at the northern end of line E1 and extends southward with a shallow southerly dip to a depth of 15 s TWT at its deepest point beneath Canova. Near the southern end of the section it reappears at 13–15 s TWT.

In several areas the reflection quality of deep reflections degrades. Examples are seen beneath the segment between shot points sevelen and Ragaz, and in the area beneath Tamins, both of which coincide also with dense population and industrialization. We feel, therefore, that this particular seismic character is not necessarily due to a change in the geologic structure, but rather be related to difficult recording environments.

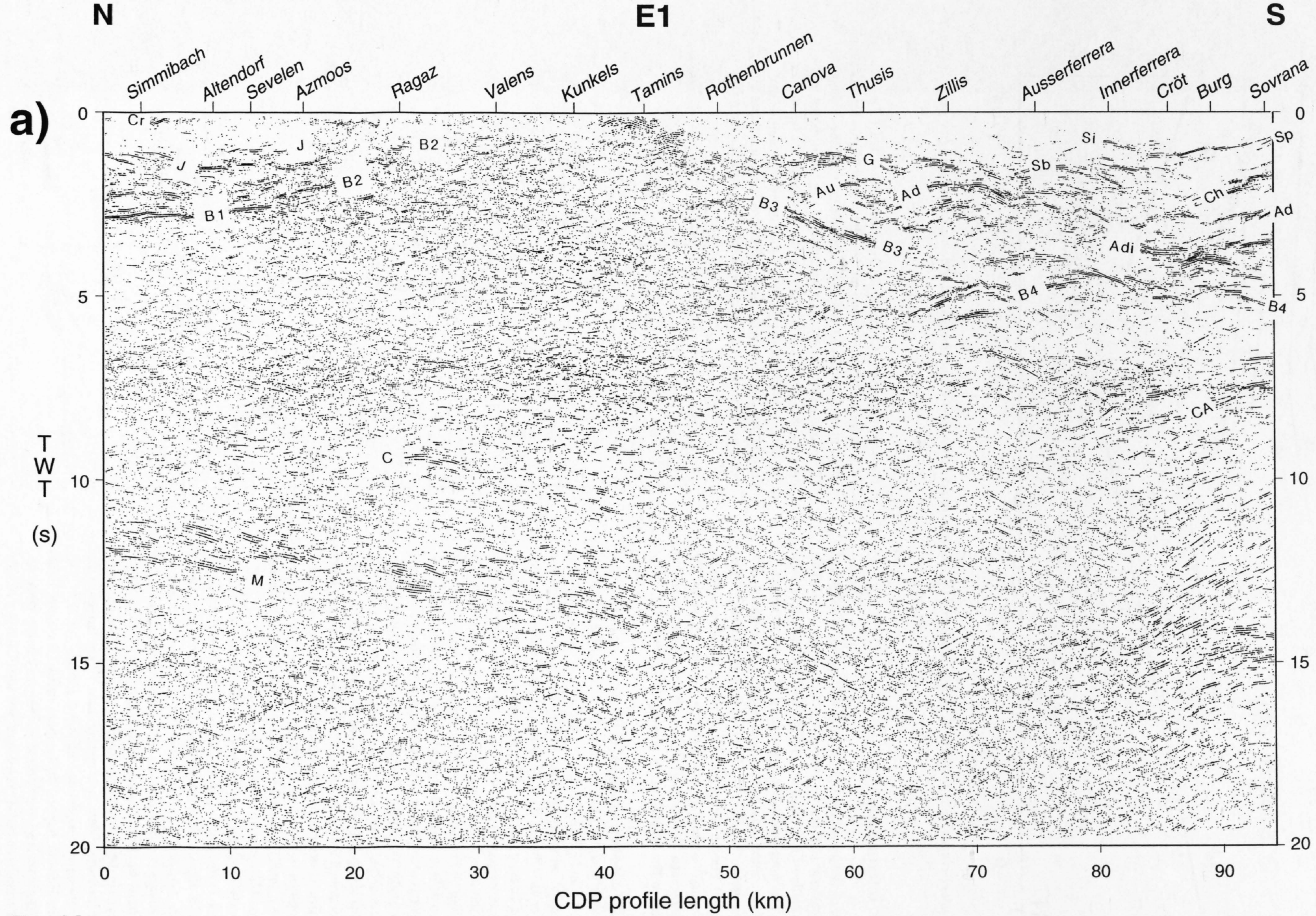

Figure 9-5a
Identification of reflection groups on unmigrated coherency enhanced Vibroseis stack. The identification is based on the evaluation of structure contour maps of potential reflectors.
Cr: top Cretaceous, J: top Jurassic, B1, B2, B3, B4: top crystalline basement of European crust (Autochthonous foreland, Aar, Gotthard, Simano), G: top Grava, Au: top Aul, Ad: top Adula, Adi: Adula internal, Ch: top Chiavenna, Sp: top Splügen, Sb: base Suretta, Si: Suretta internal, C: European Conrad, CA: Adriatic Conrad, M: Moho.

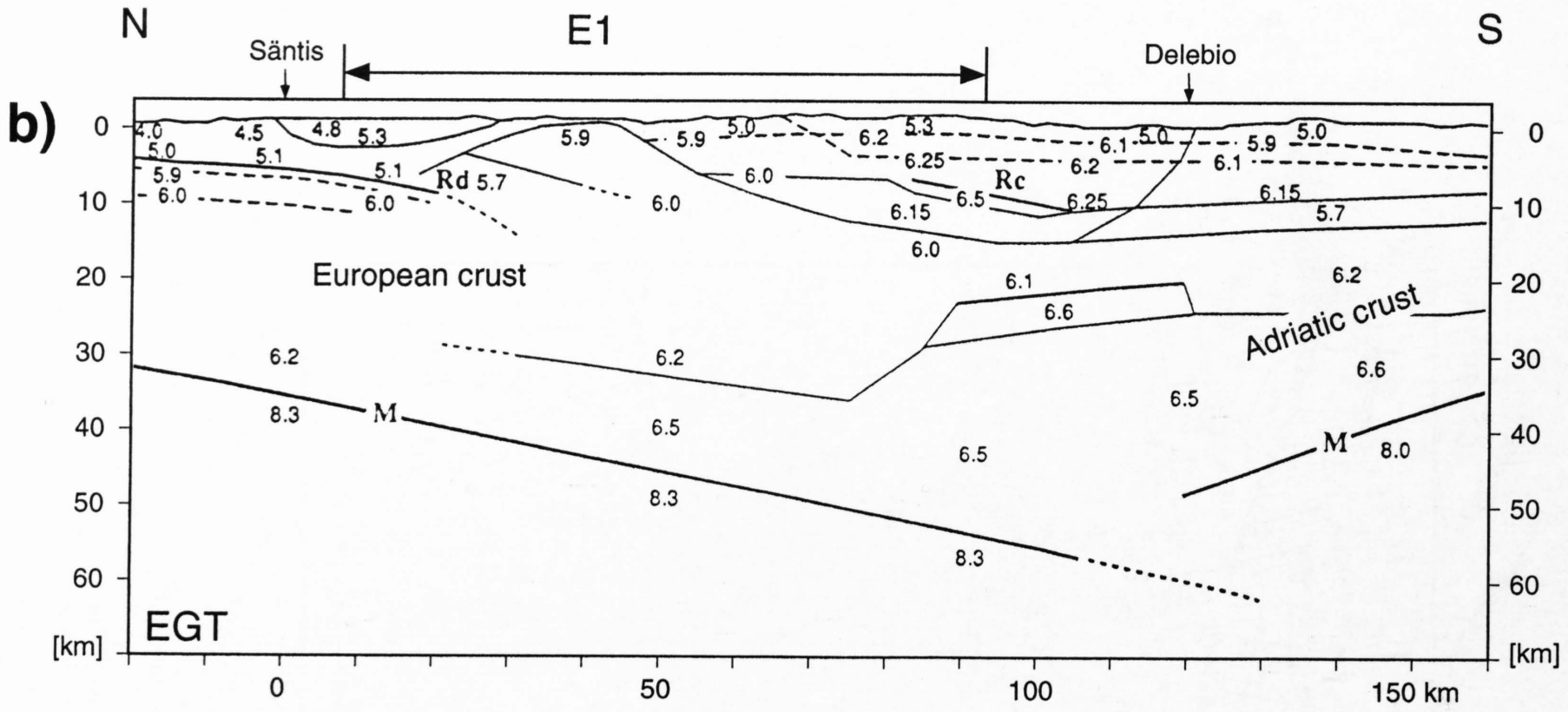

Figure 9-5 b
Refraction derived velocity model (adapted from Ye 1992). Säntis and Delebio are shot points of EGT refraction line. Note mismatch between European and Adriatic Moho.

9.2.2 Geologic interpretation

The crustal structure of this part of the Alps is fairly well known to a depth of 5–10 km due to the easterly axial plunge and the high topographic relief. This makes it possible to calibrate the reflections and to refine and laterally extend the interpretations. The three-dimensional geometry of potential reflectors such as basement-cover contacts has been analyzed using all the available surface data and their projection to depth. These results were presented by Pfiffner et al. (1990 a and b). For the deeper parts of the crust, refraction surveys and wide-angle reflections show low- and high-velocity bodies within the crust and place the Moho at a depth of around 40 km beneath Simmibach and at around 50 km beneath Thusis (Holliger & Kissling 1991, Ye 1992).

The interpretation of the s**hallow structures in the North** are discussed in detail by Pfiffner et al. in Chapter 13.1. To the north of line E1 the reflections *B1* in Figure 9-5a at 2.5 and 2.8 sTWT are from the autochthonous sedimentary cover of the foreland, which can be traced all the way across the Molasse Basin (see Pfiffner et al., Chapter 8). The strong, double-cyclic reflections stem from the top of Triassic dolomites (Röti Dolomite). somewhat weaker and less continuous reflections originate from the top of the Mesozoic carbonates. On the northern flank of the Aar massif this cover is shortened by a combination of folding and thrusting. The associated complex geometry of the reflectors leads to defocussing and scattering of the ray paths (Stäuble & Pfiffner 1991, Pfiffner et al., Chapter 13.1) resulting in the loss of coherent reflections. The seemingly "poor quality" seismic data (reflections *B2* in Figure 9-5a) nevertheless delineate the rise of the basement top from 3 sTWT (–8 km) beneath about shot point Altendorf toward the south, where it breaks surface between shot points Valens and Kunkels. Between Valens and Kunkels the basement-cover contact is actually outcropping in the tectonic window of Vättis In contrast to the seismic sections from central Switzerland (line C1, Figure 11-6 a, and Figures 9-13 and 9-14) the Aar massif basement is not seen to override Mesozoic foreland sediments in line E1.
Theshallower groupof reflections (*J* in Figure 9-5a), extending from the northern end of the line (at 1.2 s) to Azmoos, can readily be correlated with the upper and lower interface of Jurassic limestones between the Glarus and Säntis thrusts, i. e. within the Lower Glarus Nappe complex of the Helvetic nappes. The Lower Glarus Nappe complex consists of a series of imbricate thrust sheets grading into folds south of Azmoos (Helbling, 1938; Pfiffner, 1993). The interpretation given in the geologic cross section of Figure 9-8a is a downplunge projection of the surface data outcropping some 10 km farther to the west combined with 3D seismic modeling (Stäuble & Pfiffner 1993).
The basal thrust of the Helvetic nappes, the famous Glarus Thrust (see Funk et al. (1983) for a historic review), is expected immediately below these Jurassic rocks. It puts Permian red beds ("Verrucano") on top of Tertiary North-Helvetic Flysch with a displacement of about 50 km (Pfiffner, 1985) to the west of the line. It is likely that there is no Permian at the base of the Helvetic nappes because going east the basal detachment steps up from the Permian to a higher detachment level (see Pfiffner, 1993). In the transect studied the thrust possibly puts shaly Early Jurassic onto shaly-sandy Tertiary and might, therefore, not express itself seismically.

The few reflections (*Cr* in Figure 9-5a) between 0 and 1.2 s obtained from the Cretaceous limestones and marls of the Upper Glarus Nappe complex or Säntis nappe are difficult to relate to the internal structure of this thrust sheet. The poorer quality of the near-surface data can be attributed to the fact that imaging such shallow structures was not the aim of the seismic experiment. The Tertiary sediments underlying the Helvetic nappes show two types of reflection patterns: numerous short reflections in the north and a more or less transparent section in the south. The boundary between the reflective and the

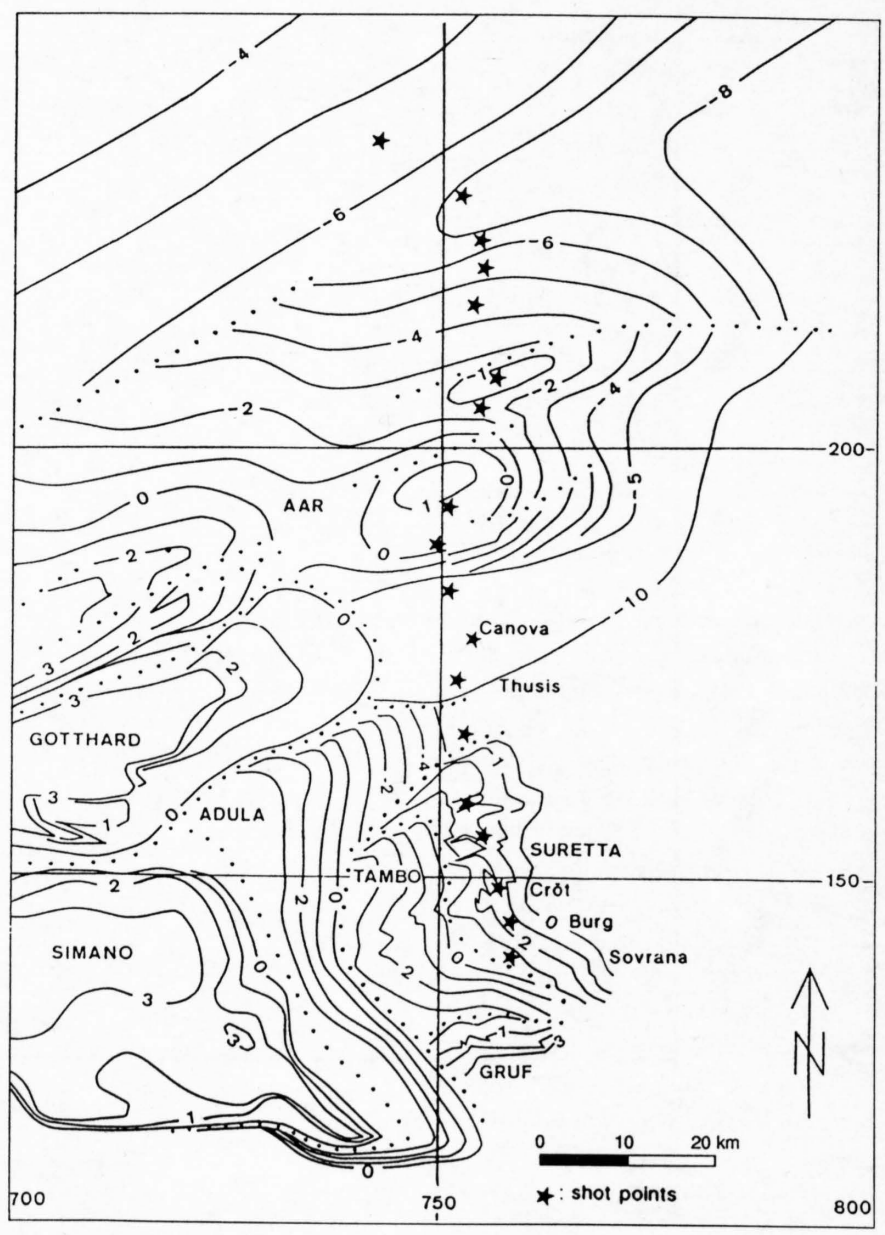

Figure 9-6
Structure contour map of "top crystalline basement" contact based on surface data (from Pfiffner et al. 1990a). Initial model. Stars denote shot points of explosion seismic data of line E1. Note bumby surfaces and cross-dip in southern part resulting in out-of-plane reflections and energy dispersal (defocussung effects).

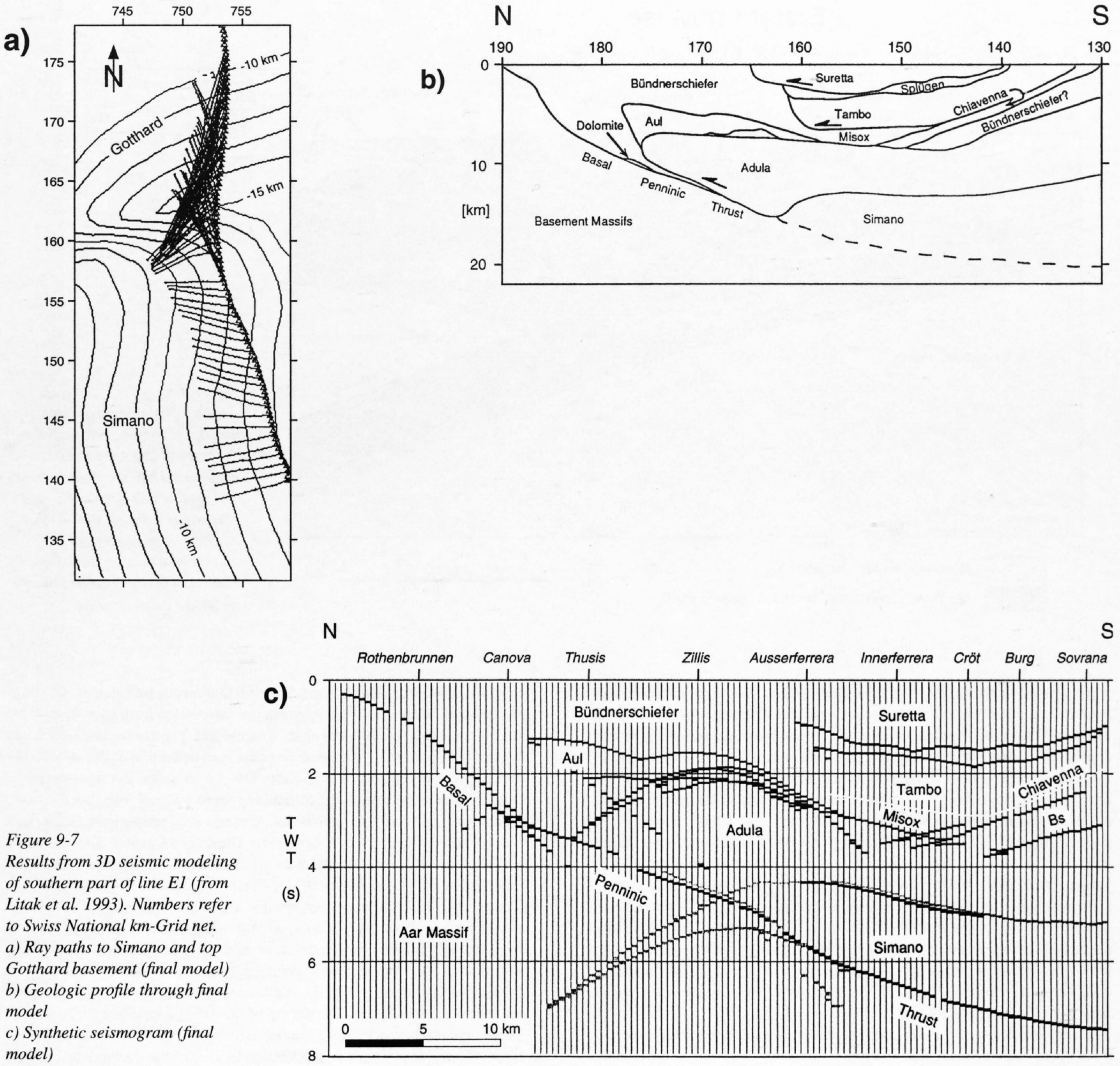

Figure 9-7
Results from 3D seismic modeling of southern part of line E1 (from Litak et al. 1993). Numbers refer to Swiss National km-Grid net.
a) Ray paths to Simano and top Gotthard basement (final model)
b) Geologic profile through final model
c) Synthetic seismogram (final model)

transparent domain is tentatively interpreted as the boundary between the UMM beds of the sub-Alpine Molasse and the North-Helvetic Flysch, as indicated by the different ornaments in Figure 9-8a. The reflective nature of the Molasse can be attributed to its lithologic character: basal turbiditic fan deposits, overlain by fine-grained deposits (shales and shaly marls) grading into a sandy and conglomeratic sequence that characterizes the Oligocene Lower Marine Molasse ("UMM" (Diem, 1986)). The repeated change from fine-grained to coarser-grained sediments at various scales may account for the generally reflective nature of the seismic section. In addition to sedimentary intercalations, tectonic imbrications known to exist farther north at the surface are expected to cause repetitions in the section studied here (see Pfiffner et al., Chapter 8). In contrast, the thick sequence of shales and sandstones of the North-Helvetic Flysch (NHF) is intensively folded (Siegenthaler, 1974), which may explain the seismically more transparent nature of this domain. The transition from flysch to molasse-type sediments is gradual in lithology, age, and location of the depocenter (e. g. Siegenthaler, 1974; Pfiffner, 1986) and therefore unlikely to produce a sharp change in the reflection pattern. In order to balance the shortened Sub-Alpine Molasse section situated farther north, a substantial amount of bedlength of Mesozoic carbonates has to be postulated in the area of the section studied. The structure of the contact between flysch and molasse in the geologic section of Figure 9-8a is intended to account for this. This point is further discussed in more detail by Pfiffner et al. in Chapter 13.1.

The interpretation of the **shallow structures in the south** is more difficult, and in some instances more than one interpretation is plausible and. Hence three models were discussed by Pfiffner et al. (1990b), who based the interpretation on the projection of surface data. Structure contour maps proved to be particularly useful in this context. The interpretation was refined subsequently. First a careful analysis of impedance contrasts based on laboratory measurements (Sellami et al. 1990) and local structure (Pfiffner et al. 1991) was undertaken. The main conclusion which could be drawn from those studies is that very good candidates for potential reflectors are Mesozoic carbonates found as thin layers sandwiched between crystalline basement blocks or within Mesozoic calcareous micaschists (Bündnerschiefer). Finally 3D seismic modeling (Litak et al. 1993) demonstrated the effects of plunging structures and improved the geometric model quantitatively. In Figure 9-7a the lateral offset between the reflection points and the seismic midpoints is about 5 km for the top of the Simano and Gotthard basement blocks. The synthetic spike seismic section shown in Figure 9-7c is derived from the "final" model displayed in 9-7b and matches many of the reflections observable in the seismic line E1 (Figure 9-2 or 9-5a).

The discussion of the individual reflection groups will proceed from top to bottom. Outcropping from south of Zillis to the southern end of the line is the Suretta nappe, a thrust sheet composed essentially of basement rocks topped by a thin cover of Mesozoic quartzites and carbonates (e. g. Milnes and Schmutz, 1978) discussed by Schmid et al. in Chapter 14. At its base the Suretta nappe overlies Mesozoic carbonates of the Splügen zone, which

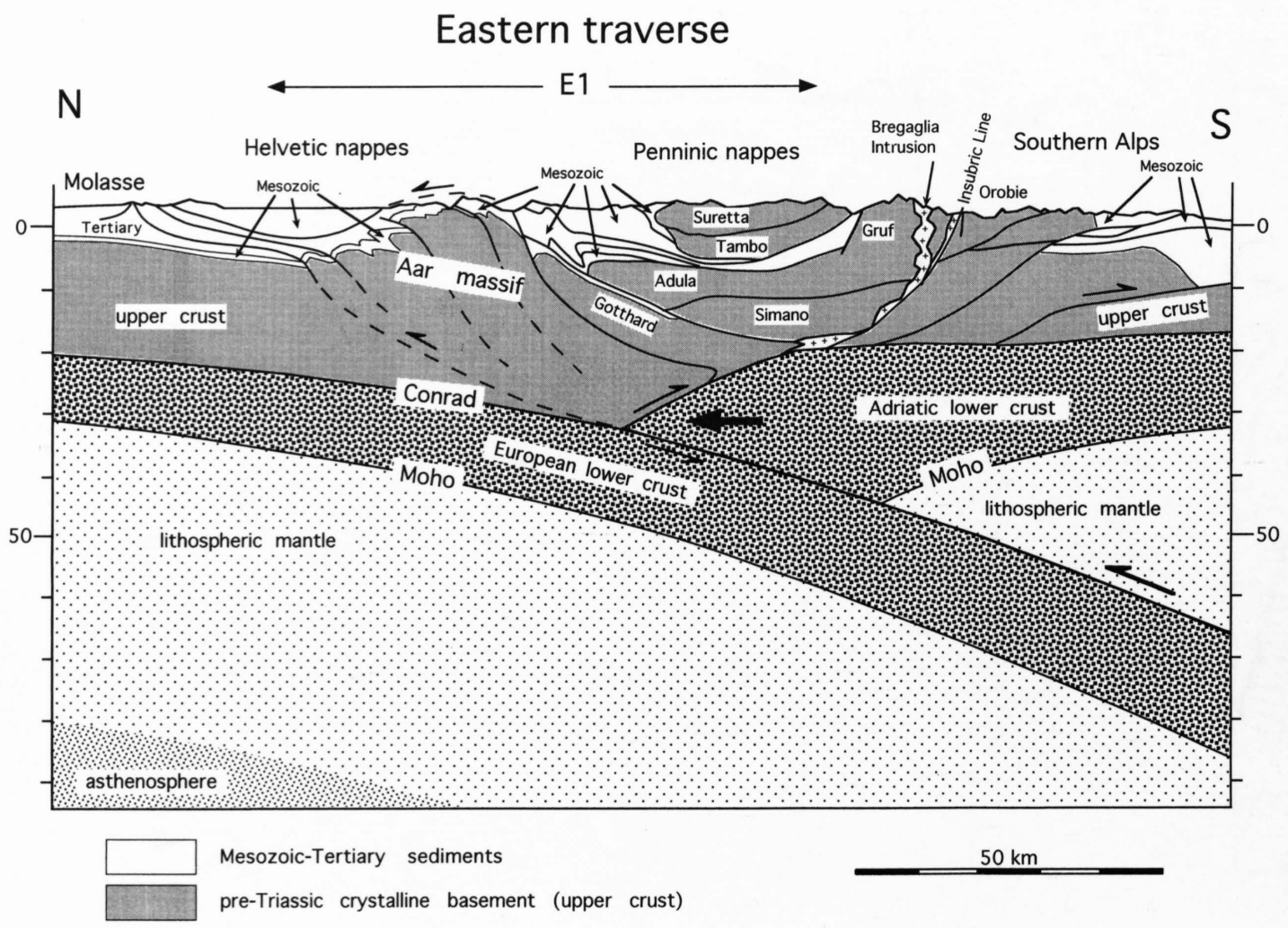

Figure 9-8
General geologic profile across the Alpine orogen, drawn along the trace of line E1, but expanded northwards into the Molasse Basin and southwards into the Po Basin. The profile displays the bivergent stacking of upper crustal flakes and the asymmetric subduction of European lower crust and mantle under the Adriatic plate.

represents a 10- to 500-m-thick layer that extends over a distance of more than 20 km. This Splügen zone can be subdivided into a lower part which represents the autochthonous cover of the Tambo basement and an upper part consisting of slices of allochthonous units (Blanc, 1965; Strohbach, 1965). Considering the regional axial plunges (cf. Pfiffner et al., 1990a), the reflections S*p* in Figure 9-5a at 1 s beneath sovrana extending to the north can readily be correlated with the Splügen zone. Using partial stacks of near-offset traces Pfiffner et al. (1991) could identify individual reflections from the top and the base of the Splügen zone, as well as contacts between ortho- and paragneisses. To the north the base of the Suretta nappe is known to steepen and reaches the surface south of Zillis. Down-plunge projections suggest that reflection S*b* originates from the base of the Suretta nappe.This nappe also contains Triassic carbonates (called "internal Trias" by Milnes and Schmutz (1978)) which form a more or less continuous band separating two basement units within the Suretta nappe and which is the probable source of the reflections S*i* at 1 s beneath Cröt.

The next unit down, the Tambo nappe, consists almost exclusively of basement rocks. It overlies the Misox zone, a thin layer of Mesozoic carbonates and schists which also contain lenses of basement rocks and ophiolitic material (metabasalts). The Misox zone is expected to lie at about 3 s beneath Cröt. Further south it rises toward the surface to overlie the Chiavenna Ophiolites (Schmutz, 1976) 10 km south of Sovrana. The Chiavenna ophiolite body is likely to be triangular shaped in a vertical cross section, but its shape is poorly constrained by surface data. As Schmutz (1976) was able to show, this ophiolite body is in an inverted position. Its northern continuation is likely to be found in the Misox zone, and thus it is possible that the Chiavenna ophiolite body overlies Mesozoic sediments, being responsible for reflection group *Ch* (see also geologic cross section of Figure 9-8a).

The Misox zone widens to the north, being composed of a number of thrust sheets of cover rocks (Gansser, 1937; Nabholz, 1945). The two topmost units, the Tomül and Grava nappes, comprise a thick monotonous sequence of argillaceous to sandy to calcareous sediments, which are called Bündnerschiefer (Nabholz, 1945; Jäckli, 1941, 1944). At their interface, the base of the Tomül unit, consists of a more or less continuous layer made up of a mélange containing carbonates overlain by ophiolitic rocks. This layer is likely to produce reflection group *G* in Figure 9-5a, which is also picked up in line E2 (see Figure 9-11). On line E2, which intersects E1 near shot point Thusis, reflection group *G* has an easterly dip (see also section 9.3). Reflection group *Au* just beneath is likely to stem from the top of the Aul thrust sheet, which consists of massive carbonates interlayered with ophiolitic rocks and which underlies Grava Bündnerschiefer.

The underlying Adula nappe consists of basement rocks topped by remnants of Triassic quartzites and carbonates. Projections of surface data (Pfiffner et al., 1990) 20 km (!) west of the seismic line place the top of the Adula nappe at around 2 s beneath Zillis and 3 s beneath Cröt. The reflections *Ad* observed at these places are thus interpreted as defining this boundary, an interpretation which is consistent with the 3D modeling results by Litak et al. (1993). To the south of the profile the Adula nappe steepens to form large-scale south facing antiforms (see Schmid et al., Chapter 22). The northerly dip of the reflection group *Ad* at 2.7 s beneath Sovrana is an indication of this steepening. Northward the situation is less clear. The Adula nappe has a steep frontal zone, similar to the Tambo and Suretta nappes (see Figure 9-6). But the Adula frontal zone does not have a constant trend and axial projection can thus only place it somewhere between shot points Thusis and Canova. The interpretation shown in Figures 9-5a and 9-8a are consistent with the observed reflections in line E2 (*Ad* in Figure 9-11), which suggests the front to be north of Thusis. According to our interpretation there are a number of reflections within the interior of the Adula nappe (*Adi* in Figure 9-5a). These might arise from strongly foliated paragneisses, contacts between paragneisses and tabular shaped Late-Variscan orthogneisses, and/or thin slabs of Mesozoic (?) carbonates contained within the Adula basement. All of these contacts and the foliation are subparallel to the top of the Adula nappe (see Pfiffner et al., 1990a, and references therein), similar to the reflection pattern, but we refrain from identifying any particular reflection in view of the uncertainties and the considerable projection distance.

The contact between the Adula nappe and the underlying Simano nappe is characterized by a thin zone of Mesozoic amphibolite grade carbonates and schists that thin southward, making the identification of the two nappes very difficult. Projection of surface data (Pfiffner et al., 1990a) places the top of the Simano nappe between 4 and 5 s beneath Ausserferrera-Sovrana and is thus correlated with reflection group *B4*. The Simano nappe is taken to encompass the underlying Leventina granite-gneiss, from which it is separated by small lenses of carbonates in the extreme south and north. To the north the Simano nappe is separated from the Lucomagno basement by the tight Molare syncline, and the Lucomagno basement is in turn separated from the Gotthard massif basement by the steeply dipping Piora zone. Following Milnes (1974), the Gotthard, Lucomagno, and Simano-Leventina basement blocks can be viewed as a single basement complex, the "Subpennine complex." The structural relationships between these basement blocks are observed at outcrop almost 50 km west of the seismic line. It is doubtful that these structures can be projected as far east as the seismic profile, and if so, cylindrical projection has certainly approached its limit (see Pfiffner, 1978, for an evaluation of the lateral continuity of folds and thrust sheets in the adjoining Helvetic zone).

The uncertainty of lateral continuity applies also for the Gotthard massif and the Tavetsch massif. The relevant question for the interpretation of the seismic data is whether or not a subsurface continuation of these basement masifs is to be expected into the area crossed by the seismic profile. The Tavetsch massif is a 5-km-thick sliver of basement rocks situated between the Aar massif and the Gotthard massif. It thins out to the east and represents the original substratum of the Axen nappe of the Helvetic nappes (see Trümpy, 1969). Both units are observed at outcrop 30 km west of the seismic profile.

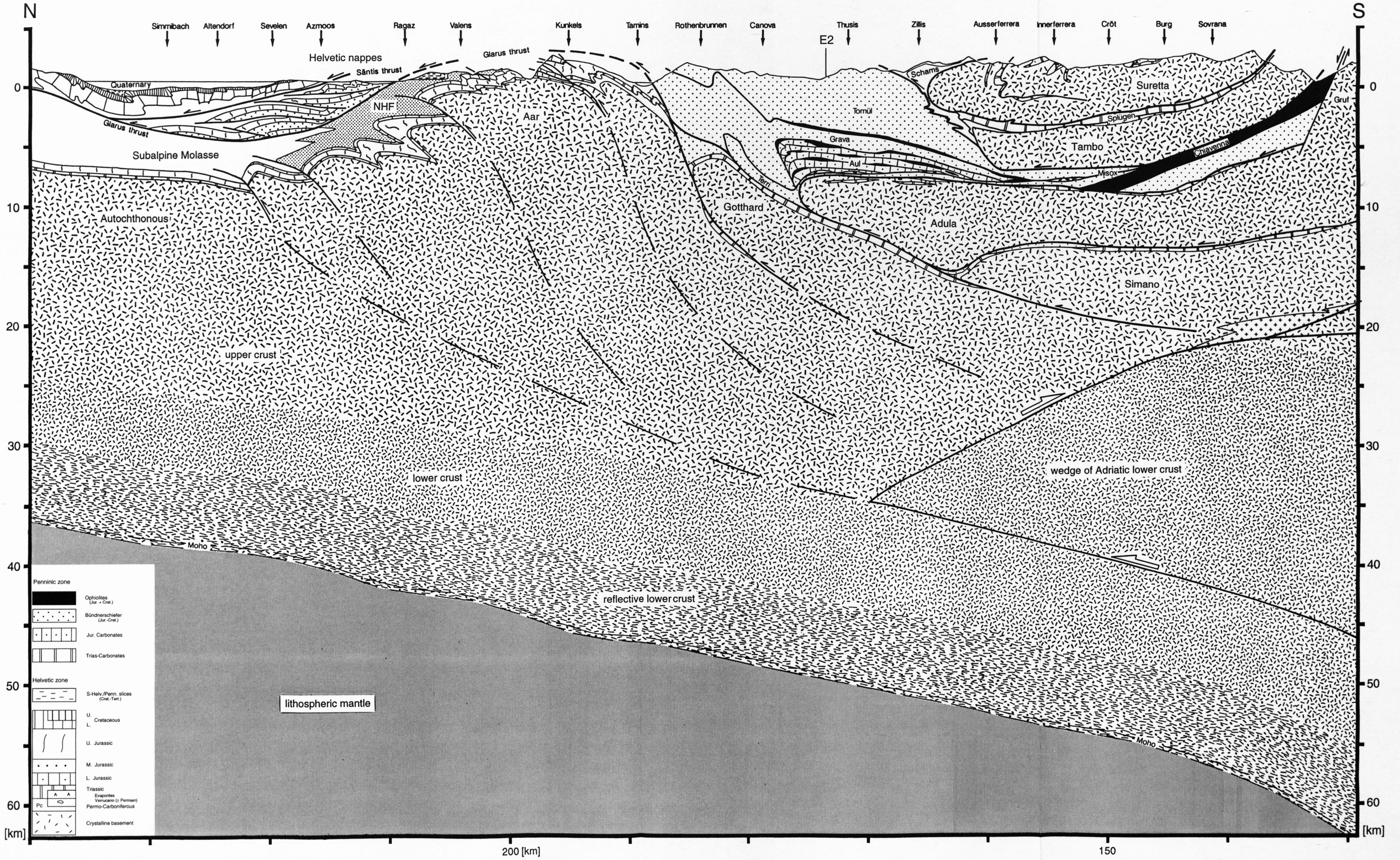

Figure 9-8a
Geologic profile along line E1 (drawn on km 755 of Swiss National Grid net) obtained from the combined interpretation of Vibroseis and explosionre-flection seismic data, and refraction seismic data. The profile is a vertical cross section through the final model obtained from 3D seismic modeling.

At its eastern end the Tavetsch massif cores an anticlinal structure in the Permian Verrucano unit. Its fold axis changes trend from WSW-ENE to WNW-ESE going east. In addition, the basal detachment of the Helvetic nappes steps up from the basement into the Mesozoic cover going east. It is probably situated in shaly Jurassic sequences along the seismic profile. All these points suggest that the Tavetsch massif is unlikely to be expected in the transect of the seismic profile E1 and does therefore not appear in our interpretation shown in Figure 9-8a. The Gotthard massif, on the other hand, probably represents the substratum of the higher Säntis-Drusberg nappe (Pfiffner, 1985; Wyss, 1986) and is more likely to be encountered in the E1 transect. Reflection group *B3* is thus interpreted to stem from the top of the Gotthard massif, the high density package at 3.5 sTWT beneath Thusis possibly representing slivers of Mesozoic carbonates which are known to occur at similar structural positions. This reflection package *B3* is also identifyable on line E2 (see Figure 9-11).

In line E1 reflection groups *B3* and *B4* are crossing each other. The N-dipping reflection group *B4* has been explained by back-thrusting in interpretation C of Pfiffner et al. (1990b). Similarly, N-dipping reflections observed in the western traverse have been interpreted to represent large scale backfolds by Steck et al. (Chapter 12), Escher et al. (Chapter 16) and Marchant & Stampfli (Chapter 24). We prefer an interpretation without large scale backfolding for the following reasons:

1) 3D seismic modeling by Litak et al (1993) suggest that the crossing of reflection groups *B3* and *B4* (beneath Zillis in Figure 9-5a) could equally well be part of a bow-tie structure resulting from a shallow synformal structure between Gotthard massif and Simano nappe (see Figure 9-7).

2) The top of the basement blocks (Aar, Gotthard and Penninic nappes) are affected by back-folding or back-thrusting which locally overturned some nappe contacts and early foliations. In the case of the Suretta nappe, a higher unit, back-folding produced even "south-verging" antiforms as discussed in more detail by Schmid et al. (Chapter 14). But the Bündnerschiefer units encountered along line E1 do not point to any significant back-folding. Also the back-folds affecting the top of the Gotthard basement farther west (along lines C1–C2 of the central traverse and in the Piora-Olivone area) seem to lose amplitude going east.

Thus, in Figures 9-8a and b the top of the Aar massif beneath Tamins-Rothenbrunnen is taken to dip steeply south. This geometry corresponds to the one observed in the Urseren zone farther west (see Pfiffner & Heitzmann, Chapter 11). This steep subsurface continuation of the Aar massif (south of Tamins in Figure 9-8a) is indicative of some sort of back-flow associated with shortening and uplift of the Aar massif basement block. Pfiffner et al. discuss the tectonic evolution of this external basement massif in Chapter 13.1 and emphasise that its structure varies along strike, the western part having been subjected to more extensive shortening in a late phase. We thus feel that the difference between the geologic profiles along the western and eastern traverse reflects in part a true difference in geologic structure.

The most prominent feature of the **deep structure** is the reflection band M in Figures 9-2 and 9-5a at 11–12 s TWT observed at the northern end and extending southward to greater depths (14.5-15.5 s TWT beneath Canova). Converting the refraction data (Holliger & Kissling 1991, Ye 1992) to a time section places the crust-mantle boundary at around 12.5 s TWT at the northern end of the section and at around 16 s TWT beneath Canova, i. e., the velocity jump associated with the refraction Moho corresponds to the bottom limit of the reflection band seen in the reflection experiment. As pointed out by Pfiffner et al. (1988), this reflection band might represent a transition zone from lower crustal to upper mantle velocities which would be beyond the resolution of refraction seismology. This reflection band, representing a reflective lowermost crust is apparent as far south as Thusis, where it disappears at 15–16 s TWT with a relatively steep southerly dip. As discussed in section 9.3. a similar observation can be made along strike line E2, where corresponding reflections from the lowermost crust disappear in an easterly direction. The EGT refraction experiment (Blundell et al. 1992, Ye & Ansorge 1990, Ye 1992), which runs parallel to E1 allows the refraction Moho to be traced farther south (see Figure 9-5b). The EGT refraction experiments indicate that the European Moho extends southward to greater depths and that a discontinuous crust-mantle boundary at a shallower depth just south of line E1 points to a crustal imbrication (see also Valasek et al. 1991, Ye 1992). Hereby a wedge of lower Adriatic crust was forced into the European crust, splitting it apart and delaminating it. The wedge of lower Adriatic crust reaches about as far north as Thusis along line E1 (see Figure 9-8a). Complex deformation is to be expected at the northern tip of this wedge and may lead to scattering and defocussing of reflected seismic rays. In the EGT-refraction experiment on the other hand, the European crust-mantle boundary has been sampled by undershooting this complex zone.

The sparse, discontinuous reflections at around 8–9 s TWT in the northern part of the section (**C** in Figure 9-5a) occur at an increase in refraction determined velocities (cf. Ye & Ansorge 1990; Valasek 1992; Ye 1992) from 6.2 to 6.5 km/s. An origin of these reflections due to the presence of fluids released in devolatilization reactions was evoked by Pfiffner et al. (1988). Some of these events are shorter than the diameter of the first Fresnel zone (limit of horizontal resolution) and may thus be due to diffractions from lateral inhomogeneities caused by irregularly shaped rock bodies rather than from horizontal layering. This velocity discontinuity, representing most likely the transition to the lower crust (Conrad discontinuity), can be traced southward to about shot point Thusis, i. e. the intersection point with line E2 (see section 9.3.). This point coincides also with the northern tip of the Adriatic wedge. The Conrad discontinuity, which is constrained by refraction seismic data, can be followed eastwards, a point discussed in more detail in section 9.5 of this chapter. Note that the position of this discontinuity as shown in Figures 9-8a and b differs from the one given by Marchant & Stampfli in Chapter 24 (Figure 24-7).

In the southern part of line E1 reflections at around 7 sTWT (*CA* in Figure 9-2) also coincide with a velocity discontinuity from 6.1 to 6.6 km/s (op. cit.). Farther north, beneath shot points Ausserferrera and Thusis this Adriatic Conrad dicontinuity dips steeply northward and is therefore not sampled in the reflection experiment.

9.2.3 Discussion and conclusion

Although the seismic line E1, which crosses a major part of the Alps, has considerably added to the knowledge of the deep structure of the Alps, additional insight was gained from the companion seismic lines through the Alps of western central and southern Switzerland. Thus, rather than trying to discuss the Alps as whole, the following discussion will focus on implications for which E1 is particularly relevant. But in order to place line E1 into the larger scale Alpine framework, the cross section of Figure 9-8a is expanded to the north, using the insight gained from the seismic lines E4, E5 and E6 crossing the Molasse basin, which are discussed in detail by Pfiffner et al. in Chapter 8, and to the south using cross sections through the Southern Alps by Schönborn (1992). The resulting, schematic geologic cross section in Figure 9-8b serves as basis for this short discussion. A more detailed discussion of this eastern transect is given by Schmid et al. in Chapter 22.

The Tertiary sedimentary infill of the North-Alpine Foredeep has been significantly shortened in its southern part, the Sub-Alpine Molasse (see Pfiffner et al., Chapter 8). The associated thrust faults level off at depth going southward and are most probably linked to shortening and uplift of the **Aar massif** (see Pfiffner et al., Chapter 13.1). In the cross section of Figure 9-8b this basement shortening is accomodated by a set of structures representing a combination of folding and faulting. The magnitude of the basement uplift from about 7 km below to 1 km above sea level requires a crustal-scale balance. It has to be noted that the amount of basement uplift becomes even more important in central Switzerland (see Pfiffner et al., Chapter 13.1); there shortening of the Jura Mountains is also related to the Aar massif basement uplift. Balancing the geologic profile of Figure 9-8b (or 9-8a) suggests that bedlengths of Mesozoic strata are shortened by about 28.5 km to an actual length of 62.5 km, as measured between a point situated at the northern end of the profile and the point beneath shot point Canova on the southern flank of the Aar massif in the south. Comparing the area of structural relief defined by the Aar massif bulge to the curvimetric shortening of the Mesozoic strata suggests a detachment of the Aar massif at some 12 km below the basement top. Going down these 12 km from the southern flank of the Aar massif puts the detachment level at the top of the Adriatic wedge. It is thus plausible that the thrust fault at the base of the Adriatic wedge which must extend northward and upward because of its significant displacement, is kinematically linked to the basal detachment of the Aar massif. It could be envisaged that the imbricate structure of the Aar massif evolved in sequence, i. e. propagated northward at the tip of the Adriatic wedge. The north-dipping thrust fault at the top of this wedge is kinematically linked to basement shortening in the Southern Alps (with south-directed thrusting of Miocene age) and to Oligo-Miocene steep south-directed thrusting on the Insubric Line. Comparing the uplift history of the Aar massif (Pfiffner et al., Chapter 13.1) and the Insubric Line (Schmid et al., Chapter 22), and considering that shortening of the Aar massif is kinematically linked to shortening of the Sub-Alpine Molasse which contains Early Miocene sediments, it follows that in Oligocene/Miocene times, both Aar massif and Insubric Line were sites of rapid uplift under ductile conditions. On the other hand much of the northward movement of the tip of the wedge is probably related to Late Miocene shortening in the Southern Alps. It thus follows that uplift of the Aar massif and along the Insubric line in this transect of the Alps was coeval and occurred as a pop-up structure, bordered by conjugate thrust faults, and that it took place at some distance ahead of the northward moving Adriatic wedge.

Inspection of the **Penninic nappes** shown in Figure 9-8b reveals that the upper crustal basement nappes form a four (or more) fold stack and thus require a substantial volume of lower crust for reasons of volumetric balancing. This volume is apparently not available in this cross section. Instead, one is forced to conclude that lower crustal material has been subducted. Subduction of lower crust has already been postulated by Laubscher & Bernoulli (1982) and Trümpy (1988). An accurate mass balance is, however, rendered difficult for the following reasons:

1. Unlike the Helvetic zone, where nappe transport was directed approximately south to north (Pfiffner, 1981, 1985), in the Penninic zone transport directions were less regular and include E-W components (see Schmid et al., Chapter 14) i. e., in and out of the section plane.
2. The thickness of the crust prior to Alpine orogeny is not yet well constrained, but it is likely that the crust had been thinned during Mesozoic rifting associated with the formation of the Tethys ocean.
3. The Moho may not behave purely as a passive interface but rather may undergo postorogenic "ordering processes" (Trappe et al., 1988). This point is particularly important for those parts of the Alps which underwent the Cretaceous to Eocene orogenic phases (Penninic, Austroalpine, and South-Alpine domains). It is possibly less relevant for the European crust of the Helvetic zone which was mainly deformed in Oligocene-Miocene times.
4. An accurate material balance should incorporate effects associated with the complex metamorphic history of the rocks involved (e. g., high-pressure metamorphism in the Adula nappe) and of the geometry of the subduction suture which is truncated by the Insubric Line near the Bergell Intrusion but which must have a continuation at depth.

The Penninic basement nappes shown in Figure 9-8b are each about 5 km thick. Considering the nappe-internal strain and structure, the original thicknesses can be estimated at 4 km (Suretta), 8 km (Tambo), 5-15 km (Adula), 15 km (Simano), which compares with the depth-to-detachment of the Gotthard (10 km) and the one derived for the Aar massif (12 km). Surface observations suggest that the geometry of these basement nappes are often controlled by lithologic contrasts, late-Variscan granitoid bodies often marking the front of such nappes. The base of these nappes, where the detachment horizon was sub-parallel to the overlying Mesozoic cover rocks, are not obviously related to lithologic contacts. Considering the evolution of the thrust belt it may be argued that the detachment level rather is controlled by temperature (weakening quartz e. g.), pressure and/or weakening due to fluid release.

In a general way **crustal shortening** within the European plate thus can be envisaged as an imbrication of upper crustal flakes detached along or slightly above the Conrad discontinuity in response to the northward moving Adriatic wedge. The lower European crust was subducted, i. e. overriden by the Adriatic wedge. Crustal thickening is thus essentially due to thickened, imbricated upper crust. The lower crust, however, also thickens slightly across line E1 according to the velocity analyses by Valasek (1992) and Ye (1992). This thickness increase is shown schematically in the geologic profile of Figure 9-8b. The southern, overriden part of this lower crust represents the substratum of the upper crustal flakes that now form the Penninic basement nappes. The latter in turn form the substratum of the Penninic cover nappes. As discussed by Schmid et al. in Chapter 14, however, this part of the European crust was stretched and thinned during the Mesozoic. These seemingly contradicting observations could be explained by shortening and imbrication of thinned lower crustal units in the footwall of the Adriatic wedge. There are, however, no reflections discernible which would highlight structures associated with this underplating.

A structure with south-directed thrusting and imbrication exists in the Southern Alps (see Schumacher et al., Chapters 10 and15, and Schmid et al. Chapter 22). Some of the north-dipping reflections beneath shot point Sovrana might in fact stem from ductile shear zones associated with South-Alpine basement flakes. On line C3 (Pfiffner & Heitzmann, Chapter 11) distinct south-dipping reflections are recognized that are likely to stem from South-Alpine thrust faults. In contrast to the northern, European part, the Adriatic lower crust beneath the Southern Alps is also thickened. This is evident from Figure 9-5b, where the top of the **Adriatic wedge**, or more precisely, the Conrad discontinuity forms a bulge. Reflections beneath reflection group *N* in Figure 9-5a are from within the Adriatic wedge and may well be related to its shortening. In any case the wedge of Adriatic lower crust which was forced into the European crust in the late stages of the Alpine collision was internally deformed. Complex deformation within the tip of the wedge may defocus and scatter seismic rays, which may explain the southward disappearance of reflections from the lowermost European crust in the near-vertical seismic profiling. The wedge overrode a slab of lower European crust in the process of collsion, peeling off and shortening the upper crust. The latter's internal deformation occurred at least in part some distance ahead of the tip of the wedge.

9.3 Interpretation of line E2: The crustal structure along strike in the eastern Swiss Alps

L. Hitz & O. A. Pfiffner

In this part of chapter 9, results of a deep seismic reflection survey located in the eastern Swiss Alps are presented. The survey was carried out in 1990 and consists of Vibroseis and dynamite recordings. The composite transect is termed E2. In contrast to the majority of the NRP 20 profiles which were recorded perpendicular to the Alpine strike, the profile E2 was recorded from WSW to ENE, parallel to the Alpine strike. It runs from Thusis to just E of Scuol in the Lower Engadine Valley (Figure 9-9b). At Thusis, line E2 intersects with line E1 (Figure 9-1) and near Scuol it intersects with line E3 (Figure 9-15) providing thus a lateral connection to the N-S trending E1 and E3 profiles as well as to the fan profiles E7 to E9. In addition, the earlier acquired seismic refraction profile ALP75 (Alpine Longitudinal Profile, Figure 9-9a) is oriented parallel to line E2. Its results are integrated in the interpretation of line E2.

9.3.1 The data

Profile E2 consists of a 21 km long Vibroseis line and an overlapping 70 km long dynamite line. Vibroseis recordings with a penetration to approximately 6 s cover the western third of the transect.

The processed dynamite and Vibroseis sections are shown in Plates 9-3 and 9-4. Both lines show a rather poor data quality for several reasons. First, the lines had to follow narrow valleys with high traffic density and railways, which results in a high ambient noise level and in a decrease of the signal/noise ratio. Second, the source energy was low, especially in the Vibroseis measurements with only 1 sweep/vibration point. Third and probably most important, the crustal structure of the Alps in N-S transects is complex with steeply N- and partly also S-dipping reflectors. The consequence of this for a seismic strike-line is strong energy scattering and the presence of out-of-plane reflections both contributing to poor data quality. Nevertheless, coherent reflected energy can be observed in both data sets. The E2 dynamite data (see Plate 9-3) are characterized by several distinctive reflection bands from

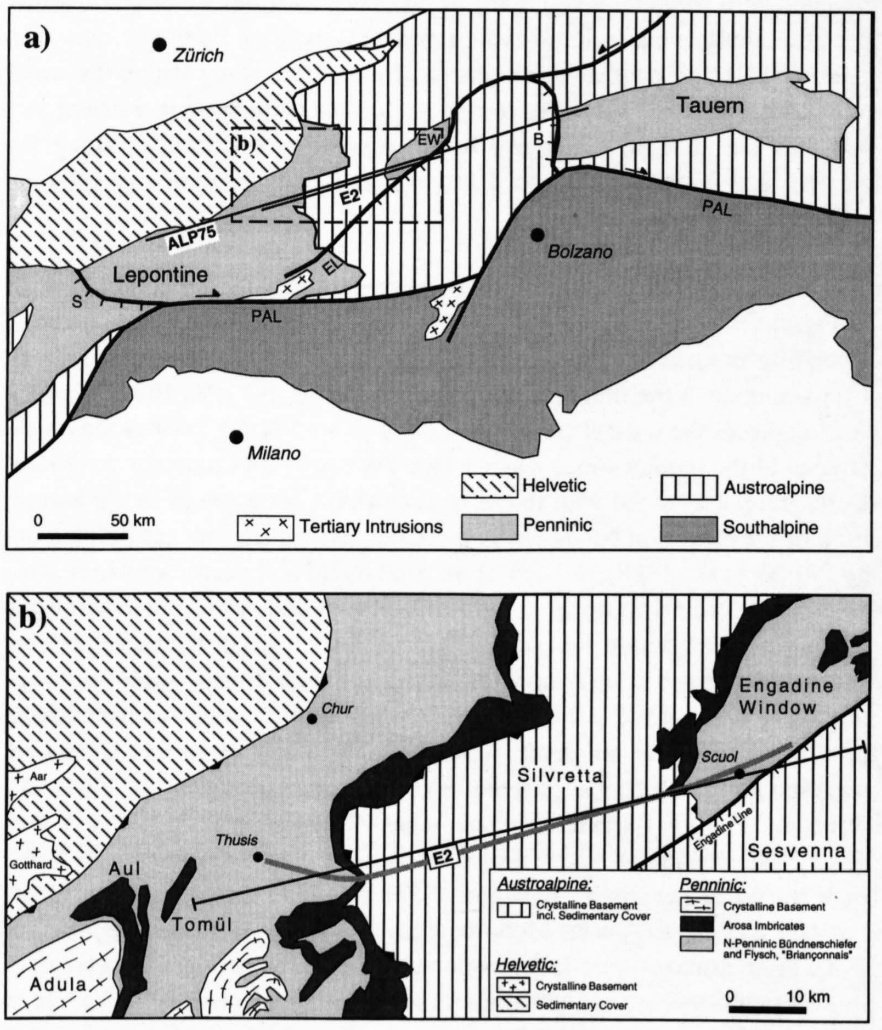

Figure 9-9
Location maps. (a) Simplified geological map of the Alps showing the locations of the E2 seismic reflection profile and the central part of the ALP75 seismic refraction profile (cf. Yan & Mechie 1989). PAL = Periadriatic lineament, EL = Engadine line, B = Brenner line, S = Simplon line, EW = Engadine window. (b) Enlarged area of (a) showing the location of the E2 processing line (dashed line) and the trace of the geological cross-section of Figure 9-12 (solid straight line).

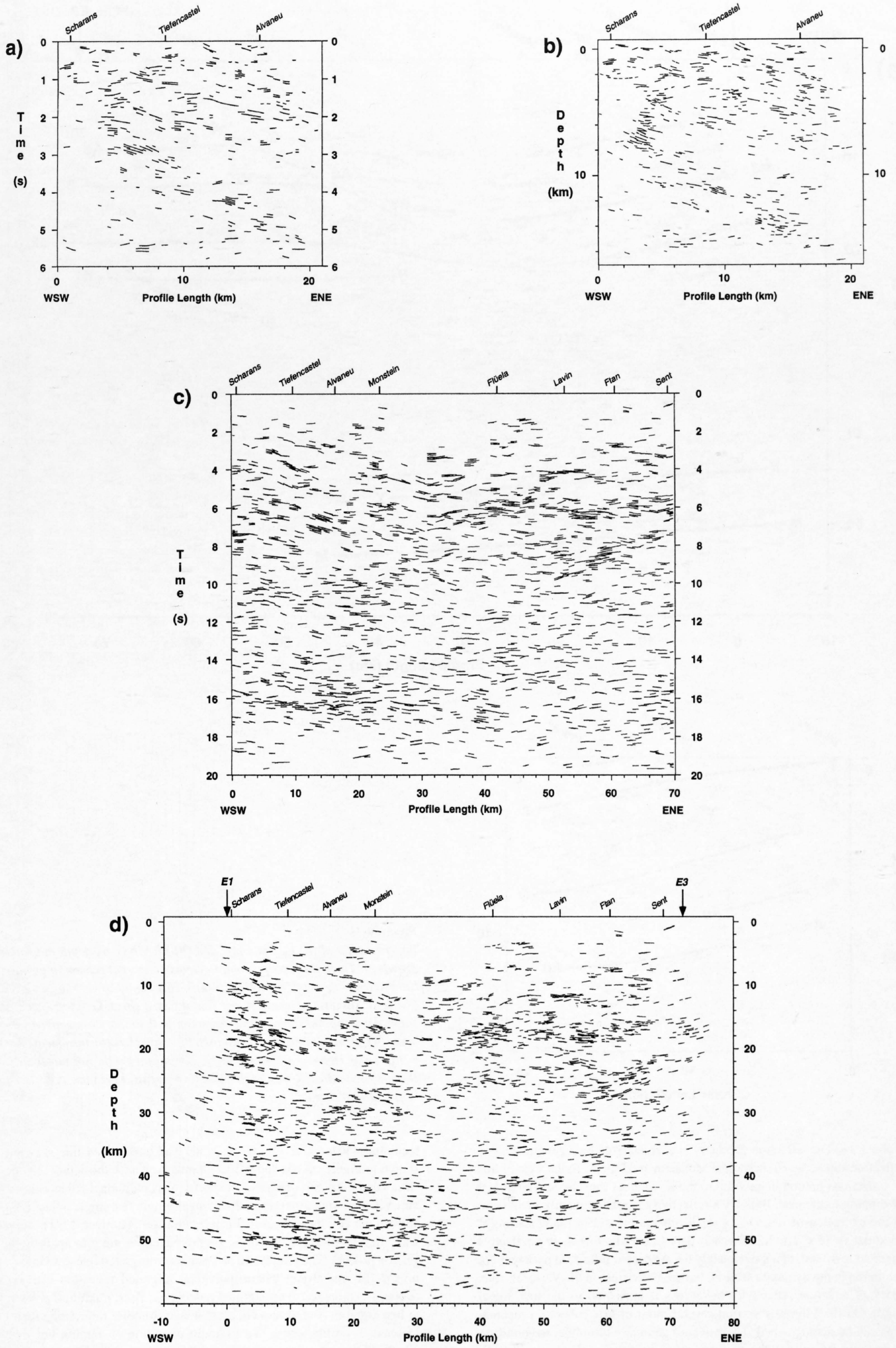

Figure 9-10
Automatic line drawings (cf. Valasek 1992) of E2 Vibroseis and E2 dynamite data. (a) E2 Vibroseis unmigrated. (b) E2 Vibroseis depth-migrated. (c) E2 dynamite unmigrated. (d) E2 dynamite depth-migrated. Horizontal to vertical scale = 1:1.
Note the increase in the dynamite profile length due to updip migration of dipping line elements.

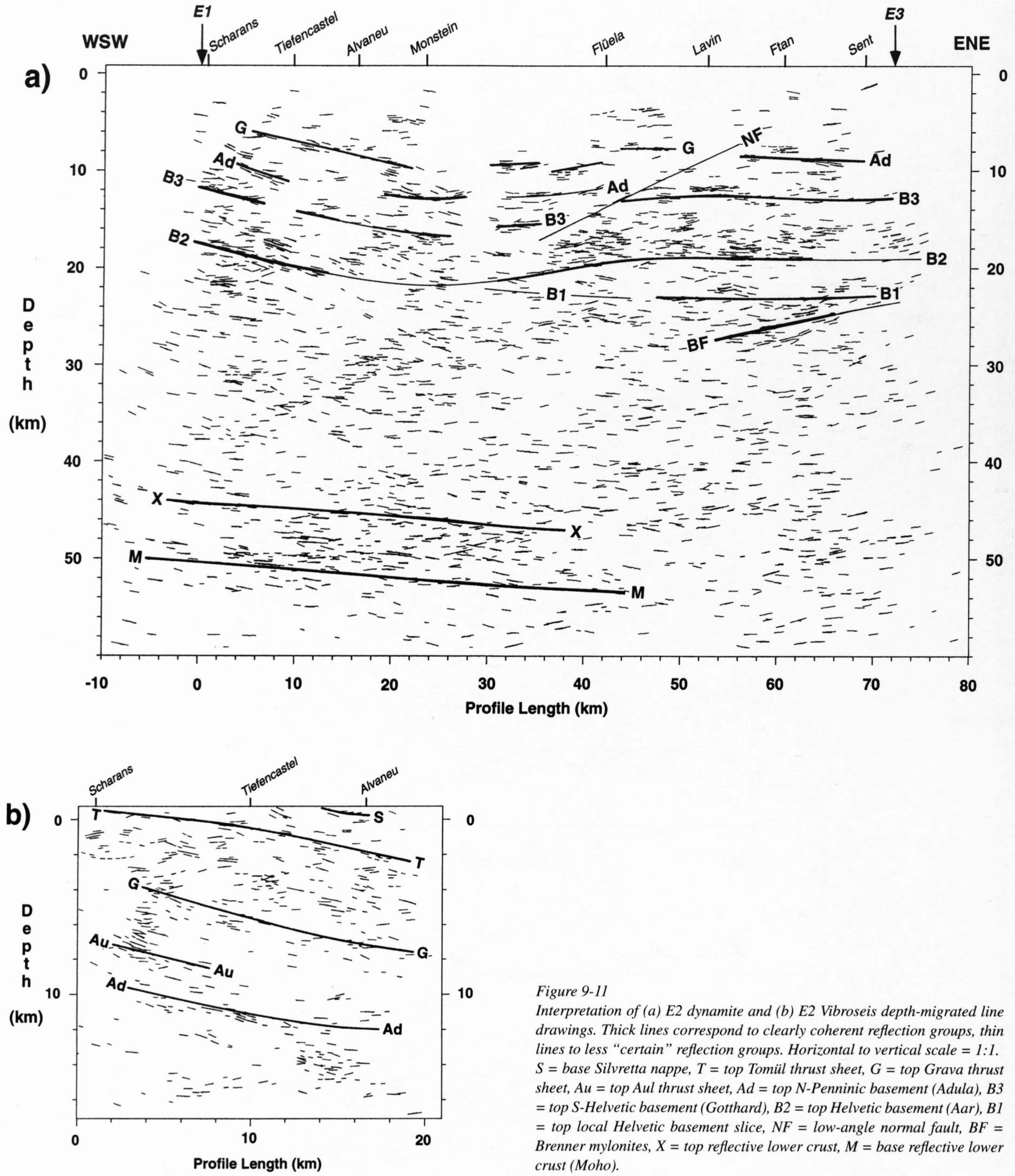

Figure 9-11
Interpretation of (a) E2 dynamite and (b) E2 Vibroseis depth-migrated line drawings. Thick lines correspond to clearly coherent reflection groups, thin lines to less "certain" reflection groups. Horizontal to vertical scale = 1:1. S = base Silvretta nappe, T = top Tomül thrust sheet, G = top Grava thrust sheet, Au = top Aul thrust sheet, Ad = top N-Penninic basement (Adula), B3 = top S-Helvetic basement (Gotthard), B2 = top Helvetic basement (Aar), B1 = top local Helvetic basement slice, NF = low-angle normal fault, BF = Brenner mylonites, X = top reflective lower crust, M = base reflective lower crust (Moho).

1 to about 9 s. The reflection geometry is characterized by a general change in reflection-dip between shotpoints Monstein and Flüela. To the west of this area, reflections predominantly dip to the E, whereas they are subhorizontal to W-dipping to the east. Below 9 s reflectivity is predominantly incoherent with the exception of a 1.5 to 2 s thick reflection band in the W starting at approximately 15 s. The E2 Vibroseis data (see Plate 9-4) show a reflective upper crust to a depth of approximately 6 s. As deeper reflection packages are encountered in the dynamite section, but are not visible in the Vibroseis line, the lack of coherent reflectivity below 6 s is attributed to the low signal strength. On the Vibroseis section several more or less coherent reflection groups can be distinguished. Their overall geometry closely corresponds to the reflection geometry in the western part of the dynamite section with individual reflection groups dipping predominantly to the E.

For the purpose of depth-migration, the seismic data presented in Plate 9-4 were transformed into line drawings using a computer-based line drawing technique (Valasek & Frei, chapter 4). The unmigrated line drawings are shown in Figures 9-10a and 9-10c. Comparison with the actual seismic data shows that the computer-based method depicts individual reflections very accurately including also minor dip-changes within one single reflection. Upon subsequent ray theoretical depth-migration (cf. Holliger 1991), curved or wavy line segments representing single reflections are torn apart by the migration process. The effects can be seen in the migrated line drawings of Figures 9-10b and 9-10d where individual migrated reflection elements are shorter as compared to unmigrated reflections. Thus, migration gives at least at first sight an overall less coherent image. Another migration effect is the increase in profile length due to updip migration of dipping line elements which in the case of the dynamite section adds another 20 km to the initial profile (Figure 9-10d). Depth-migration was performed using a velocity structure based on the results of the nearby ALP75 refraction profile (cf. Yan & Mechie 1989, Figure 9-13).

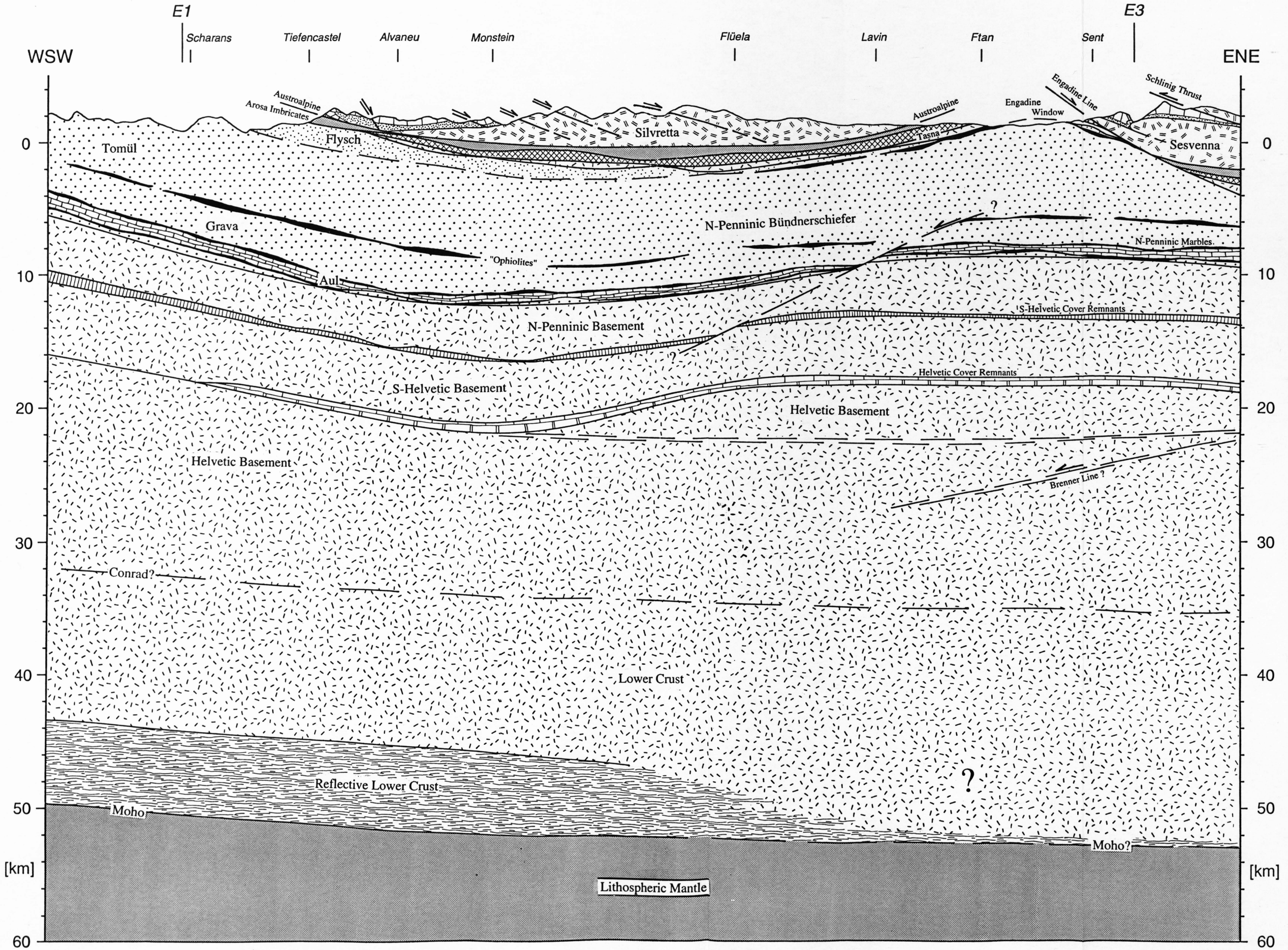

Figure 9-12
Crustal-scale cross-section based on the interpretation of the E2 dynamite and Vibroseis data, the parallel oriented ALP75 refraction profile, the intersecting reflection profiles E1 and E3, and surface geology. The cross-section follows the straight line indicated in Figure 9-9b. No vertical exageration. Coordinates correspond to the Swiss National grid net.

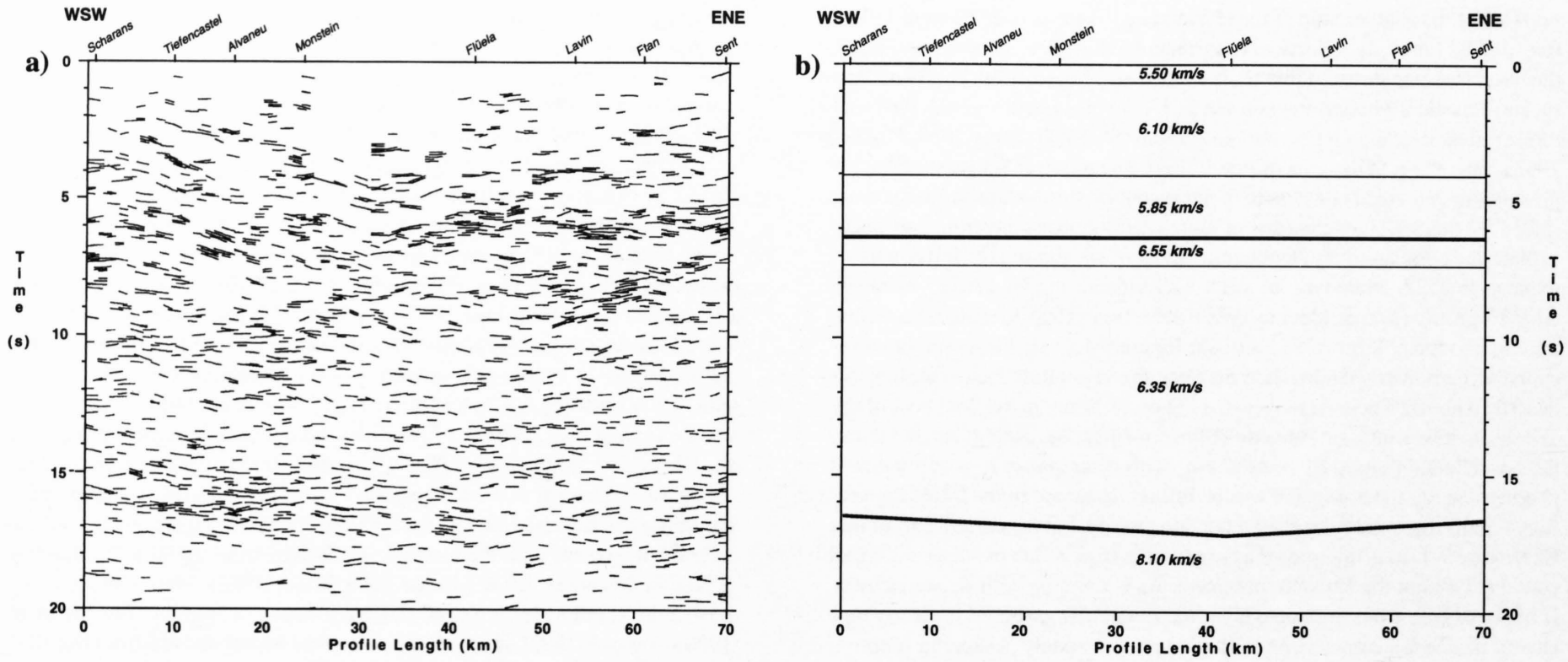

Figure 9-13
Comparison between (a) unmigrated E2 reflection data and (b) the corresponding extract of the parallel oriented ALP75 velocity-depth model by Yan & Mechie (1989). The base of the reflected energy at around 6 s and the base of the reflective lower crust at approximately 16.5 s correspond well to two pronounced velocity discontinuities in the velocity-depth model (thick lines). Horizontal to vertical scale = 1:1 at an average crustal velocity of 6 km/s.

9.3.2 Geologic interpretation

The test of a good interpretation is consistency. This statement is especially valid for the deep seismic reflection data of line E2 with its low signal/noise ratio. Accordingly, the following information was used for the interpretation of the E2 data: (1) reflection geometry; (2) surface geology along the transect based on the works by Brauchli & Glaser 1924, Willhelm 1929, Eugster & Leupold 1930, Bearth et al. 1935, Spaenhauer et al. 1940, Jäckli 1941, Nabholz 1945, Cadisch 1953, Cadisch et al. 1963, Trümpy 1980, Stutz & Walter 1983, Eichenberger 1986, Behrmann 1988, Selverstone 1988, Schmid & Haas 1989, Schmid & Froitzheim 1993, Pfiffner et al. 1990a; (3) interpretations of line E1 by Pfiffner et al. 1988, 1990b, 1991, Frei et al. 1989, Mueller 1990, Valasek 1992 and Litak et al. 1991, 1993; and (4) refraction derived velocity-depth models by Egloff 1979, Noack 1984, Yan & Mechie 1989 and Ye 1992. In a first interpretative step, migrated reflections forming coherent reflection groups were identified (Figure 9-11, thick lines). Then, the identified reflection packages were, if possible, joined together over the entire profile length considering also less "certain" reflection groups (Figure 9 -11, thin lines). Finally, the resulting structural interpretation was iteratively compared with the above-mentioned geological and geophysical data base in order to obtain maximum consistency. In the following, the results of this interpretation procedure are presented starting with the structurally highest tectonic unit and proceeding downwards to the base of the crust. The interpretation is summarized in the geological cross-section of Figure 9-12.

Austroalpine, Arosa imbricate and Briançonnais units: As mentioned earlier, the WSW–ENE running E2 profile parallels the general strike of the Alpine chain. As a consequence, only two major Alpine tectonic units, the Austroalpine zone (represented by the Silvretta and Sesvenna nappes) and the underlying Penninic zone (represented by the Arosa imbricate, Briançonnais (Tasna nappe in the E) and N-Penninic Bündnerschiefer and Flysch units) are exposed along the line (Figure 9-9b). Surface correlation indicates that the base of the Austroalpine Silvretta nappe lines up with shallow reflections between shotpoints Tiefencastel and Alvaneu in the Vibroseis data (*S* in Figure 9-11b). In the dynamite data, the Austroalpine base is not imaged due to the large-offset recordings. The seismic record of this discontinuity is hence very sparse and its construction in the crustal cross-section of Figure 9-12 is predominantly based on geological surface maps (cf. Willhelm 1929, Bearth et al. 1935, Spaenhauer et al. 1940, Cadisch et al. 1963) and a structure contour map specifically constructed thereof. The position of the underlying Arosa imbricates, marking the oceanic suture between Briançonnais and Austroalpine units, and the position of the Briançonnais units themselves are again poorly constrained by the seismic data, although a velocity increase in the ALP75 seismic refraction profile from 5.5 km/s to 6.1 km/s (Figure 9-13, Yan & Mechie 1989) might be attributed to ophiolitc rocks found within the Arosa imbricates as well as in the topmost Bünderschiefer units of the Engadine window (Figure 9-9b). It can however not be used for constructing structural details. As a consequence, the geometry of the Arosa and Briançonnais units is again based on surface geological data and thus somewhat speculative at depth.

N-Penninic cover nappes and basement: Updip projections of reflection packages *T*, *G* and *Au* (Figure 9-11) suggest that these reflections stem from the N-Penninic Bündnerschiefer unit. The latter consists of several tectonic subunits or thrust sheets, which contain predominantly shaly-sandy calcareous micaschists with intercalated layers of marbles and ophiolitic rocks (cf. Jäckli 1941, 1944, Nabholz 1945, Cadisch 1953). Using laboratory P-wave velocity measurements by Sellami et al. (1990) and first arrivals, Pfiffner et al. (1991) argued that high reflection coefficients result from juxtaposition of these rock types. On the other hand, complexely deformed lenses of dolomites and ophiolitic rocks, as they are observed at surface, are expected to scatter the seismic energy and thus decrease the signal coherency. Only regular and larger scale structures within the N-Penninic Bündnerschiefer are therefore likely to produce coherent reflected energy. One such structure are massive carbonates found at the top of the Tomül thrust sheet (Willhelm 1929, Jäckli 1944) and westward up-dip projection of reflection group *T* is consistent with this interpretation. In a similar way, reflection group *G* can be attributed to the marble-basalt layer seperating the Tomül thrust sheet from the underlying Grava thrust sheet. This interpretation is consistent with the E1-interpretations by Pfiffner et al. (1990b, 1991) and Litak et al. (1991, 1993). Reflection group *Au*, being again in good agreement with the E1-interpretations, may well stem from the Aul thrust sheet (Figure 9-9b) which contains large bodies of marbles and several slivers of ophiolitic rocks (Nabholz 1945). Due to the lower resolution of the dynamite data, *Au* cannot be clearly seperated from the next deeper reflection group *Ad*. For the geologic interpretation, the top of the Aul thrust sheet along the dynamite section is thus placed at the top of reflection group *Ad*, which is attributed to the top of the N-Penninic Adula basement nappe directly underlying the Aul thrust sheet. This interpretation results from the correlation with the E1-interpretations by Pfiffner et al. (1990b), which itself was derived from surface data (structure contour maps by Pfiffner et al. 1990a), as well as by Litak et al. (1993) who validated the interpretation by 3D seismic modeling. The observed lateral discontinuity of the described reflection groups is explained by variations in subsurface geology and by strong local energy scattering along complex structures.

Helvetic Basement: Based on the correlation with the top of the of the S-Helvetic basement in line E1 (*B3* in Figure 9-5a), reflection group *B3* (Figure 9-11a) is interpreted as the top of the S-Helvetic Gotthard "massif". Reflectivity of this discontinuity is explained by remnants of autochthonous Mesozoic sediments and by a mylonitic fabric due to thrusting along the basal Penninic thrust. Also based on E1, reflection group *B2* (Figure 9-11a) is attributed to the top of the Helvetic Aar massif basement. Along the E1 transect, the contact between the Helvetic Aar massif and the overlying S-Helvetic Gotthard thrust-sheet puts basement rocks onto basement rocks. This configuration lacks the appropriate impedance contrast to generate strong reflections in the E1 data. The marked difference in the seismic ex-

pression of the southern top of the Helvetic basement in lines E1 (non-reflective) and E2 (strongly reflective) is attributed to difference in structural style: the basal Helvetic thrust in line E1 is located at the base of the Permian "Verrucano" clastics, whereas towards the E, i. e. in the area of line E2, the basal thrust ramps laterally up into middle Jurassic shales (Trümpy 1969, Pfiffner 1993). Therefore, in the area of line E2, Triassic to lower Jurassic sediments presumably remained attached to their crystalline substratum and were overridden by the S-Helvetic basement unit. Such lithologic layering can easily explain the comparatively strong reflectivity of the top of the Helvetic basement in line E2. Moreover, in the velocity-depth model derived from the ALP 75 profile (Yan & Mechie 1989), reflection group *B2* coincides with a thin high-velocity layer (6.55 km/s, see Figure 9-13). This layer might correspond to carbonates sandwiched between the crystalline basement units as described above. There is, however, a big discrepancy in the thickness of the Triassic to lower Jurassic Helvetic sediments (max. est. 500 m) and the thickness of reflection group *B2* (max. 2 km). This discrepancy is possibly due to geometrical ray focussing and will be further discussed in the following section. Finally, the weakly defined reflection group *B1* in the eastern part of line E2 (Figure 9-11a) is interpreted as originating from a slab of Mesozoic rocks contained within the Helvetic basement. As is the case with *B2*, reflectivity is likely to stem from lithologic layering. Reflection group *B1* is clearly registered in line E3 (see section 9.4) where it is strongly S-dipping (approx. 25°) and ends approximately 10 km N of the intersection with E2. We therefore conclude that *B1* represents an out-of-plane reflection and that the Mesozoic sediments which caused the reflections are probably absent vertically beneath E2. In the geological cross-section of Figure 9-12, the base of the overlying Helvetic basement slice is thus drawn as a discrete shear zone.

Normal Faults: Updip projection of reflection group *BF* (Figure 9-11a) yields a surface position near the western end of the Tauern window. This western margin is defined by a W-dipping low-angle normal fault (Figure 9-9a), termed Brenner Line (Selverstone 1988) or Sterzing-Steinach mylonite zone (Behrmann 1988). The normal fault shows a minimum vertical throw of 10 km (Lammerer 1988) and is related to final movements in the unroofing history of the Tauern window, which started at latest in the Early Oligocene (Selverstone 1988). Displacements along the Brenner Line are associated with strong mylonitization in an up to 400 m thick mylonite belt (Behrmann 1988). Reflection group *BF* could thus be tentatively interpreted as acoustic response to the Brenner mylonites. Another possibility, not implying such large distance correlations, would be to consider reflection group *BF* as a side swipe associated with the Adriatic wedge, since the lack of lower crustal reflectivity beneath *BF* could be the consequence of deep crustal deformation by the indenting wedge (see below). When following the upper crustal reflections over the entire profile length, a W-dippinig zone offsetting reflection groups *Ad* and *B3* can be noted (*NF* in Figure 9-11a). With the exception of some W-dipping reflections, this zone lacks reflectivity (Figure 9-10d). Correlation of reflection groups *Ad* and *B3* across *NF* suggests a normal fault displacement. These observations lead us to the postulation of a W-dipping low-angle normal fault cutting across the upper crustal nappe stack. At the surface, this fault zone might be related to a system of NNW–SSE trending brittle faults cutting all the tectonic units of the Engadine window. Kläy (1957) suggests that this fault system plays an important role in the uplift and formation of the Engadine window. If this correlation between the postulated normal fault and the brittle faults observed at surface is correct, it may be argued that the shear zone flattens towards the E and that the brittle faults represent associated high-angle faults in the hanging wall. This structural relation can also be observed in the Turba mylonite zone where high angle brittle faults cut across the hanging wall of the mylonite zone (Nievergelt et al. 1996).

Lower Crust and Moho: In line E2, clearly coherent reflectivity in the lower crust is only found between *X* and *M* (Figure 9-11a). This stands in contrast to the intersecting line E1 and the EGT refraction profile where besides a reflective lowermost crust, a reflective Conrad discontinuity (C in Figure 9-5a) and a corresponding velocity increase from 6.2 to 6.5 km/s (Figure 9-5b) can be observed. The lack of a reflective Conrad discontinuity in line E2, however, is in agreement with ALP75 velocity-depth models (Yan & Mechie 1989, Noack 1984) and with the intersecting line E3, where a well-defined Conrad discontinuity is absent, too. We can therefore conclude that the Conrad discontinuity along E2 is not a sharp boundary and generates neither coherent near-vertical nor wide-angle reflections. In order to distinguish nevertheless between upper and lower crust in the E2-interpretation, we extrapolated the Conrad discontinuity from the N and W, where it is defined by both seismic methods (section 9.5, Egloff 1979, Ye 1992).
As mentioned above, coherent reflectivity in the lower crust is observed in the western part of line E2, where it forms an approximately 6 km thick reflective zone between *X* and *M* (Figure 9-11a). The comparatively strong reflectivity corresponds to the seismic character of the lowermost crust in line E1 near the intersection, as well as to lower crust sampled in many other areas (cf. Klemperer et al. 1986). Numerical modeling shows that a subhorizontal layering of laminae with low and high seismic velocities explains best the high reflectivity of the lower crust (cf. Sandmeier & Wenzel 1986). In the case of the Alps, Rey (1993) suggested that the layering might have been produced by Variscan post-thickening crustal extension and low-P granulite facies metamorphism of the lower crust in late Carboniferous to Permian times. The characteristic lower crustal reflectivity, however, diminishes towards the E (Figure 9-11a). The decrease in reflectivity could be the effect of (1) recording conditions (cf. Smithson 1986), (2) scattering of the seismic wave front in a structurally complex overburden (cf. Raynaud 1988, Carbonell & Smithson 1990) or (3) scattering of the seismic energy within a complex lower crust (cf. Valasek et al. 1991, Pfiffner et al.1991). Argument (1) can be excluded, as recording conditions did not change significantly along the E2 transect. Arguments (2) and (3) are discussed in the following section. The base of the crust in the E2 transect, i. e. the reflection Moho, is placed at the bottom of the reflection group between *X* and *M* (Figure 9-11a). This is in good agreement with the Moho depth derived from the ALP75 refraction profile in this area (Yan & Mechie 1989, Noack 1984). Moreover, at the intersection, it coincides with the reflection Moho of line E1 (Pfiffner et al. 1990b, Valasek 1992) and with the refraction Moho derived from the EGT data (Ye 1992). As the reflection Moho is not defined in the eastern part of E2, the Moho depth in this area is entirely based on the southward extrapolation of strong Moho reflections from line E3 (see section 9.4).

9.3.3 Discussion and conclusion

Data quality: In comparison to the intersecting lines E1 and E3, the seismic data quality of line E2 is poor. Low signal/noise ratio due to a high ambient noise level and intense energy scattering along complex structures is an inherent problem for all three deep seismic surveys, although probably not everywhere to the same degree (ambient noise is lowest in line E3). However, what clearly distinguishes line E2 from the other profiles is the fact that it runs parallel to the Alpine strike. In the area of intersection between lines E1 and E2, steeply S- and partly also N-dipping potential reflectors are very likely to exist (Figure 9-8a). Thus, significant out-of-plane energy is to be expected in line E2. If interfering destructively, such out-of-plane reflections can break up the recorded wave fronts significantly, resulting in a loss of signal coherency. In special geometrical configurations, however, constructive interference might result in thick zones of multcyclic reflections. This might well be the case for the southern Aar massif with its concave-like geometry (Figure 9-8a or b) and could explain the difference in thickness between reflection group *B2* (up to 2 km) and the thickness of the sandwiched Triassic to Lower Jurassic cover sediments (up to 500 m) responsible for the reflections.

Comparison between seismic reflection and refraction data: Comparison of the E2 reflection data with the velocity model derived from the ALP 75 refraction profile by Yan & Mechie (1989) reveals good agreement in two major crustal boundaries (Figure 9-13): (1) comparison reveals a good fit between the base of the reflective lower crust and the refraction Moho, defined by a velocity jump from 6.35 km/s to 8.1 km/s and (2) the band of reflected energy at approximately 7 s correlates well with a thin high-velocity layer of 6.55 km/s underlying a velocity inversion zone of 5.85 km/s. The remaining velocity discontinuities cannot be clearly linked to the E2 reflectivity pattern. From this comparison it can however be concluded, that velocity discontinuities with velocity contrasts > 5% in the ALP75 refraction profile are indeed reflective in the E2 reflection profile.

Partial lack of lower crustal reflectivity: As pointed out in the previous paragraph, the poor lower crustal reflectivity in the eastern half of line E2 is most probably related to strong energy scattering along complex structures. A comparison of the upper crustal architecture of line E1 (intersecting E2 in the W) and line E3 (intersecting E2 in the E) reveals a similarly complex upper crustal structure. It thus seems unlikely that an increase in the complexity of the upper crust, i. e. scattering of the seismic energy in the overburden, could explain the observed disappearance of lower crustal reflectivity. On the other hand, a southward decay of lower crustal reflections is also observed in line E1 (S of the intersection with E2). There, it coincides with the northern front of the Adriatic wedge consisting of lower crust. The disappearance of a reflective lower crust in E1 has thus been attributed to energy scattering in a complexly deformed lower crust associated with this indenting wedge (Pfiffner et al. 1991, Valasek et al. 1991). Between the western and the eastern NRP 20 transects, Valasek (1992) deduced a WSW–ENE strike for the northern front of the wedge. Its further continuation towards the E can be indirectly assessed from the shortening within the Southern Alps (as argued by

Pfiffner et al. 1991, the wedge's length should balance with the length of the upper crustal flakes stacked up in the Southern Alps). Judging from the shortening estimates gathered from balanced N–S profiles across the Southern Alps (Schönborn 1992), the wedge's northern front may well retain its WSW–ENE strike and may even extend farther N than the eastern end of line E2. The disappearance of the lower crustal reflections towards the E in line E2 may thus also be explained by scattering of the seismic energy due to deep-crustal deformation by the indenting Adriatic wedge.

Geologic interpretation: It has to be stressed that, given the relatively poor data quality of line E2, the geologic interpretation presented here is certainly not the only possible solution, although the integration of complementary data like the intersecting profiles E1 and E3, the refraction profile ALP 75 and surface geology presents strong constraints. Moreover, it has to be kept in mind that any crustal geologic cross-section represents a strongly simplified image of the crust, because of the limited resolution of the available geological and geophysical data. With these restrictions in mind, the most important information in the geologic context gathered through line E2 are (Figure 9-12): (1) The S-Helvetic and N-Penninic basement units appear to be continuous along strike. (2) The axial dip of upper crustal units, which is also observed at surface, rapidly decays towards the E. This decay may be attributed to the presence of a Helvetic basement slice underneath the Engadine tectonic window, which induces an uplift of of the overlying units. (3) The domal antiform forming the Engadine window does not seem to affect the underlying basement. This means that the N-Penninic Bündnerschiefer units must be detached from their crystalline substratum. (4) Both the Brenner line (if this interpretation is followed) and the postulated normal fault in the upper crust along line E2 indicate E–W extension. Seismic refraction data (Yan & Mechie 1989) do not point to a significant uplift of the crustal base associated with this extension. Consequently, extension might be related to N-S shortening and vertical thickening. Based on surface observation, syncompressional E-W extension in the Eastern Alps was already postulated by Behrmann (1988), Selverstone (1988) and Ratschbacher et al. (1991b) and was modeled by Ratschbacher et al. (1991a). The extension recorded in E2 can be dated as "post-nappe" as it affects e. g. the basal Penninic thrust (Figure 9-12). Since the latter is post Early Eocene (see Schmid et al., Chapter 14), E-W extension along E2 is dated as Late Eocene or younger, i. e. coeval with extension linked to the Tauern uplift (Selverstone 1988). (5) The NE part of the Engadine line (Figure 9-9b) is a normal fault with an estimated minimum vertical throw of 4 km in the area of scuol (Schmid & Haas 1989, schmid & Froitzheim 1993). If the Brenner line is taken to be responsible for reflection group *BF*, the Engadine and Brenner lines would form a set of conjugate normal faults. In this case, the Austroalpine crustal lid situated between these two faults is essentially downfaulted, accentuating the structural highs of the Engadine and Tauern windows (Figure 9-14). Note that a conjugate fault geometry does not necessarily imply contemporaneous activity.

Summarizing, the following conclusions can be drawn:

(1) The seismic data quality in the E2 strike-line is poor as compared to N–S oriented seismic dip-lines. The difference in data quality is attributed to the destructive interference of reflected out-of-plane energy.
(2) Velocity contrasts in excess of 5% in the ALP75 refraction profile proved to be reflective in the E2 reflection profile. Consequently, where available, seismic refraction results should be integrated in the interpretation of deep-seismic reflection data.
(3) Reflectivity of the lowermost crust is poor in the eastern half of line E2 as compared to the western half. This is speculatively attributed to scattering of the seismic energy due to deformation of the lower crust by the indenting Adriatic wedge.
(4) The S-Helvetic and N-Penninic basement units appear to be continuous along strike.
(5) The axial dip of upper crustal units rapidly decays towards the east. This might be attributed to the presence of a Helvetic basement slice underneath the Engadine window, which induces an uplift of the overlying units.

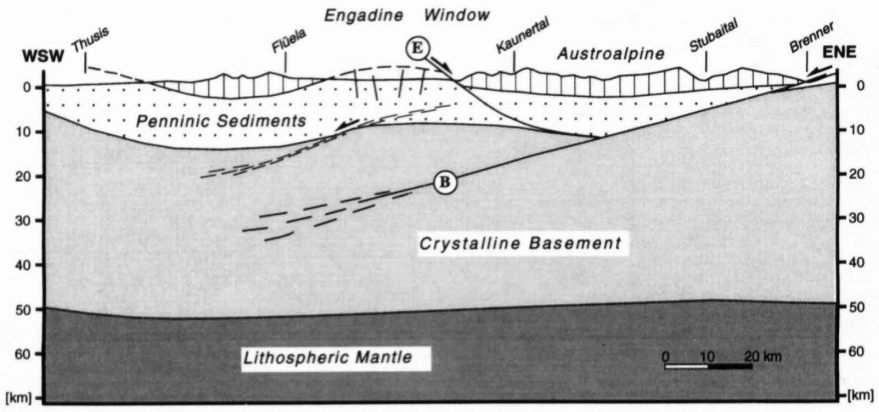

Figure 9-14
Tectonic model along strike showing a possible relationship between the Engadine line (E) with the Brenner line (B) as a set of conjugate normal faults. Normal faulting leads to the formation of a downfaulted Austroalpine crustal block situated between the two faults.
The model follows the ALP75 trace indicated in Figure 9-9a and includes data from Kläy (1957), Behrmann (1988), Selverstone (1988), Yan & Mechie (1989) and Schmid & Froitzheim (1993).

9.4 Interpretation of line E3: The deep structure of the Engadine window

L. Hitz & O. A. Pfiffner

This section presents the results of a deep seismic reflection survey located at the eastern margin of the Engadine tectonic window (Figure 9-15). The survey consists of two short dynamite lines which are combined into a composite transect termed E3. Line E3 crosses all the major tectonic units of the lower Engadine valley including the so-called Engadine line, a major structural discontinuity in the eastern Swiss Alps. In addition, line E3 intersects line E2 just east of Scuol (Figure 9-15). Combined with the E2 transect, line E3 was intended to clarify the deep structure of the Engadine window, a tectonic window which Termier (1904) referred to as "the most beautiful example to cite".

9.4.1 The data

Line E3 was recorded in the fall of 1991 in a joint operation of the Geophysical Institutes of Clausthal (FRG), Munich (FRG), Münster (FRG), Leoben (A), Zürich (CH) and a private Swiss company. A total of 6 dynamite shots were fired, each with a 30 kg charge. They were recorded by a 14.3 km long receiver spread consisting of five different registration units in the Uina and Sinestra valleys (Clausthal, Munich, Münster, Zürich and GeoExpert), and by a separate 4.8 km long receiver spread in the Fimber valley (Leoben). This configuration resulted in two separate CDP-processing lines (Figure 9-15),

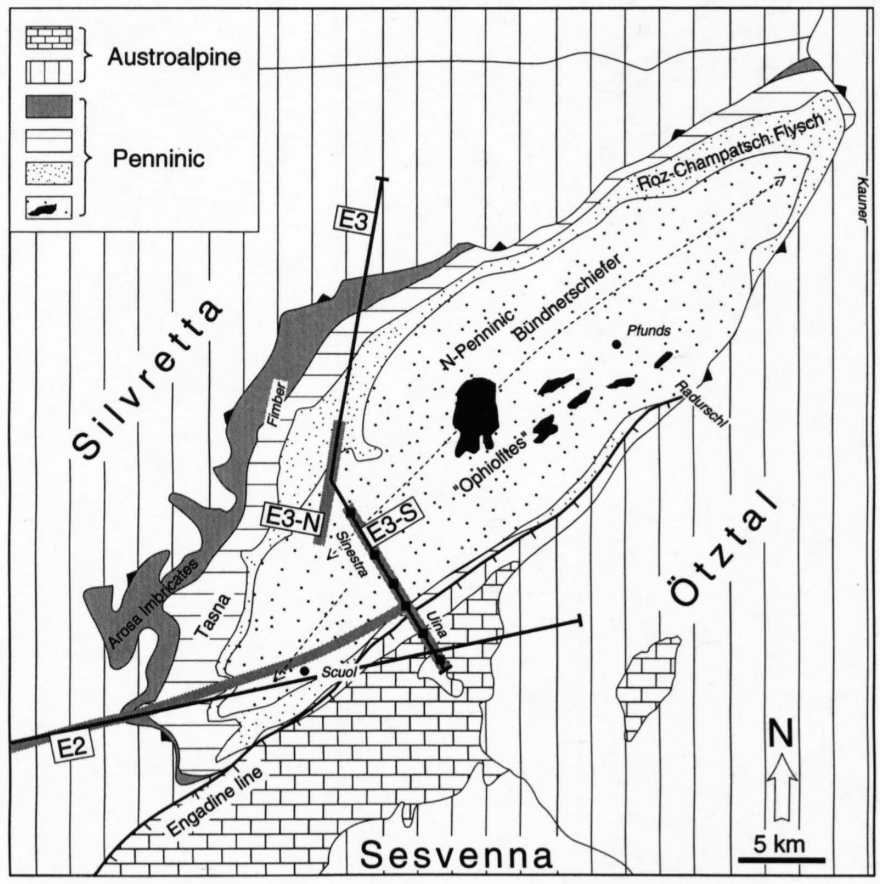

Figure 9-15
Simplified tectonic map of the Engadine tectonic window showing the location of the E3 transect consisting of the seismic reflection profiles E3-North (E3-N) and E3-South (E3-S), and part of the intersecting seismic reflection profile E2.
Grey lines = CDP-processing lines, black squares = shot locations, black straight lines = traces of geological cross-sections, dashed lines with arrows = crest-lines of the Engadine antiform (cf. Cadisch et al. 1963).

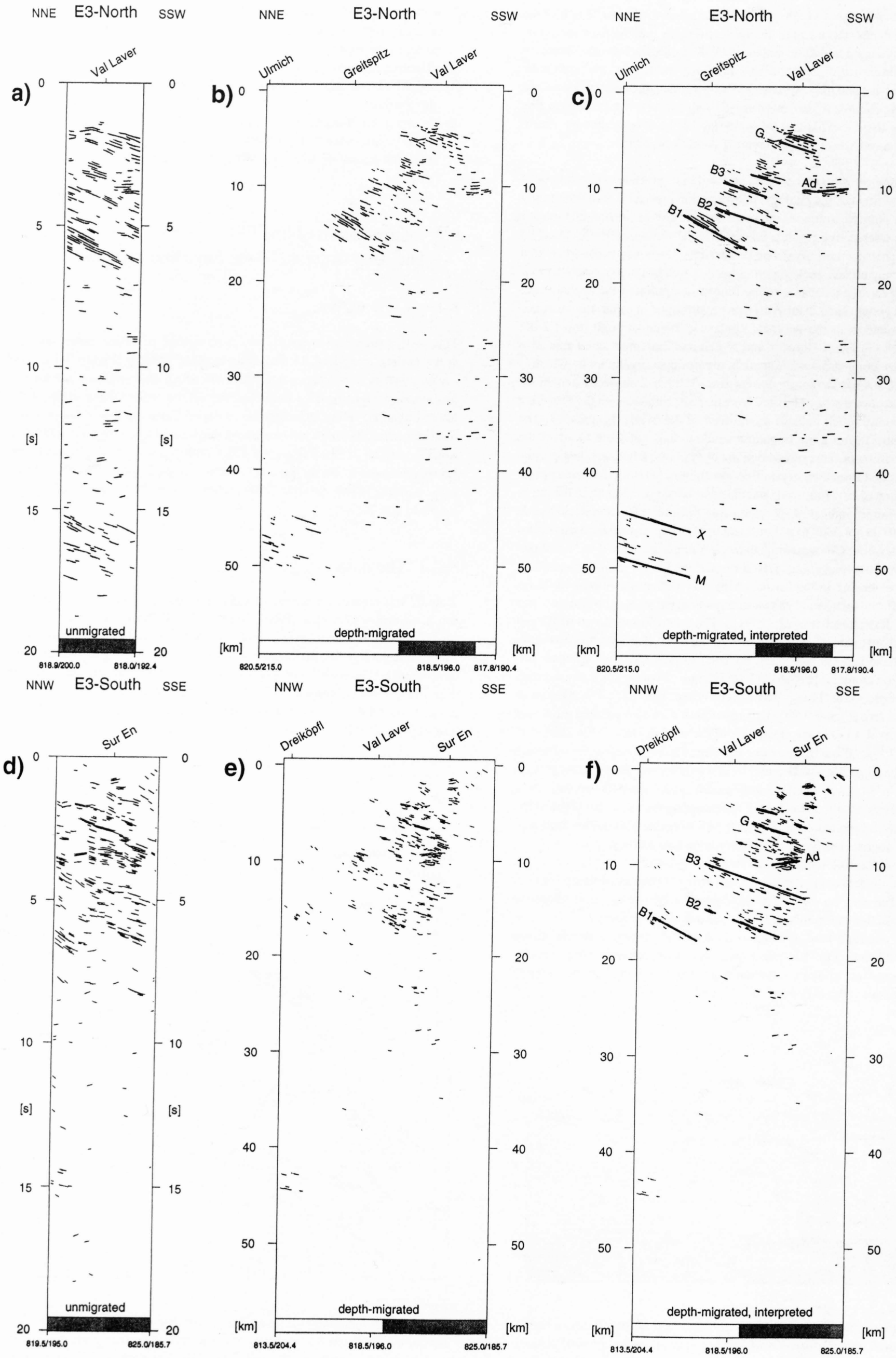

Figure 9-16
Automatic line drawings of the E3 seismic reflection data. Data are shown in unmigrated (a and d), depth-migrated (b and e) and interpreted form (c and f). Lettered reflection groups are discussed in the text. Horizontal to vertical scale = 1:1.
Note the increase in profile length due to up-dip migration of dipping line elements.

one oriented SSE–NNW (E3-South), and one oriented SSW–NNE (E3-North). The data were treated at the processing center of the ETH Zürich using standard processing procedures troughout. Due to the unique character of every individual shot-gather and the low CDP coverage (max. 5), however, special processing parameters and methods of determing them had to be designed (cf. De Haas 1992). The processed data are presented in Plates 9-5 and 9-6.

E3-South (Plate 9-6, see also Figure 9-16d) shows strong reflections in the upper 8 s dipping predominantly to the SSE. Below 8 s, reflectivity is very poor. The most prominent reflection group is characterized by two-cyclic, high-amplitude reflections dipping from 2.0 s in the NNW to 3.5 s in the SSE. Below this group, a subhorizontal to slightly NNW-dipping reflective zone can be observed. The latter is followed by two SSE-dipping reflection groups, one from 4 to 5.5 s in the SSE, the other from 5 to 6.5 s in the SSE. Upper crustal reflectivity ends with a strongly SSE-dipping reflection group at 6 s in the NNW. Reflectivity in the shallowmost part of line E3 between 0 and 1.5 s is rather erratic. Note, however, a change in reflection geometry from subhorizontal to NNW-dipping in the central part to SSE-dipping in the southern part of the line.

Similar to E3-South, E3-North (Plate 9-5, see also Figure 9-16a) shows a strongly reflective upper crust starting with an approximately 1 s thick reflective zone from 2 s in the NNE to 3 s in the SSW. This is followed by a reflection group with a marked change in reflection geometry: in the SSW, reflections are subhorizontal to NNE-dipping, whereas towards the NNE they are SSW-dipping. Below the latter, a 2 s thick zone with constantly SSW-dipping reflection packages can be observed marking the base of the reflective upper crust. In contrast to the similarity of upper crustal reflectivity, E3-North shows strong SSW-dipping reflections also in the lowermost crust between 15 and 17 s.

For the purpose of depth-migration, the seismic data (Plates 9-5 and 9-6) were transformed into automatic line drawings (Figure 9-16a and d) using a program developed by Valasek (1992; see Valasek & Frei, chapter 4). Ray-theoretical depth-migration (cf. Holliger 1991) was done using a velocity structure derived from the ALP 75 velocity-depth model by Yan & Mechie (1989). The depth-migrated line drawings are shown in Figure 9-16b and e. Note that up-dip migration of dipping line elements increased the profile length considerably and that the identification of the above described reflection groups, which is easy in Figure 9-16a and d, is less evident in the depth-migrated line drawings of Figure 9-16b and e.

9.4.2 Geologic interpretation

In a first interpretative step, depth-migrated coherent reflection groups were laterally correlated and labeled (Figure 9-16c and f). In a second step, these reflection groups were projected parallel to the regional strike (WSW-ENE, see inset in Figure 9-17) onto a common trace termed E3 (Figure 9-15). The result of this procedure can be seen in the simplified line drawing of Figure 9-17. Note that the projected reflection groups line up smoothly, indicating that distortions due to projection are moderate. The next step in the interpretation involved the correlation of the simplified line drawing with the geophysical and geological database available for the study area. The geophysical database consists of the intersecting E2 seismic reflection profile (section 9.3), the intersecting ALP 75 seismic refraction profile (cf. Yan & Mechie 1989, Noack 1984) and two seismic experiments in the area E of Pfunds (Scheliga 1971, Giese & Prodehl 1976). Geologic data include geologic and tectonic maps (Kläy 1957, Cadisch et al. 1963, Trümpy 1972, Oberhauser 1980), structure contour maps (Stutz & Walter 1983) and various other studies regarding the geology of the Lower Engadine valley (cf. Cadisch 1953, Trümpy 1980, Schmid & Haas 1989, Mattmüller 1991, Schmid & Froitzheim, 1993). It should be noted that the domal structure of the Engadine window prohibits reflection correlation with geologic outcrops by means of projections, as done in the case of E1. The identification of individual reflections is thus mainly based on the correlation with the intersecting line E2 and the ALP 75 velocity-depth model. In the following, the results of the geologic interpretation, summarized in the geologic cross-section of Figure 9-19, are presented.

Shallow crust: Due to large off-set recordings and low CDP-coverage, reflections from the shallowmost crust are predominantly absent. Only in the southernmost part of line E3 where offsets are smallest, shallow reflectivity can be observed (Figure 9-17). There, line E3-South shows some faint strongly SSE-dipping reflections at 1 to 1.5 s at the line's southern end (Figure 9-18). By up-dip projection, they match with the Engadine line, a normal fault with an estimated vertical throw of 4 km in the area of Scuol (Schmid & Haas 1989). Reflectivity might stem from the juxtaposition of contrasting lithologies, as downfaulting along the Engadine line places Austroalpine basement (Sesvenna) next to Penninic sediments (Bündnerschiefer unit). The interpretation of the Austroalpine units, the Arosa imbricates and the Briançonnais unit (Tasna nappe) as shown in Figure 9-19 is mainly based on surface data by Kläy (1957) and Oberhauser (1980) for the northern part, and Cadisch et al. (1963), Stutz & Walter (1983), Schmid & Haas (1989) and Schmid & Froitzheim 1993 for the southern part. At the NE margin of the Engadine window, Scheliga (1971) reported strong reflections at 1.1 s TWT (~1.5 km b.s.l.) from a seismic reflection experiment in the Kauner valley (Figure 9-15). Giese & Prodehl (1976) attributed these reflections to the contact between Penninic Bündnerschiefer and Austroalpine basement.

N-Penninic cover nappes and basement: Extrapolation of surface data suggests that the short, predominantly SSE-dipping reflections between 2 and 7 km depth (Figure 9-17) originate from within the N-Penninic Bündnerschiefer unit. Reflectivity is likely to stem from intercalated large-scale lenses of ophiolitic rocks observed also at surface (cf. Koller & Höck 1987). Reflections labeled *G* in Figure 9-17 are speculatively attributed to a more or less continuous ophiolitic layer, similar to the one encountered in lines E1 and E2. In the W, this layer is correlated with the Grava thrust sheet, a subunit of the N-Penninic Bündnerschiefer unit (see sections 9.2 and 9.3).

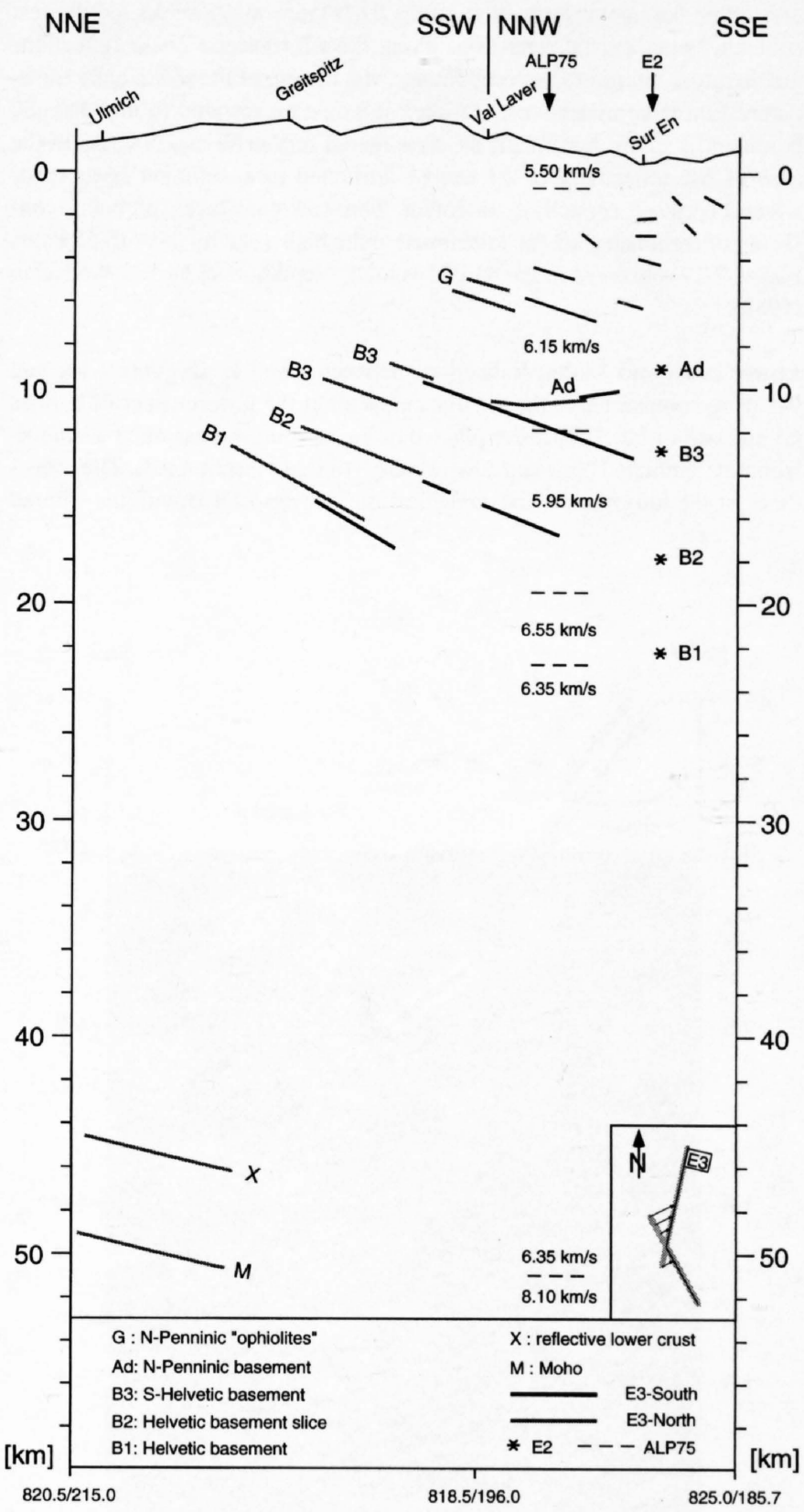

Figure 9-17
Simplified line drawing resulting from the projection (see inset) of coherent reflection groups of lines E3-South and E3-North (Figure 9-16c and f) onto the common E3 trace indicated in Figure 9-15. Note that the migrated reflection groups of the two lines line up smoothly indicating that distortions due to projection are moderate.
Stars = intersecting reflection groups of line E2 (Figure 9-11), dashed lines = intersecting discontinuities from the ALP75 velocity-depth model by Yan & Mechie (1989). Vertical to horizontal scale = 1:1.

Based on the correlation with E2, the next deeper reflection group *Ad* (Figure 9-17) is interpreted as marking the top of a large-size N-Penninic basement unit, which in the W corresponds to the Adula nappe. Reflection group Ad forms an exception in the E3 reflection geometry as it is subhorizontal to slightly NNE-dipping. Together with the underlying reflection group *B3*, *Ad* forms a triangle indicative of the northern end of this Penninic basement nappe. The reflectivity of *Ad* is tentatively attributed to the impedance contrast between crystalline basement rocks (Adula) and high-velocity marbles and basalts of the overlying Aul thrust sheet (cf. Pfiffner et al. 1991, Sellami et al. 1990).

Helvetic basement: Reflection group *B3* (Figure 9-17) can be correlated with the top of the S-Helvetic basement unit imaged in line E2. In line E1, this discontinuity corresponds to the top of the Gotthard unit and is identical with the basal Penninic thrust. Reflectivity is explained by possible remnants of S-Helvetic cover-sediments (Triassic dolomites) and/or a velocity anisotropy produced by mylonitization along the basal Penninic thrust. In the ALP 75 velocity-depth model by Yan & Mechie (1989), the corresponding velocity discontinuity marks the top of a velocity inversion zone (Figure 9-17). Similar to line E2, the next deeper reflection group *B2* can be attributed to the top of a local Hevetic basement slice underlying the Engadine window. Reflectivity could stem from Mesozoic carbonates interlayered with crystalline basement. Reflection group *B1* (Figure 9-17) marks the deepest coherent upper crustal reflections along the E3 transect. These reflections are therefore interpreted as originating from the top of the seismically transparent European upper crust. As such it would correspond to the Helvetic basement, i. e. the Aar massif as encountered further W and NW. As in the case of *B2*, reflectivity of *B1* can be attributed to a sediment layer sandwiched between crystalline basement. This sediment layer, probably consisting of carbonates, might correspond to the high-velocity layer (6.55 km/s, Figure 9-17) observed in the ALP75 velocity-depth model by Yan & Mechie (1989).

Lower crust and Moho: Reflections between *X* and *M* (Figures 9-16c and 9-17) are comparable to the seismic character of the lowermost crust in lines E1 and part of E2. They are explained as the seismic expression of a subhorizontally laminated high-and-low velocity structure (section 9.3). The reflectivity of the lowermost crust as well as the one associated with the Conrad discontinuity is, however, absent in most of line E3. This observation is in agreement with the eastern part of the intersecting line E2, where a reflective lower crust and a reflective Conrad discontinuity are not observable either. This lack of reflectivity is speculatively attributed to Alpine deep-crustal deformation resulting in strong scattering of the seismic energy (see discussion in section 9.3). The Conrad discontinuity shown in the crustal cross-section of Figure 9-19 is thus based on extrapolated data from the N and W only (section 9.5, Egloff 1979, Ye 1992). It was drawn to indicate that a differentiation between upper and lower crust along E3 is nevertheless likely to exist.
The base of the crust, i. e. the reflection Moho, is placed at the bottom of the reflection package between *X* and *M*. It dips about 13° to the SSW. As the reflection package tapers off to the S, the Moho as shown in Figure 9-19 corresponds solely to an extrapolation of *M*. This extrapolated Moho discontinuity, however, fails to match the refraction-derived Moho by Yan & Mechie (1989) by approximately 3 km (Figure 9-17). The misfit is indicative of depth-distortions due to out-of-plane energy in the ALP 75 refraction data.

9.4.3 Discussion and conclusion

Correlation between E2/ALP 75 and E3: The strongly SSE-dipping reflections in line E3 indicate that reflected out-of-plane energy in the seismic strike-lines E2 and ALP 75 has to be expected. It is thus not surprising that none of the intersecting E2-reflection groups (depth-migrated along strike) and ALP 75-discontinuities exactly match the migrated reflection groups of line E3 (Figure 9-17). Correlation of the E3 seismic data with the results of lines E2 and ALP 75 is nevertheless possible and facilitates the identification of the individual reflections. Moreover, a limited amount of 3D structural information can be gained in the area of intersection. There, the WSW–ENE striking E2 profile shows subhorizontally oriented Penninic and Helvetic basement units, whereas in line E3, the same basement units are dipping SSE (Helvetic units) or NNW (Penninic unit). Consequently, an ENE-strike (~055° N) can be deduced for the basement units underlying the Engadine window, which closely corresponds to the regional strike observed at surface (Kläy 1957, Cadisch et al. 1963). The good agreement in strike between units at the surface and deep basement units suggests that the formation of the Engadine window may be closely linked to deformation within the underlying basement (see below).

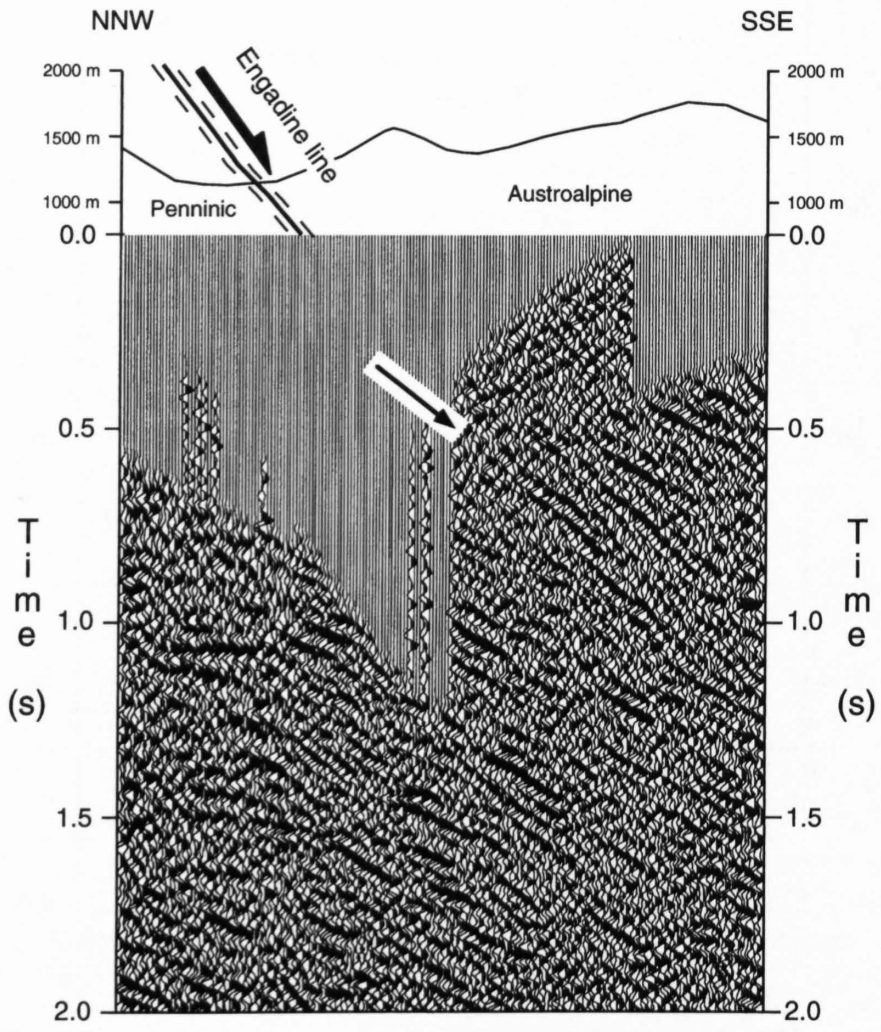

Figure 9-18
Extract of the southernmost part of the E3 reflection data (see also Plate 9-6). SSE-dipping reflections (arrow) can be correlated with the Engadine line at surface which essentially acts as a normal fault in the investigatea area. Note the change from subhorizontal reflections in the NNW to SSE-dipping reflections in the SSE. This change in orientation is attributed to dragfolding associated with faulting along the Engadine line.

Geologic interpretation (Figure 9-19): The geologic interpretation of line E3 shows that the Engadine tectonic window is underlain by an up to 10 km thick pile of N-Penninic Bündnerschiefer. The latter is probably composed of a number of thrust sheets, as indicated by coherent reflectivity within the Bündnerschiefer. These units form the core of the domal antiform constituting the Engadine window. This antiform apparently does not significantly affect the underlying basement units, which is compatible with the E2-interpretation (Figure 9-12) where the basement units underneath the Engadine window are subhorizontally oriented. From this it can be concluded that the N-Penninic Bündnerschiefer units must be detached from the underlying basement nappe-stack during window formation, i. e. they may be regarded as forming a large-scale detachment fold.
Another result of the geologic interpretation of line E3 is that the Engadine window seems to be underlain by a Helvetic basement slice (HBS). The latter is also recognized along strike in line E2, where it laterally ends towards the W in the area between shot points Monstein and Flüela (Figure 9-12). The HBS-basement slice is thus of limited lateral extent, seemingly restricted to the area of the Engadine window and could thus be responsible for the axial plunge of this structural high.

Engadine line: Based on paleostress analysis and large-scale nappe correlation, the Engadine line (Figure 9-15) has recently been recognized as a post-collisional tectonic lineament along which oblique slip and block rotation took place in Late Tertiary times (Schmid & Froitzheim 1993). In the area of line E3, the Engadine line essentially acts as a brittle normal fault with down-faulting of the SE block (Figure 9-19). The vertical throw is estimated to be approximately 4 km (Schmid & Haas 1989). On a large scale, movements along this part of the Engadine line juxtaposes Austroalpine basement and N-Penninic Bünderschiefer. Such a lithologic contrast should give rise to steep reflections and to a lateral P-wave velocity change. SSE-dipping reflections correlating with the surface position of the Engadine line can indeed be observed in the E3 data (Figure 9-18). The reflections dip about 55° to the SSE at depth, which is within the dip range expected from geologic surface data. Moreover, a change in reflection orientation from subhorizontal between 1 and 1.5 s to SSE-dipping further S can be observed in the Bündnerschiefer units below the Engadine fault (Figure 9-18). This change may reflect drag-folding in the fault's footwall (Schmid & Froitzheim 1993).
The expected P-wave velocity change across the Engadine line was in fact

E3

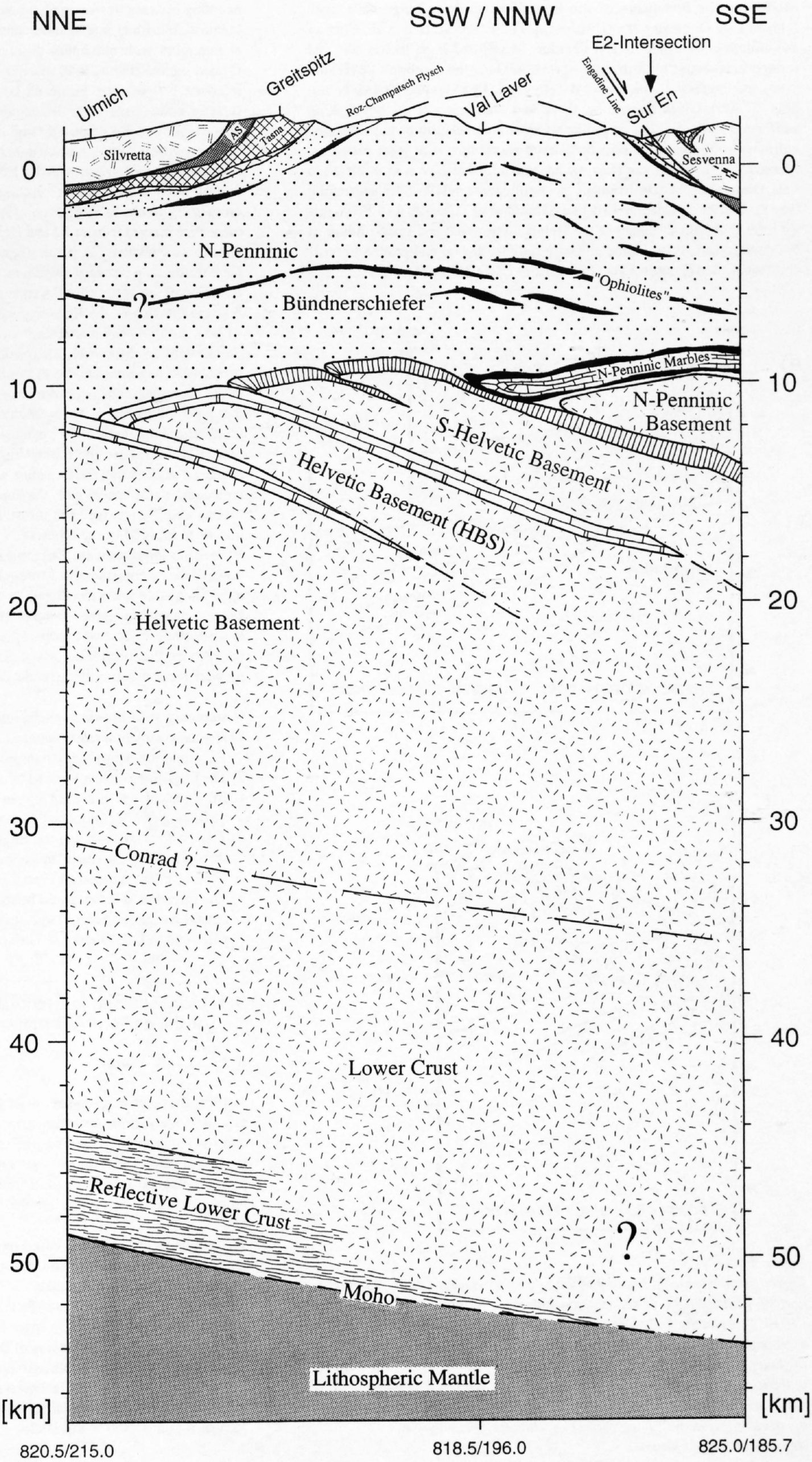

Figure 9-19
Crustal-scale cross-section through the Engadine tectonic window based on the interpretation of the E3 seismic reflection data, the intersecting seismic profiles E2 and ALP75 and surface geology. The trace of the cross-section is indicated in Figure 9-15. Coordinates correspond to the Swiss National grid net. No vertical exageration.

observed in a short seismic refraction profile in the Radurschl valley where travel times could not be explained without assuming a lateral inhomogeneity (Scheliga 1971, Giese & Prodehl 1976). The derived lateral velocity change was attributed to the contact between the juxtaposed Austroalpine basement and N-Penninic Bündnerschiefer.

Model for the formation of the Engadine window: Large-scale open folds of Late Oligocene age (Domleschg-Phase, see Schmid et al., Chapter 14) affecting Austroalpine and Penninic units trend E–W to NE–SW and formed in response to dextral transpression along the Insubric line (Figure 9-8b) and the coeval intrusion of the Bregaglia (30 Ma) and Novate batholiths (27 Ma). Given the similar shape and orientation of the NE-striking antiform constituting the Engadine window a correlation of the Engadine uplift with this phase of post-collisional shortening is at least plausible. Moreover, thrusting in the Helvetic basement further NW is also related to Late Oligocene – Early Miocene post-collisional NNW–SSE shortening (see Pfiffner et al, Chapter 13.1 and Schmid et al., Chapter 14). From this we infer that both thrusting in the Helvetic basement and open folding of N-Penninic and Austroalpine units are roughly coeval and related to post-collisional shortening in Late Oligocene to Early Miocene times.

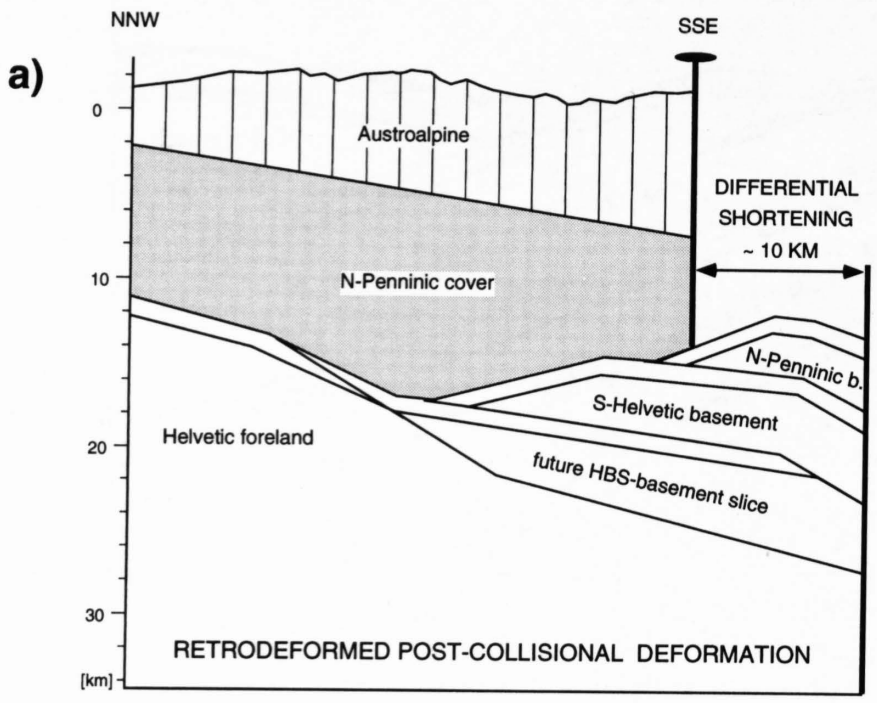

Figure 9-20
Tectonic model for the formation of the Engadine window. (a) Retrodeformation of post-collisional deformation shows a differential shortening of ~10 km between the Austroalpine lid and the European basement suggesting a decoupling between the two units. (b) Post-collisonal shortening leads to the indentation of an upper crustal wedge bounded by a passive back thrust at the top and an active NW-vergent thrust at the bottom. The indentation is associated with detachment folding, local uplift and extension resulting in the present-day domal shape of the Engadine tectonic window.
No vertical exaggeration.

Using area- and line-length balancing methods, retrodeformation of the post-collisional structures in a NNW-SSE cross-section across the Engadine window shows that shortening associated with the formation of the HBS-basement slice is in the order of ~12.5 km, whereas unfolding of the basal Austroalpine thrust in the section considered corresponds to a shortening of ~2.5 km only (Figure 9-20a). The striking difference in shortening suggests a decoupling between the Austroalpine lid and the European basement units during post-collisional deformation. Such a decoupling is likely to be positioned at interfaces with maximum differences in rock strength. In the retrodeformed section (Figure 9-20a), a major detachment could be expected at the interface between the European basement and the N-Penninic Bündnerschiefer units (large-scale detachment and thrusting of the Penninic cover nappes followed this contact throughout the Swiss Alps). Thus, our model includes a protruding European upper crustal wedge bounded by a passive back-thrust at the top and an active NNW-vergent thrust at the bottom (Figure 9-20b). Such passive back-thrust models have been reported from various orogens by Banks & Warburton (1986). Assuming (1), that the HBS-basement slice imaged in lines E2 and E3 is restricted to the area of the Engadine window (see above), (2), plane strain in the area considered and (3), a complete decoupling between Bündnerschiefer and European basement, the indentation of the upper crustal wedge must lead to a local uplift of maximally 8 km in the area of the Engadine window. This local uplift, accomodating ~12.5 km of post-collisional shortening, leads to the domal shape of the Engadine window. Moreover, the resulting tectonic uplift of ~8 km, which is probably an overestimate due to assumption (3), is likely to induce extension in the overlying units. An expression of this extension could be found in the the Late Oligocene – Early Miocene activity along the Engadine line (Schmid & Froitzheim 1993), extensional brittle faults in the Engadine window (Kläy 1957) and the E2 low-angle normal fault (section 9.3). Summarizing we suggest that the Engadine window is essentially the result of post-collisional deformation with the superposition of large-scale detachment-folding above a passive back thrust, local uplift and extension in Late Oligocene to Early Miocene times.
Viewed at a large scale, the Engadine structural high could be coeval with the uplift of the external massifs. Moreover, it seems possible that the HBS-basement slice underlying the Engadine window is arranged in a right-step en-échelon manner in respect to the external basement uplifts. Such a geometry is compatible to dextral transpression with NNW-SSE directed shortening between the European and Adriatic plates in Late Tertiary times, as suggested by plate reconstructions by e. g. Savostin et al. (1986).

In summary, the following conclusions may be drawn:

1) A good correlation exists between reflections as observed in lines E2 and E3, rendering the geologic interpretation relatively reliable.
2) The Engadine window is cored by an up to 10 km thick pile of N-Penninic Bündnerschiefer underlain by an ENE-striking basement nappe-stack consisting of N-Penninic and Helvetic basement units.
3) The antiform constituting the Engadine window does not seem to affect the underlying basement units implying that the N-Penninic Bündnerschiefer must be detached from the basement during window formation.
4) The Engadine window could be the result of the indentation by an upper crustal wedge producing large-scale detachment folding, local uplift and extension in Late Oligocene to Early Miocene times.

9.5 Deep seismic fan-recordings and a 3D crustal model of the eastern Aar massif

L. Hitz & O.A. Pfiffner

In 1986, the receiver spread of the E1 seismic reflection profile was additionally used for various far-offset measurements. They included both in-line and fan-recordings. In the first part of this section the fan data shall be described in detail and their geologic interpretation will be given. In a second part, the elaborated network of 2D profiles will be combined into a 3D crustal model to get new insight into the structure of the eastern Aar massif uplift.
The results of this work are based on two fundamental assumptions, which are necessary to locate the reflecting subsurfaces in the seimic fan data. The assumptions are: (1) CDP equals CMP and (2) the CDP-lines run parallel to the true dip of the imaged subsurface. Assumption (1) allows the positioning of the individual CDP-lines in space (Figure 9-21), whereas assumption (2) allows a correct depth conversion of the reflection data by means of ray-theoretical depth migration. Both assumptions are crude approximations of the true situation. Valasek (1992), however, showed that mispositioning due to these assumptions is minimal for moderately dipping crustal layers (0° to 15°) such as observed in this study.

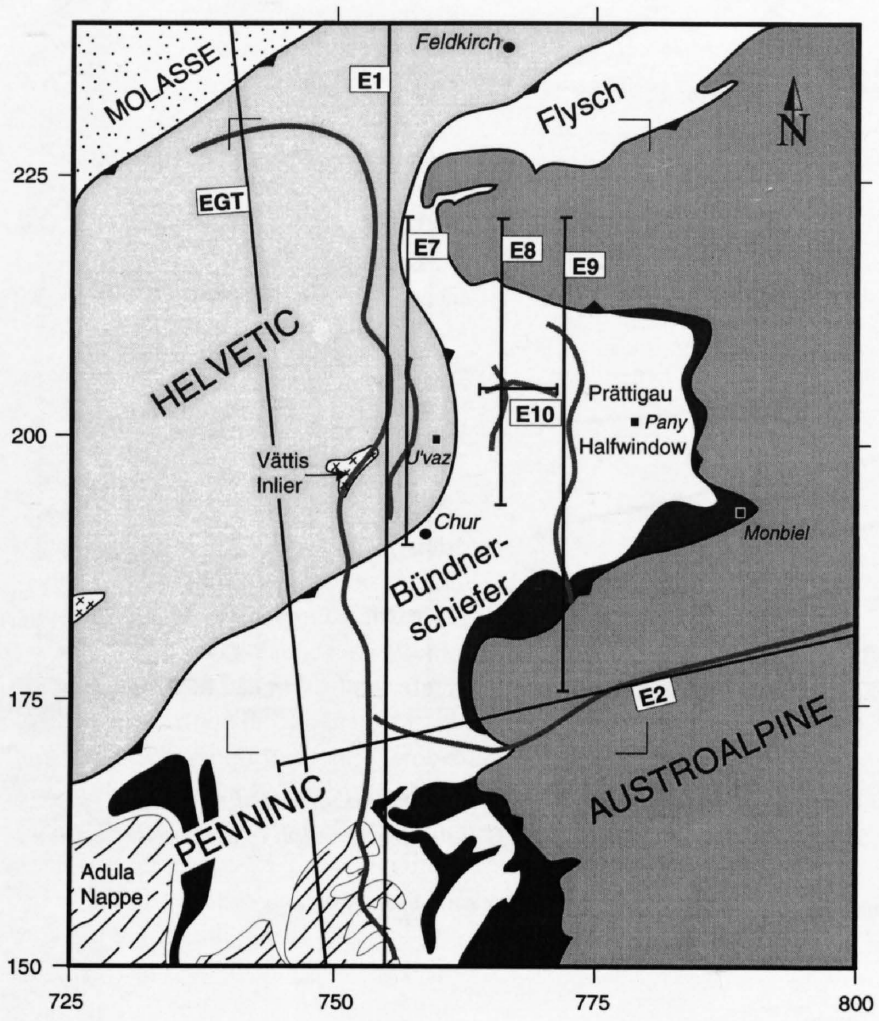

Figure 9-21
Simplified tectonic map of the study area with locations of NRP 20 seismic reflection lines and the EGT seismic refraction line. Grey lines correspond to CDP postions, straight black lines correspond to the traces of geological cross sections. Squares indicate fan-shot locations and rectangles show locations of Figures 9-28 and 9-29. Coordinates are given in the Swiss National Grid system.

9.5.1 The data

The reflection seismic fan data presented here consist of 7 dynamite shots with a 300 kg charge each. Two shots were fired from shot-location "Untervaz" (760.230/198.660, average lateral offset 5.4 km). They were recorded in the rolling 240 channel receiver-spread of line E1. With a CDP spacing of 40 m, the resulting CDP-line from the two shots measures 19.2 km. In the following, the "Untervaz" line will be referred to as line E7. From the second shot-location "Pany" (778.660/202.500, average lateral offset 23 km), only one shot was fired resulting in a 9.6 km long CDP-line. It will be referred to as line E8. Finally, from shot location "Monbiel" (791.850/192.230, average lateral offset 40 km) four shots were fired giving rise to a 33.9 km long CDP-line. It will be referred to as line E9. In addition to the three fan profiles, a 4.3 km long near vertical line situated between lines E8 and E9 was recorded by the Institute of Geophysics of the ETH Zürich (Figure 9-21). The line consists of two dynamite shots of 1.5 kg charge each and will be referred to as line E10. The seismic sections E7 to E9 are presented Plates 9-7 to 9-9. Line E10 is shown in Figure 9-22.

Line E7 (see Plate 9-7) is characterized by an approximately 1.5 s thick reflection package dipping from 12 s in the N to 13 s in the S. In addition, a conspicuous subhorizontal reflection band can be seen at 9.5 s. It is included in the interpretation, as it can be correlated with reflection bands of the same character in neighboring profiles. Line E8 (see Plate 9-8) shows a well developed deep reflection package dipping southward from 12 to 13 s. Its thickness is in the order of 2 s. North-dipping reflections at 11 s and south-dipping less coherent reflections between 9 and 10 s are also present. The strong reflectivity at 7 s in the center of E8 will not be considered for interpretation due to its very limited extension and also due to the apparent lack of equivalent reflections in the nearby profiles. Line E9 (see Plate 9-9) essentially reveals the same deep reflectivity as the previous two profiles: a south-dipping reflection package from 12.5 to 14 s with a thickness in the order of 1.5 to 2 s, and a less coherent south-dipping reflection band from 10 to 12 s. Despite their small lateral extension, north-dipping reflections at 6 s between horizontal km 30 and 34, and south-dipping reflections at 4 to 6 s between km 20 and 27 should be noted. As will be shown below, they can be correlated with reflections in the line E2 (section 9.3) and in the E10 profile. In contrast to the fan data, the near-vertical line E10 (Figure 9-22) provides information of the uppermost crust. It shows two distinct apparently east-dipping reflections at 1.2 to 1.6 s and 1.8 to 2.3 s, respectively. At the western end of the profile, the lower reflection band flattens out, whereas the upper band looses its strong reflectivity almost completely. Sporadic reflections below the lower reflection band are considered as random noise from a nearby timber factory. For the purpose of the geologic interpretation, a computer-based transformation of the reflection seismic data into line drawings (Valasek 1992) followed by ray-theoretical depth migration (Holliger & Kissling 1991) were performed. Velocities for depth migration were derived from a velocity model used by Valasek (1992) for line E1, which represents a simplified version of the findings of the EGT refraction profile by Ye (1992). The above described reflections were then identified on the depth migrated sections. The results of this processing are shown in the simplified line drawing of Figure 9-23. Note that up-dip migration of reflections considerably increased the profile lengths. The length of the geologic profiles of Figures 9-24 to 9-27 is thus determined by the length of the migrated sections (Figure 9-21).

9.5.2 Geologic interpretation

Looking at the seismic sections E7 to E9 (see Plates 9-7 to 9-9) it is clear, that the profiles yield only information of the deep crust. They can, however, be complemented by surface geological data and by the seismic lines E1, E2 and E10, which all contain shallow data. It becomes thus possible to construct geological cross-sections from the surface down to the crust-mantel boundary. The cross sections along lines E7 to E10 are shown in Figures 9-24 to 9-27. In the following, it will be explained how they were constructed, beginning with the base of the crust and ending with the highest sedimentary units.

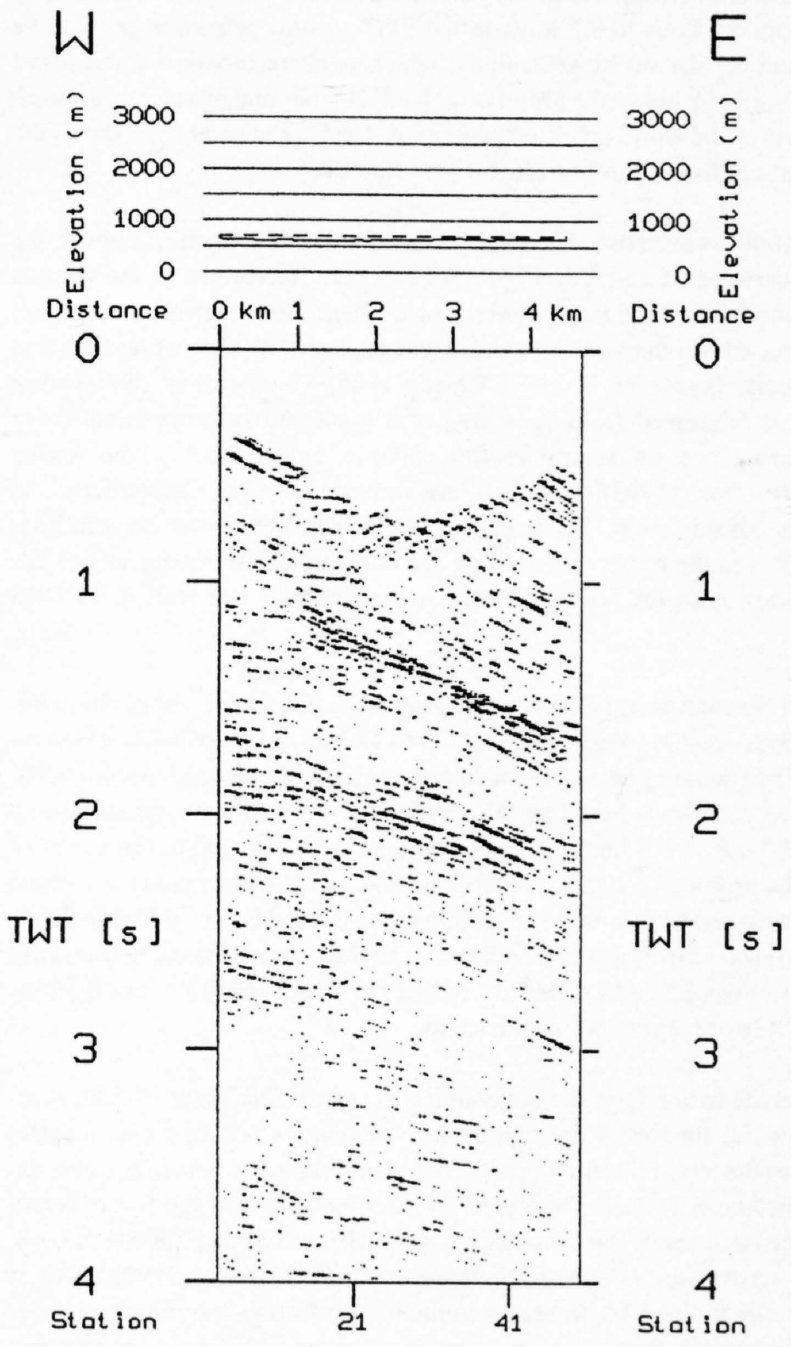

Figure 9-22
Unmigrated near-vertical seismic line E10 showing two destinct apparently east-dipping reflections at 1.2 to 1.6 s and 1.8 to 2.3 s respectively. At the western end of the profile, the lower reflection band flattens out, whereas the upper band looses its strong reflectivity almost completely. For location see Figure 9-21.

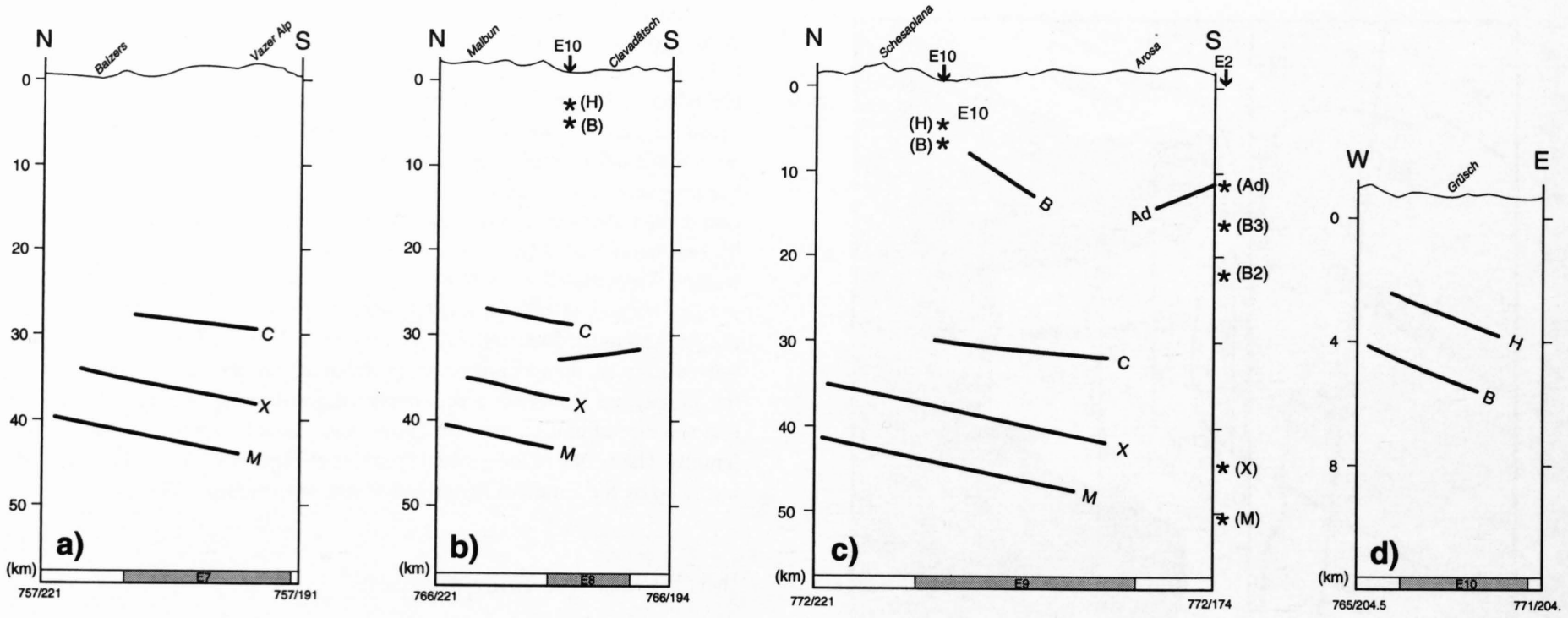

Figure 9-23

Depth-migrated reflections considered for interpretation of (a) line E7, (b) line E8, (c) line E9 and (d) line E10. Stars correspond to migrated reflections of intersecting profiles. White bars at the bottom of each section correspond to the profile length added by the migration process (up-dip migration of dipping reflections). Coordinates are given in the Swiss National Grid system.

M: Moho, X: top of laminated lower crust, C: Conrad, Ad: top of Adula basement nappe, B: top of Aar massif, H: top of Infrahelvetic cover.

Moho discontinuity: In all three fan profiles, the base of the deepest reflection package (*M* in Figure 9-23 a-c) corresponds to the base of the crust, i. e. the Moho discontinuity. This interpretation is based on (a) depth position and dip of reflection group M, which can be correlated with a P-wave velocity jump from 6.5 km/s to 8.3 km/s in the EGT seismic refraction profile (Ye 1992) and (b) the strong reflectivity, which is characteristic for the lower crust immediatly above the Moho in all NRP 20 lines and in many other sampled areas of the world (cf. Klemperer et al. 1986). The southward dip of the Moho ranges from 9° in line E7 to 12° in line E8.

Laminated lower crust: The highly reflective bands immediatly above the Moho (between M and *X* in Figure 9-23a-c) are interpreted as the seismic expression of a laminated lower crust. Such heterogeneous reflection fabrics have been derived from numerical models with alternating high and low velocity layers (cf. Braile & Chiang 1986). Geologically, the layering may have originated from stretching of a thickened heterogeneous lower crust during post-thickening crustal collapse. In the case of the Alpine lower crust, Rey (1993) suggests a late Variscan age (late Carboniferous to Permian) for this event. The thickness of the laminated lower crust in lines E7 to E9 is in the range of 5 to 6 km and compares with the one in line E1, the Western Alps (cf. Valasek 1992) or the Pyrenees (cf. Bois & ECORS 1991).

Conrad discontinuity: The conspicuous reflection bands above the laminated lower crust in a depth range of 9.5 to 12 s (*C* in Figure 9-23a-c) are interpreted as marking the top of the lower crust, i. e. the Conrad discontinuity. This interpretation is based on the correlation with a p-wave velocity jump from 6.2 km/s to 6.5 km/s with similiar depth position and dip in the EGT refraction profile (Ye 1992). In addition, the Conrad discontinuity is defined by the same erratic line-up of short reflections in line E1 (*C* in Figure 9-5a). The southward dip of this discontinuity is slightly smaller than the Moho dip with 7° in lines E7 and E9, and 10° in line E8. This implies a minor thickening of the lower crust towards the south.

Aar massif: In line E10, the lower reflection band (*B* in Figure 9-23d) is interpretated as the top of the crystalline basement, which in the area corresponds to the top of the Aar massif. This interpretation is based on a correlation with line E1, where the top of the Aar massif marks the last coherent reflection band above the Conrad reflections (*B1* and *B2* in Figure 9-5a), i. e. the Aar massif itself is seismically transparent (Pfiffner et al. 1990b). This is also the case in line E10, where no continuous reflections can be found under reflection band B. Reflectivity possibly stems from a high-velocity dolomite layer imediately above the crystalline basement (see also section 9.2). The shallower reflection band in line E10 (*H* in Figure 9-23d) is interpreted as the basal thrust of the allochthonous Helvetic nappes. Reflectivity of *H* is explained by lithological velocity contrasts, which are possibly enhanced by velocity anisotropies along the thrust plane. The observed loss of reflectivity towards the western end of line E10 (Figure 9-22) suggests, that the reflectors might change their orientation from an apparent E-dip to a more horizontal orientation. In this case, coherent seismic energy would reflect out of the E10 receiver spread and thus would explain the loss of coherent reflections towards the W. The implied westward flattening could further indicate, that the crest of the ENE-dipping Aar massif culmination is situated immediatly to the W of the migrated section. Assuming that this interpretation is correct, joining of this Aar crest with the Aar crest exposed in the Vättis inlier (Figure 9-21) results in an orientaion of the Aar massif's crest-line of approximately 060/20. This orientation in turn agrees well with the surface orientation of major fold axes in the crystalline basement, which were formed during the basement uplift (Pfiffner 1977). Additional seismic information of the basement top is available from line E9. There, south-dipping reflections at 4 to 6 s between horizontal km 20 to km 27 (see Plate 9-9) can easily be correlated with the basement top recorded in line E10 (B in Figure 9-23c and d). The considerably less coherent reflectivity of B in line E9 as compared to line E10 is explained by an increased structural complexity of the reflecting surface in the N–S profile and by a more intense scattering of the wavefront in the fan data due to its longer travel distance.

As recording offsets were generally too large to register the top of the crystalline basement in the fan profiles, the top of the Aar massif must be projected from surface and from subsurface positions recorded in lines E1 and E10. For the Aar massif's crest-line, the orientation of 060/20 deduced above was used for projection. As a second key-structure, the deepest basement position north of the culmination, the Aar depression, was used. To find out the latter's orientation, all the seismic lines crossing this depression were examinated (W1, C1, E1, see Pfiffner et al., Chapter 13.1). The depth of the Aar depression varies between –8.1 km in line W1, –9.6 km in line C1 and –9.0 km in line E1. On a map, the points lie on a remarkably straight line striking N65°E. As depth varies only minor with distance (variations between C1 and E1 is only 0.6 km corresponding to a dip angle of 0.3°), the dip of the depression for the projection purpose is set to 0°. Consequently, the Aar depression north of the culmination is projected along 065/00 into the fan profiles. For the further construction of the basement top between projected crest and depression, the two points were joined by a straight line, which serves as an envelope for the northern flank of the Aar massif. Its more detailed geometry was then taken from the modeled structure of the E1 profile by Stäuble & Pfiffner (1991) and Stäuble et al. (1993).

Gotthard "massif": The Gotthard "massif", outcropping in the central Alps, is seismically imaged in lines E1, E2 and E3 (see sections 9.2 to 9.4). The latter's eastern continuation is thus quite well established and allows the prediction, that the northern part of the Gotthard "massif" should be encountered in the southern end of line E9. Due to large offset recordings, however, no reflections from the Gotthard top can be observed. The depth and the geometry of the Gotthard "massif" as shown in the cross-section along E9 (Figure 9-26) is thus purely based on projections from line E1 and on the correlation with line E2.

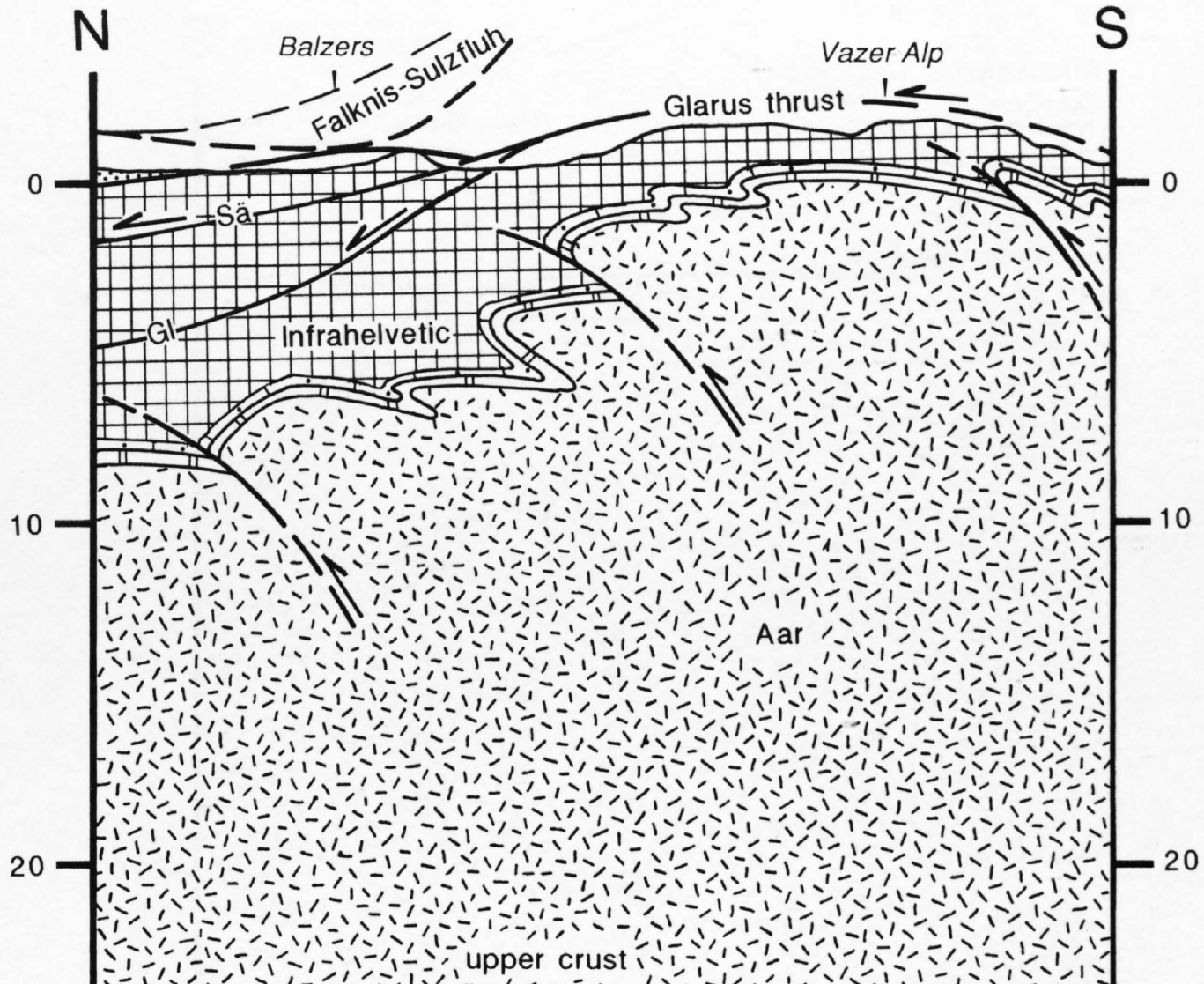

Figure 9-24
Geologic cross section along line E7 based on the interpretation of the seismic data (see Plate 9-7 and Figure 9-23a) and on projections from surface data and line E1 (see Figure 9-8). The trace of the cross section is straight N-S and follows km 757 of the Swiss National Grid system.

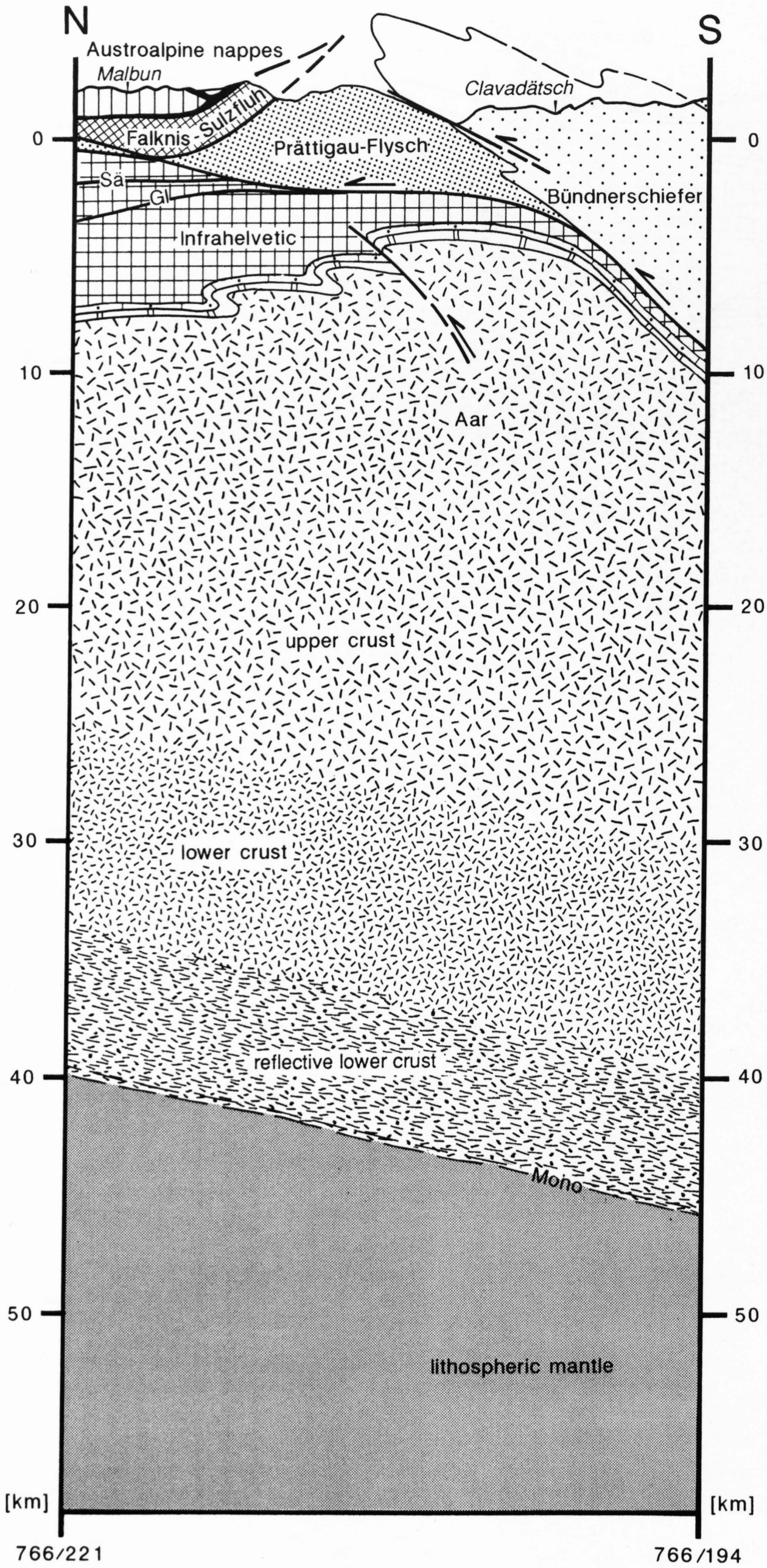

Figure 9-25
Geologic cross section along line E8 based on the interpretation of the seismic data (see Plate 9-8 and Figure 9-23b), projections from surface data and the line E1 cross section (see Figure 9-8) and on the interpretation of the intersecting line E10 (see Figure 9-27). The trace of the cross section is straight N–S and follows km 766 of the Swiss National Grid system.

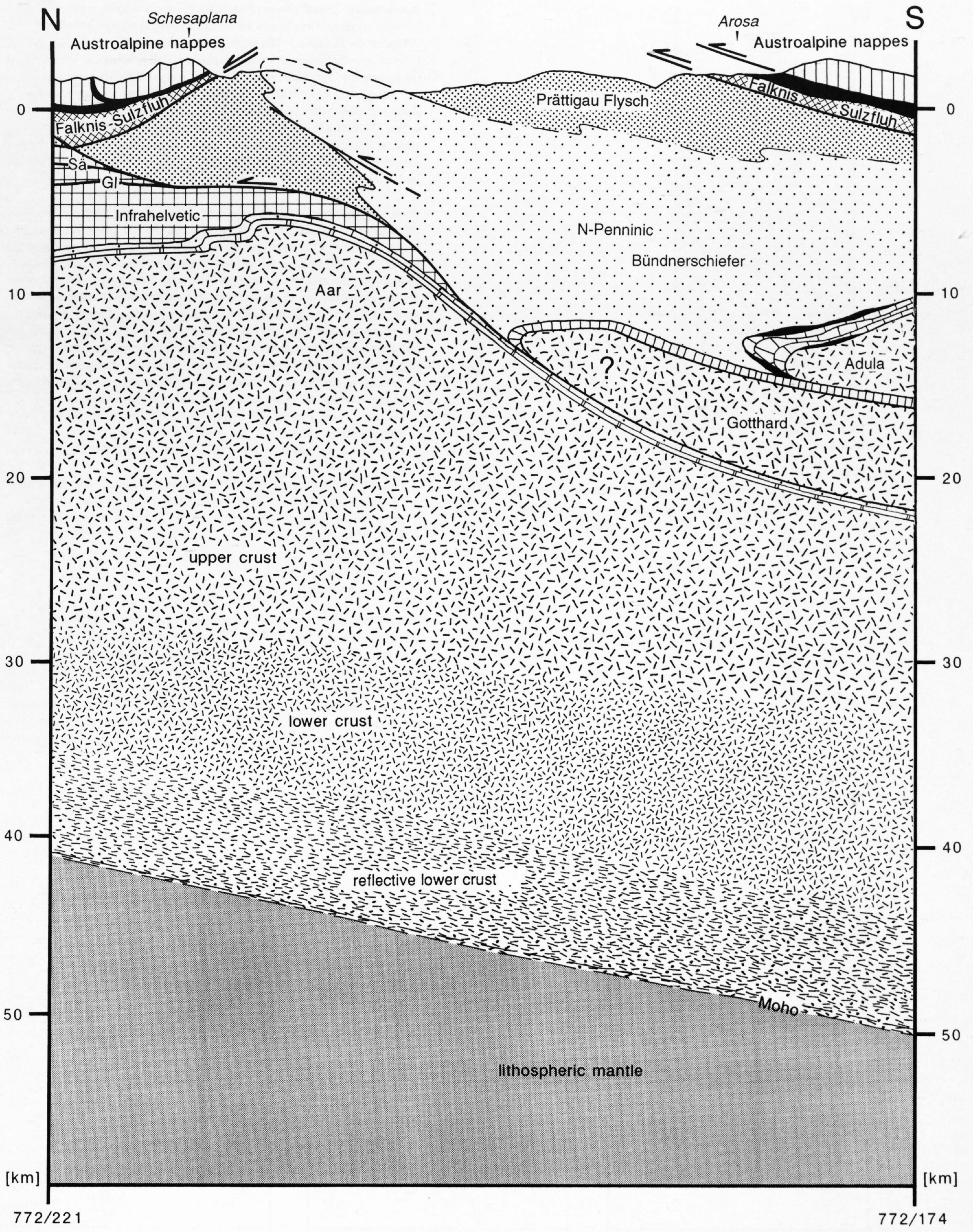

Figure 9-26
Geologic cross section along line E9 based on the interpretation of the seismic data (see Chapter 4 and Figure 9-23c), projections from surface and the E1 cross section (see Figure 9-8) and on the interpretations of the intersecting lines E10 (see Figure 9-27) and E2 (see Figure 9-12). The trace of the cross section is straight N–S and follows km 772 of the Swiss National Grid system.

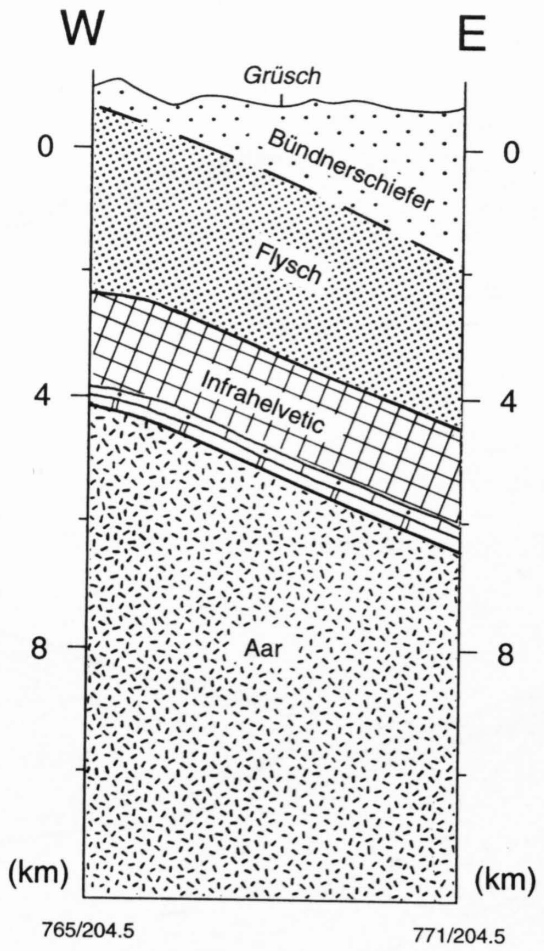

Figure 9-27
Geologic cross section along line E10 based on the interpretation of the seismic data (see Figure 9-22). The trace of the cross section is straight W–E and follows km 204.5 of the Swiss National Grid system.

Adula nappe: In line E9 (see Plate 9-9), the north-dipping reflections at 6 s between horizontal km 30 and km 34 can be correlated with reflections from the top of the Penninic Adula nappe in line E2 (*Ad* in Figure 9-23c). Reflectivity of this discontinuity can be explained with lithological velocity contrasts between cover sediments and the Adula crystalline basement rocks. The top of the Adula nappe is also seismically imaged in line E1 (see section 9.2). Joining the northern Adula front in line E1 with the corresponding structure in line E9 results in a Adula tip line with an orientation of 060/25. This orientation is comparable to the trend of the main structural elements of the Aar massif as described above and to the result of 3D seismic modeling along E1 by Litak et al. (1993).

Overlying sedimentary units: For the overlying sedimentary units, seismic information is available only from lines E1, E2 and E10. However, due to the strong ENE dip of the basement, there is an excellent surface control on the higher units. The azimuth for projection was kept constant at N65°E, corresponding to the average strike of the basement structures described above. The projection dip was chosen according to the positions of the structures involved, i. e. 20° for a position above the Aar crest, 0° for a position above the Aar depression and a linearly interpolated value for a position between crest and depression. These projection trajectories are based on the assumption, that the basement uplift essentially controls the axial plunge of the higher tectonic units, a point that will be discussed in the next section. The following sources of surface data were used to constrain the projections:

Helvetic Zone: Pfiffner 1977 and 1978, Trümpy 1980, Pfiffner et al. 1990a, Pfiffner 1993.

Bündnerschiefer and Prättigau Flysch: Nänny 1948, Nabholz 1951, Christ & Nabholz 1959.

Falknis-Sulzfluh nappes and Arosa imbricates: Lorenz 1901, Brauchli & Leupold 1915, Trümpy 1916, Cadisch 1922, Allemann et al. 1985.

Austroalpine nappes: Oberhauser 1970, Tollmann 1976, Oberhauser 1980, Allemann et al. 1985.

9.5.3 3D model

The interpretations discussed above, together with the results of lines E1, E2 (sections 9.2 and 9.3) and the EGT refraction profile (Ye 1992) form a dense network of 2D crustal information (Figure 9-21). Based on this network, structure contour maps for the following discontinuities were constructed: the Moho (Figure 9-28a), the top of the laminated lower crust (Figure 9-28b), the top of the lower crust, i. e. the Conrad (Figure 9-28c) and the top of the crystalline basement (Figure 9-29). The 3D geometry of the three lower crustal layers were obtained by linear interpolation between data points and sub-

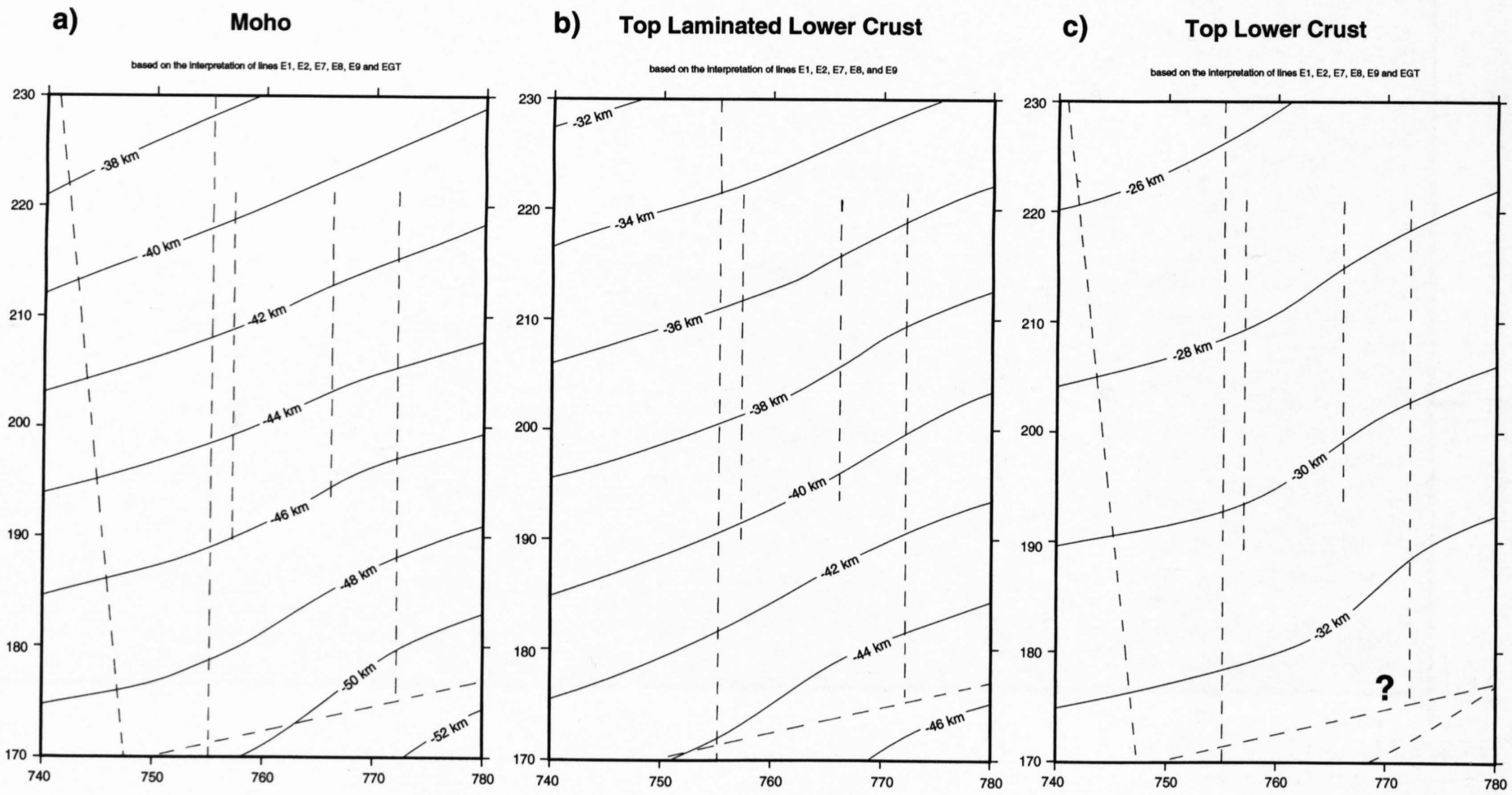

Figure 9-28
Stucture contour maps of the deep crustal discontinuities imaged in the seismic reflection lines E1, E2, E7, E8 and E9 and in the EGT seismic refraction profile (stippled straight lines, see also Figure 9-21). The depth accuracy is estimated to be in the order of ± 2 km. All discontinuities show similar and simple 3D geometries with a constant ENE strike and dip angles between 12° (Moho and top of the laminated lower crust) and 8° (Conrad).

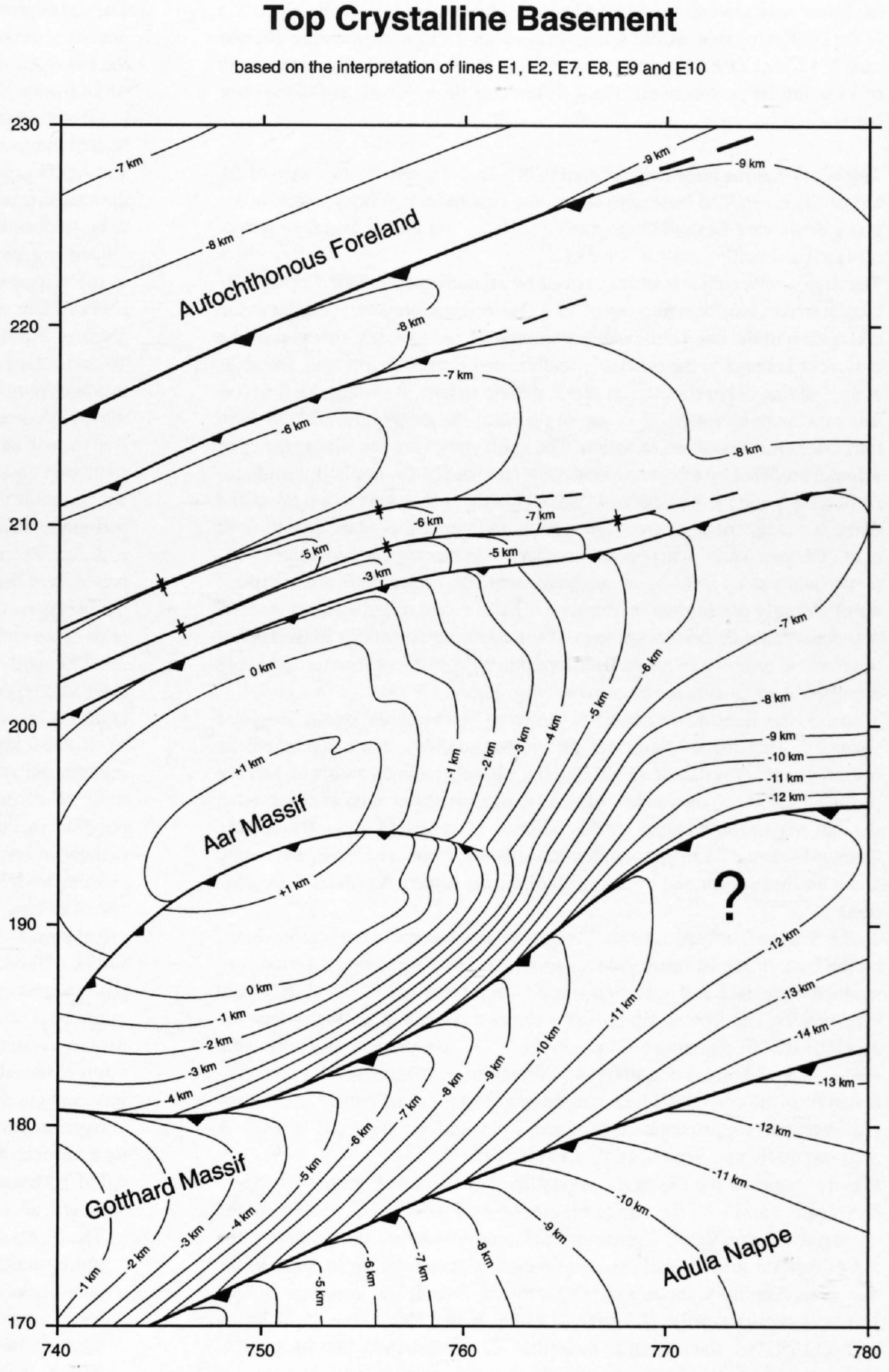

Figure 9-29
Structure contour map of the the top of the crystalline basement imaged in lines E1, E2, E7, E8, E9 and E10 (see also Figures 9-21 and 9-28). The depth accuracy is estimated to be in the order of 0 (surface control) to ± 1.5 km. The 3D geometry reveals complicated domal surfaces formed by a combintion of fold-and-thrust tectonics. The structural disharmony with respect to the lower crust (see Figure 9-28) implies a crustal decoupling mechanism during the formation of the basement uplifts and nappes (Aar, Gotthard, Adula).

sequent smoothing with a 2 km long running average filter (program INTERPS by Valasek 1992). Contouring of the top basement surface was entirely made by hand. The accuracy of the vertical position of the different interfaces is largely controlled by the velocity function used for depth-migration and decreases with dip and time (cf. Holliger 1991 for migration error analysis). The resulting vertical error for a velocity fluctuation of 0.2 km/s relative to 6.0 km/s are approximately 1.8 km for the Moho discontinuity, 1.2 km for the Conrad discontinuity and a maximum of 0.5 km for top basement surface. As Valasek (1992) and Litak et al. (1993) have shown, depth distortions in N–S profiles caused by side-swipes measure approximately 0.5 km for the Moho and Conrad discontinuities, and up to 1 km for the top of the crystalline basement in the area considered. The depth accuracy are thus roughly estimated to be in the order of ± 2 km for the Moho, the top of the laminated lower crust and the Conrad discontinuity, and around ± 1.5 to 0 km (surface control) for the top of the crystalline basement.

Moho discontinuity (Figure 9-28a): The European Moho contours are constrained by both reflection and refraction seismic data. The Moho geometry reveals a smooth surface with an average strike of N70°E and an average dip of 12°. Comparison with the Moho map in this area by Valasek (1992) shows a remarkably good agreement in strike and dip, with depth positions differing by a maximum of 1 km. The good agreement illustrates the relatively simple and continuous geometry of the European Moho, considering that Valasek's map is based on a far less dense network of 2D seismic lines. In addition, the good fit between the refraction and the reflection derived Moho illustrates, that the two methods are imaging the same discontinuity.

Top of laminated lower crust (Figure 9-28b): The top of the laminated lower crust is constrained by seismic reflection data only. As might be expected from the 2D data, the 3D geometry of the top of the laminated lower crust is nearly identical with the Moho geometry. The two discontinuities are seperated by 5 to 6 km. This thickness compares to the ones determined in the central and western portions of the Swiss Alps (cf. Valasek 1992). However, it is only half the thickness of the laminated lower crust found in DEKORP profiles in the European foreland (cf. DEKORP 1990). Assuming a pre-Alpine origin of this structure (Rey 1993), it is possible that the reduced thickness resulted from crustal thinning and stretching during Mesozoic rifting.

Conrad discontinuity (Figure 9-28c): The contoured surface of the top of the lower crust, i. e. the Conrad discontinuity, is constrained by seismic reflection and refraction data. However, it has to be stressed, that the Conrad discontinuity is very poorly defined in the reflection seismic data and that the interpretation is thus somewhat speculative. The actual Conrad geometry might be more complex as appears in Figure 9-28c. With this restriction in mind, the Conrad geometry strongly resembles the geometries of the underlying surfaces. The slightly smaller average dip angle (8°, as compared to 12° for the Moho and the laminated lower crust) implies a minor thickening of

the lower crust towards the SSW. The same observation is made by Ye (1992) in the EGT refraction profile. Comparison with the Conrad structure contour map of Valasek (1992) reveals differences in depth and strike by a maximum of 2 km and 10°, respectively. These differences lie within the estimated error bounds.

Top of crystalline basement (Figure 9-29): The structure contour map of the top of the crystalline basement shows the first basement body encountered going downward from the topographic surface. The map is based on reflection data and geological surface data.

The map's NW corner is characterized by an undisturbed SSE dipping surface. It strikes N66°E with a dip of 10°. This orientation is very similar to the orientation of the deep crustal discontinuities. Consequently, this part of the basement belongs to the relatively undisturbed European foreland. Immediately S of the –9 km structure contour, the top basement surface starts to rise to a maximum elevation of +1 km in the Vättis inlier (Figure 9-21) to form the eastern Aar massif culmination. The uplift shows the overall geometry of a dome, bordered by a depression in the N (marked by the northernmost basement thrust) and by the Gotthard "massif" in the S. The northern flank of the dome is characterized by overturned folds and thrust slices (see also Pfiffner et al., Chapter 13.1), whereas the southern side reveals a less complex geometry with a steep SSE-dip of approximately 50°. To the ENE, the basement uplift strongly diminishes in amplitude. In fact, one might suspect that the Aar massif culmination ceases to exist some kilometers further ENE and that basement shortening might be transferred to an equivalent structure possibly arranged in an en-échelon pattern (see also Figure 13-25).

To the S, the eastern Aar massif is shown to be overthrust by the Gotthard "massif". This second basement unit is considerably less constrained. Its overall geometry is that of a ENE dipping, slightly reclined antiform, lacking positive indications of internal fold-and-thrust structures such as observed in the Aar massif. In addition to this contrast in structural style, the eastern Gotthard "massif" seems to widen towards the WSW and ENE, indicating that it has been deformed by the uplift of the the eastern Aar massif culmination.

To the S of the Gotthard "massif", the crystalline basement top is represented by the front of the Penninic Adula nappe. The latter's geometry is well constrained by surface and reflection seismic data (see also Litak et al. 1993 and section 9.2). The frontal Adula nappe shows a change in geometry from an overturned ENE plunging antiform in the WSW to a more or less horizontal wedge-shaped body in the ENE. An average axial plunge of 20° can be deduced from the contours which is comparable to the axial plunge of the eastern Penninic nappe stack determined from surface data (cf. Milnes & Schmutz 1978, and Schmid et al., Chapter 14).

When comparing the top of the crystalline basement in Figure 9-29 (based on seismic data) with the one in Figure 9-6 by Pfiffner et al. (1990a, based on surface data solely), significant differences emerge. For example, the top of the Aar massif N of the culmination is deeper by up to 3 km in the new map. Similarly, the top of the Gotthard "massif" at coordinates 750/180 is at approximately –1.5 km in Pfiffner et al. (1990a) but at –4 km in Figure 9-29. It is interesting to note, that 3D seismic modeling by Litak et al. (1993) already pointed into exactly this direction. In addition, the top basement contour in the new map is more structured, illustrating that the cover sediments at the surface conceal important basement structures at depth.

9.5.4 Discussion and conclusion

The results of the deep seismic fan recordings show, that the crust-mantle boundary, the top of the laminated lower crust and the Conrad discontinuity (Figure 9-28a-c) have similar 3D geometries with ENE strikes and dips between 12° (Moho, top laminated lower crust) and 8° (Conrad). The thickness of the laminated lower crust remains constant at around 5 to 6 km, whereas the thickness of the lower crust increases from 12 km in the N to 16 km in the S. This thickening is also reported from other NRP 20 transects and the EGT refraction profile (Valasek 1992, Ye 1992). It indicates, that collision tectonics affected the European lower crust as far N as the external massifs.

In sharp contrast to the simple geometry of the lower crustal units, the top of the crystalline basement is structurally much more complex with reliefs of up to 10 km. The relief and the associated disharmony with the underlying units suggests, that not only the nappes (Adula etc.), but also the basement "massifs" (Aar, Gotthard) must be considered allochthonous. This implies that an intracrustal decoupling mechanism must have taken place during the formation of the basement units. The decoupling horizon must be situated somewhere between the top of the lower crust and the top of the crystalline basement. It has been suggested that velocity inversion zones found beneath the Alps are possible candidates for such detachments (cf. Mueller 1990), owing to the presence of elevated fluid pressures.

The structure of the allochthonous basement units is visible from the mapped pattern of the surface geology (Figure 9-21). For example, the embayment of the basal Austroalpine thrust fault E of Vättis (with the sudden change in strike from a N–S to a SW–NE) can be linked to the Aar massif culmination in the subsurface. Similarly, S of Chur, the strike change from NE–SW to N–S of the Austroalpine base can be linked to the topography of the Gotthard and Adula units (note that this strike change at surface mimics the trend of the structure contours at subsurface). The basement topography is thus taken to be responsible for the general shape of the Prättigau halfwindow (as postulated e. g. by Staub 1934), a fact which is also sustained by the orientation of the principal foliation plane in the Bündnerschiefer, dipping SSE in the area of Chur and E in the area of line E10 (Figure 9-21, Dreibündenstein phase of Pfiffner 1977).

To understand the eastern end of the Aar-Gotthard culmination in a larger tectonic framework, it is useful to inspect the geometry of its western counterpart. As discussed by Pfiffner et al. in Chapter 13.1, the western end of the Aar massif and the Aiguilles Rouges-Mt. Blanc massifs are relayed in a right-step en-échelon manner. Burkhard (1988) postulated a N–S oriented wrench fault in the Rawil depression in between. It can be shown, though, that major fold hinge lines in the Helvetic zone (Morcles and Doldenhorn e. g., see Pfiffner 1993) are also relayed en-échelon and the geologic interpretation of line W1 (see Pfiffner et al., Chapter 13.1) does not point towards the existence of a wrench fault. A similar en-échelon pattern can be postulated at the end of the Aar-Gotthard culmination. Here, the eastern end of the Aar-Gotthard culmination could be relayed with the "Engadine uplift" in a right-step en-échelon manner. As discussed in section 9.4., the ENE striking antiform associated with the Engadine window itself and outlined by the basal Austroalpine thrust, is cored by Penninic cover nappes (Bündnerschiefer units). This antiform is locally uplifted in response to the formation of a NW-vergent basement slice underlying the Engadine window. It seems possible, that this latter basement slice is arranged in a right-step en-échelon manner in respect to the eastern external basement uplift. In addition, considering lines W1, C1 and E1, the northernmost thrust fault of the Aar massif seems to have a constant ENE strike along the entire basement uplift. This orientation is comparable to the strike of Variscan structures in the European foreland like e. g. the Permo-Carboniferous basement trough in NE-Switzerland (Sprecher & Müller 1986). Based on the similarity in orientation, it might be postulated, that the northernmost basement thrust represents a reactivated Variscan structure controling the position of the external basement uplift in the Alps.

Returning to the investigated area, it can be said, that fan shooting into an existing near-vertical deep seismic measurement setup, combined with a short near-vertical measurement, has proven to be very useful in obtaining a detailed 3D crustal model. The new insights gained from this 3D model can be summarized as follows:

1) The Moho discontinuity, the top of the laminated lower crust and the Conrad discontinuity have all similar and simple 3D geometries with a constant strike to the ENE and dip angles between 8° and 12°. The laminated lower crust has a constant thickness of 5 to 6 km, whereas the lower crust thickens from 12 km in the NNW to approximately 16 km in the SSE. This change in lower crustal thickness might reflect mild lower crustal thickening during Tertiary compression.
2) The 3D geometries of the top of the crystalline basement contacts reveal complicated domal surfaces formed by a combination of fold-and-thrust tectonics. The structural disharmony with respect to the lower crust implies a crustal decoupling mechanism during the formation of the basement uplifts and nappes. The decoupling horizon must be situated between the Conrad discontinuity and the top of the crystalline basement.
3) Comparison of surface data and the top-basement geometry clearly reveals a kinematic link between the shape of the Prättigau halfwindow and the formation of the Aar massif culmination.

Acknowledgements

J. Ansorge, G. Eisbacher and R. Marchant are thanked for reviewing this chapter. Many thanks go also to E. Lanz and S. Sahli for plotting and drawing assistance. We would like to thank in particular J. Ansorge, N. Froitzheim, M.R. Handy, E. Kissling, St. Mueller, St. Schmid and G. Schreurs for comments on early versions of this chapter and many fruitful discussions. H. Horstmeyer and P. Valasek are thanked for introducing L. H. to seismic data processing.

Plates 9-1 to 9-9

SWISS NATIONAL SCIENCE FOUNDATION

86-NF-E1 (DYNAMITE)

FINAL STACK

1: 200'000

RECORDING PARAMETERS

SPREAD LAYOUT	19.2 km
CHANNELS	240
SOURCE TYPE	Dynamite
SOURCE DEPTH	10-75 m
CHARGE SIZE	10-400 kg
GROUP INTERVAL	80 m
GEOPHONE TYPE	10 Hz
GEOPHONE PATTERN	24 in line / 76.6 m
INSTRUMENTATION	SERCEL 348
FIELD FILTERS	HC 62.5 Hz / NT 50 Hz
COVERAGE	1 - 4
SAMPLING RATE	4 ms
RECORDING LENGTH	60 s
RECORDED BY	PRAKLA SEISMOS AG
DATE RECORDED	Sept. 1987

PROCESSING PARAMETERS

1. Demultiplex and gain recovery
2. Trace editing
3. Crooked line geometry
4. Time variant trace equalisation
5. Predictive deconvolution
6. Time variant bandpass filter
7. Field static corrections
8. NMO-Correction
9. CDP-Sort
10. Mute application
11. CDP-Stack
12. Resample to 8 ms
13. Time variant bandpass filter
14. Time variant trace equalisation
15. Strong coherency filter
16. Time variant trace equalisation

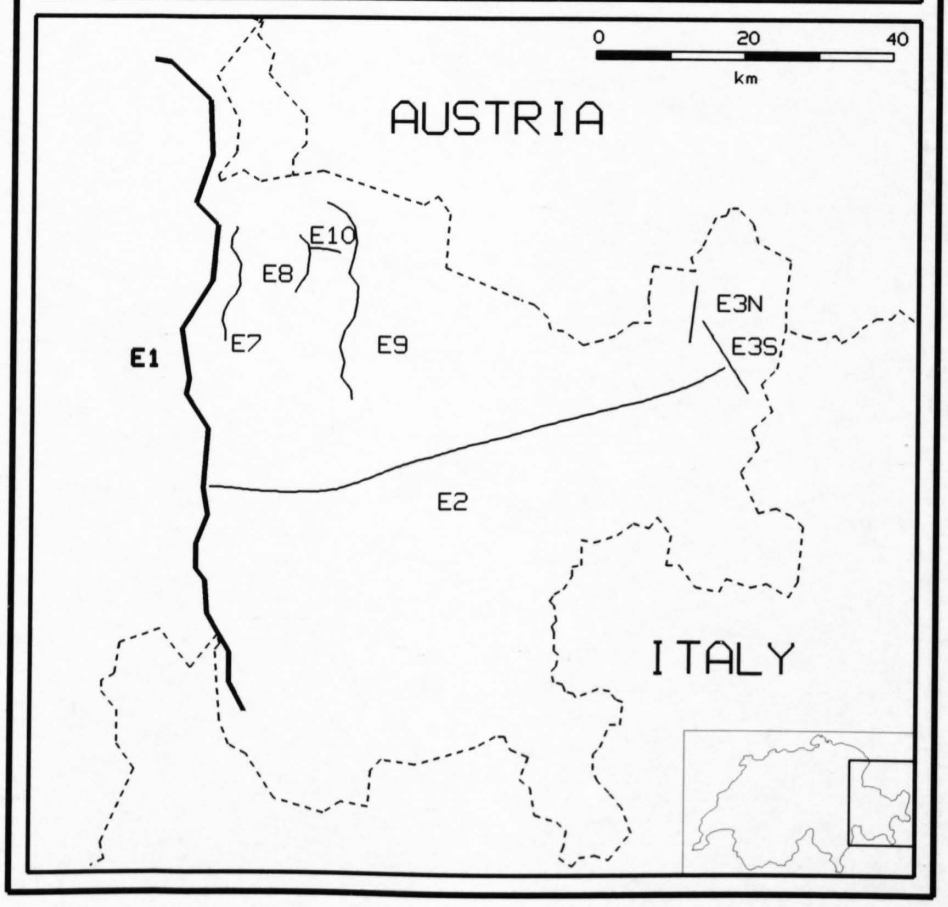

E1 (86-NF-D1)

N

S

Sevelen
Untervaz
Innerferrera

Simmibach Altendorf | Azmoos | Ragaz | Valens | Kunkels | Tamins | Canova | Thusis | Zillis | Ausserferrera | Croet | Burg | Savrana

Elevation (m) 3000 2000 1000 0

Distance 0 km 10 20 30 40 50 60 70 80 90km

TWT [s] 0 2 4 6 8 10 12 14 16 18 20

Station 1001 1100 1200 1300 1400 1500 1600 1700 1800 1900 2000 2100 2200 2300 2472

SWISS NATIONAL SCIENCE FOUNDATION

86-NF-E1 (VIBROSEIS)

FINAL STACK

1: 200'000

RECORDING PARAMETERS

SPREAD LAYOUT	9720-200-x-200-9720 m
CHANNELS	240
SOURCE INTERVAL	80 m
SOURCE TYPE	Vibroseis
SOURCE LAYOUT	6 Vibrators at 12 m
SWEEP FREQUENCY	10-48 Hz
SWEEP LENGTH	60 s
SWEEPS/VP	4
GROUP INTERVAL	80 m
GEOPHONE TYPE	10 Hz
GEOPHONE LAYOUT	24 in-line / 76.6 m
INSTRUMENTATION	SERCEL 348
FIELD FILTERS	HC 62.5 Hz
COVERAGE	120 (nominal)
RECORDING MODE	unsummed and uncorrelated
SAMPLING RATE	4 ms
RECORDING LENGTH	64 s
RECORDED BY	PRAKLA SEISMOS AG
DATE RECORDED	Sept. 1986

PROCESSING PARAMETERS

1. Demultiplex with gain recovery
2. Vibroseis whitening (AGC 500 ms)
3. Vibroseis correlation
4. Vertical summing
5. Crooked line geometry
6. CDP-Sort
7. Resample to 8 ms
8. Time variant trace equalisation
9. Spectral balancing
10. Bandpass filter 5/11-40/50 Hz
11. Predictive deconvolution
12. Bandpass filter 4/8-40/50 Hz
13. NMO-Correction
14. Mute application
15. Surface consistent residual statics
16. CDP-Stack
17. Elevation correction to reference datum
18. Predictive deconvolution
19. Time variant bandpass filter
20. Strong coherency filter
21. Time variant trace equalisation

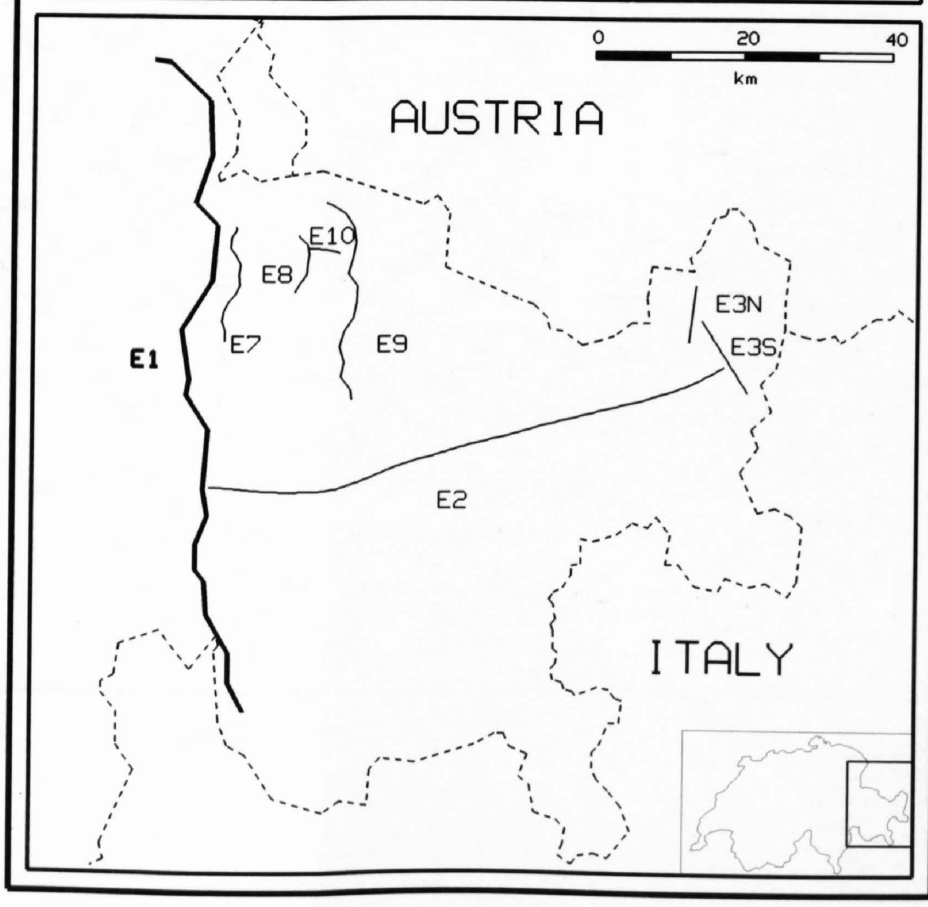

E1 (86-NF-V1)

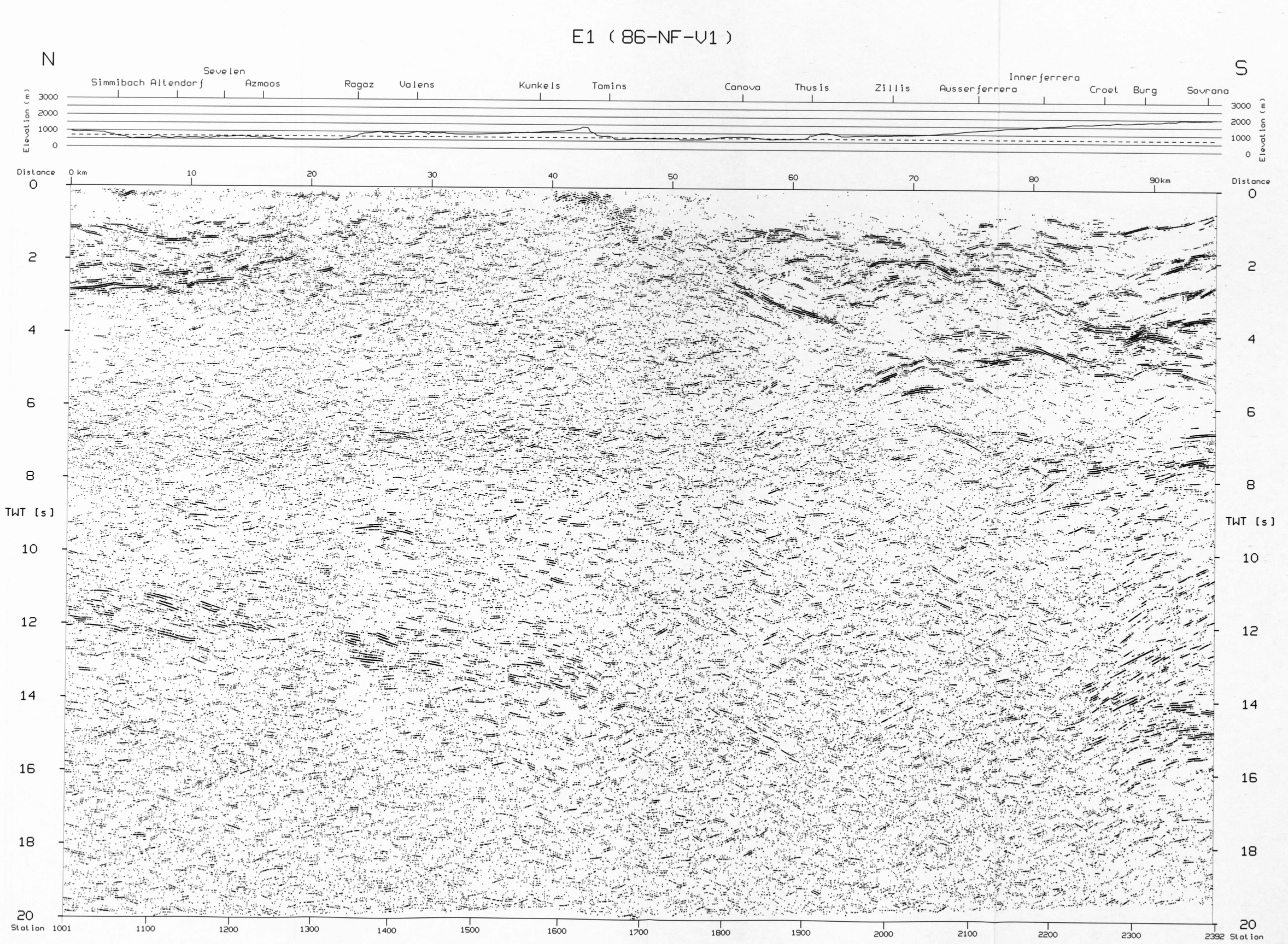
N
S
Sevelen
Simmibach
Altendorf
Azmoos
Ragaz
Valens
Kunkels
Tamins
Canova
Thusis
Innerferrera
Zillis
Ausserferrera
Croel
Burg
Sovrana
Elevation (m)
3000
2000
1000
0
Distance
0 km
10
20
30
40
50
60
70
80
90km
TWT [s]
0
2
4
6
8
10
12
14
16
18
20
Station
1001
1100
1200
1300
1400
1500
1600
1700
1800
1900
2000
2100
2200
2300
2392

SWISS NATIONAL SCIENCE FOUNDATION

90-NF-E2 (DYNAMITE)

FINAL STACK

1: 200'000

RECORDING PARAMETERS

SPREAD LAYOUT	35.5 km
CHANNELS	336
SOURCE TYPE	Dynamite
SOURCE DEPTH	25-80 m
CHARGE SIZE	100 kg (average)
GROUP INTERVAL	100 m
GEOPHONE TYPE	10 Hz
GEOPHONE PATTERN	24 in line
INSTRUMENTATION	SERCEL 368
FIELD FILTERS	HC 89 Hz
COVERAGE	1 to 3
SAMPLING RATE	4 ms
RECORDING LENGTH	45 s
RECORDED BY	PRAKLA SEISMOS AG
DATE RECORDED	Oct. 1990

PROCESSING PARAMETERS

1. Demultiplex and gain recovery
2. Trace editing and resample to 8 ms
3. Line geometry
4. Application of field statics
5. Band pass filter
6. Notch filter: 16.67 Hz
7. Spectral balancing
8. Time variant scaling
9. Despiking
10. F/K-Filter
11. NMO-Correction
12. First break mute
13. CDP-Sort
14. CDP-Stacks in shot domain
15. CDP-Edit
16. CDP-Stack
17. Time variant bandpass filter
18. Strong coherency filter

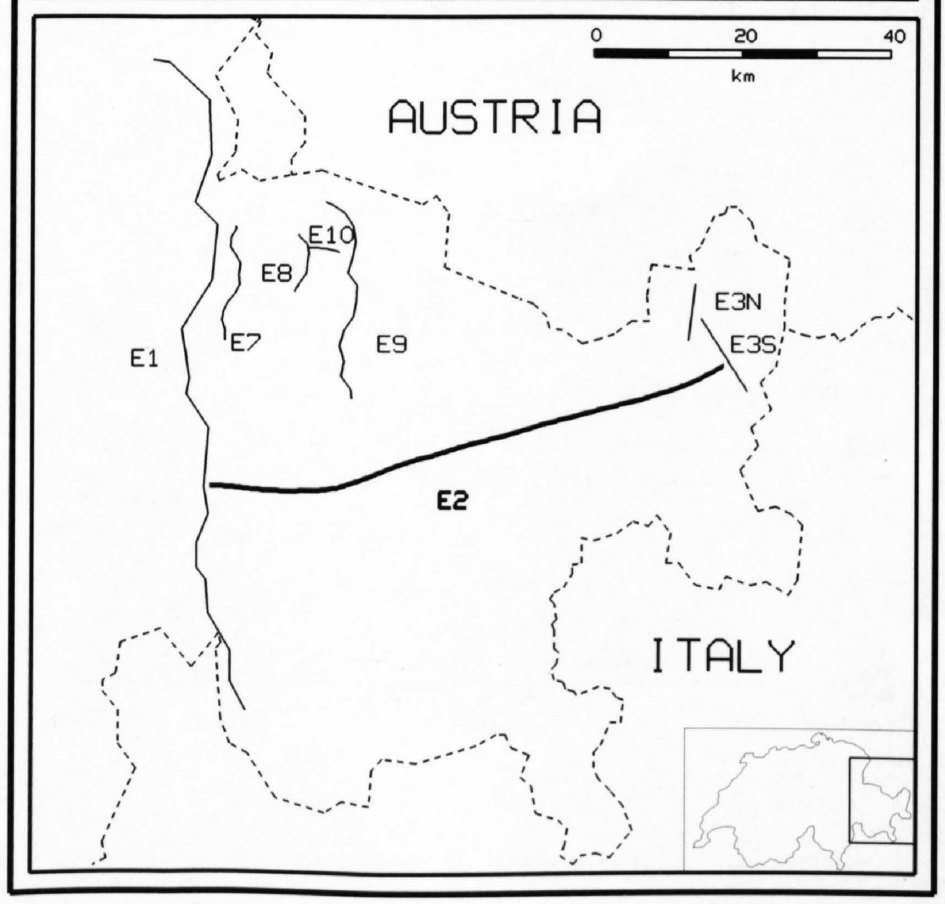

E2 (90-NF-04/05)

WSW

ENE

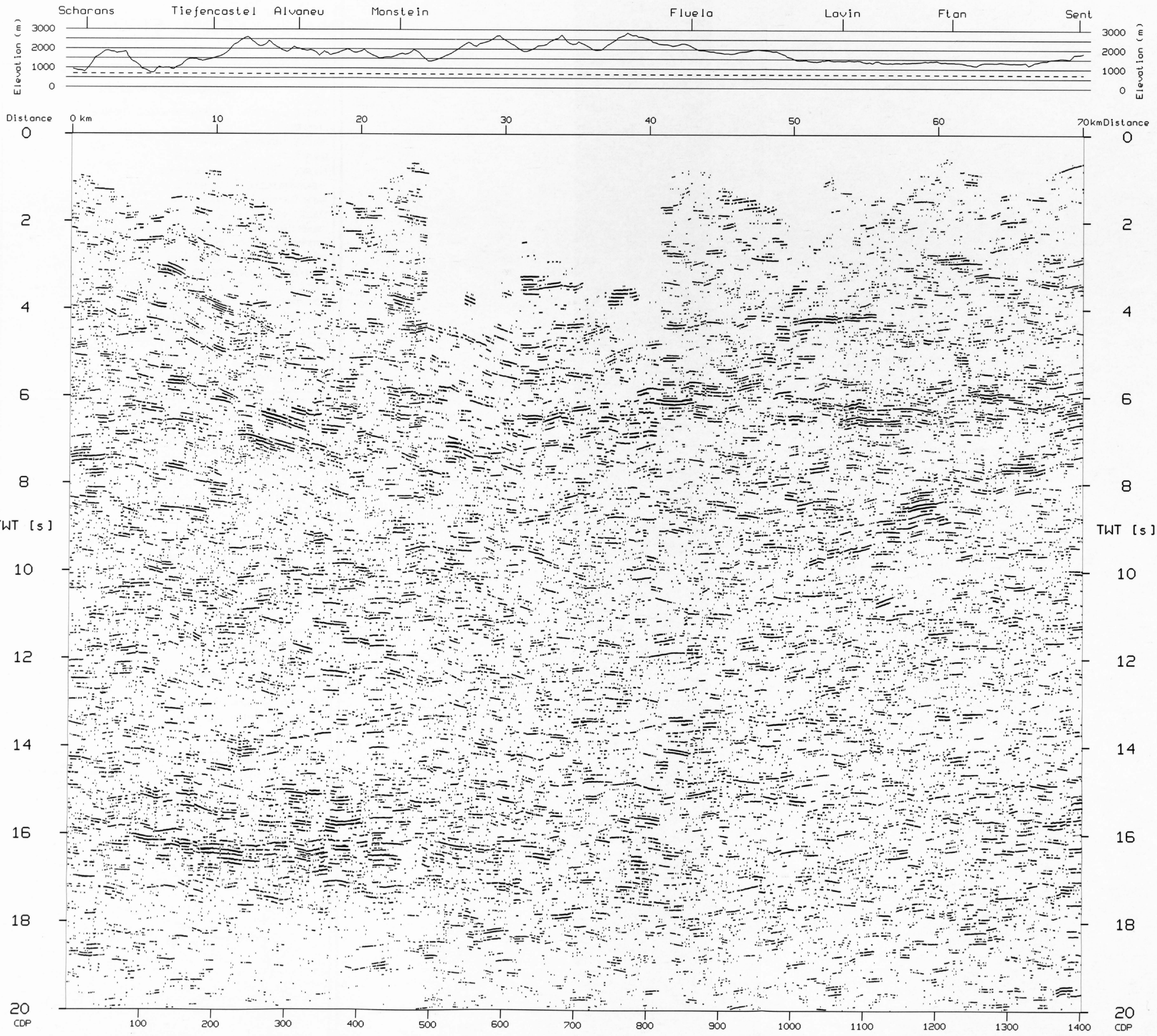

SWISS NATIONAL SCIENCE FOUNDATION

90-NF-E2 (VIBROSEIS)

FINAL STACK

1: 100'000

RECORDING PARAMETERS

SPREAD LAYOUT	15050-100-x-100-15050 m
CHANNELS	300
SOURCE INTERVAL	50 m
SOURCE TYPE	Vibroseis
SOURCE LAYOUT	5 Vibrators
SWEEP FREQUENCY	10-80 Hz
SWEEP LENGTH	60 s
SWEEPS/VP	1
GROUP INTERVAL	100 m
GEOPHONE TYPE	10 Hz
GEOPHONE LAYOUT	24 in line
INSTRUMENTATION	SERCEL 368
FIELD FILTERS	LC 8 Hz
COVERAGE	300 (nominal)
RECORDING MODE	Demultiplexed
SAMPLING RATE	4 ms
RECORDING LENGTH	75 s
RECORDED BY	PRAKLA SEISMOS AG
DATE RECORDED	Oct. 1990

PROCESSING PARAMETERS

1. Reformatting and gain recovery
2. Trace editing
3. Line geometry
4. CDP-Sort
5. Predictive deconvolution
6. Bandpass filter 6/10-75/85 Hz
7. Scaling
8. Application of field static corrections
9. Elevation to floating datum
10. Spiking deconvolution
11. Bandpass filter 8/12-70/100 Hz
12. NMO-Correction
13. Mute application
14. Surface consistent residual statics
15. Subsurface consistent residual statics
16. CDP-Stack
17. Time variant bandpass filter
18. Coherency filter
19. Time variant trace equalisation
20. Strong coherency filter

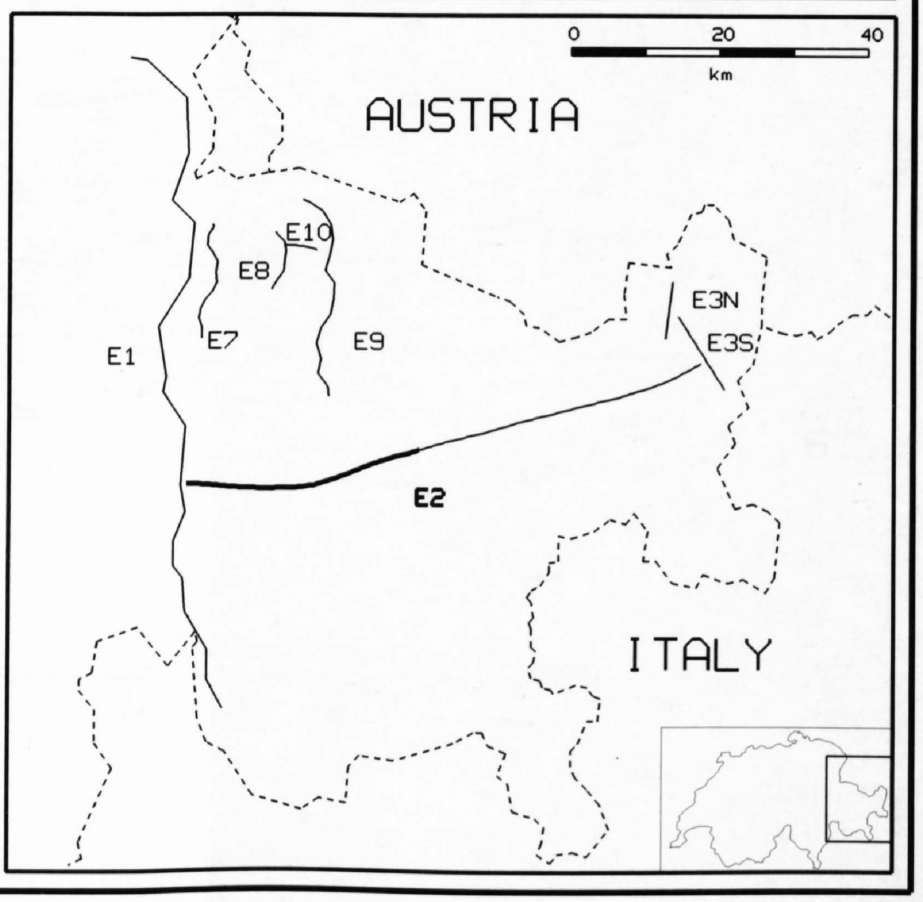

E2 (90-NF-V4)

WSW

ENE

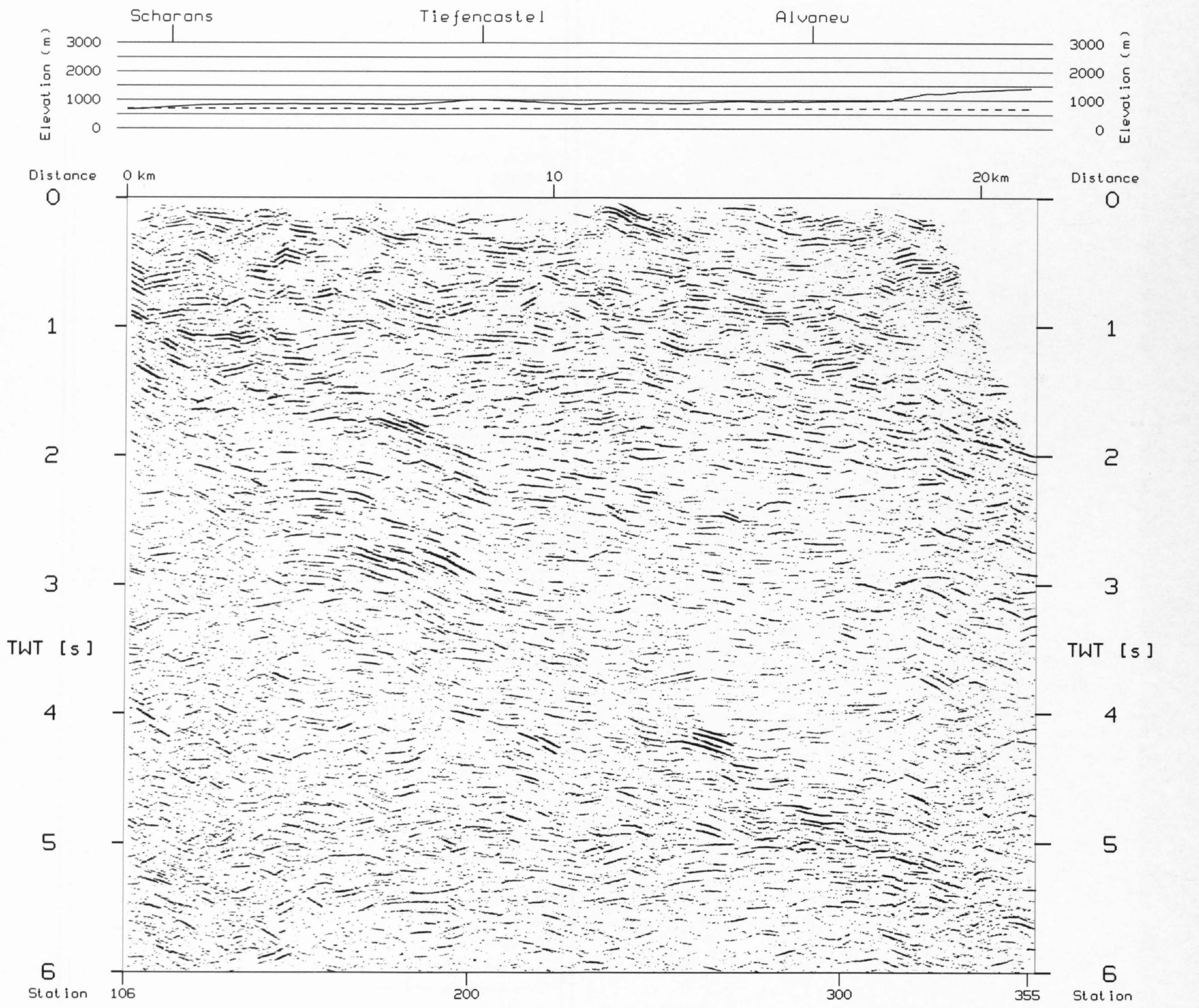

SWISS NATIONAL SCIENCE FOUNDATION

91-NF-E3N (DYNAMITE)

FINAL STACK

1: 200'000

RECORDING PARAMETERS

SPREAD LAYOUT	4.75 km
CHANNELS	48 / 48
SOURCE TYPE	Dynamite
SOURCE DEPTH	30 m
CHARGE SIZE	30 kg
GROUP INTERVAL	50 m
GEOPHONE TYPE	10 Hz
GEOPHONE PATTERN	12
INSTRUMENTATION	SERCEL 338HR / 338B
FIELD FILTERS	HC 125 Hz
COVERAGE	1-2 (nominal)
SAMPLING RATE	2 ms
RECORDING LENGTH	24 s
RECORDED BY	Geophys. Inst. Leoben
DATE RECORDED	Oct. 1991

PROCESSING PARAMETERS

1. Demultiplex
2. Resampling to 4 ms
3. Zero time correction
4. Static correction
5. Time variant scaling
6. Time variant bandpass filter
7. Spectral balancing
8. F/K filter
9. Despiking
10. Resampling to 8 ms
11. NMO-Correction
12. Mute application
13. Editing of optimum single coverage
14. CDP-Sort
15. CDP-Stack
16. Time variant bandpass filter
17. Coherency enhancement

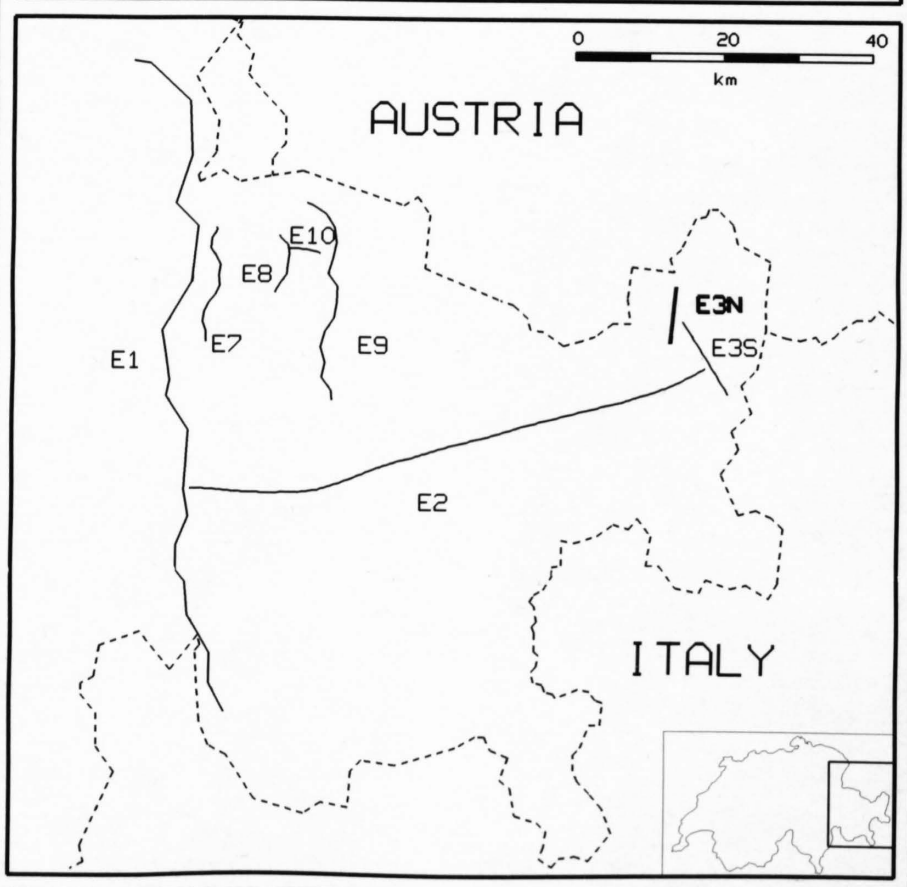

E3-North

NNE SSW

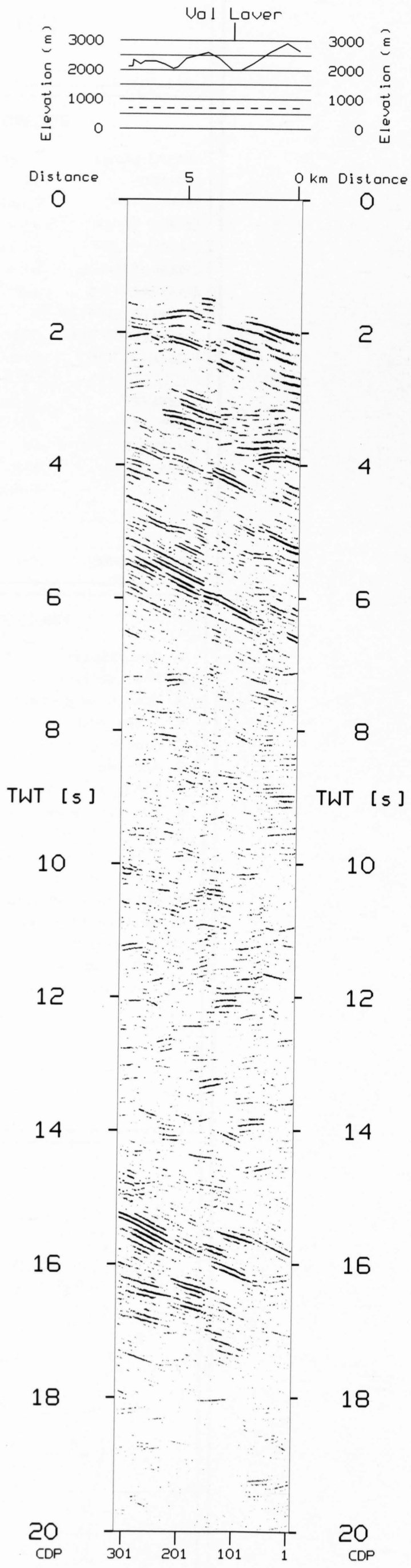

SWISS NATIONAL SCIENCE FOUNDATION

91-NF-E3S (DYNAMITE)

FINAL STACK

1: 200'000

RECORDING PARAMETERS

SPREAD LAYOUT	11 km
CHANNELS	48 / 48 / 96 / 48 / 48
SOURCE TYPE	Dynamite
SOURCE DEPTH	30 m
CHARGE SIZE	30 kg
GROUP INTERVAL	50 m
GEOPHONE TYPE	4.5 / 4.5 / 10 / 4.5 / 4.5 Hz
GEOPHONE PATTERN	6 / 6 / 12 / 6 / 6
INSTRUMENTATION	DFS-V/SERCEL 338/DFS-V/DFS-IV/BISON
FIELD FILTERS	No/LC 0.5 HC 125 NT 50/No/HC 124/ LC 4 HC 125 Hz
COVERAGE	11 (max.)
SAMPLING RATE	2 / 2 / 2 / 2 / 4 ms
RECORDING LENGTH	60 / 60 / 60 / 39 / 20 s
RECORDED BY	ETH / Muenchen / Muenster Clausthal / GeoExpert
DATE RECORDED	Oct. 1991

PROCESSING PARAMETERS

1. Demultiplex
2. Shot sorting
3. Zero time correction
4. Trace editing
5. Static correction
6. Scaling
7. Bandpass filter 4/8-28/40 Hz
8. Predictive deconvolution
9. Spectral balancing
10. Time variant bandpass filter
11. NMO-Correction
12. Mute application
13. Editing of selected CDP's
14. CDP-Sort
15. CDP-Stack
16. Coherency filter

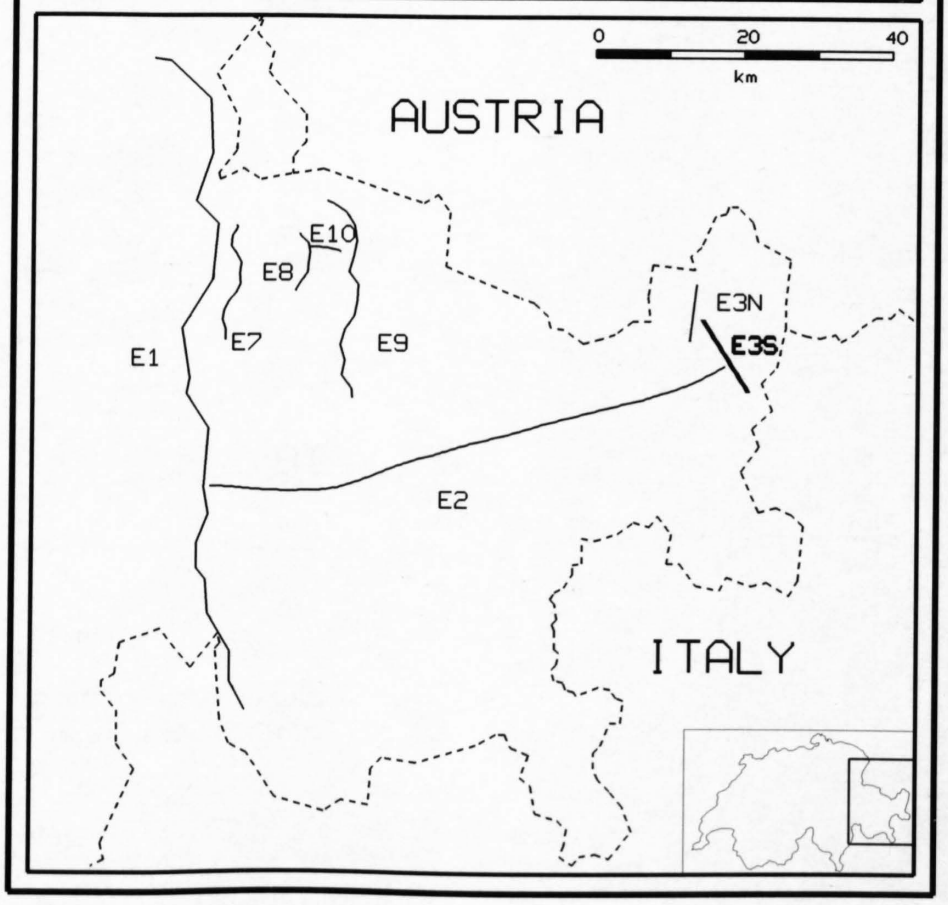

SWISS NATIONAL SCIENCE FOUNDATION

86-NF-E7 (DYNAMITE)

FINAL STACK

1: 200'000

RECORDING PARAMETERS

SPREAD LAYOUT	19.2 km
CHANNELS	240
SOURCE TYPE	Dynamite
SOURCE DEPTH	30 m
CHARGE SIZE	350 kg
GROUP INTERVAL	80 m
GEOPHONE TYPE	10 Hz
GEOPHONE PATTERN	24 in line / 76.6 m
INSTRUMENTATION	SERCEL 348
FIELD FILTERS	HC 62.5 Hz / NT 50 Hz
COVERAGE	1-2 (nominal)
SAMPLING RATE	4 ms
RECORDING LENGTH	60 s
RECORDED BY	PRAKLA SEISMOS AG
DATE RECORDED	Sept. 1987

PROCESSING PARAMETERS

1. Demultiplex and gain recovery
2. Resample to 8 ms
3. Line geometry
4. Application of field statics
5. Spectral balancing
6. Predictive deconvolution
7. Spiking deconvolution
8. Time variant bandpass filter
9. Mute application
10. Scaling
11. F/K-Filter
12. Time variant lowpass filter
13. NMO-Correction
14. Strong coherency filter

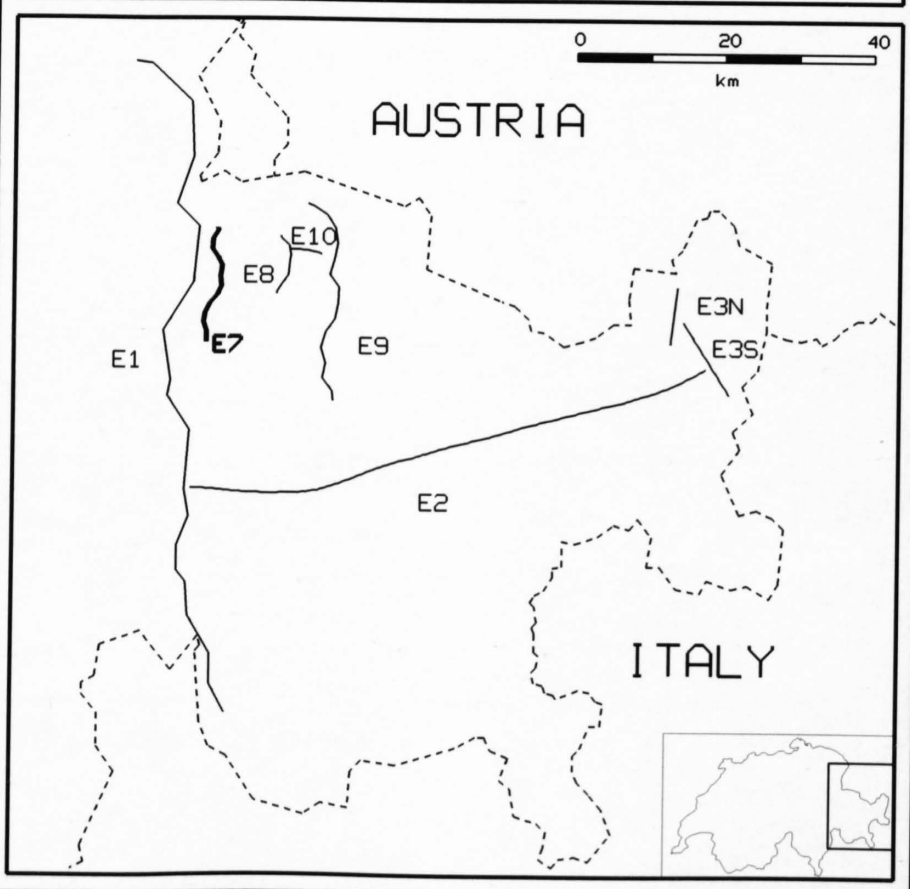

E7 (UNTERVAZ FAN SHOT)

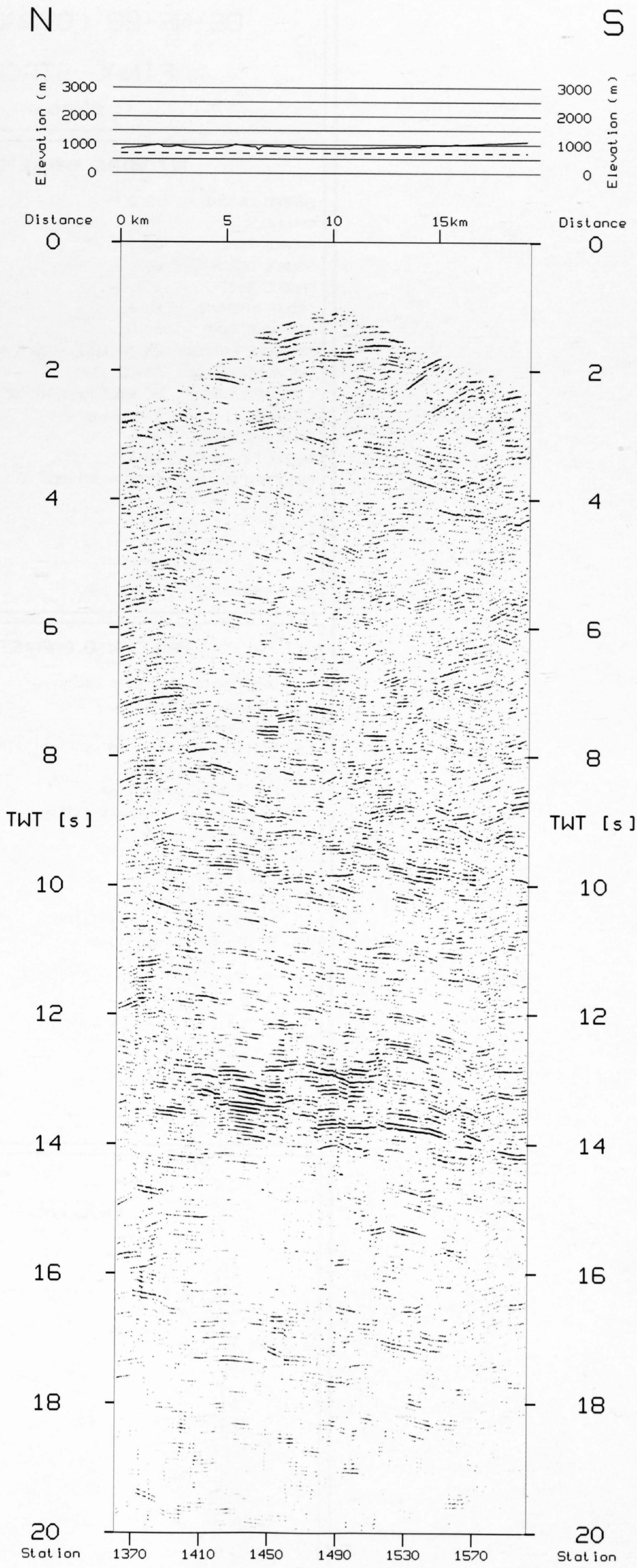

SWISS NATIONAL SCIENCE FOUNDATION

86-NF-E8 (DYNAMITE)

FINAL STACK

1: 200'000

RECORDING PARAMETERS

SPREAD LAYOUT	19.2 km
CHANNELS	240
SOURCE TYPE	Dynamite
SOURCE DEPTH	60
CHARGE SIZE	200 kg
GROUP INTERVAL	80 m
GEOPHONE TYPE	10 Hz
GEOPHONE PATTERN	24 in line / 76.6 m
INSTRUMENTATION	SERCEL 348
FIELD FILTERS	HC 62.5 Hz / NT 50 Hz
COVERAGE	1 (nominal)
SAMPLING RATE	4 ms
RECORDING LENGTH	60 s
RECORDED BY	PRAKLA SEISMOS AG
DATE RECORDED	Sept. 1987

PROCESSING PARAMETERS

1. Demultiplex and gain recovery
2. Resample to 8 ms
3. Line geometry
4. Application of field statics
5. Spectral balancing
6. Spiking deconvolution
7. Time variant bandpass filter
8. Mute application
9. Scaling
10. F/K-Filter
11. NMO-Correction
12. Time variant lowpass filter
13. Strong coherency filter

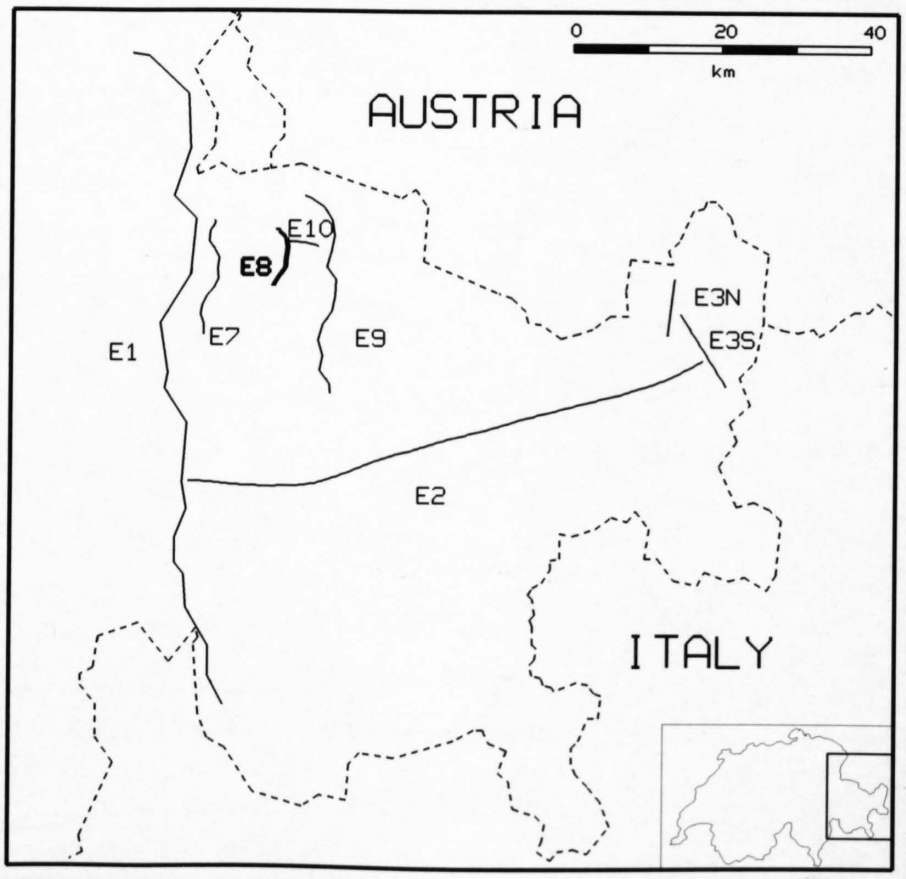

E8 (PANY FAN SHOT)

N S

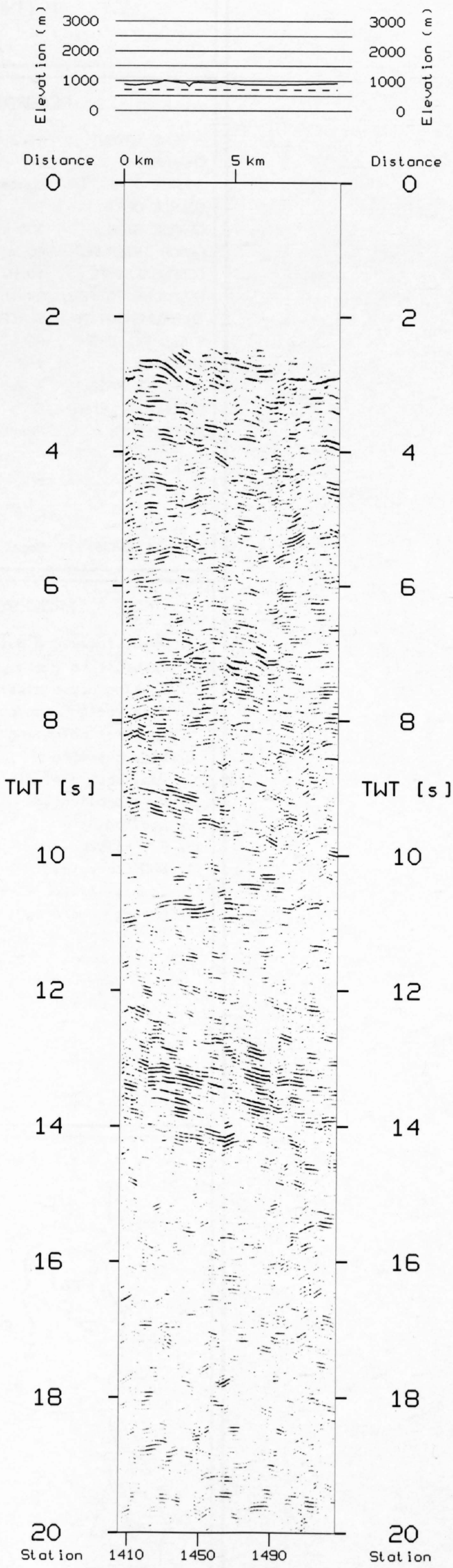

SWISS NATIONAL SCIENCE FOUNDATION

86-NF-E9 (DYNAMITE)

FINAL STACK

1: 200'000

RECORDING PARAMETERS

SPREAD LAYOUT	19.2 km
CHANNELS	240
SOURCE TYPE	Dynamite
SOURCE DEPTH	50
CHARGE SIZE	300 kg
GROUP INTERVAL	80 m
GEOPHONE TYPE	10 Hz
GEOPHONE PATTERN	24 in line / 76.6 m
INSTRUMENTATION	SERCEL 348
FIELD FILTERS	HC 62.5 Hz / NT 50 Hz
COVERAGE	1-2 (nominal)
SAMPLING RATE	4 ms
RECORDING LENGTH	60 s
RECORDED BY	PRAKLA SEISMOS AG
DATE RECORDED	Sept. 1987

PROCESSING PARAMETERS

1. Demultiplex and gain recovery
2. Resample to 8 ms
3. Spiking deconvolution
4. Time variant bandpass filter
5. Spectral balancing
6. Line geometry
7. Application of field statics
8. Mute application
9. Scaling
10. F/K-Filter
11. NMO-Correction
12. Lowpass filter 16/22
13. Strong coherency filter

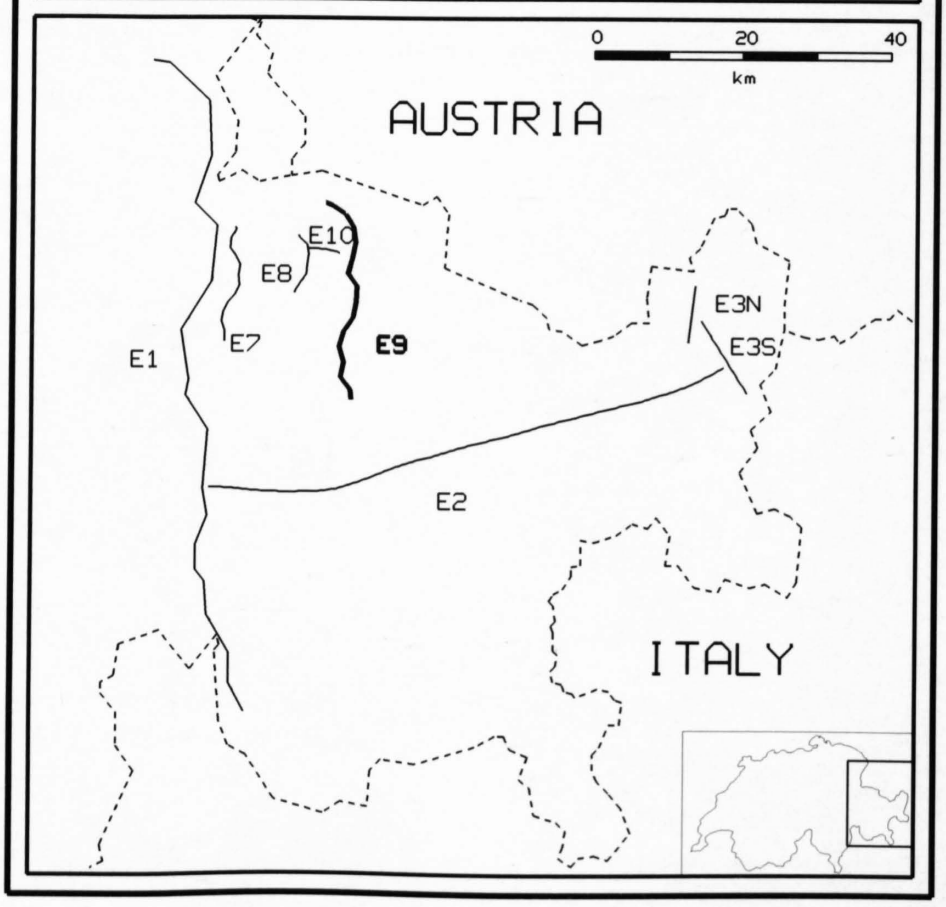

E9 (MONBIEL FAN SHOT)

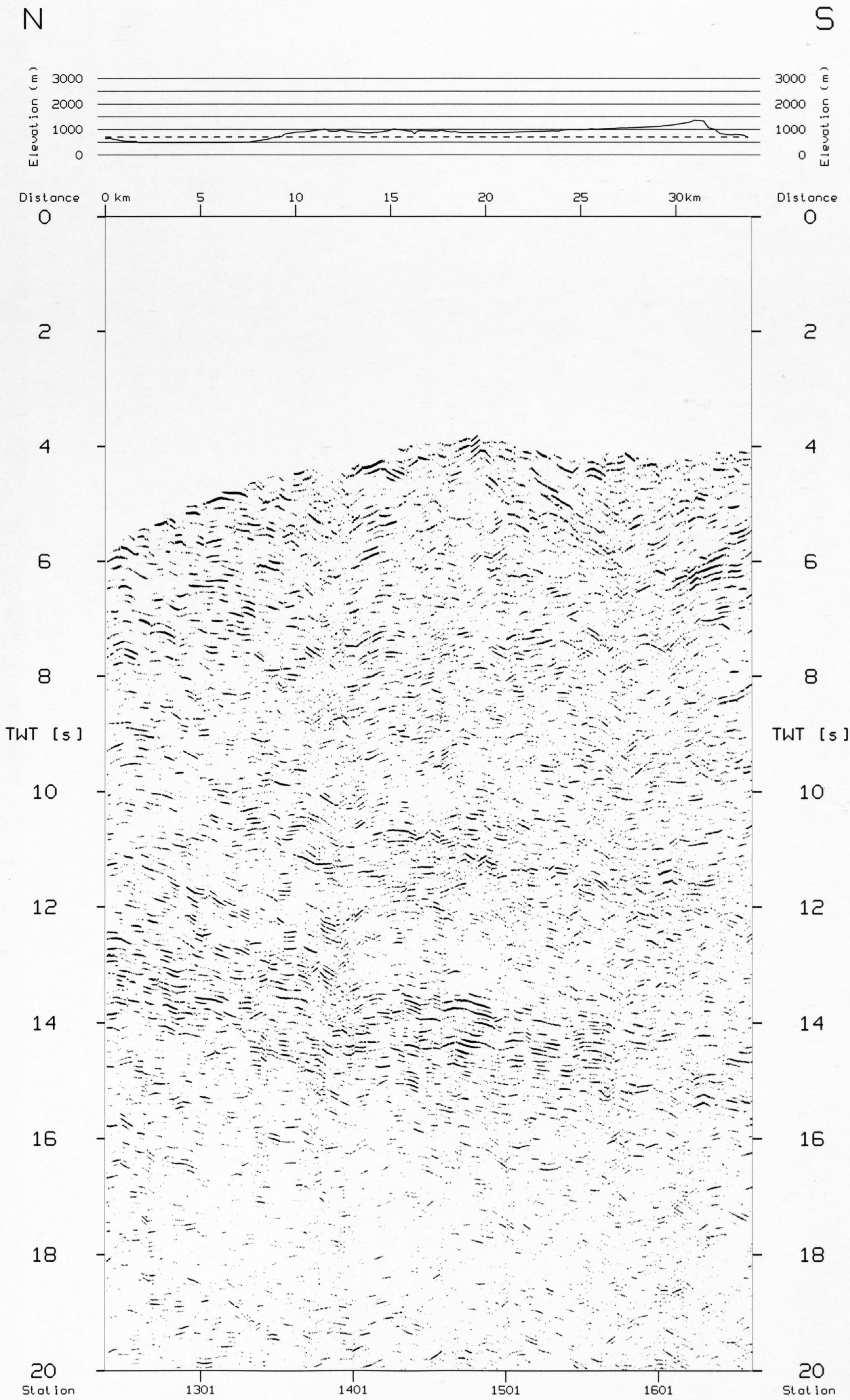

10 Geological interpretation of the seismic profiles through the Southern Alps (lines S1–S7 and C3-south)

M. E. Schumacher

Contents

10.1 Introduction

By the early 1980s the results from seismic reflection profiling for hydrocarbon exploration in the Po plain provided clear evidence for a Middle to Late Miocene southern foreland fold-and-thrust belt of the Alps, buried below Pliocene and Quaternary deposits (Pieri & Groppi 1981). In its northern continuation, however, no seismic reflection data on the deep structure of the Southern Alps were available until NRP 20 and CROP did their recent deep seismic-reflection survey (Figure 10-1).

The southern and central traverses of NRP 20 reveal new, basic insights into the southern, deep-crustal collisional structures of the Alps. However, geological interpretations of the seismic data from this area meet with particular difficulties. The profiles cross the western Southern Alps in a geologically extremely complex part with a polyphase deformation history, near the internal hinge of the Alpine arc (Schumacher et al., Chapter 15). Moreover, the distinct 3D structural setting aggravates the uncertainties about the significance of pre-migration stacked reflection data (Valasek et al. 1990; Frei et al., Chapter 3). Nevertheless, a reasonable connection between the rather difficult reflection data and the geological surface data is attempted at a local and regional scale.

The geological discussion of the seismic profiles through the Southern Alps is organized in three sections. They are, from east to west, the Generoso, the Lugano and the Malcantone sections. The tentative geological cross sections are constructed along straight lines following the processing lines of the reflection profiles shown on the map of Figure 10-1. Registration lines and shot points of the dynamite charges can be taken from Figure 2-1 of Chapter 2. For a detailed discussion about acquisition, processing and presentation of the reflection data see Frei (Chapter 2), Frei et al. (Chapter 3) and Valasek & Frei (Chapter 4).

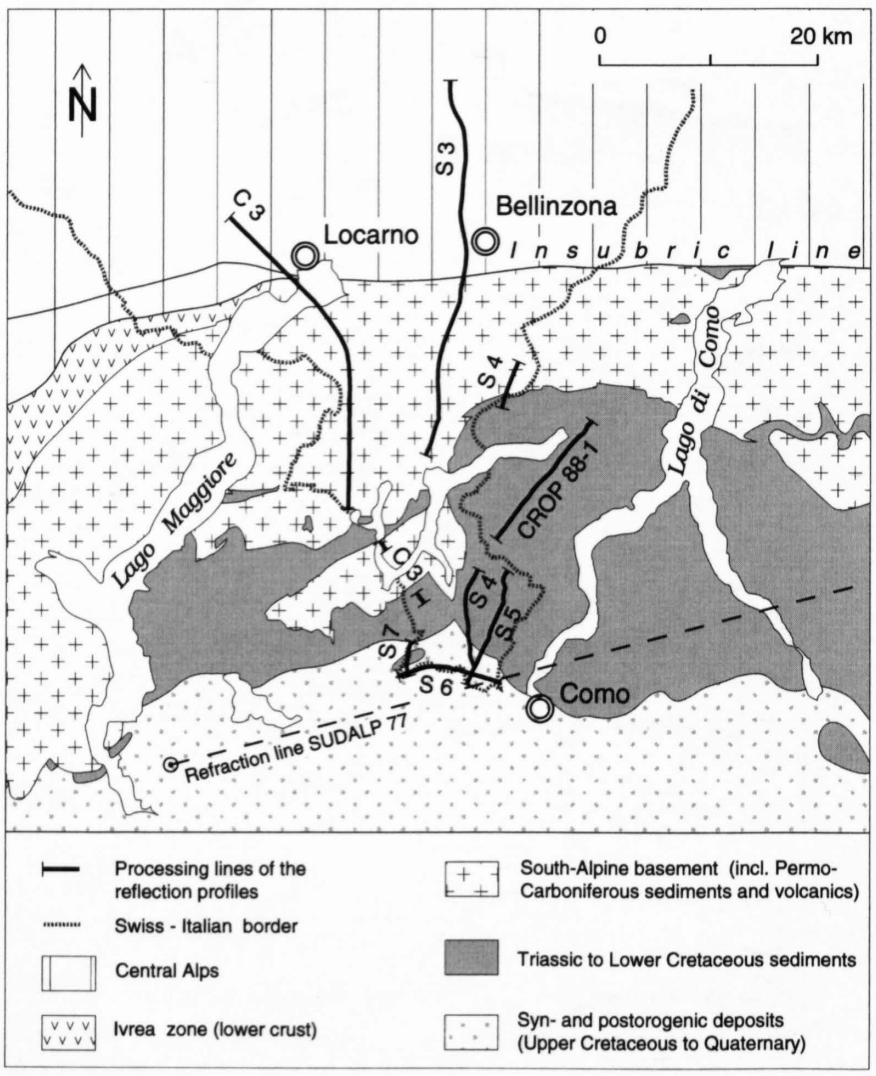

Figure 10-1
Location of the seismic-reflection profiles (processing lines) through the Southern Alps between Lago Maggiore and Lago di Como. Southern traverse: lines S3-7 and CROP 88-1; Central Traverse: line C3.

10.2 The Generoso section (lines S4, S5, S6 and CROP 88-1)

The structural setting of the Monte Generoso area between the Lugano and the Lecco transverse zones (Figure 10-2), is dominated by south-vergent sedimentary décollement nappes. Stratigraphically this segment is characterized by the thick Norian to Liassic syn-rift deposits of the Monte Generoso basin (von Bistram 1903, Lehner 1952, Bernoulli 1964, Sarti et al. 1991, Bertotti et al. 1993). The Lugano and Lecco transverse zones originated as Mesozoic extensional fault-systems which bordered the Generoso basin, as documented by sedimentary facies and thickness changes across them (Wiedenmayer 1963, Bernoulli 1964, Lichtensteiger 1986). They were reactivated as complex transfer zones (Laubscher 1985, Schumacher 1990) during the Alpine orogeny. Large portions of the Upper Triassic basin fill were back-thrust to the north along the Monte Grona line (Laubscher 1985) and other associated north-directed thrusts.

East of Lago di Como, the basement units of the two Orobic nappes (San Marco unit and Mezzoldo unit of Schönborn 1992) which are well exposed north and east of the Grigne plunge axially towards the Generoso area (Figure 10-2). The San Marco unit (Upper Orobic nappe) continues across Lago di Como forming the Val Colla ramp-fold, wedged to the south into the Carnian shales and evaporites below the syn-rift deposits of the Generoso basin (Laubscher 1985). The Mezzaldo unit plunges below the Grigne.

At the surface, the Monte Generoso unit is divided by the Generoso thrust into an northern, upper part and a southern, lower part (Bernoulli 1964, cf. Figure 10-10). Both units show intense, internal folding of the well stratified

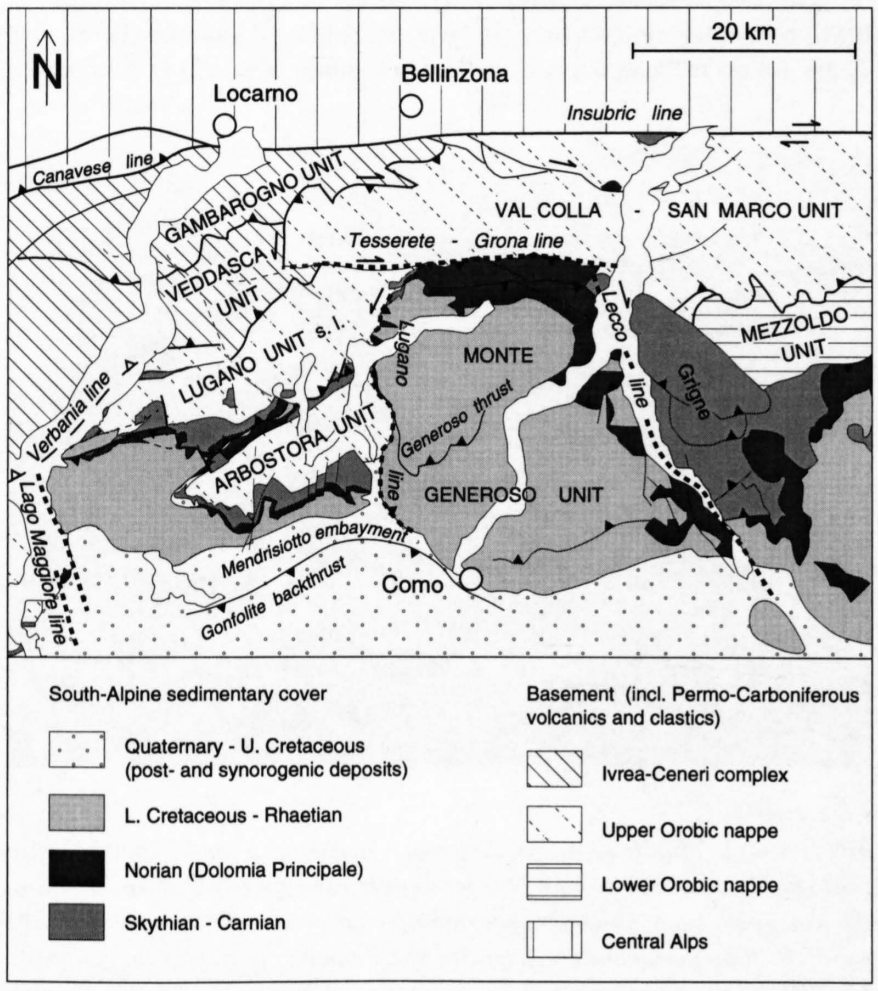

Figure 10-2
Geological map of the investigated area with the main tectonic elements.

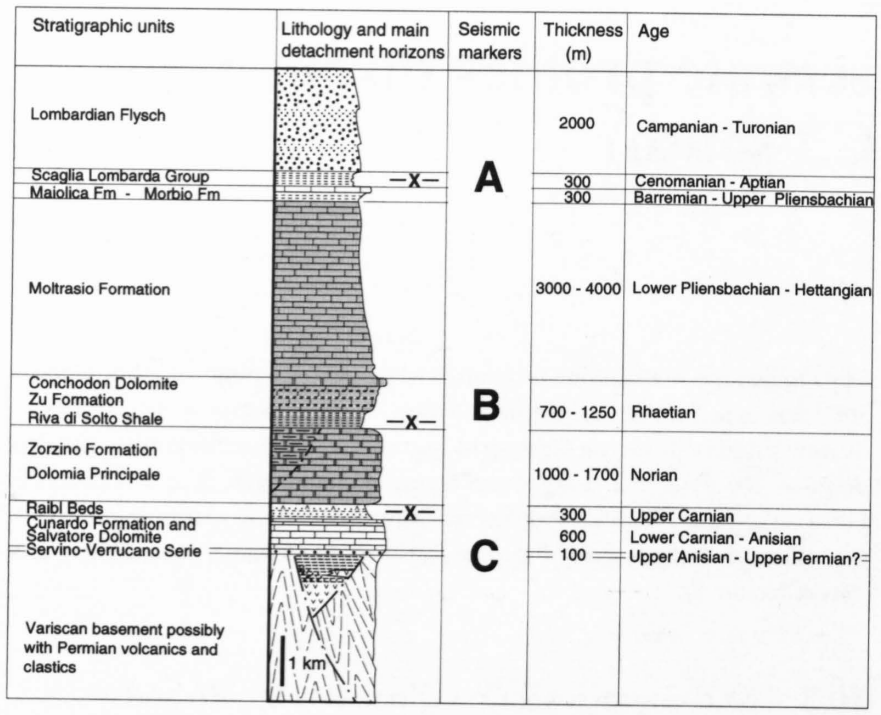

Figure 10-3
Stratigraphy of the Monte Generoso basin. Syn-rift deposits are grey-shaded. The seismic markers A, B, C are reflection bands, not individual horizons; marker A: top Maiolica – base Lombardian Flysch; marker B: Rhaetian; marker C: top basement, assumed to be represented approximately by the envelope at base of the reflective Mesozoic rocks.

Liassic basinal limestone (Moltrasio Formation). This contrasts with the more rigid deformational behaviour of the Triassic carbonates piled up as thrust sheets in the Grigne and along the Grona line.
To the southwest, the southern part of the Generoso unit dips with 60° or more below the back-thrust South-Alpine Molasse (Gonfolite Lombarda) forming a frontal triangle structure (Bernoulli et al. 1989). However, in detail the situation is complicated by overturning of the frontal limb and by additional frontal imbrication (Repossi 1929, Lüdin 1983).
The stratigraphy of the Monte Generoso basin is summarized in Figure 10-3. Norian to Middle Liassic syn-rift deposits change significantly their thickness in west-east direction, reaching their maximum to the west near the Lugano master fault (Bernoulli 1964, Bertotti 1991). However, no comparable thickness changes can be observed in north-south direction. The thickness values inferred from surface geology (Bernoulli 1964, Bertotti 1991) are only applicable to the Monte Generoso unit. For the deeper tectonic units, however, facies changes may be well possible and generally reduced thicknesses are expected.
Figure 10-4 shows the sequence of syn-rift deposits exposed on the western border of Lago di Como. The morphologically outstanding band at the top of the reflective Rhaetian sequence is formed by the competent carbonates of the Conchodon Formation overlain by the thick Liassic Moltrasio Formation. Below follow the alternating marls and limestones of the Zù Formation and

Figure 10-4
The Norian to Middle Liassic sedimentary sequence of the Monte Generoso basin at Monte di Tremezzo on the western border of Lago di Como (view to the W). The morphologically outstanding Conchodon Formation forms the top of the Rhaetian sequence, overlain by the thick Liassic Moltrasio Formation. Below the Conchodon cliff follows the alternating marl-limestone sequence of the Zù Formation, underlain by the Riva di Solto Shale. In the lower right corner appears the Norian Dolomia Principale.

the Riva di Solto Shale at the bottom. The whole Rhaetian sequence at this locality has a thickness of about 1000 m (Burchell et al. 1990). Down to the right the top of the Norian Dolomia Principale can be recognized.

Line S5

The vibroseis data from line S5 along Valle di Muggio are shown as coherency-enhanced final stack in Plate 10-9 and as unmigrated line drawing together with the surface geology in Figure 10-5. Figure 10-6 shows the geological interpretation of line S5 with the position of the main reflections after migration.
The first good reflection band B in the north at 1,5 s TWT can be correlated with the alternating Rhaetian carbonates and shales. The position of these reflections agrees with the estimated thickness of about 4 km for the overlying Liassic cherty limestone (Moltrasio Formation) based on surface geological data (Bernoulli 1964). The intensely folded Liassic Moltrasio Formation appears hardly reflective. The transparent domain immediately below the Rhaetian could represent the Norian Dolomia Principale. Some imbrication of the Rhaetian reflectors can be well recognized and points to a local detachment at the base of the Rhaetian (Riva di Solto Shale).
To the south, on Figures 10-5 and 10-6, between 0 s and 1s TWT the strong, steeply south-dipping reflections A correspond probably roughly to the marly Upper Cretaceous Scaglia Group between the limestone of the Maiolica Formation and the clastics of the Lombardian Flysch.
Between the two reflecting domains, A and B, an Alpine transpressively reactivated part of the Mesozoic Lugano fault is suspected. It appears to be confirmed by the drastically reduced thickness of the Liassic rocks to the south, if the reflections P are correlated with Triassic (Rhaetian?) rocks. A reverse component of the Alpine Lugano fault can be recognized from the displaced Maiolica/Scaglia boundary.

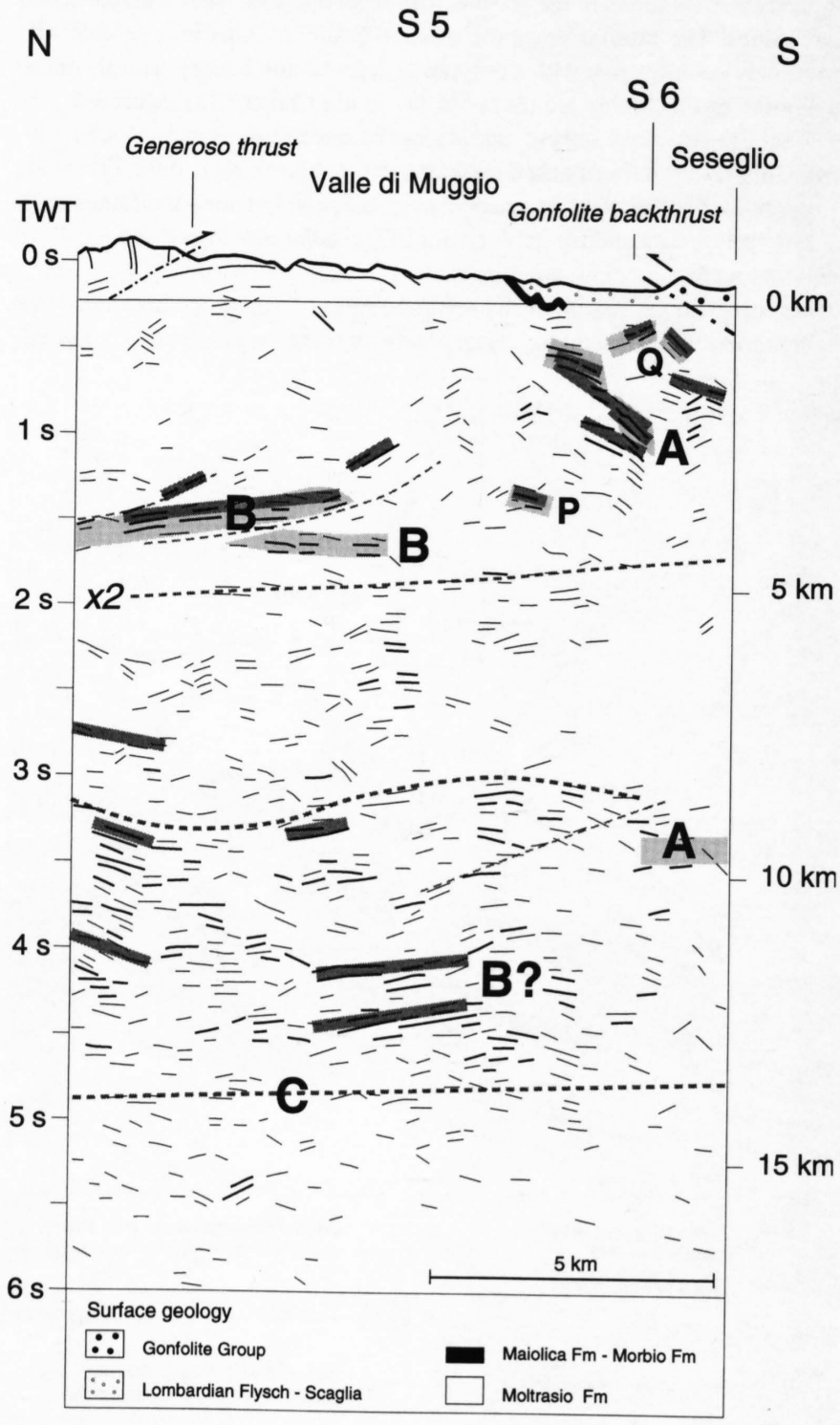

Figure 10-5
Unmigrated, handmade line-drawing of the vibroseis profile S5 with tentative geological correlations (see Figure 10-3 and discussion in the text). The km-scale is based on an assumed average P-wave velocity of 6 km/s.

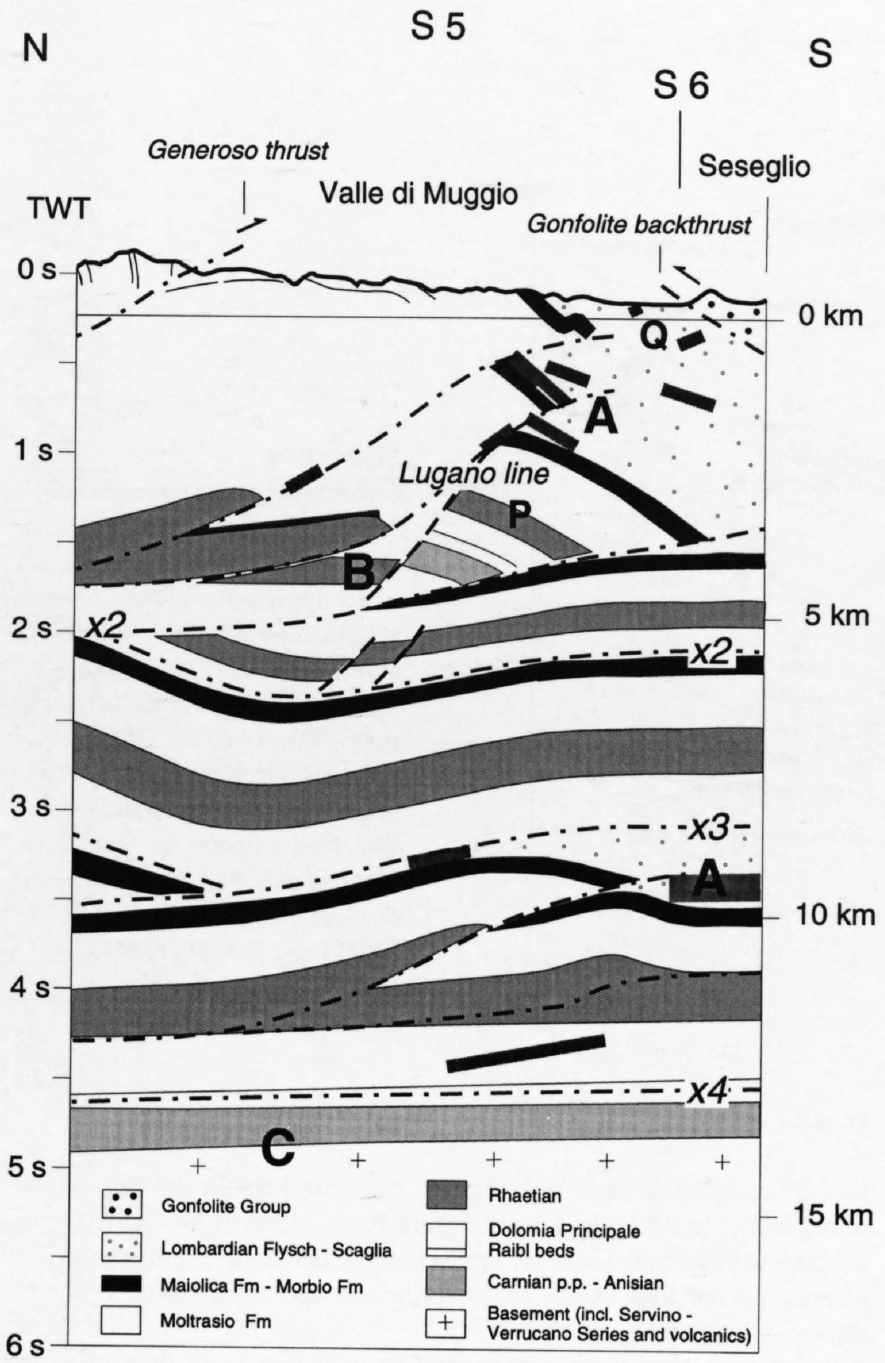

Figure 10-6
Tentative geological interpretation of the upper part of line S5 showing the position of the main reflectors after migration (discussion in the text). x2, x3 and x4 mark the supposed basal thrust planes of the various South-Alpine nappes (see Table 10-1).

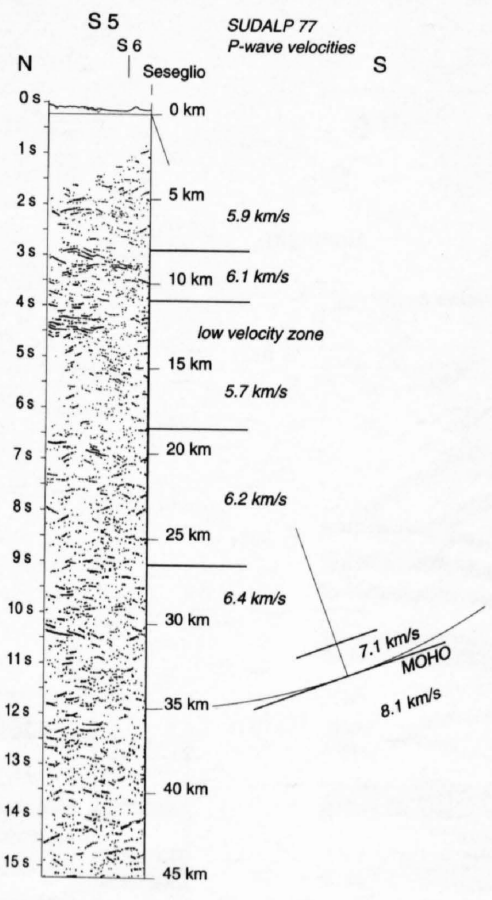

Figure 10-7
Coherency-enhanced dynamite data of line S5 (shot Seseglio) compared with P-wave velocities of the intersecting seismic-refraction profile SUDALP 77 (after Deichmann et al. 1986), plotted to the right. The boundaries of the velocity domains at the deepest crustal levels are shown in a migrated position (Ye 1992). There are no distinct reflections recognizable at the level of the refraction Moho, nor does this level mark the base of sporadic reflections.

Reflections Q show a synformal geometry after migration and suggest intense folding of the Lombardian Flysch below the backthrust of the Gonfolite Lombarda (Bernoulli et al. 1989).

The horizontal reflection pattern near 2 s TWT (approximately 5 km depth) contrasts with the inclined reflections above and this discordance is explained by a thrust *x2* separating the two domains. To the south this thrust cuts across the Mesozoic Lugano fault, whereas towards the north it may level off into the Carnian Raibl shales.

The top of the autochthonous basement C seems to be located at a depth of about 14 km below sea level. Immediately above the basement a domain of reflections between 3 s and 5 s TWT may represent the lowermost, autochthonous or parautochthonous Mesozoic cover unit. Thus, the total thickness of the sedimentary rocks above the basement seems to be at least 14 km. Because the thickness of the undisturbed sedimentary sequence in this area ranges from 4 to 7 km (and is probably no more than 10 km, compare Figure 10-3), the rocks which lie above the basement must be tectonically repeated, as implied by the apparent repetitions of the reflective intervals interpreted as Maiolica and Rhaetian.

The reflections A at about 3 s to 3.5 s TWT appear to correspond to the top of the Lower Cretaceous (Maiolica Formation) and base of the "mid"- Cretaceous (Marne di Bruntino and Sass della Luna Formations) as documented by AGIP seismic lines (e. g. Mattavelli and Margarucci 1992). Lines S5 and S6 intersect and these reflections can be correlated with the very pronounced reflection band at 3.5 s TWT on line S6 (Figure 10-12). Based on these correlations an original thickness of about 4 to 5 km is estimated for a basal cover unit, locally increased by some minor internal imbrication. Between this basal Mesozoic cover unit and the Generoso unit, there is space for another large sedimentary nappe, probably consisting of Norian to Lower Cretaceous strata (Figure 10-6).

The dynamite data of line S5 (see Plate 10-8 and Figure 10-7) clearly confirm the location of the basement/cover contact at about 14 km. The Cretaceous reflections A at about 3s TWT are here even better documented than by the vibroseis data.

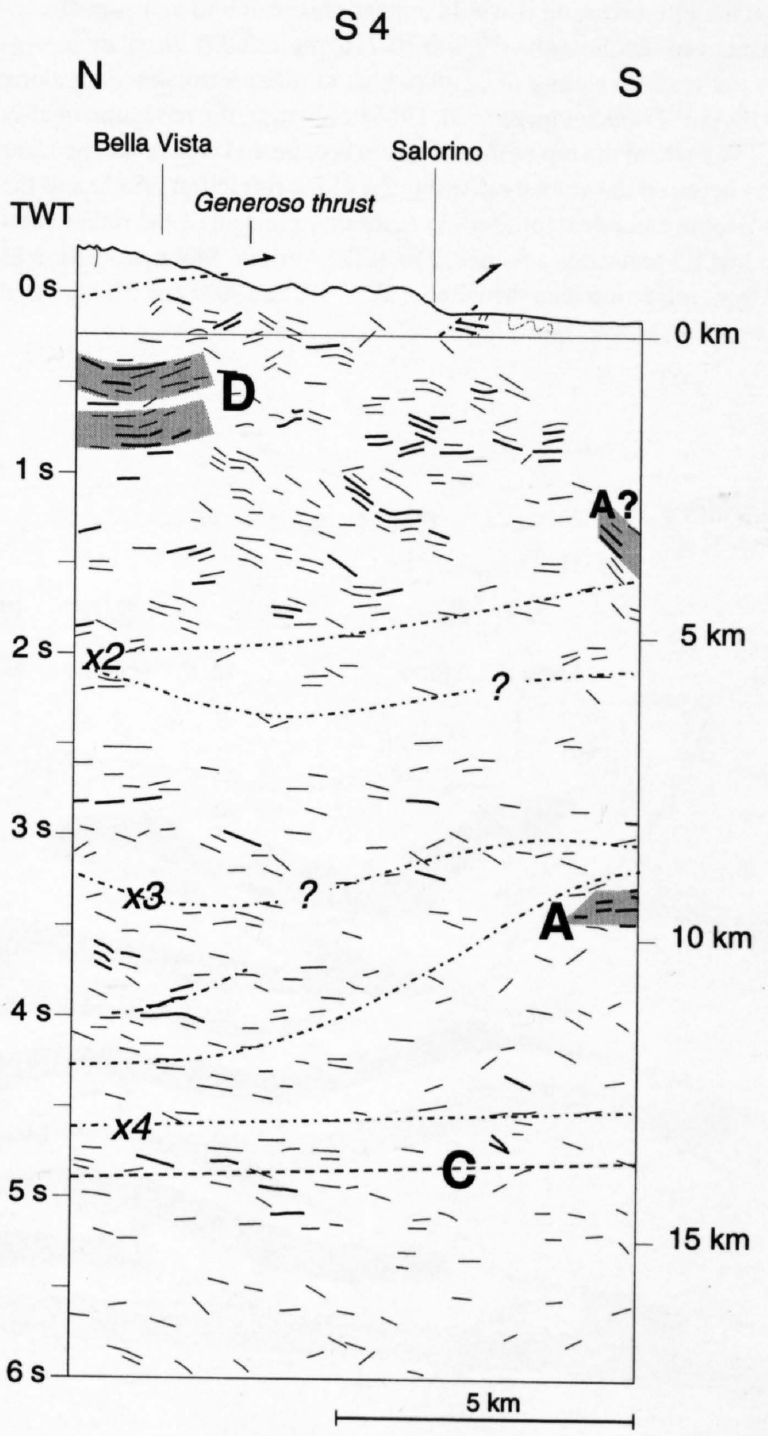

Figure 10-8
Unmigrated, handmade line-drawing of the vibroseis profile S4 with tentative geological correlations (discussion in the text). x2, x3 and x4 are supposed thrust planes of the South-Alpine nappes (see Table 10-1).

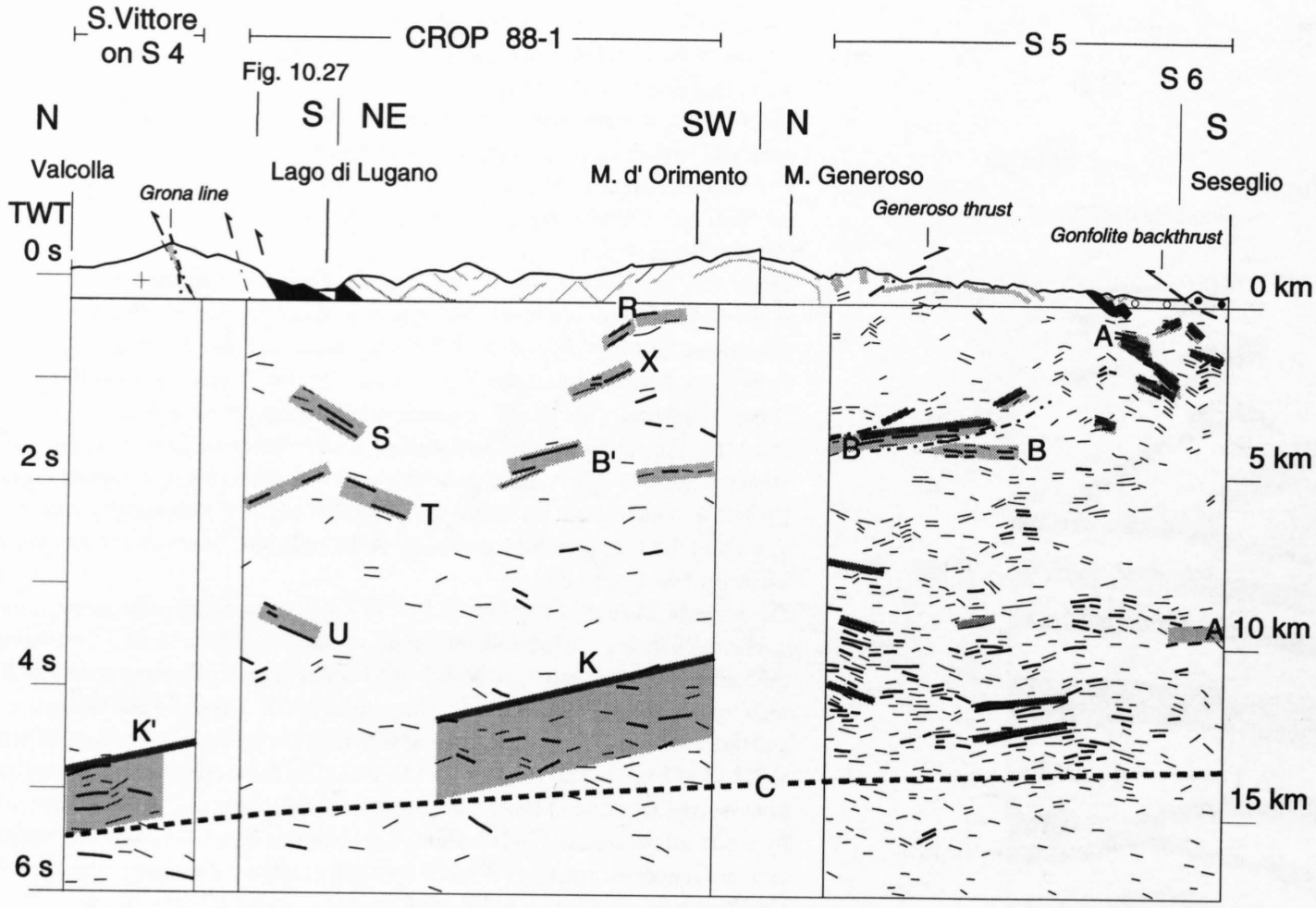

Figure 10-9
Combined section through the Monte Generoso area. Unmigrated, handmade line-drawings of the upper parts of the explosion seismic lines S4 (shot San Vittore) and CROP 88-01 (shots San Pietro, Montoni and Bollette) and the vibroseis line S5, with a tentative geological correlation of the main reflections (grey-shaded). For the discussion see text and compare Figure 10-10. Surface geology after Lehner (1952) and Beroulli (1964).

The longitudinal seismic-refraction profile SUDALP 77 (Ansorge et al. 1979) crosses line S5 near the Swiss/Italian border (Figure 10-1). Hence for a crustal scale interpretation it would appear reasonable to compare the reflection data from shot Seseglio (Figure 10-7) to the velocity distribution suggested by ray-trace modeling of amplitude controlled refraction data along profile SUDALP 77 (Deichmann et al. 1986). However, the reflection quality below 5s TWT where the top of the basement is expected is poor and no clear correlation between the velocity distribution of the refraction profile and the reflection profile can be established. In particular the data of the rather short reflection line S5 precludes a recognition of the Adriatic Moho at – 35 km as expected from refraction data (Mueller et al. 1980, Ye 1992) and a distinction between upper and lower crust.

Line S4

Line S4 branches off from line S5 near Chiasso and continues northward almost parallel to the Lugano fault (Figure 10-1). North of M. Generoso, the Italian line CROP 88-1 was set up to continue line S4 in NE-direction. Coherency-filtered final stacks of the explosion and vibroseis data sets are shown in Plates 10-6 and 10-7.
A tentative geological interpretation of an unmigrated line drawing of the vibroseis data from line S4 is shown in Figure 10-8. Although data quality is very poor, some observations can be made by comparison with the better data of line S5 (Figure 10-5). The reflections D between 0 s and 1 s TWT below Bella Vista on line S4 (Figure 10-8) seem to be at variance with the seis-

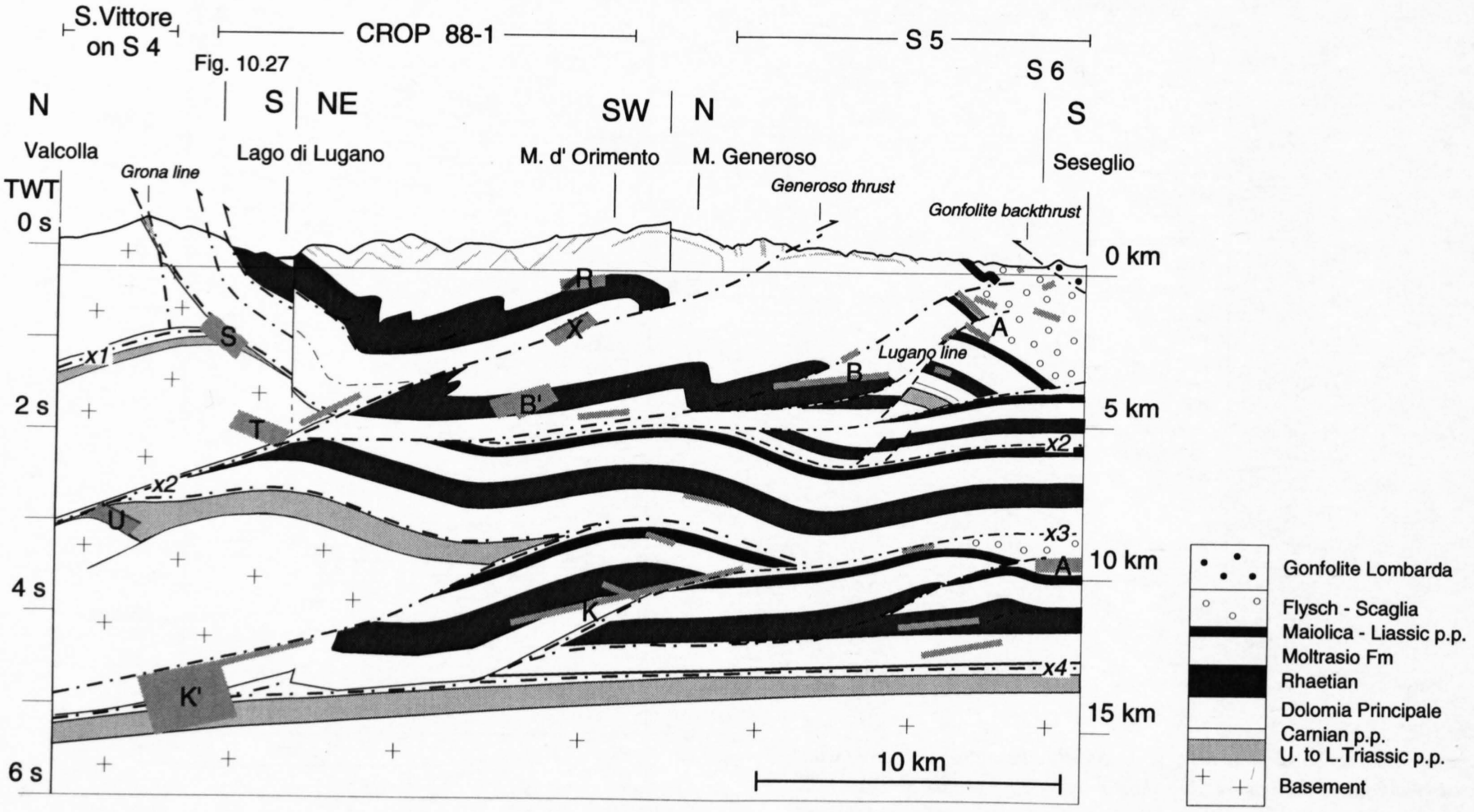

Figure 10-10
Tentative geological interpretation of the Generoso section (compare Figure 10-9) with the main reflectors (grey-shaded) in a migrated position (modified after Schumacher 1994). x1, x2, x3 and x4 mark the supposed thrust planes of the South-Alpine nappes (see Table 10-1).

mically transparent Moltrasio Formation on line S5. However, considering the location of line S4 close to the Lugano fault system these reflections may originate from lateral reflectors to the west and/or document a Mesozoic fault step (Bernoulli 1964, p. 54-55) with a reduced thickness of the Moltrasio Formation. In this case, the reflections D could be well attributed to Triassic rocks (compare line S7, Figure 10-17). The rather chaotic reflection pattern below Salorino is obviously the expression of the intense deformation at the front of the Generoso unit and probably also due to 3D-effects (side swipes).

The subhorizontal reflections A at about 3.5 s TWT may correspond to the Cretaceous reflectors A of line S5, interpreted to mark approximately the top of the "autochthonous" Mesozoic.

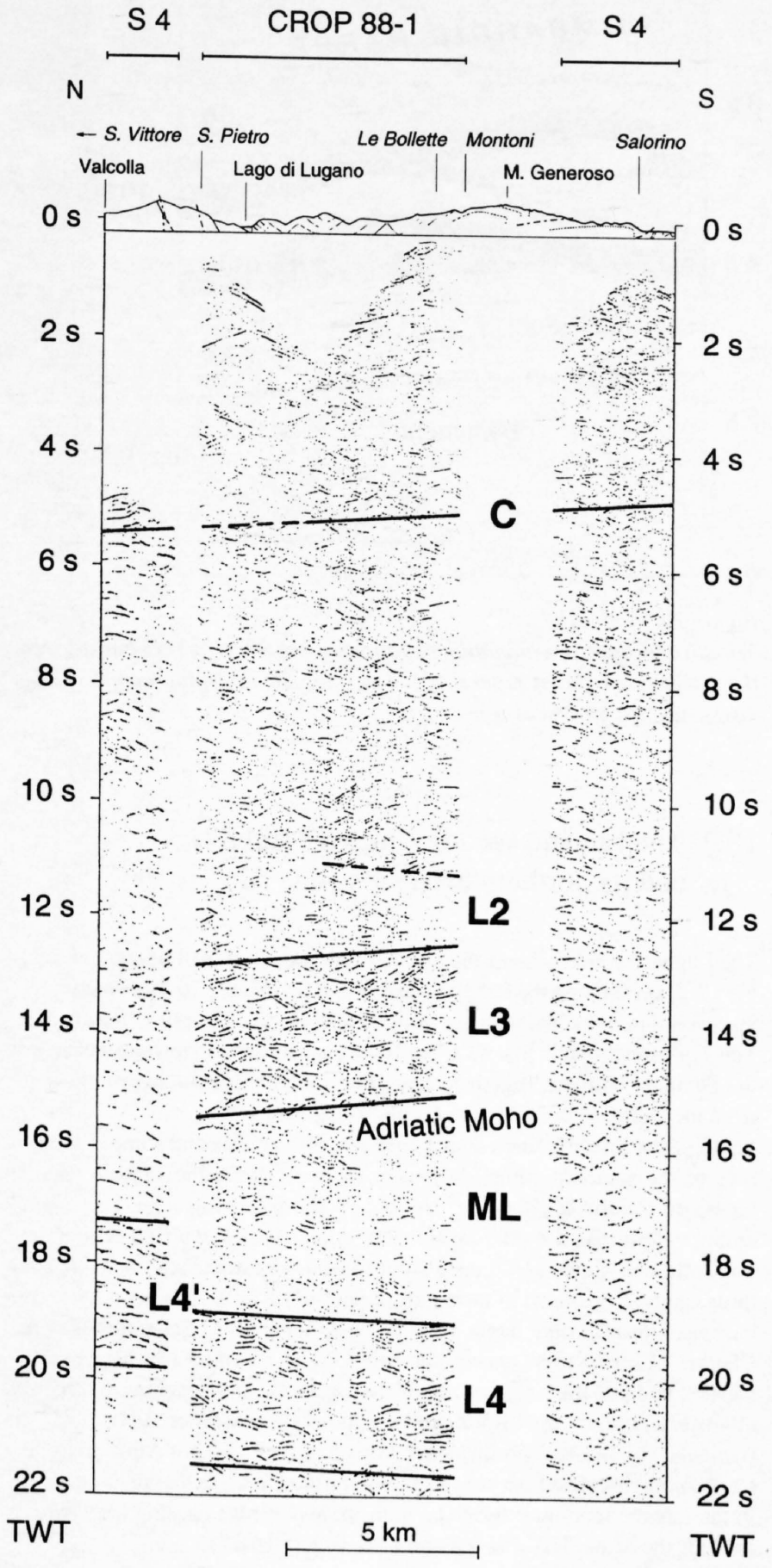

Figure 10-11
Coherency-enhanced, unmigrated explosion seismic data of the combined line S4/CROP 88-1 with tentative geological correlation of the deep-crustal parts. C: top basement beneath the Generoso area; L2, L3: Adriatic lower crust with Adriatic Moho at the base; L4, L4': European lower crust with European Moho at the base; ML: possibly Adriatic mantle lithosphere.

Line CROP 88-1

Line CROP 88-1 is a dynamite profile consisting of three single shots. No vibroseis was recorded. The data near the surface are discussed in the context of the entire shallow part of the Generoso section shown by the combined profile in Figures 10-9 and 10-10. This profile is composed of three segments: a northern segment with the data of shot San Vittore registered on line S4, the dynamite line CROP 88-1 and the vibroseis line S5 to the south (Figure 10-1). The combination of these segments offers the best chance to decipher the rather poor reflections of CROP 88-1 and to yield some additional information about the subsurface structure of the Generoso area. However, the common mid-points (CMP) used to determine the location of the reflectors in the San Vittore segment are based on the simple assumption of horizontal reflectors.

Reflections B' fit well with the prolongation of the Rhaeatian reflector B and are thus considered to be the continuation of the latter towards north. After migration, the reflections X seem to line up with the Generoso thrust at the surface. Therefore the reflections R can possibly again be attributed to Triassic (Rhaetian?) rocks, but belonging to the upper part of the Generoso unit.

The reflection bands S and T may originate from the south-dipping Triassic carbonates and shales south of the Monte Grona line (Lehner 1952, Bertotti 1991) at the front of the Orobic basement. Reflection band U, however, is interpreted as the base of the sedimentary cover of the southern limb of a deeper basement ramp-fold (Figure 10-10). This ramp-fold is part of an intermediate Lombardic nappe between the Orobic nappes on top and the imbricated basal Mesozoic units below. The latter, well documented on line S5, continue along line CROP 88-1, giving rise to the reflections K. They taper off towards the north and could be even responsible for the distinct north-dipping reflections K' of shot San Vittore.

For the discussion of the deep-crustal configuration along the Monte Generoso section, the coherency-enhanced dynamite data of lines S4 and CROP 88-01 are shown in Figure 10-11 down to a depth of 22 s TWT. The top of the lower crust along the lines S4 and CROP 88-01 was estimated by Valasek (1992) in his three-layer crustal velocity model to be approximately at 8–9 s TWT or 25 km depth.

Particularly interesting are the two reflective domains L3 and L4 separated by a transparent domain ML on the CROP line because they point to a possible redoubling of the Moho below the Southern Alps. The base of the apparently north-dipping domain L3 between 12 s and 15 s TWT seems to correlate roughly with the seismic-refraction Moho (Ye 1992). That means the Adriatic Moho arrives at a depth of 46–47 km under the northern Generoso massif. Consequently the transparent zone ML below represents Adriatic mantle lithosphere.

The reflections L4 between 19 s and 22 s TWT may well represent a fragment of European lower crust and of European Moho at its base. To the north, on the San Vittore part of line S4 south-dipping reflections L4' are documented between 17 s and 20 s TWT and can be also interpreted as European lower crust. This reflection zone, however, appears to be shifted up vertically in the order of 1.5 s TWT (4.5 km) with respect to the lower reflective zone L4 on CROP 88-1. This could at least partly result from the 7 km lateral offset between the southern end of S4 San Vittore segment and the northern end of the CROP segment (Figure 10-1) and would signify a dip to the southeast for this European Moho fragment.

The lower crustal reflections L3 above the Adriatic Moho seem separated by a more transparent domain L2 from a still higher reflective zone. This alternation becomes, more obvious on lines S3 and C3 (see below) and leads one to assume lower crustal stacking.

Line S6

The W-E trending vibroseis line S6 follows the front of the backthrust South-Alpine Molasse (Gonfolite Lombarda) along a curved line (Figure 10-2). It covers the mainly buried, complex structures of the Mendrisiotto embayment and connects line S5 of the Generoso section with line S7 of the Lugano section (Figure 10-1). A coherency-enhanced final stack of line S6 is shown in Plate 10-10.

As on line S5, the seismic reflection pattern from the sedimentary cover units on line S6 can be divided into three parts (Figures 10-12 and 10-13):

1) From the surface down to a depth of about 2 s TWT (corresponding to roughly 6 km) the seismic reflection pattern is very chaotic. This is not surprising since line S6 investigates the strongly deformed frontal part of the Orobic nappe-system wedged under the South-Alpine Molasse. In addition, the Lugano transverse zone is expected to pass somewhere through the eastern half separating the Generoso basin from the Arbostora swell. Both tectonic elements are incorporated in the Orobic nappe system and hence detached from their original substratum. Near the western end of line S6 at the locality Gaggiolo (Stabio) a well was drilled into the Middle Liassic

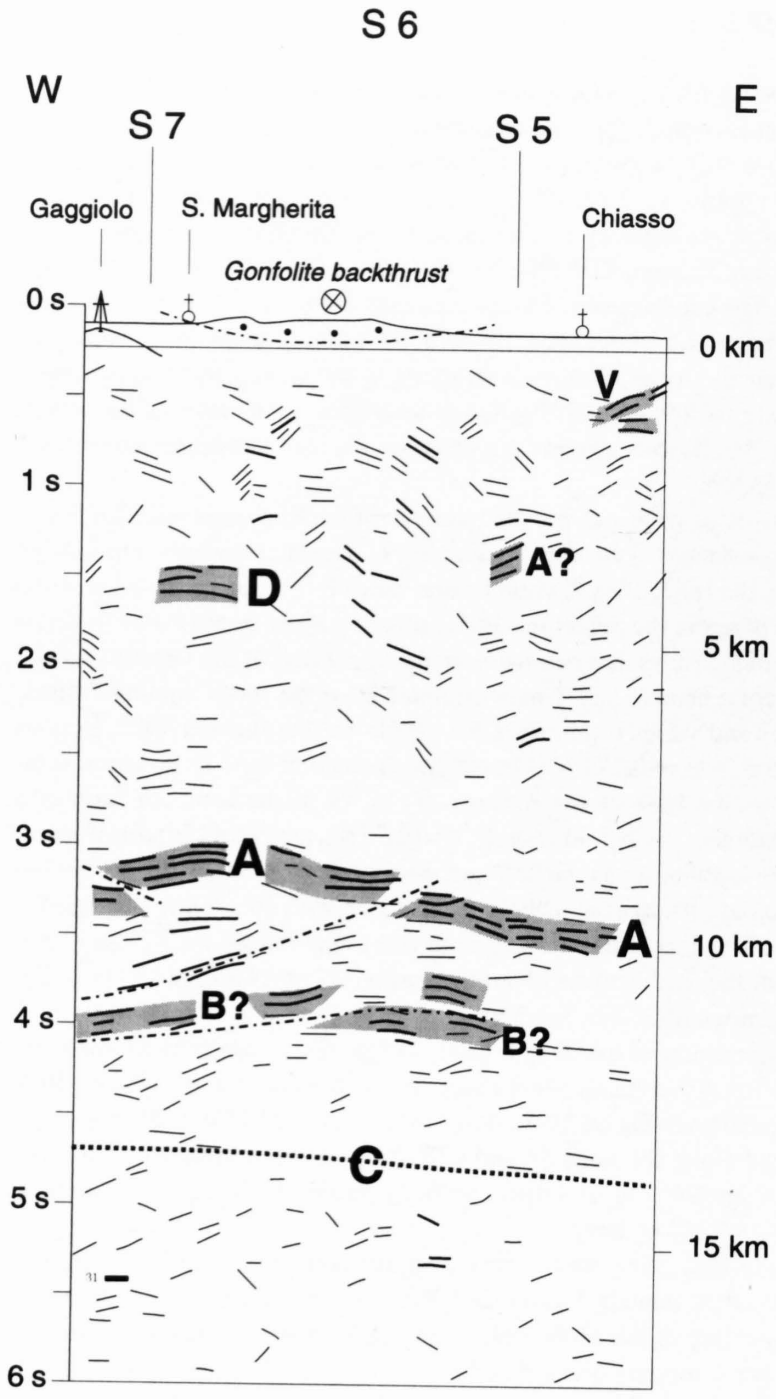

Figure 10-12
Unmigrated, handmade line-drawing of the vibroseis profile S6 with tentative geological correlations (see Figure 10-13 and discussion in the text).

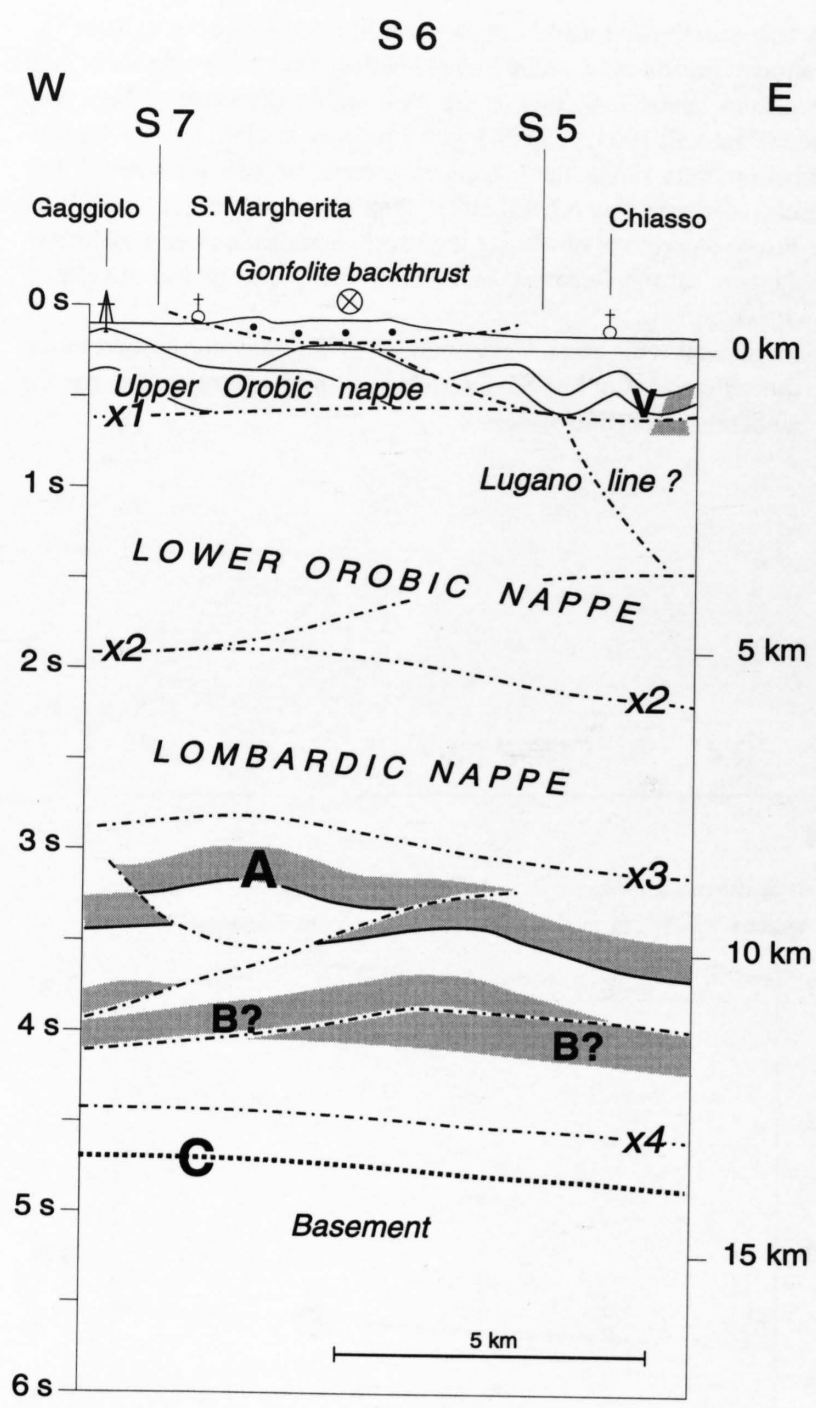

Figure 10-13
Tentative tectonic interpretation of vibroseis line S6. x1, x2, x3 and x4 show the conjectured thrust planes of the various South-Alpine nappes (Table 10-1). See text for discussion.

(Domeriano) rocks of the Stabio anticline (compare line S7, Figure 10-17) which is obviously detached in the Raibl beds in front of the Arbostora ramp-fold (front of the Upper Orobic nappe west of Lugano transverse zone, compare Figure 10-21; Schumacher et al., Chapter 15). The SSE-dipping (Arbostora) and SW-dipping (Generoso) limbs of the frontal ramp-folds may well cause lateral seismic reflections from the north. This seems to be the case for the reflection band D which can be correlated with the south-dipping reflection band D on line S7 (Figures 10-15 and 10-16) and may be attributed to Middle Triassic carbonates. The apparently west-dipping reflections V may be correlated to the SW-dipping base of the intensely folded Scaglia Group and Lombardian Flysch (Vonderschmitt 1940). These reflections appear to be truncated at the base by a shallow thrust and they cover the top of the Mesozoic Lugano fault (compare line S5 Figures 10-5 and 10-6).

2) Between 2 s and 3 s TWT, line S6 appears seismically more transparent. This may be because of the presence of a rather monotonous carbonate sequence lacking seismically significant interfaces.

3) Strong reflections are present between 3 s and 4.5 s TWT. The excellent reflection band A, composed of 3 or 4 distinct horizons, is interpreted as the base of the upper part of the Lower Cretaceous (Marne di Bruntino, Sass della Luna and Scaglia). This reflective zone between the top of the Maiolica and the base of the Lombardian flysch is well known from AGIP seismic lines (Quattrone et al. 1990, Mattavelli and Margarucci 1992). The domed geometry of this reflection band is probably mainly due to imbrication rather than to the curved line geometry. This becomes evident when reflection band A is compared to the corresponding reflections A on line S5 (Figure 10-5). The bulge could be the expression of a small WSW-ENE trending (lateral?) ramp-fold. The basal imbricates seem to be detached along the reflective horizon B which is interpreted as the Rhaetic sedimentary sequence. The top of the autochthonous basement C, according to line S5, is expected at 4–5 s TWT, equivalent to 12–15 km depth.

10.3 The Lugano section (lines S3 and S7) and its northern extension (line S1)

The Lugano section crosses the Southern Alps west of the Lugano line (Figure 10-2) comprising the seismic lines S3 and S7 (Figure 10-1). From line S3 vibroseis and dynamite data are available, from line S7 only vibroseis data. The explosion seismic line S1 extends the Lugano section towards north into the Penninic domain. Together, they offer a crustal section across the Alps from the Gotthard massif to the Po plain (Figure 10-28).

South of the Insubric line various gneisses, micaschists and some amphibolites of the southern Alpine basement crop out along the Lugano section (compare Reinhard 1964). At the surface the following Alpine structural units can be distinguished from N to S (Figures 10-2): Ivrea-Ceneri complex, Val Colla-San Marco unit, Lugano unit s.l. and Arbostora anticline. The latter three can be considered to form part of the early Alpine, probably Late Cretaceous, Upper Orobic nappe (Figure 10-2, Table 10-1; Schumacher et al., Chapter 15). However, during the Late Oligocene and Early Miocene the western end and the northern rim of the Upper Orobic nappe were structurally overprinted by the Insubric deformations (Schumacher 1990, 1991). In particular the Insubric northwestern corner of the Southern Alps, the Ivrea-Ceneri complex (Schumacher 1995), was pushed towards the SE. To the east, in the Lugano section, it formed a transpressive wedge causing back-thrusts towards the N and NW along its roof (cf. Figure 10-21).

Line S7

Line S7 is only 3.5 km long and covers the area between the southern limb of the Arbostora ramp-fold to the north (Schumacher 1990, Schumacher et al., Chapter 15) and the back-thrust Gonfolite Lombarda (South-Alpine Mo-

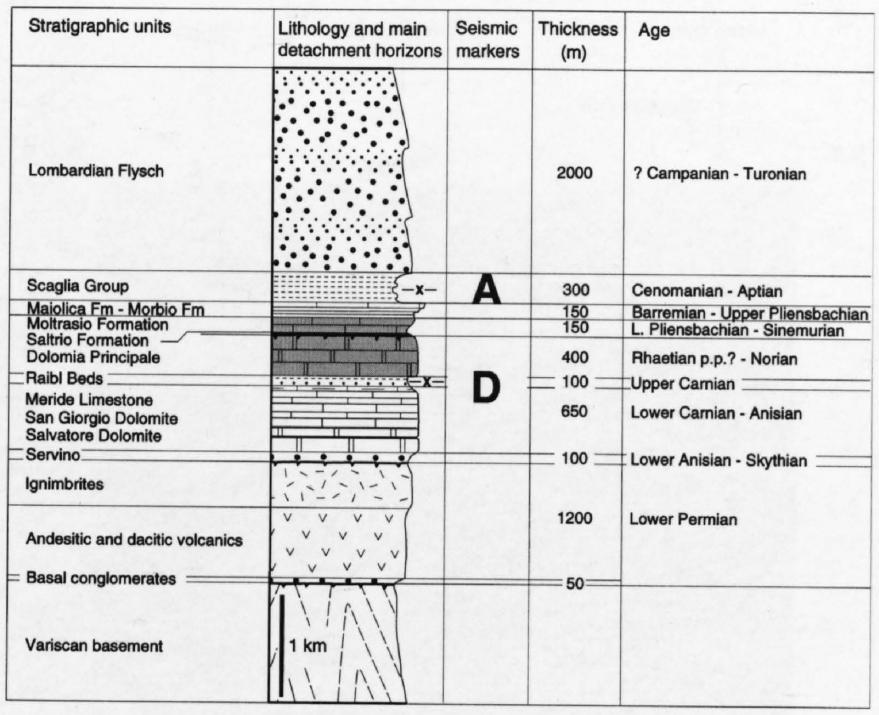

Figure 10-14
Stratigraphy of the Arbostora swell in the area north of line S7. The thin grey interval corresponds to the syn-rift deposits (compare Figure 10-3). The seismic marker D corresponds to unidentified Triassic sediments. Data from Senn (1924) and Kälin & Trümpy (1977).

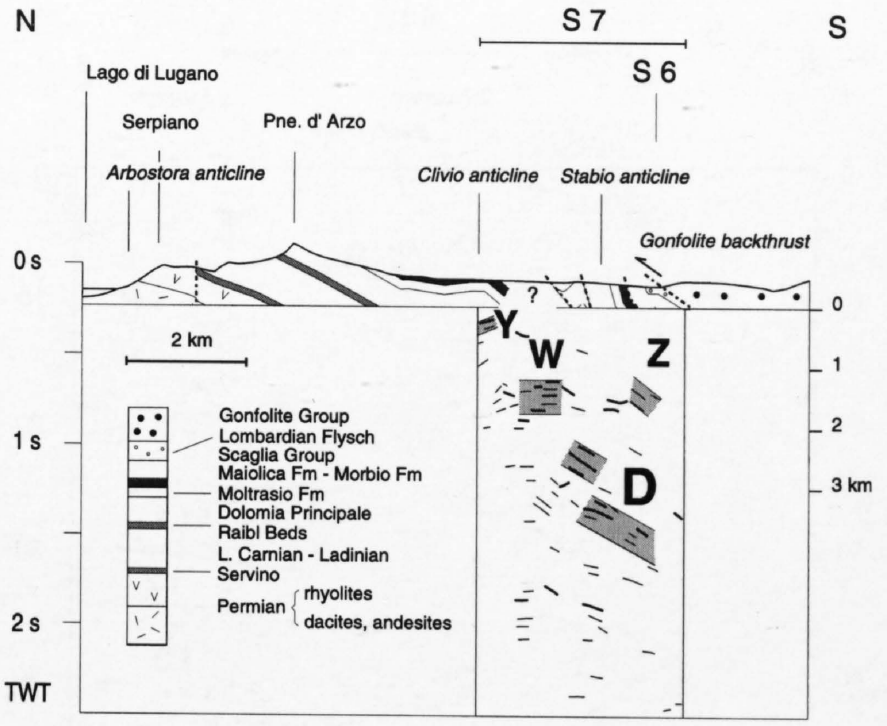

Figure 10-16
Unmigrated, handmade line-drawing of line S7 (main reflections are grey-shaded) and geological surface data (from Senn 1924) in the northern continuation.

lasse) to the south (Bernoulli et al. 1989). The coherency-enhanced final stack of this vibroseis line is shown in Plate 10-11.
Figure 10-14 shows the stratigraphy used to interpret line S7 based on data from the south-dipping Permo-Mesozoic cover immediately to the north (Senn 1924). The thickness of the Norian to Middle Liassic syn-rift deposits is drastically reduced compared to the Generoso section (Figure 10-3). The condensed Saltrio Formation documents the Arbostora swell during the Rhaetian to Early Liassic stage of rifting (Kälin & Trümpy 1977, Wiedenmayer 1963).

The seismic data from the upper part of line S7 are presented together with the intersecting western end of line S6 on Figure 10-15. Figure 10-16 shows a line drawing of the unmigrated data of line S7, with the discussed main reflections grey-shaded, and the geological surface data (Senn 1924). The same reflections after migration are shown together with the geological interpretation in Figure 10-17.
The short reflection bands Y and Z could indicate an additional narrow anticline in the shallow subsurface between the Clivio anticline and the Stabio anticline (cf. Senn 1924). These minor structures are interpreted as secondary structures of the badly distorted frontal wedge-into-split-apart triangle associated with back-thrusting of the Gonfolite Lombarda (Bernoulli et al. 1989).
The lower one of the two south-dipping reflections D correlates with the horizontal reflections D on the W–E trending crossline S6 (Figure 10-15) justifying migration in N–S direction. Migration places the reflection bands D to the north of the flat-lying reflections W (Figure 10-17). The reflection bands D and W can be attributed to Mesozoic sediments. However, as the dip of the

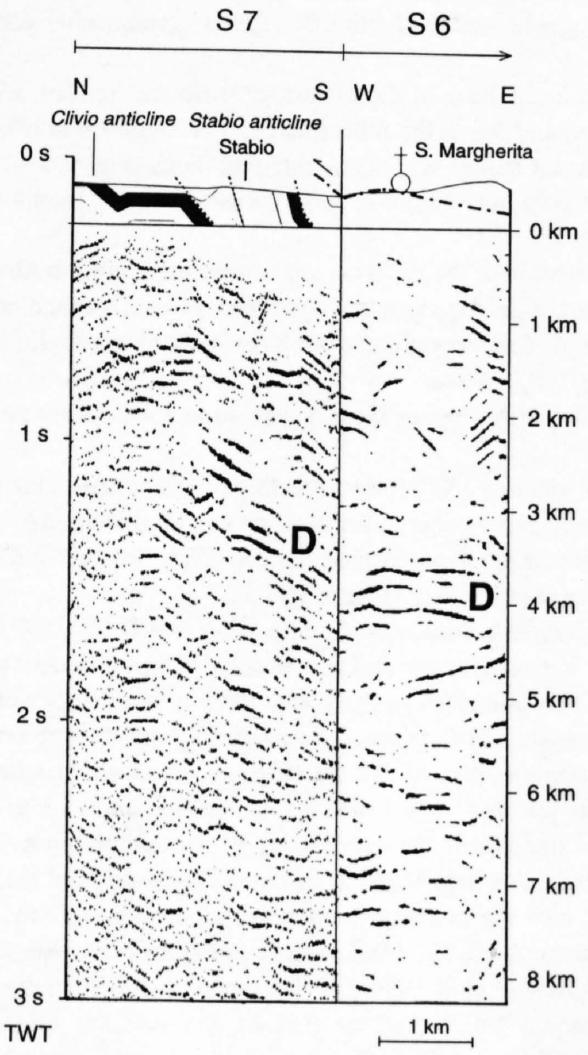

Figure 10-15
Coherency-enhanced, unmigrated vibroseis data from the upper part of line S7 (compare Figure 10-16) and of the intersecting western end of line S6 for comparison. The reflection bands D on both lines can be correlated.

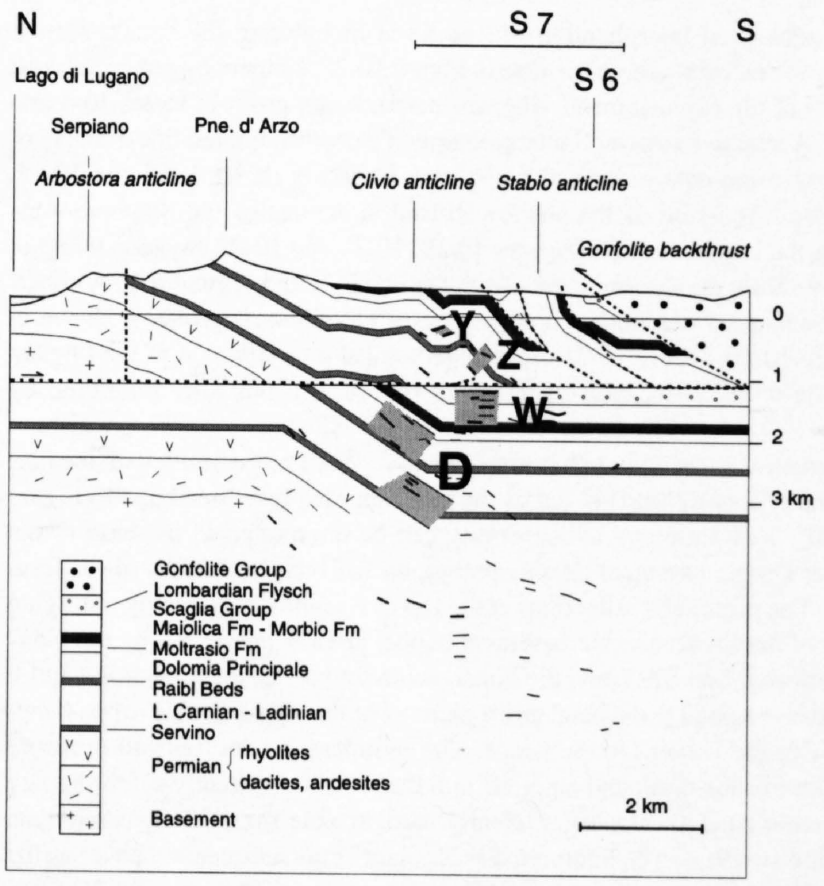

Figure 10-17
Tentative geological interpretation of line S7 showing the main reflections (grey-shaded) in a migrated position (discussion in text).

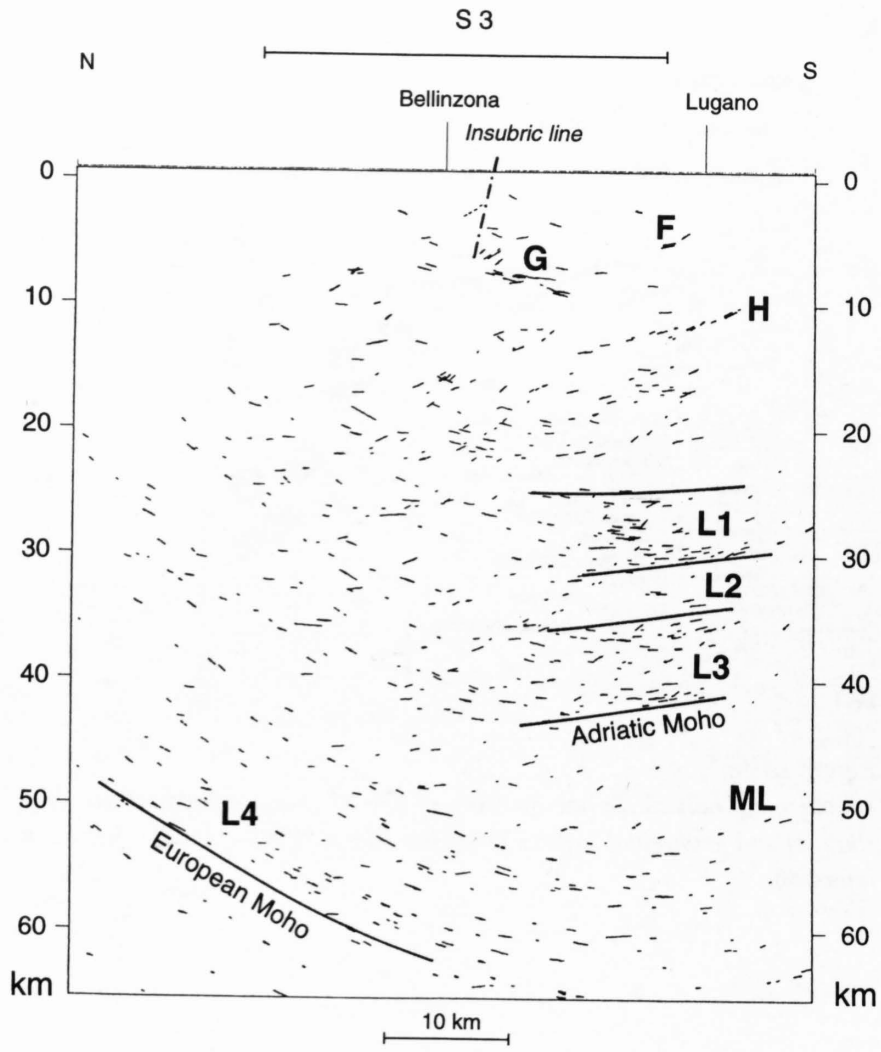

Figure 10-18
Tentative structural interpretation of the depth-migrated line drawing (from Valasek 1992) of the dynamite profile S3 (compare Figure 10-28). F: base of the Upper Orobic nappe, x1; G: probably lower part of the Mesozoic sedimentary cover of a deep Lombardic basement ramp-fold; H: parautochthonous Mesozoic sediments; L1-L3: Adriatic lower crustal units; L4: European lower crust; ML: possibly Adriatic mantle lithosphere.

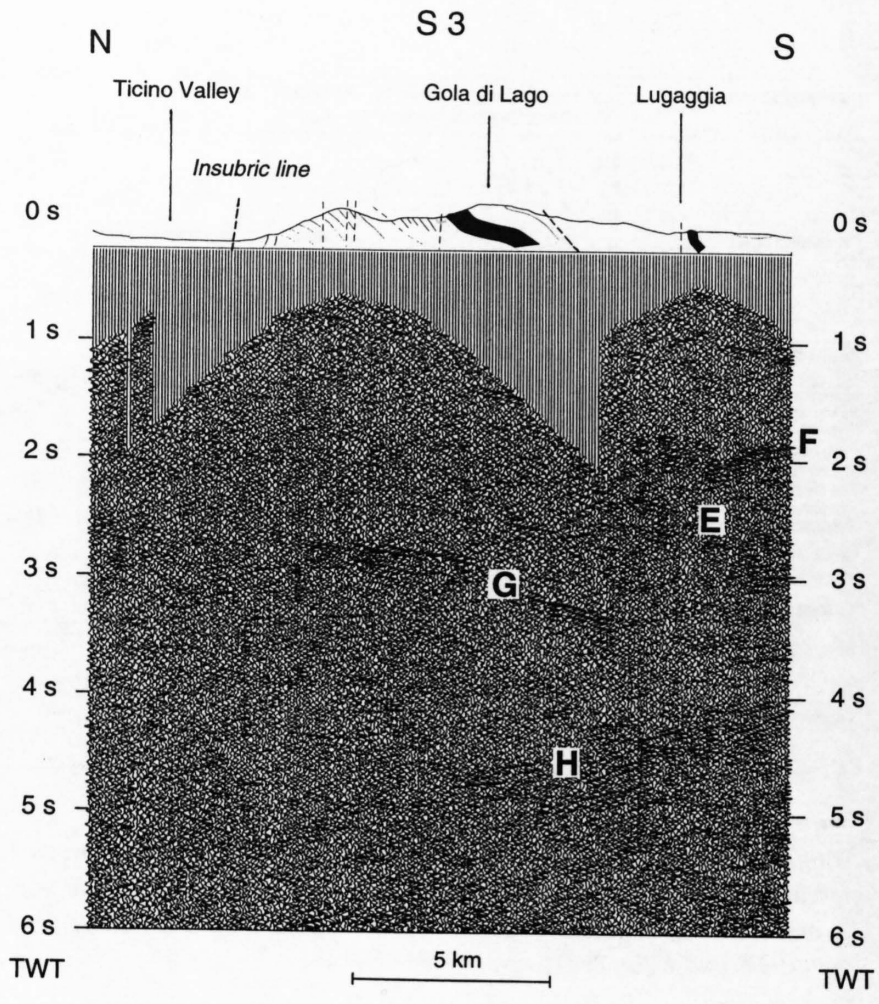

Figure 10-19
Unmigrated dynamite data from the upper part of line S3 (compare Figures 10-20 and 10-21). For the discussion of the reflection bands E–H see text.

Mesozoic cover flattens at the surface south of Pne. d' Arzo the reflections D are not a simple extension of the south-dipping Arbostora cover. They rather form the frontal limb of a deeper ramp fold below the Arbostora ramp-fold (Figures 10-17 and 10-21; Schumacher et al., Chapter 15). No significant reflections can be recognized on line S7 below 2 s108108 TWT.

Line S3

The geological interpretation of line S3 is included in the crustal section along the entire southern traverse in Figure 10-28. Coherency-enhanced final stacks of the explosion and vibroseis data sets are given in Plates 10-4 and 10-5. A tentative structural interpretation of a depth-migrated line drawing of the explosion data processed by Valasek (1992) is shown in Figure 10-18. For the discussion of the shallow crustal structures of the Southern Alps along the Lugano section Figures 10-19, 10-20 and 10-21 are added. Figure 10-19 shows the dynamite data from the upper, South-Alpine part. A coherency-enhanced and migrated upper part of the vibroseis profile is shown in Figure 10-20. Figure 10-21 offers a geological interpretation of the Lugano section with the location of the main reflection bands after migration by hand.

Informative is the domain between 1 s and 3 s TWT to the south with the horizontal reflection bands E, cut by the north-dipping reflection band F (Figure 10-20). This structural unconformity can be interpreted as the base of the Upper Orobic basement nappe ramping up flat-lying sediments of the footwall. The prominent reflections at the top of E could document the flat-lying base of the Lower Orobic basement nappe, already postulated by the interpretation of line S7. Thus, the upper, southern half of the reflection band F could correspond to the basal thrust plane *x1* of the Upper Orobic nappe ramping over the Lower Orobic nappe. The sediments in the footwall probably continue to the north and taper off into the narrow apparently south-dipping reflection band G. The latter, clearly recognizable from the dynamite data (Figure 10-19), can be interpreted as remnant of the sedimentary cover on the frontal limb of another deep-seated basement ramp-fold (Figure 10-21; compare also Figure 10-10 and Schönborn 1992).

This ramp-fold is thrust over apparently north-dipping Mesozoic sediments suggested by a 2 km (0.6-0.7 s TWT, Vp = 6 km/s) thick band of strong reflections H at the base of the South-Alpine orogenic wedge. To the north, these basal (meta)sediments reach down to a depth of about 15 km and hence to upper greenschist facies metamorphic conditions (450° C and 4 kbar).

The basal Mesozoic sediments at the frontal tip of the Southern Alps are documented by the subsurface data from the Po plain (AGIP line 3 of Pieri & Groppi 1981 and Cassano et al. 1986). Together with the NRP 20 data they now permit a first approximation of the overall geometry of the South-Alpine orogenic wedge (Laubscher 1990a, Schumacher 1990, Schönborn 1992).

Compared to the base of the Mesozoic sediments on line S5 (Figure 10-9) the position and dip of the reflection band H suggest that H is located in the roof of a basal duplex and is not autochthonous (Figure 10-21). However it was apparently not subject to large thrusting and is therefore called "Parautochthon".

The continuation of the basal detachment of the Southern Alps into the more internal part of the Alps remains undefined. From a mechanical point of view one can argue for decoupling at the base of an "orogenic lid" (Figure 10-28; Laubscher 1983, 1994).

The steeply north-dipping Insubric mylonite zone cannot be recognized on line S3.

Between 6 s and 8 s TWT (corresponding to 18 km and 24 km depth in Figure 18) a rather chaotic pattern of reflections can be attributed to a highly mobile amphibolite facies metamorphic middle crust, possibly interfingering with some lower crustal flakes (Figure 10-28).

Seismic refraction data (e. g. Mueller et al. 1980, Ye 1992) determine the boundary between upper and lower crust (Conrad discontinuity) at about 8 s TWT. This coincides roughly with the top of a pile of alternating reflective and transparent domains documented by the seismic reflection data in the southernmost part of line S3 (Figures 10-18 and 10-28). In the upper part of this pile (8 s – 14 s TWT) two reflective zones, L1 and L3, are separated by a transparent domain L2. They are interpreted as a lower crustal stack with the Adriatic Moho at its base. The position of the Adriatic Moho coincides with the velocity jump from 6.9 km/s to 8.1 km/s below the Insubric line at about 15 s TWT as inferred from refraction along line Lago Bianco-Verona (Egloff 1979, Deichmann et al. 1986). In this case the transparent domain ML would be part of the Adriatic lithospheric mantle, whereas for the transparent domain L2 seismic refraction velocities suggest lower crustal material.

Another reflective domain L4 appears around a depth of 16 s to 21 s TWT (48 km to 63 km, in Figure 10-18). It could represent a remnant of European lower crust and Moho subducted below the Adriatic plate.

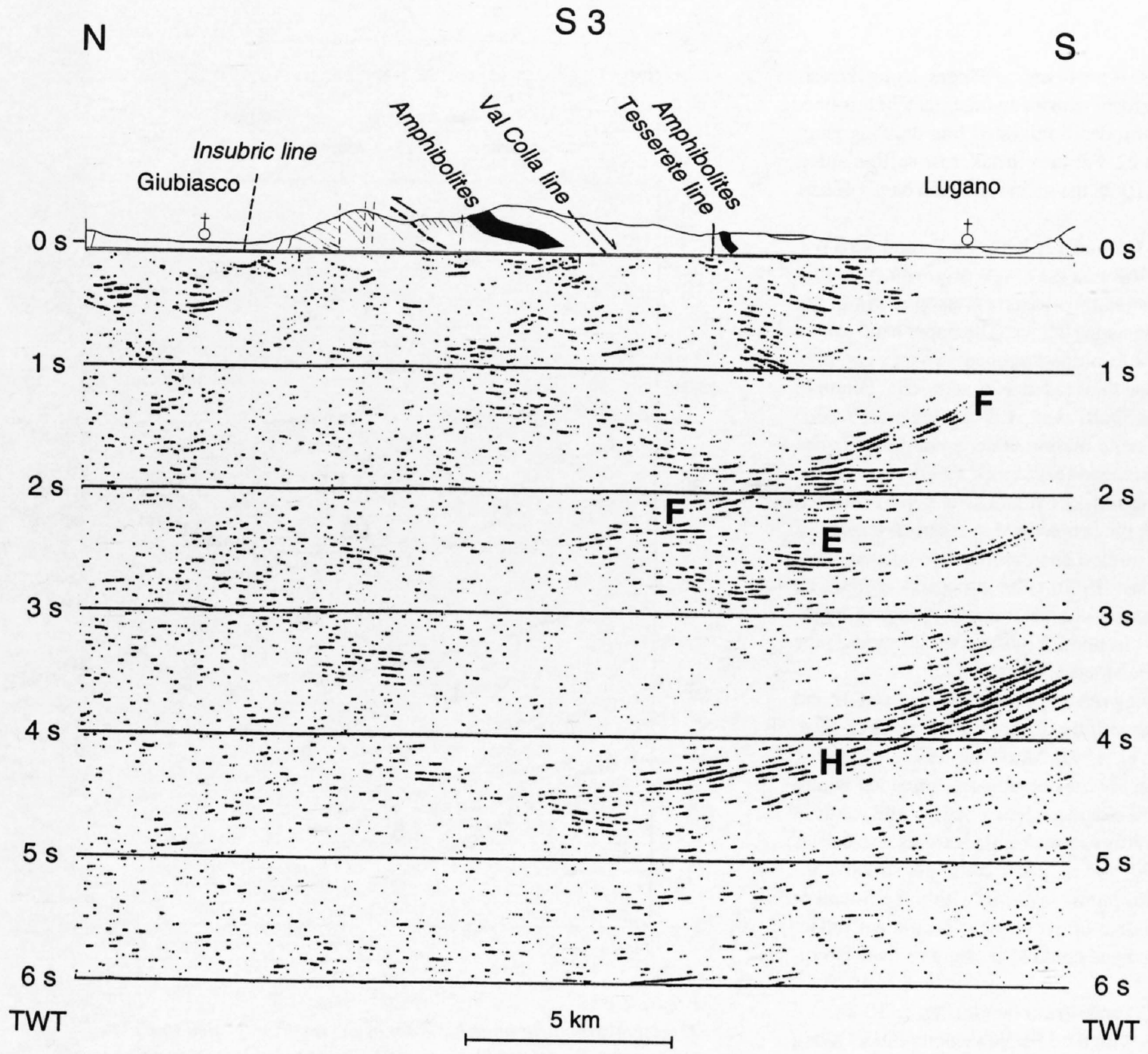

Figure 10-20
Coherency-enhanced, time-migrated upper part of vibroseis profile S3 with surface geology (see Figure 10-21 and discussion in the text).

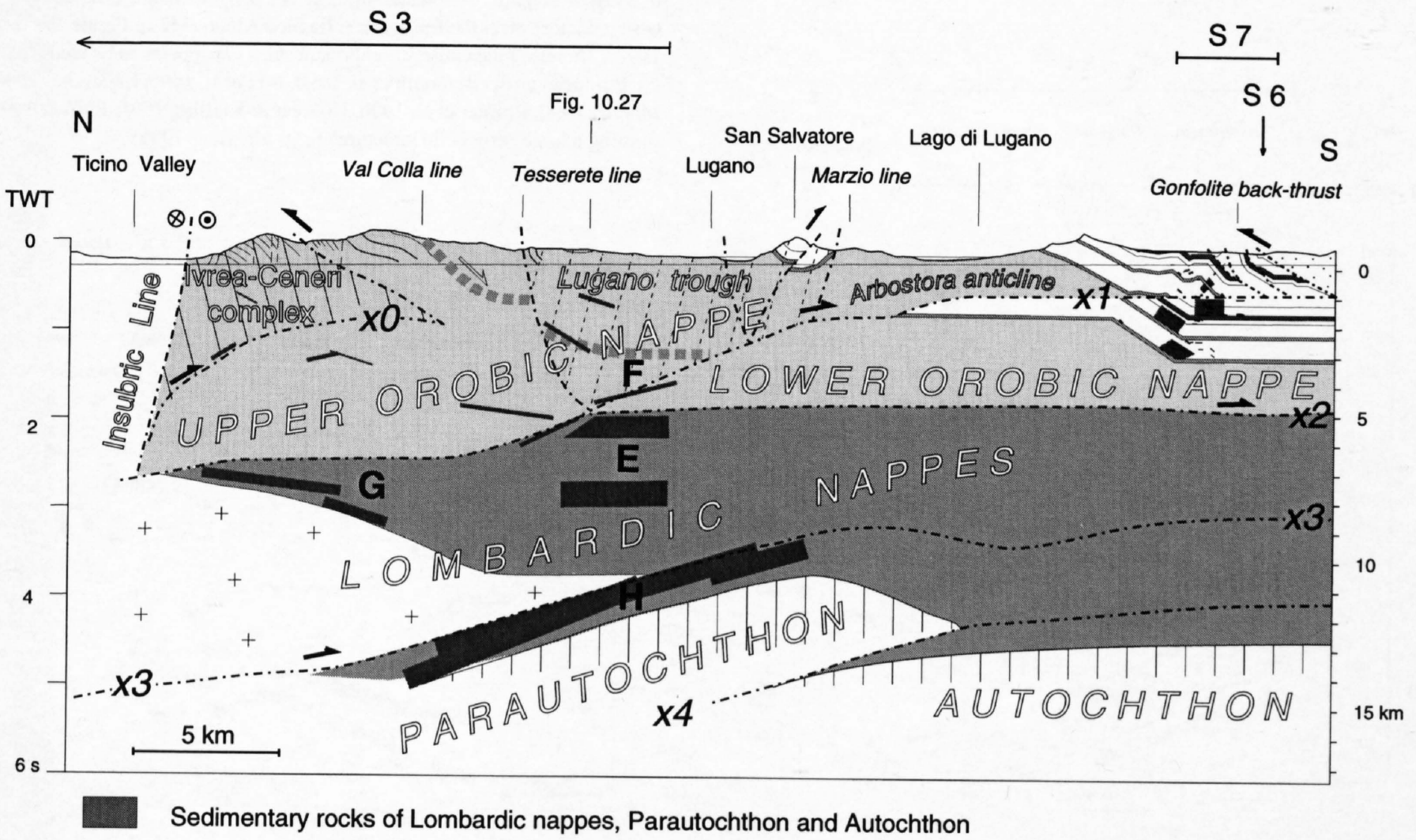

Figure 10-21
Geologic profile along the Lugano section (lines S3 and S7) based on the interpretation of hand-migrated data (main reflectors grey-shaded). x0, x1, x2, x3 and x4 are supposed thrust planes separating the various South-Alpine nappes (see Table 10-1). See text for discussion.

Line S1

The dynamite line S1 was recorded across the Penninic nappes, along the Calanca valley. Plate 10-1 shows the coherency-enhanced final stack of this line. A tentative structural interpretation of a depth migrated line drawing from Valasek (1992) is shown on Figure 10-22. For the crustal cross section along the entire southern traverse on Figure 10-28 the main reflection bands of line S1 were migrated by hand.

The two horizontal reflection bands (1) and (2) between 2 s and 4 s TWT (6–12 km depth) beneath shot point Valbella may well originate from thin layers of metasediments, separating crystalline basement nappes within the flat laying northern part of the Penninic nappe edifice. The upper band can be correlated with the base of the Simano-Leventina-Lucomagno nappe complex (e. g. Frei et al. 1989). Below this nappe the existence of additional Penninic basement nappes seems possible (Bernoulli et al. 1990). However, repetitions of seismic markers due to large scale folding under amphibolite facies metamorphic conditions can not be excluded (e. g. Steck 1990).

The south-dipping reflections (3) at around 4 s TWT (12 km depth) between shot points Hinterrhein and Valbella fit the conjectured southern extension of the Gotthard massif cover. Near the surface this basement/cover contact is subvertical or even overturned (Probst 1980). The proposed correlation therefore suggests flattening of the contact at greater depth. Along strike reflections (3) match with reflections B4 in line C2 of the central traverse (see Figures 11-3 and 11-6 of Pfiffner & Heitzmann, Chapter 11).

Of particular interest is the north-dipping reflection band (4) between 3 s and 5 s (9–15 km depth), often correlated with the Insubric mylonite belt (e. g. Bernoulli et al. 1990, Heitzmann et al. 1991, Marchant 1993). However, lithologic layering, e. g. lenses of amphibolites or marbles contained within granitic gneisses and micaschists in the Southern Steep belt, would result in higher impedance contrasts than anisotropy of mylonitic textures and fabrics (Kern 1990, Siegesmund & Kern 1990) and may also cause constructive interference of reflected energy. Thus lithologic layering within the Southern Steep belt may be an excellent candidate to cause these prominent reflections. On the other hand this reflection band could also originate from a remnant of the Alpine ophiolitic suture.

The reflective domains (7) between 20 and 40 km depth (Figure 10-28) are interpreted as lower crust, in harmony with the seismic velocity model along the EGT by Ye (1992) based on refraction data. They seem to form a wedge tapering off towards the N. However, the top of these probably mainly Adriatic lower crustal units is located about 5 km higher than in the southern part of line S3. This observation and the structural discordances within the lower crustal stack seem to point also to south-vergent thrusting and wedging.

The south-dipping reflection band (9) at about 50 km depth can be interpreted as a fragment of European lower crust (compare lowermost reflective crust of Pfiffner & Hitz, Chapter 9, and Pfiffner & Heitzmann, Chapter 11). Its base coincides with the European refraction Moho (M2 in Figure 10-28; Ye 1992). Therefore the entire lower crustal stack (7) appears to be wedged into the European crust (Bernoulli et al. 1990, Frei et al. 1990, Laubscher 1990b, Mueller 1990, Pfiffner et al. 1990, Holliger & Kissling 1991, Pfiffner 1992), forming a large "crocodile structure" (e. g. Meissner 1989).

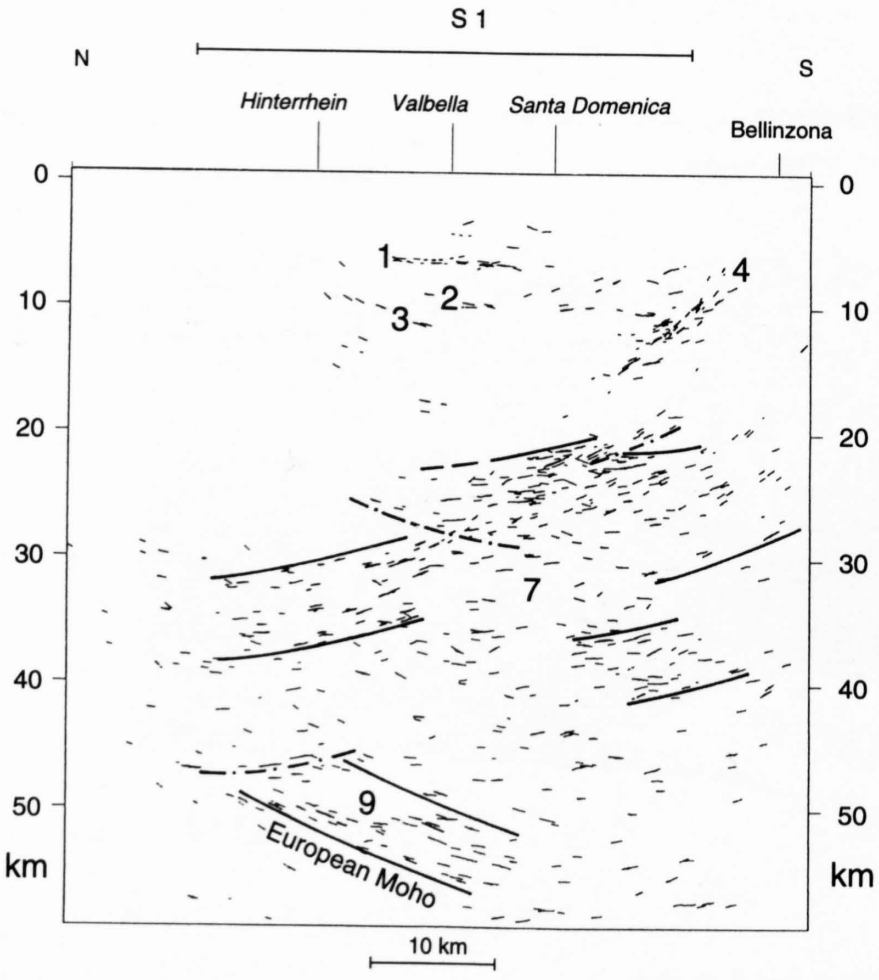

Figure 10-22
Tentative structural interpretation of the depth-migrated line drawing (from Valasek 1992) of the dynamite profile S1 (see Figure 10-28 and discussion in the text).

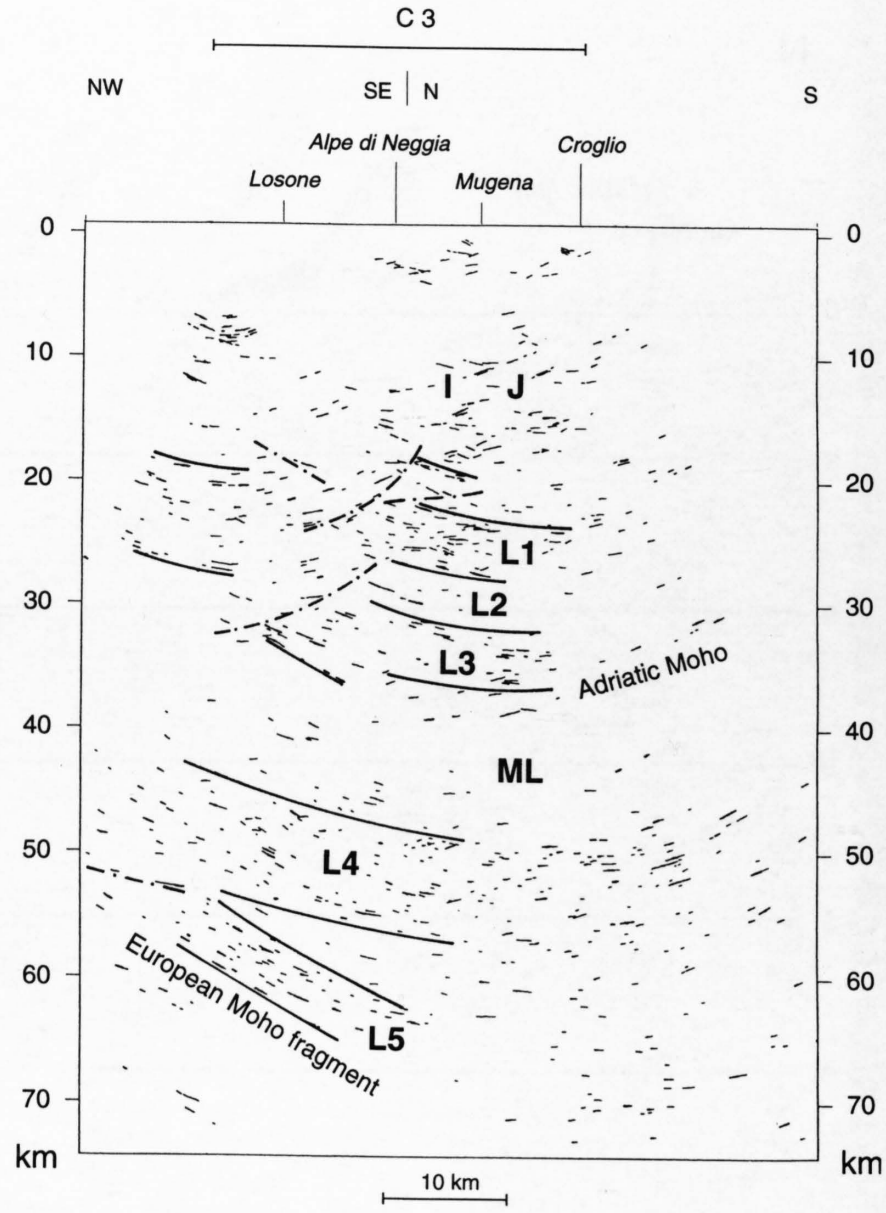

Figure 10-23
Tentative structural interpretation of the depth-migrated line drawing (from Valasek 1992) of the dynamite profile C3. I, J: (meta)sedimentary layers near the base of the South-Alpine orogenic wedge; L1 – L3: Adriatic lower crustal units; L4, L5: probably European lower crustal units; ML: possibly Adriatic mantle lithosphere. See also Figure 11-4.

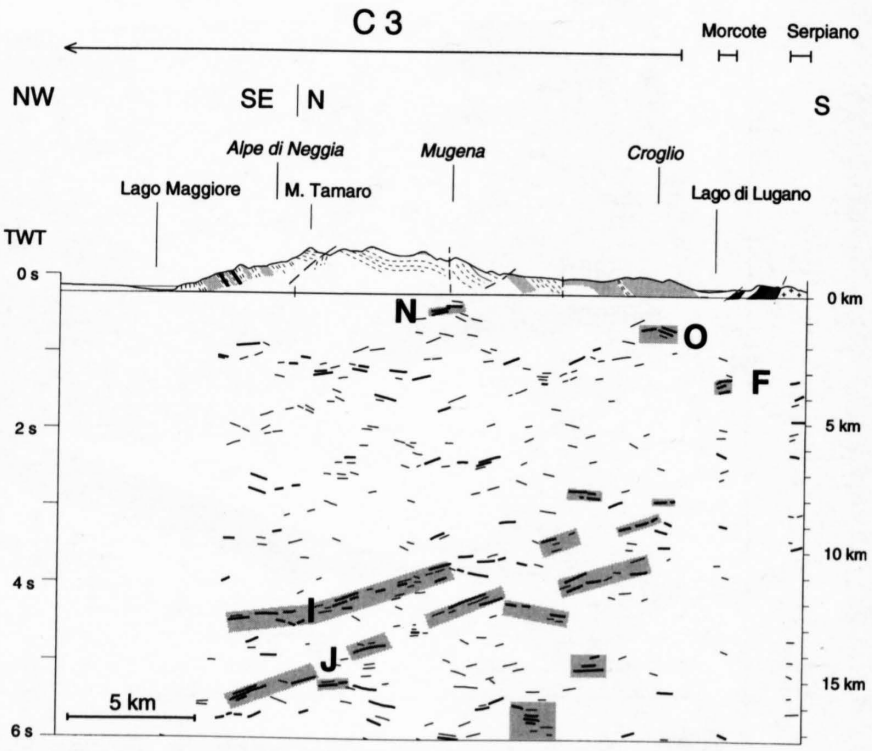

Figure 10-24
Unmigrated, handmade line-drawing of the upper and southern part of line C3 with main reflections bands grey-shaded (see Figure 10-25 and discussion in the text).

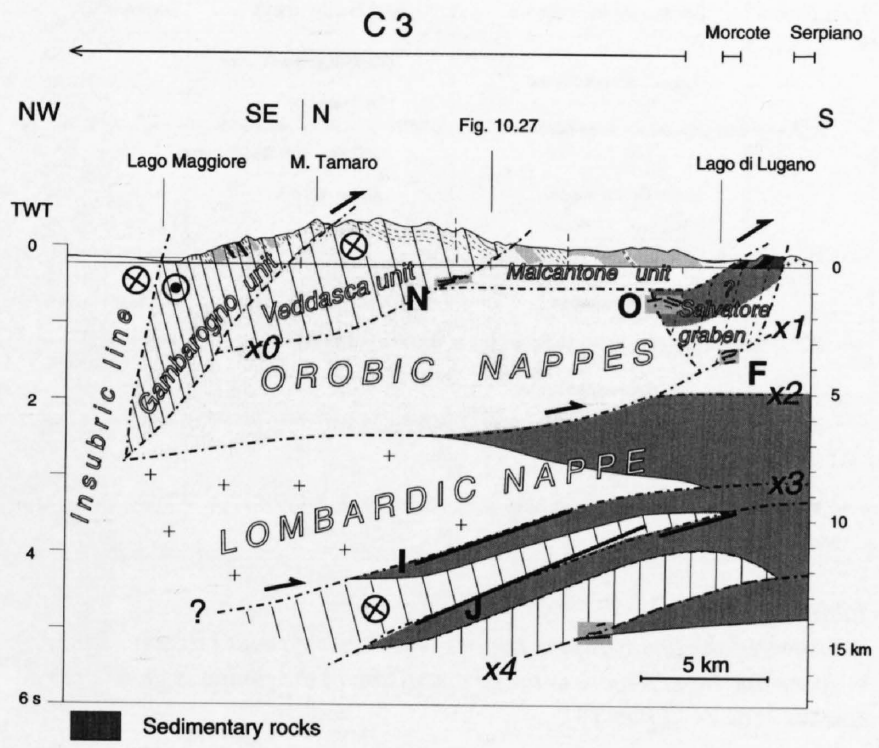

Figure 10-25
Tentative geological profile along the Malcantone section based on the interpretation of hand-migrated data (main reflectors grey-shaded) from the upper part of line C3 (discussion in the text). x0, x1, x2, x3 and x4 are supposed thrust planes of the various South-Alpine basement nappes (see Table 10-1 and compare S3, Figure 10-21).

10.4 The Malcantone section (line C3)

The Malcantone section follows the dynamite line C3 crossing the Insubric line near Losone, west of Locarno (Figure 10-1). It turns from NW–SE into N-S direction near Monte Tamaro and has its southern end in the Tresa valley south of Malcantone. In addition, shot Croglio was registered to the south along two short line segments near Morcote and Serpiano.

Along the Malcantone section two units of the Ivrea-Ceneri complex (Schumacher 1995), the Gambarogno and the Veddasca units, are wedged into and overlie, respectively, the Upper Orobic nappe (Figure 10-2). They both continue to the west across Lago Maggiore, and their overall transport direction was towards southeast (Schumacher et al., Chapter 15). In front of the Ivrea-Ceneri complex the Malcantone unit (part of the Lugano unit s.l.) was peeled off from the roof of the Upper Orobic nappe and was thrust probably about 3 to 5 km to the south over the sediments of the San Salvatore graben (Figure 10-25).
Petrographically the entire basement cropping out along the Malcantone section belongs to the Ceneri zone, consisting of amphibolite facies granitic gneisses, paragneisses, amphibolites and ultramafics (Reinhard 1964, Boriani et al. 1977). It is separated from the Permian volcanic rocks of the Arbostora anticline to the south by the strongly disturbed Mesozoic sedimentary rocks of the narrow Salvatore-Val Cuvia belt (Figure 10-2 and 10-25).

Line C3

The coherency-enhanced final stack of this line is shown in Plate 10-12. In order to discuss this line on the scale of the entire crust, a tentative structural interpretation of a depth-migrated line drawing from Valasek (1992) is shown in Figure 10-23. This aspect is also discussed by Pfiffner & Heitzmann in Chapter 11 in the context of the Central Traverse (cf. Plate 11-1 and Figure 11-4). However, for the discussion of the shallow crustal structures of the Southern Alps along the Malcantone section and to compare them with those along the Lugano section, Figures 10-24 and 10-25 are added.
Figure 10-24 shows an unmigrated, handmade line-drawing of the South-Alpine, upper part of line C3 and Figure 10-25 its tentative geological interpretation after migration. Reflections N are located in the continuation of the Arosio thrust at the base of the Veddasca unit. They may be correlated with the cataclastic rocks of this fault zone. Reflections O could originate from sediments of a possible extension of the Salvatore trough below the overthrust Malcantone unit. The reflection band F can be correlated with the base of the Upper Orobic nappe, ramping over the Lower Orobic nappe (compare line S3, Figure 10-21). To the north, the base of the Orobic basement nappes appears to reach down to 7 km depth. The sedimentary rocks underlying the Orobic nappes seem not to extend as far north as in the Lugano section.

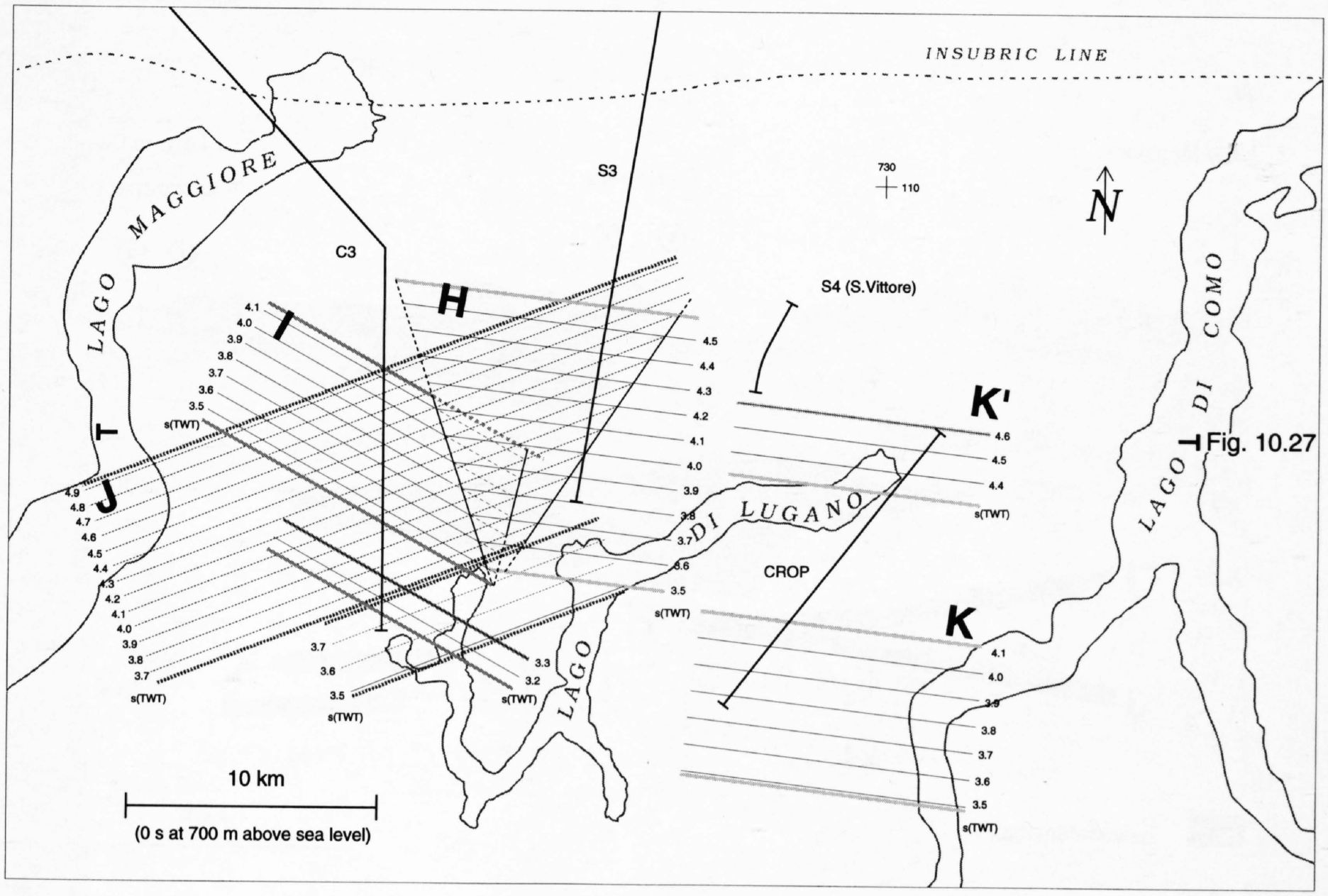

Figure 10-26
Map of isochrons (two-way travel time [TWT] in seconds) from the top of the parautochthonous Mesozoic (respectively base of the Lombardic nappes) after updip migration (assuming planar reflectors H – K). Compare Figures 10-10, 10-21, 10-25 and 10-27.

Although line C3 passes nearby the easternmost outcrops of the Ivrea zone with its lower crustal rocks (e. g. Schmid 1993) and crosses the eastern end of the Bouguer anomaly attributed to the Ivrea body (Giese 1968, Kissling 1980), no evidence for an eastern subsurface continuation is given by the seismic reflection data.

Particularly interesting are the two reflection bands I and J (SAT 1 and SAT 2 of Pfiffner & Heitzmann , Chapter 11) from the base of the South-Alpine orogenic wedge. How do they correlate with basal reflection band H on line S3? Because the reflection bands I and J continue across the kink of line C3 near Monte Tamaro (Figures 10-24 and 10-25), their true dips to the NE and NW, respectively, can be estimated, assuming planar reflectors. Their contours are represented by isochrons, and to get the true dip of the reflectors the isochrons are migrated perpendicular to strike (the migrated contour map is shown in Figure 10-26). The two reflective layers I and J converge towards the east where they meet with the reflection band H (line S3). Their geometric configuration suggests an oblique ramp with a basal thrust sheet wedging out towards the Lugano section. This is illustrated by the geologic W–E section shown in Figure 10-27. Similar to reflection band H on line S3, the two reflective zones I and J on line C3 are interpreted as Mesozoic (meta)sedimentary layers, the transparent domain between them as basement.

Deeper data, displayed in Figure 10-23, show both, N- and S-dipping reflections between –18 km and – 40 km (6 s – 13 s TWT). The upper boundary of this domain harmonizes with the change from upper to lower crustal P-wave velocities indicated by refraction data. The lower boundary roughly corresponds to the location of the north-dipping Adriatic refraction Moho. A transparent domain L2, separating this domain into an upper and a lower reflective zone, L1 and L3, tapers off towards the north. The whole configuration (L1 – L3) is interpreted as a lower crustal stack (compare Figure 10-28). The transparent domain ML of about 10 km thickness (beneath L3) probably represents lithospheric mantle of the Adriatic plate.

The 10 km thick reflective domain L4 still further down forms an apparently open synclinal structure between –42 km and –57 km (14 s and 19 s TWT) after migration. These reflections too can be interpreted to be of lower crustal origin. The bottom of the lowermost, 5 km thick band of apparently SE-dipping reflections L5, between –54 km and –66 km (18 s and 22 s TWT), can be interpreted as a fragment of the European Moho.

Main thrusts	South - Alpine nappes	Basement parts	Sedimentary parts
TOP	Ivrea - Ceneri complex	Gambarogno unit Veddasca unit	
x0	*Late Oligocene - Early Miocene (= INSUBRIC)*		
	Upper Orobic nappe	Val Colla - San Marco unit Lugano unit s. l. Arbostora unit	Grigne Salvatore - Val Cuvia belt
x1	*Late Cretaceous - Paleogene(?) (= OROBIC)*		
	Lower Orobic nappe	Mezzoldo unit	Generoso unit
x2	*Paleogene(?) - Middle Miocene (= OROBIC and LOMBARDIC)*		
	Lombardic nappe system		Milan belt
x3	*Middle Miocene - Late Miocene (= LOMBARDIC)*		
	Parautochthon		
x4	*Middle Miocene - Late Miocene (= LOMBARDIC)*		
BOTTOM			

Table 10-1
Relations of the South-Alpine nappes and thrust systems (x0, x1, x2, x3, x4) in space and time. A more detailed discussion of the timing is given in Schumacher et al. (Chapter 15).

10.5 Discussion and conclusions

The NRP 20 seismic-reflection profiles through the Southern Alps are compatible with the concept of a pile of nappes including crystalline basement and sedimentary rocks, above an "autochthonous" to "parautochthonous" basement whose top is at -14 km beneath the Monte Generoso area (Figure 10-10). A schematic overview of the South-Alpine nappes and the associated thrust faults in the investigated area is given in Table 10-1. Together with the subsurface data from the Po plain the NRP 20 data allow to determine the overall geometry of the South-Alpine orogenic wedge.

In order to give an idea about the three-dimensional nappe geometry a W–E geological cross section (Figure 10-27) was added to the geological interpretations of the N-S sections (Figures 10-10, 10-21 and 10-25). Three tectonic levels are distinguished from the top to the bottom: 1) the Orobic nappe sys-

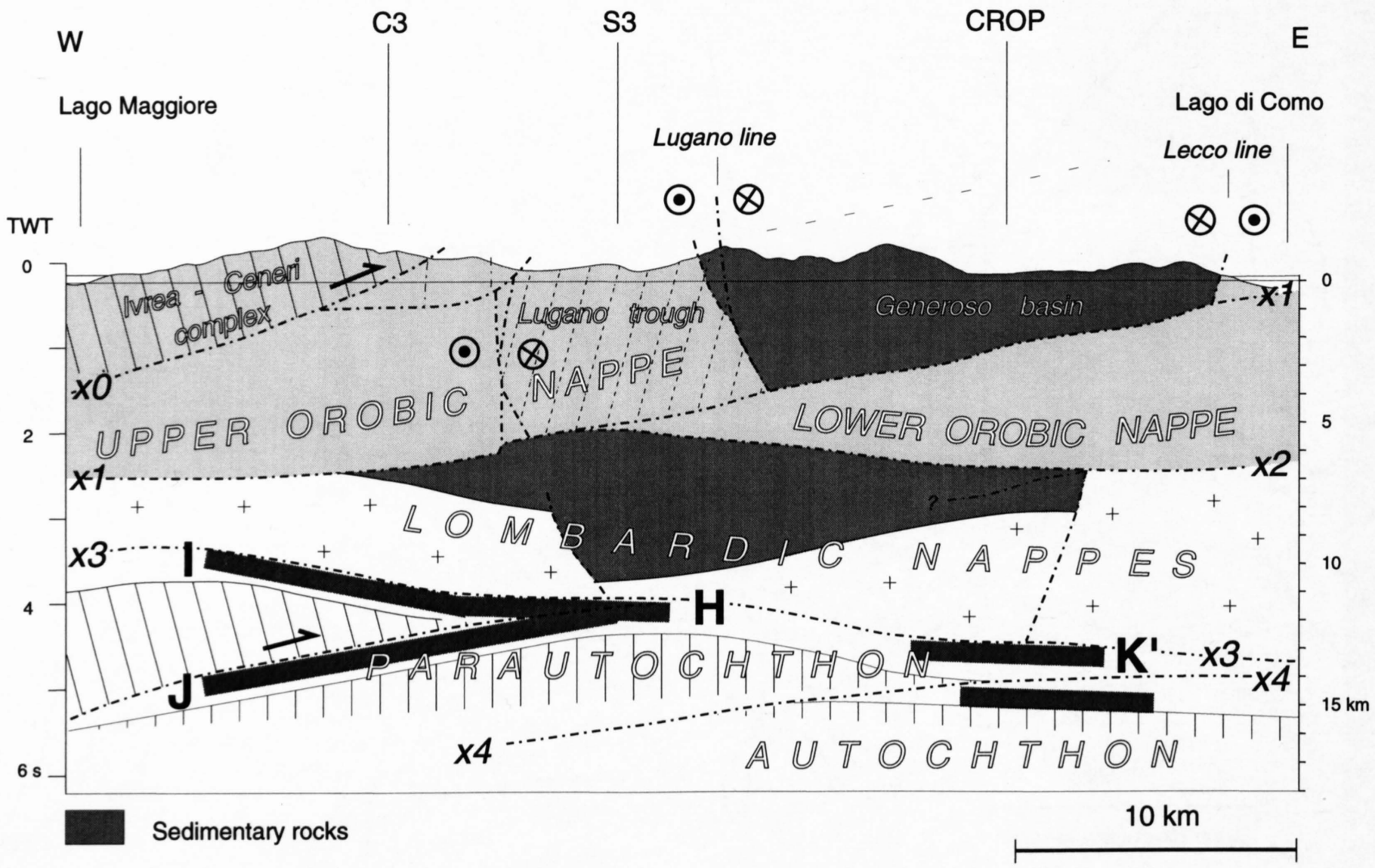

Figure 10-27
Geologic profile in W–E direction across the western Southern Alps between Maccagno on Lago Maggiore and Bellano on Lago di Como (for location see Figure 10-26). The geometry of the basal imbricates results from the migrated isochrons on Figure 10-26. Time to depth conversion is based on an average P-wave velocity of 6 km/s. x0, x1, x2, x3 and x4 are the supposed thrust planes of the various South-Alpine nappes (see Table 10-1 and discussion in the text).

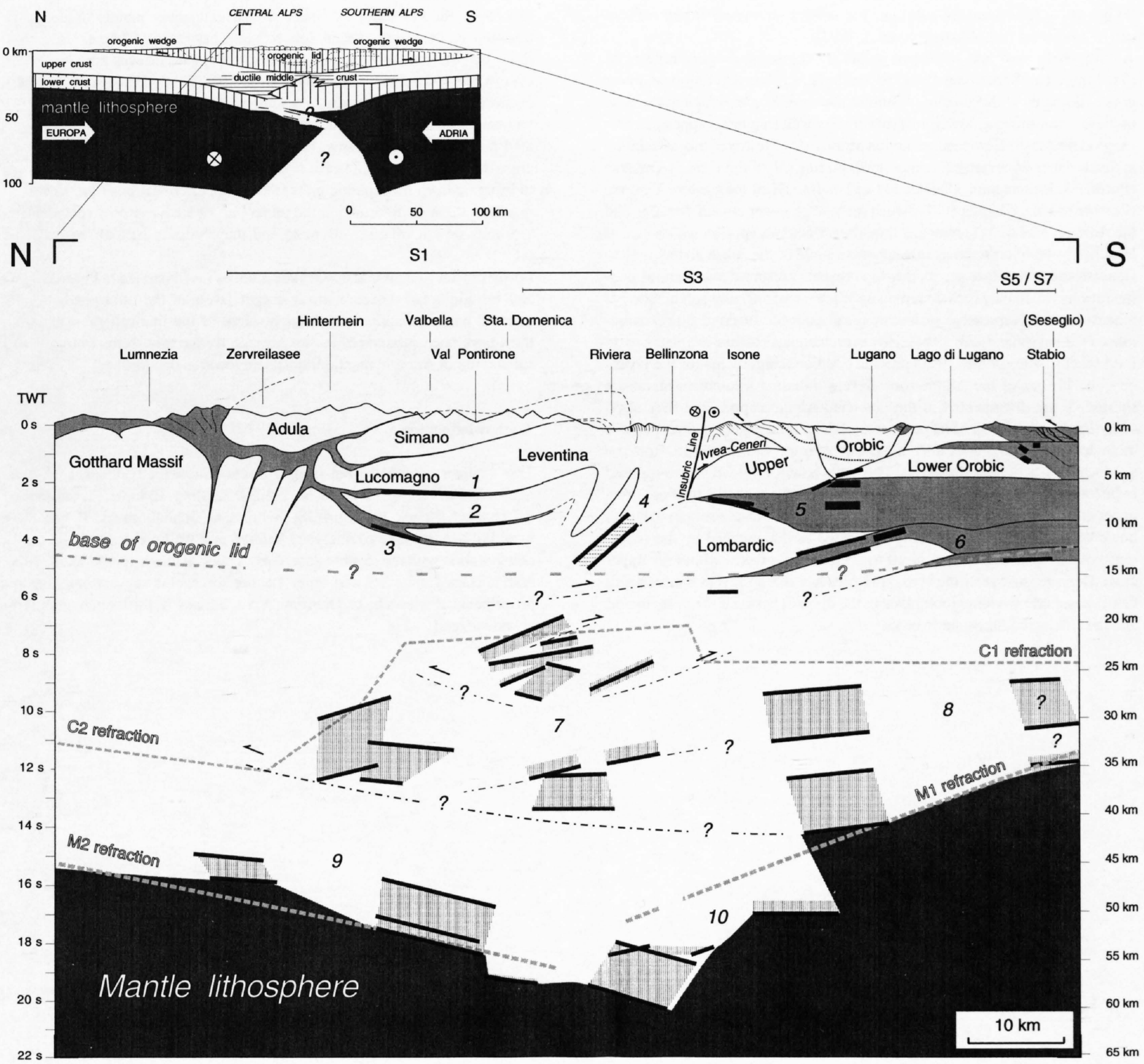

Figure 10-28

General crustal profile along the southern traverse showing the main reflection bands and reflective domains (narrow vertical ruling) in a hand-migrated position. The km-scale is based on the assumption of an average P-wave velocity of 6 km/s. light grey: Mesozoic to Tertiary sediments and metasediments; white: crystalline crustal rocks; dark grey: lithospheric mantle. The locations of the refraction Moho (M1: Adriatic Moho, M2: European Moho) and the top of the refraction lower crust (C1: Adriatic Conrad, C2: European Conrad) are adapted from Ye (1992). The conjectured base of the orogenic lid (after Laubscher 1994) is shown schematically. This basal detachment becomes better defined towards the frontal parts (orogenic wedges) than it is in the internal part. (1)-(3) dividing sedimentary layers of the Penninic nappes, (4) probable extension of the Southern Steep zone, (5) sediments of the Lombardic nappes (Milan belt), (6) parautochthonous sediments, (7) lower crustal stack (probably mainly of Adriatic and subordinately of European origin), (8) Adriatic lower crust, (9) European lower crustal fragments, (10) upper mantle flakes and deep crustal fragments.

The schematic lithospheric section across the Alps (in the upper left corner; modified after Laubscher 1994) gives the location of the crustal profile within the entire collision zone.

tem (Upper Orobic nappe and Lower Orobic nappe) axially plunging to the WSW, 2) the Lombardic nappe system and 3) the basal duplexes (Parautochthon). In addition, the Ivrea-Ceneri complex is thrust towards southeast over the western end of the Upper Orobic nappe. Interestingly, the sedimentary rocks below the Orobic nappes seem to extend much further to the north on line S3 than on adjacent sections both west and east. This may be explained by assuming a Mesozoic basin in the Lombardic nappe system similar to the Generoso basin in the Orobic nappe system (Figure 10-27).

In all geological sections, the top of the basal Mesozoic sediments (H, I, J, K') is taken from the migrated isochrons in Figure 10-26, converted to depths with an average P-wave velocity of 6 km/s. Based on these data, an additional thrust sheet between the "Parautochthon" and the Lombardic nappes is shown in the west of Figure 10-27, tapering off towards east. Take note of the structural trends of the imbricated basal sediments in Figure 10-26 which parallel the southern Alpine front at the surface (Mendrisiotto embayment).

The main results of the South-Alpine seismic-reflection data (southern traverse) for the deep crustal configuration of the Alps are summarized in Figure 10-28. The top of the lower crust (Conrad discontinuity) below the Southern Alps of Ticino is not clearly defined by the seismic reflection pattern but can be estimated using refraction data (Ye 1992) and stacking velocities (Valasek 1992) to be at a depth of approximately 20 km to 25 km (C1 in Figure 10-28). The base of the lower crust, the Adriatic Moho, is better constrained. It dips to the north from – 35 km below Chiasso (Seseglio in Figure 10-28) to approximately – 45 to – 50 km below the Insubric line, which agrees with the position of the refraction Moho (M1 in Figure 10-28; ETH Working Group on Deep Seismic Profiling 1991). The divergence of the Adriatic Conrad and Moho discontinuities towards the Central Alps suggests wedging of the lower crust towards south, in addition to prominent wedging towards north (Adriatic wedge). This may have resulted in a lower crustal stack with a complicated internal structure (7 in Figure 10-28; cf. Laubscher 1994), possibly including also some upper mantle slices. However, the data

do not allow for an unique solution, and several alternative interpretations can be discussed (e. g. Musacchio et al. 1993).

A completely new and important result are the south-dipping reflections (9 in Figure 10-28) between 45 and 65 km depth, attributed to European lower crustal domains with European Moho at the base. The envelope at the base of these south-dipping, lowermost reflective crustal fragments appears to correspond well to the European refraction Moho (M2). However, this correlation is much better documented farther north on line C1 of the Central Traverse (Pfiffner & Heitzmannn, Chapter 11) and on line E1 of the Eastern Traverse (Pfiffner & Hitz, Chapter 9). Between these deep lower crustal domains and the Adriatic Moho (M1) above, a transparent domain appears which can, at least partly, be interpreted as lithospheric mantle of the Adria plate.

Deep-seismic sounding across the Alps reveals present-day structural configurations which may include remnants of previous, different subduction geometries and transpressive structures (e. g. possible inverted flower structures, cf. Laubscher 1983, 1994). However, material balance estimates (e. g. Laubscher 1990c, 1990d, 1991) provide additional arguments for the geometry and history of the Alpine root. Several hundred kilometers of crustal shortening are documented in the obducted Alpine nappes and they obviously imply subduction of large masses of deep lithospheric counterparts. A main detachment has to separate the obducted upper crustal nappes from the subducted parts of the lithosphere. This detachment level which is supposed to be located near the brittle-plastic transition can be seen like the base of an upper crustal "orogenic lid" (Laubscher 1983). The lithosphere below the lid, however, is not simply and totally subducted as documented by the occurrence of eclogites and lower crustal to upper mantle flakes within the upper crust. Deep seismic profiling across the Alps has also shown as a main result that lithospheric wedging took place in the domain between the orogenic lid and the subducted lithospheric roots.

Moreover, the obduction of lower crustal and upper mantle units, as for example in the Ivrea system (cf. Schumacher et al., Chapter 15), illustrates that the domain of the upper crustal orogenic lid was not always and everywhere completely decoupled from the deeper lithosphere. Largely decoupled were the thin-skinned nappes. Less or no decoupling has to be assumed when or where deeply rooted wrench-fault systems and associated thick-skinned structures, like the Ivrea system, cut across the whole crust. In this case transpressive obduction may be an efficient mechanism to bring up deep lithospheric units into an upper crustal position. However, in a later stage of deformation the upper part of such a deeply rooted structure may be cut off from its roots and may become part of the orogenic lid.

Lower crustal wedges and upper mantle flakes (as illustrated in Figure 10-28) call for additional detachments at deeper levels of the lithosphere. Again, material balance requires that large portions of the lithospheric substratum must have been subducted. For an Adriatic wedge this seems to imply also subduction of Adriatic mantle lithosphere towards the north.

Acknowledgements

This Chapter benefited from fruitful discussions with J. Ansorge, D. Bernoulli, R. Fantoni, R. Freeman, W. Frei, E. Kissling, E. Lanz, H. Laubscher, P. Lehner, T. Noack, St. Müller, St. Schmid, G. Schönborn and P. Valasek. I would like to thank Eva Lanz, Paul Valasek and Walter Frei for their helpful collaboration with the seismic data plots. A special thank goes to Daniel Bernoulli, Hans Laubscher and Peter Lehner for useful suggestions and improvements. Reviews by C. Doglioni, A. Escher and A. Pfiffner are gratefully acknowledged.

Plates 10-1 to 10-12

SWISS NATIONAL SCIENCE FOUNDATION

88-NF-S1 (DYNAMITE)

FINAL STACK

1: 200'000

RECORDING PARAMETERS

SPREAD LAYOUT	19.2 km
CHANNELS	240
SOURCE TYPE	Dynamite
SOURCE DEPTH	50 m
CHARGE SIZE	185-1200 kg
GROUP INTERVAL	80 m
GEOPHONE TYPE	10 Hz
GEOPHONE PATTERN	24 in-line
INSTRUMENTATION	SERCEL 368
FIELD FILTERS	HC 178 Hz
COVERAGE	1 - 3
SAMPLING RATE	4 ms
RECORDING LENGTH	60 s
RECORDED BY	PRAKLA SEISMOS AG

DATE RECORDED Sept. 1988

PROCESSING PARAMETERS

1. Demultiplex and gain recovery
2. Time variant bandpass filter
3. Resample to 8 ms
4. F/K-Filter
5. Crooked line geometry
6. CDP-Sort
7. Field static corrections
8. NMO-Correction
9. Predictive deconvolution
10. Time variant bandpass filter
11. CDP-Stack
12. Time variant trace equalisation
13. Strong coherency filter

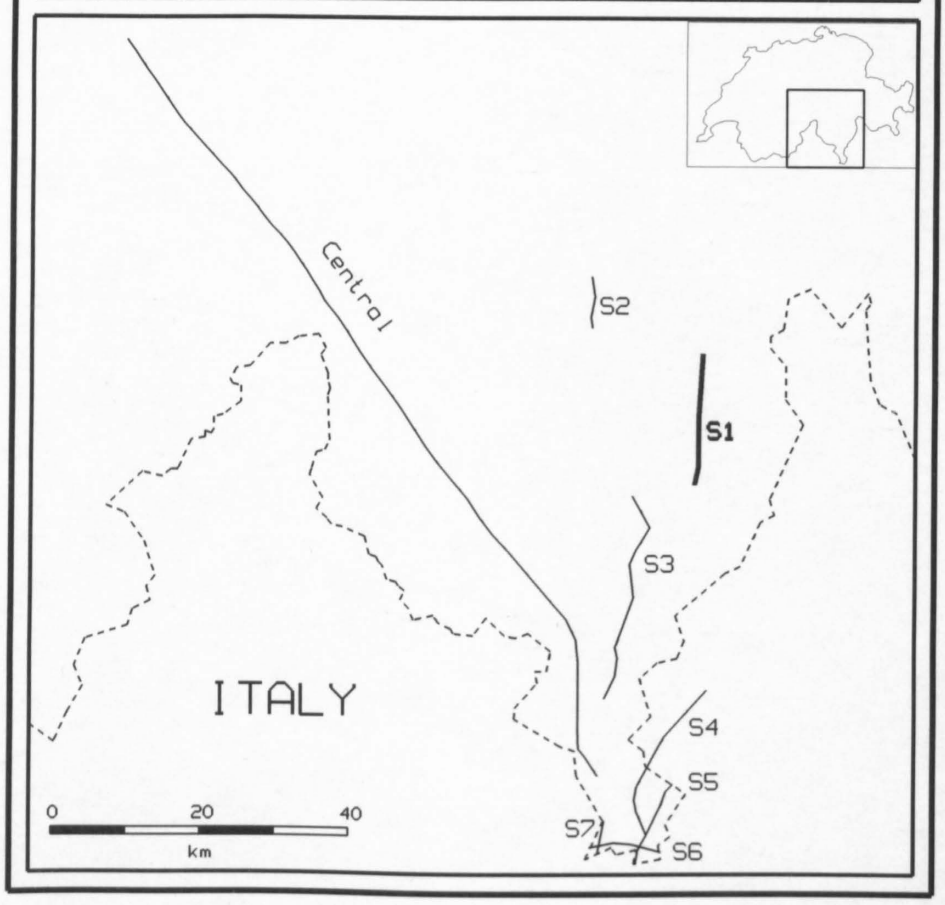

S1 + VALS (DFSV)

N

S

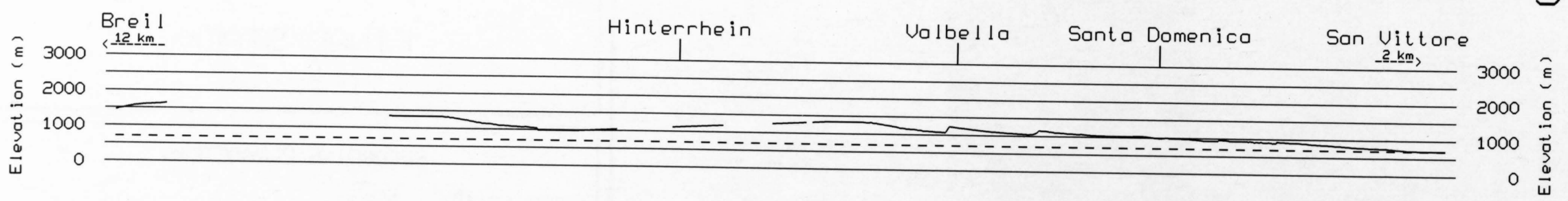

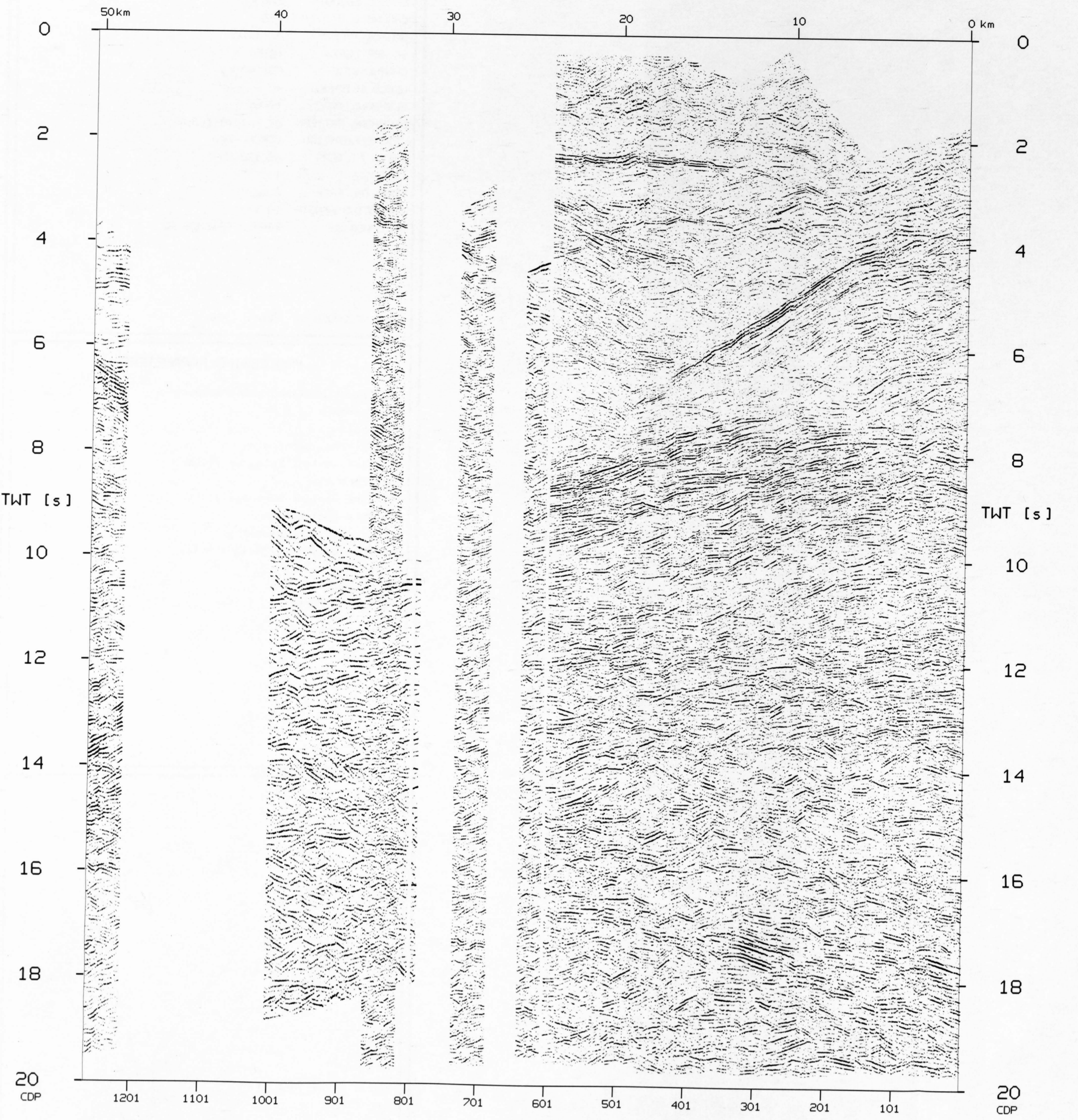

SWISS NATIONAL SCIENCE FOUNDATION

88-NF-S2 (DYNAMITE)

FINAL STACK

1: 200'000

RECORDING PARAMETERS

SPREAD LAYOUT	7.6 km
CHANNELS	192
SOURCE TYPE	Dynamite
SOURCE DEPTH	18-50 m
CHARGE SIZE	85-100 kg
GROUP INTERVAL	40 m
GEOPHONE TYPE	10 Hz
GEOPHONE PATTERN	24 spaced 1.3 m
INSTRUMENTATION	SERCEL 368
FIELD FILTERS	HC 178 Hz
COVERAGE	1
SAMPLING RATE	2 ms
RECORDING LENGTH	60 s
RECORDED BY	PRAKLA SEISMOS AG
DATE RECORDED	Sept. 1988

PROCESSING PARAMETERS

1. Demultiplex and gain recovery
2. Resample to 8 ms
3. Scaling
4. Spiking deconvolution
5. Time variant bandpass filter
6. Trace mix
7. Time variant bandpass filter
8. Mute application
9. Crooked line geometry
10. Application of field statics
11. NMO-Correction
12. CDP-Sort
13. Strong coherency filter

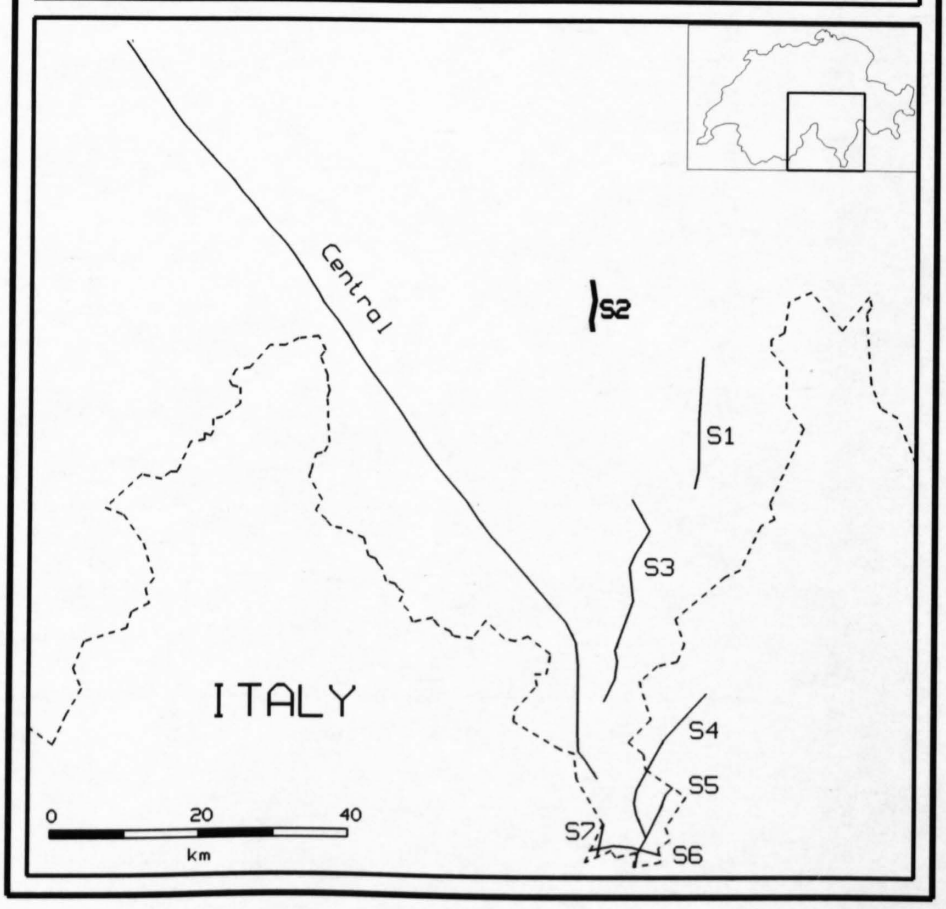

S2 (88-NF-D2)

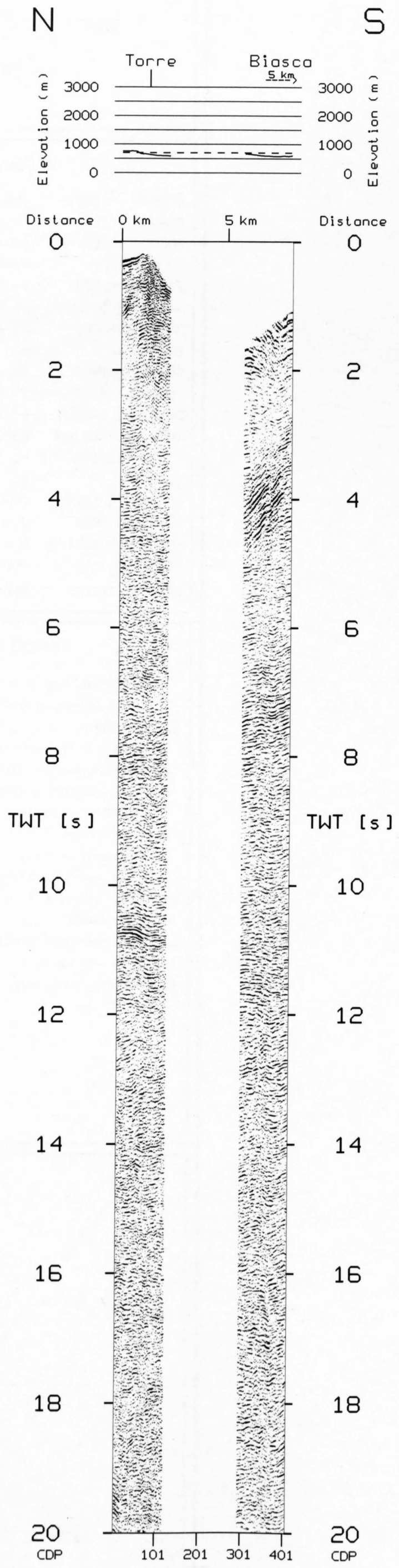
N
S
Torre
Biasca
5 km
Elevation (m)
3000
2000
1000
0
Distance
0 km
5 km
0
2
4
6
8
TWT [s]
10
12
14
16
18
20
CDP
101
201
301
401

SWISS NATIONAL SCIENCE FOUNDATION

88-NF-S2 (VIBROSEIS)

FINAL STACK

1:100'000

RECORDING PARAMETERS

SPREAD LAYOUT	2420-60-x-60-2420 m
CHANNELS	120 / 192
SOURCE INTERVAL	40 m
SOURCE TYPE	Vibroseis
SOURCE LAYOUT	3 Vibrators
SWEEP FREQUENCY	10-60 Hz
SWEEP LENGTH	20 s
SWEEPS/VP	6
GROUP INTERVAL	40 m
GEOPHONE TYPE	10 Hz
GEOPHONE LAYOUT	24 spaced 1.3 m
INSTRUMENTATION	SERCEL 368
FIELD FILTERS	HC 178 Hz
COVERAGE	60 (nominal)
RECORDING MODE	correlated and demultiplexed
SAMPLING RATE	2 ms
RECORDING LENGTH	6 s
RECORDED BY	PRAKLA SEISMOS AG
DATE RECORDED	Sept. 1988

PROCESSING PARAMETERS

1. Reformatting and gain recovery
2. Line geometry and survey data assignment
3. CDP-Sort
4. Time variant trace equalisation
5. Spiking deconvolution
6. Time variant bandpass filter
7. Field static corrections
8. NMO-Correction
9. Subsurface consistent res. static corrections
10. Time variant bandpass filter
11. Time variant trace equalisation
12. CDP-Stack
13. Time variant bandpass filter
14. Time variant trace equalisation
15. Strong coherency filter

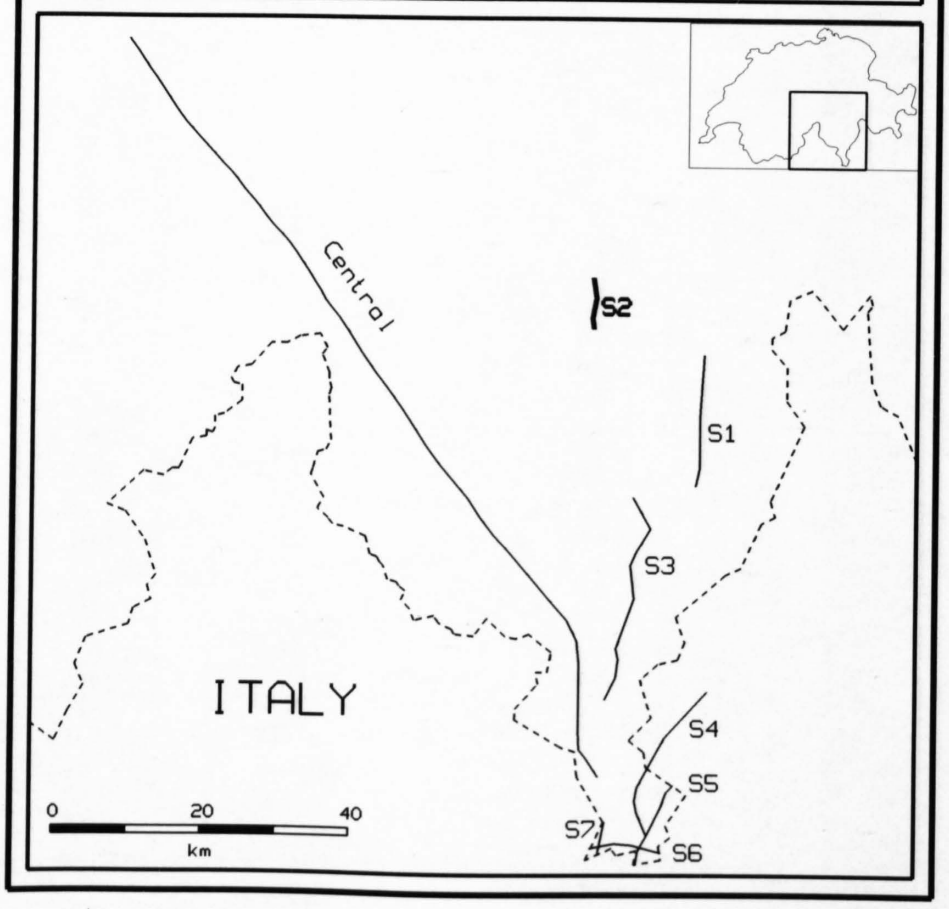

S2 (88-NF-V2)

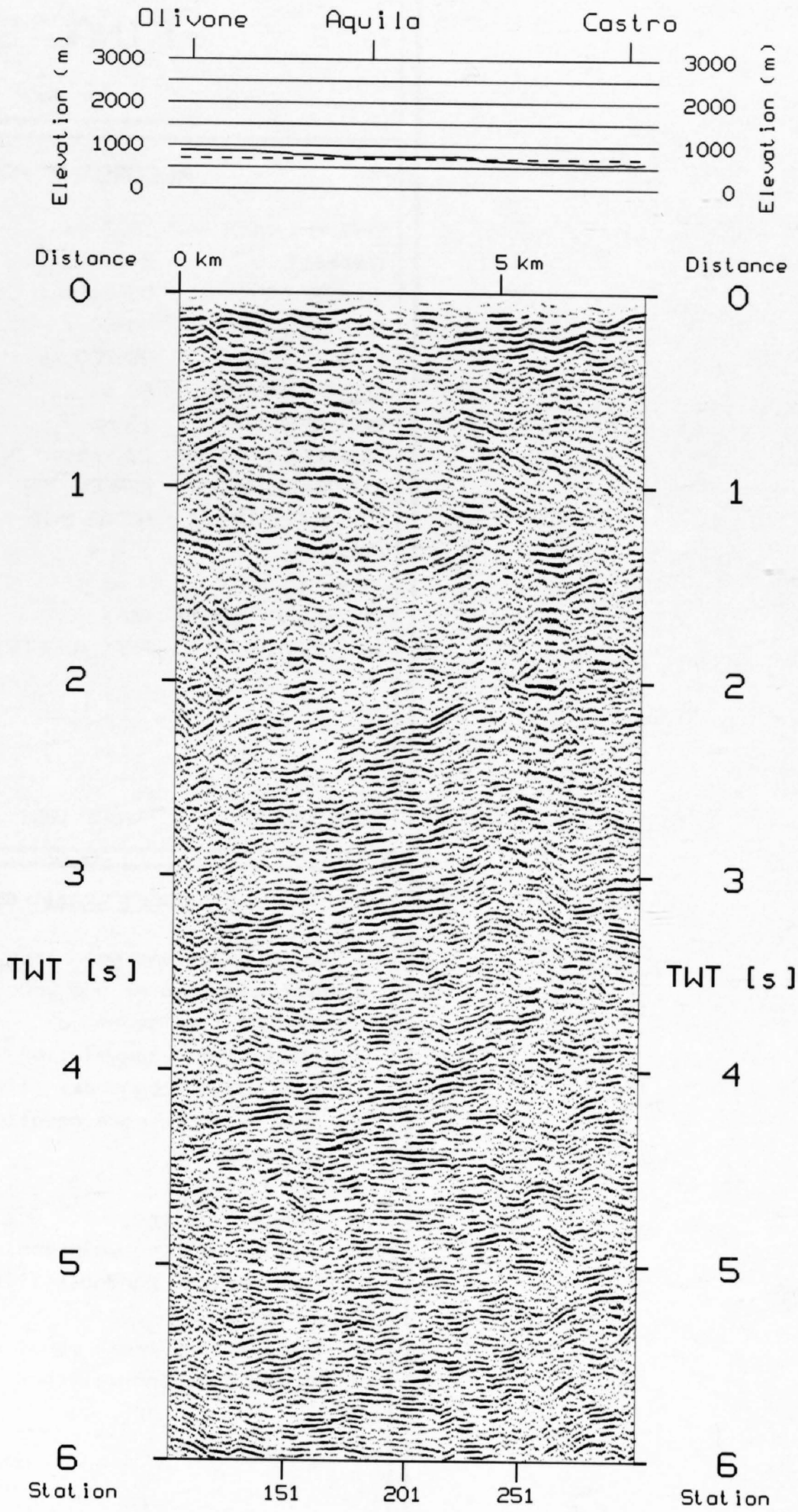
N
S
Olivone
Aquila
Castro
Elevation (m)
3000
2000
1000
0
Distance
0 km
5 km
0
1
2
3
4
5
6
TWT [s]
Station
151
201
251

SWISS NATIONAL SCIENCE FOUNDATION

88-NF-S3 (DYNAMITE)

FINAL STACK

1: 200'000

RECORDING PARAMETERS

SPREAD LAYOUT	19.2 km
CHANNELS	240
SOURCE TYPE	Dynamite
SOURCE DEPTH	40-60 m
CHARGE SIZE	35-200 kg
GROUP INTERVAL	80 m
GEOPHONE TYPE	10 Hz
GEOPHONE PATTERN	24 spaced 3.3 m
INSTRUMENTATION	SERCEL 368
FIELD FILTERS	HC 88.8 Hz
COVERAGE	1 - 4
SAMPLING RATE	4 ms
RECORDING LENGTH	60 s
RECORDED BY	PRAKLA SEISMOS AG
DATE RECORDED	Sept. 1988

PROCESSING PARAMETERS

1. Demultiplex and gain recovery
2. Resample to 8 ms and trace editing
3. Crooked line geometry
4. Predictive deconvolution
5. Time variant bandpass filter
6. Time variant trace equalisation
7. CDP-Sort
8. Field statics
9. NMO-Correction
10. Predictive deconvolution
11. Time variant bandpass filter
12. CDP-Stack
13. Time variant trace equalisation
14. Strong coherency filter

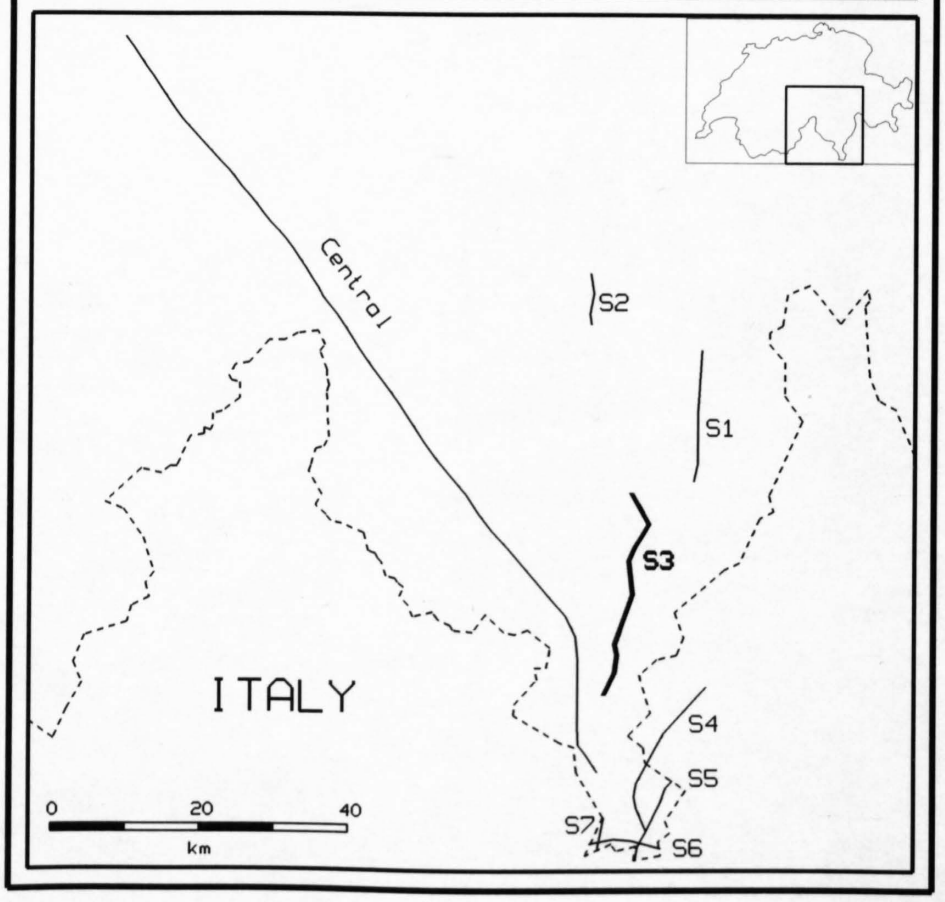

Plate 10-4

S3 (88-NF-D3)

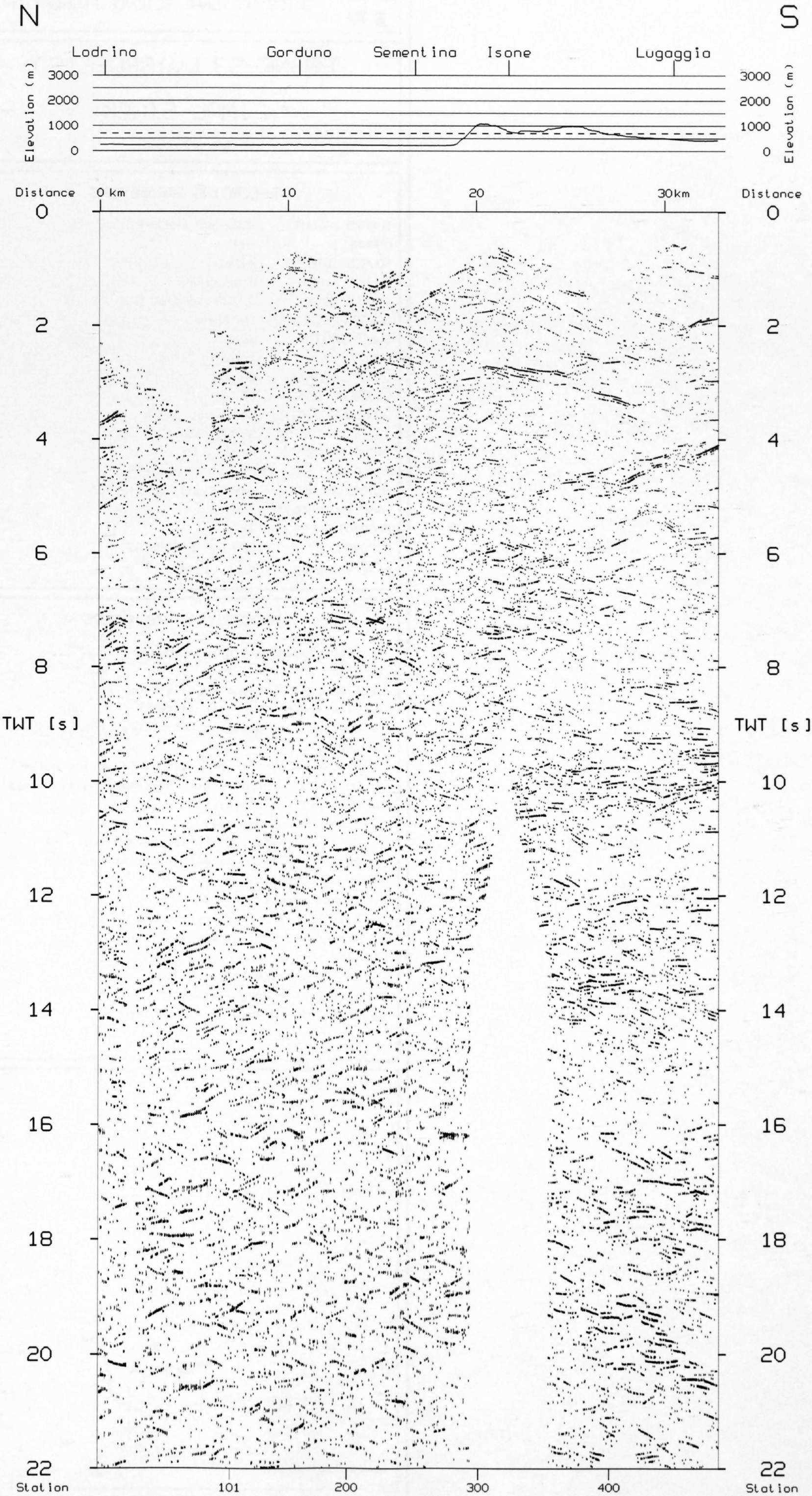
N
S
Lodrino
Gorduno
Sementina
Isone
Lugaggio
Elevation (m)
3000
2000
1000
0
Distance
0 km
10
20
30km
TWT [s]
0
2
4
6
8
10
12
14
16
18
20
22
Station
101
200
300
400

SWISS NATIONAL SCIENCE FOUNDATION

88-NF-S3 (VIBROSEIS)

FINAL STACK

1: 200'000

RECORDING PARAMETERS

SPREAD LAYOUT	9720-200-x-200-9720 m
CHANNELS	240
SOURCE INTERVAL	40 m
SOURCE TYPE	Vibroseis
SOURCE LAYOUT	6 Vibrators at 5 m
SWEEP FREQUENCY	10-40 Hz
SWEEP LENGTH	60 s
SWEEPS/VP	1 to 4
GROUP INTERVAL	80 m
GEOPHONE TYPE	10 Hz
GEOPHONE LAYOUT	24 spaced 3.3 m
INSTRUMENTATION	SERCEL 368
FIELD FILTERS	HC 88.8 Hz
COVERAGE	2 x 120 (nominal)
RECORDING MODE	summed and correlated
SAMPLING RATE	4 ms
RECORDING LENGTH	24 s
RECORDED BY	PRAKLA SEISMOS AG
DATE RECORDED	Sept. 1988

PROCESSING PARAMETERS

1. Demultiplex with gain recovery
2. Trace editing
3. Time variant trace equalisation
4. Time variant bandpass filter
5. Crooked line geometry (20 m CDPs)
6. CDP-Sort
7. Elevation static correction to floating datum
8. Data dependent suppress. of random noise bursts
9. Predictive deconvolution
10. Time variant bandpass filter
11. Surface consistent static corrections
12. Residual CDP consistent static corrections
13. NMO-Correction
14. Iterative median stack
15. Elevation static correction to datum (700 m)
16. Time variant trace equalisation
17. Time variant bandpass filter
18. Moving average trace mixing
19. Strong coherency filter
20. Trace mix (2-fold horizontal sum)

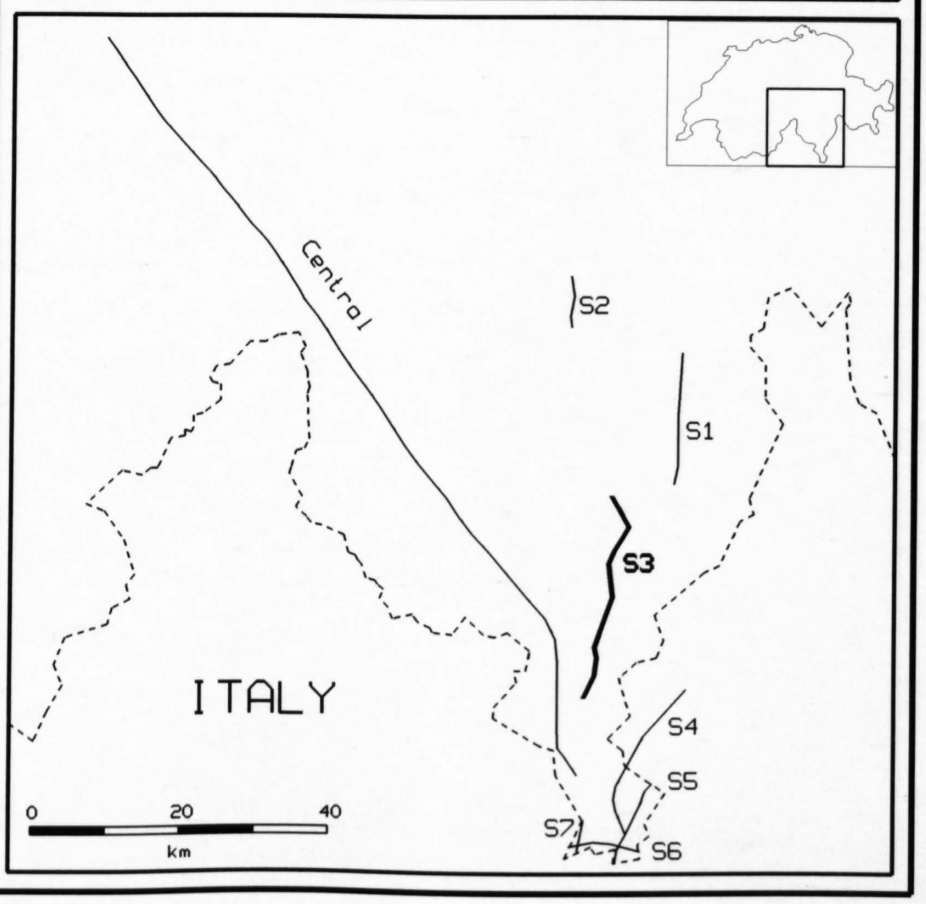

S3 (88-NF-V3)

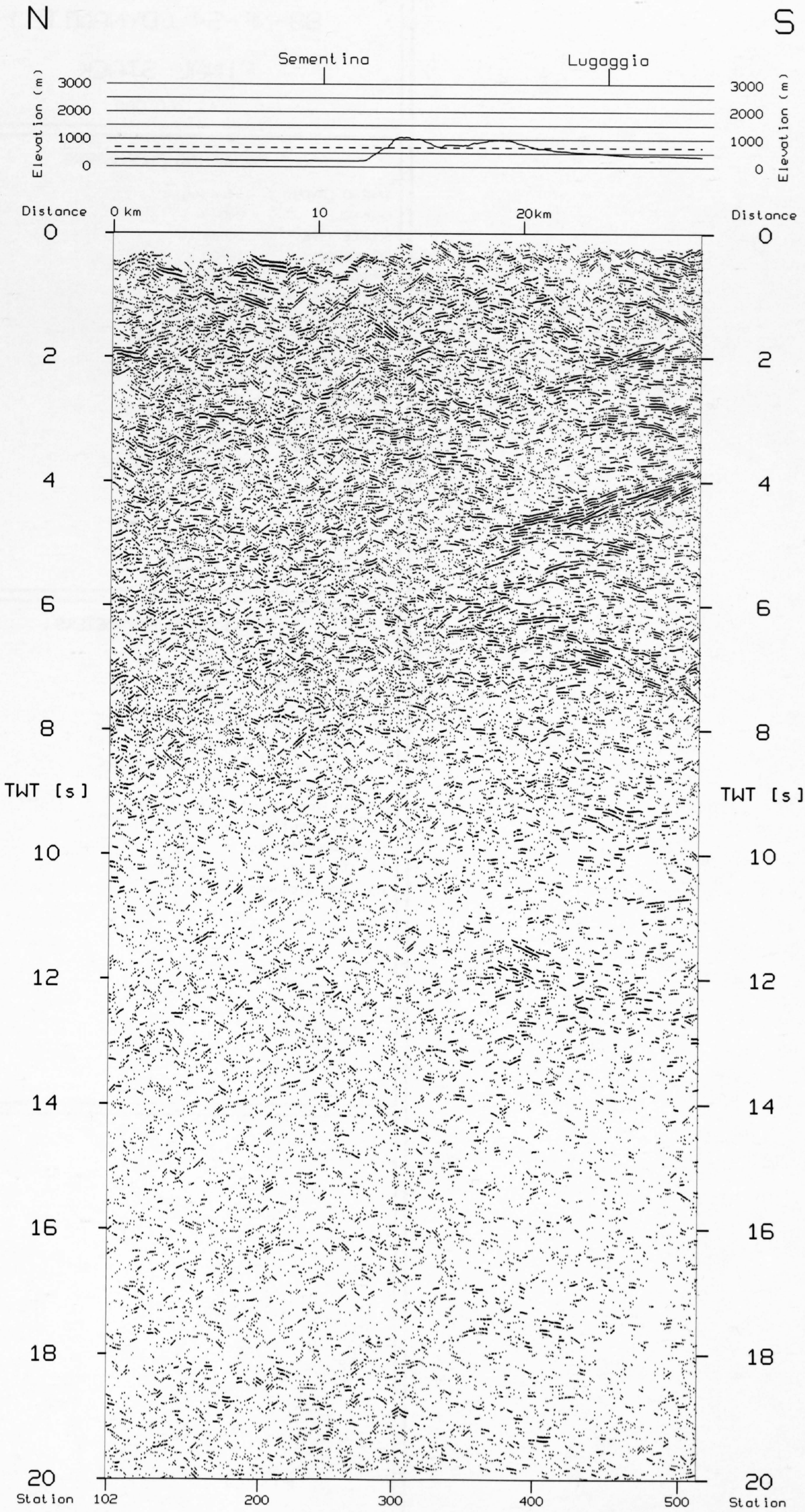
N
S
Sementina
Lugaggio
Elevation (m)
3000
2000
1000
0
Distance
0 km
10
20km
0
2
4
6
8
TWT [s]
10
12
14
16
18
20
Station
102
200
300
400
500

SWISS NATIONAL SCIENCE FOUNDATION

88-NF-S4 (DYNAMITE)

FINAL STACK

1: 200'000

RECORDING PARAMETERS

SPREAD LAYOUT	14.4 km
CHANNELS	240
SOURCE TYPE	Dynamite
SOURCE DEPTH	10-30 m
CHARGE SIZE	25-100 kg
GROUP INTERVAL	60 m
GEOPHONE TYPE	10 Hz
GEOPHONE PATTERN	24 spaced 2.5 m
INSTRUMENTATION	SERCEL 368
FIELD FILTERS	HC 88.8 Hz
COVERAGE	1 - 3
SAMPLING RATE	4 ms
RECORDING LENGTH	60 s
RECORDED BY	PRAKLA SEISMOS AG
DATE RECORDED	Sept. 1988

PROCESSING PARAMETERS

1. Demultiplex and gain recovery
2. Resampling to 8 ms
3. Crooked line geometry
4. Predictive deconvolution
5. Time variant bandpass filter
6. Time variant trace equalisation
7. CDP-Sort
8. Application of field statics
9. Mute application
10. NMO-Correction
11. CDP-Stack
12. Strong coherency filter

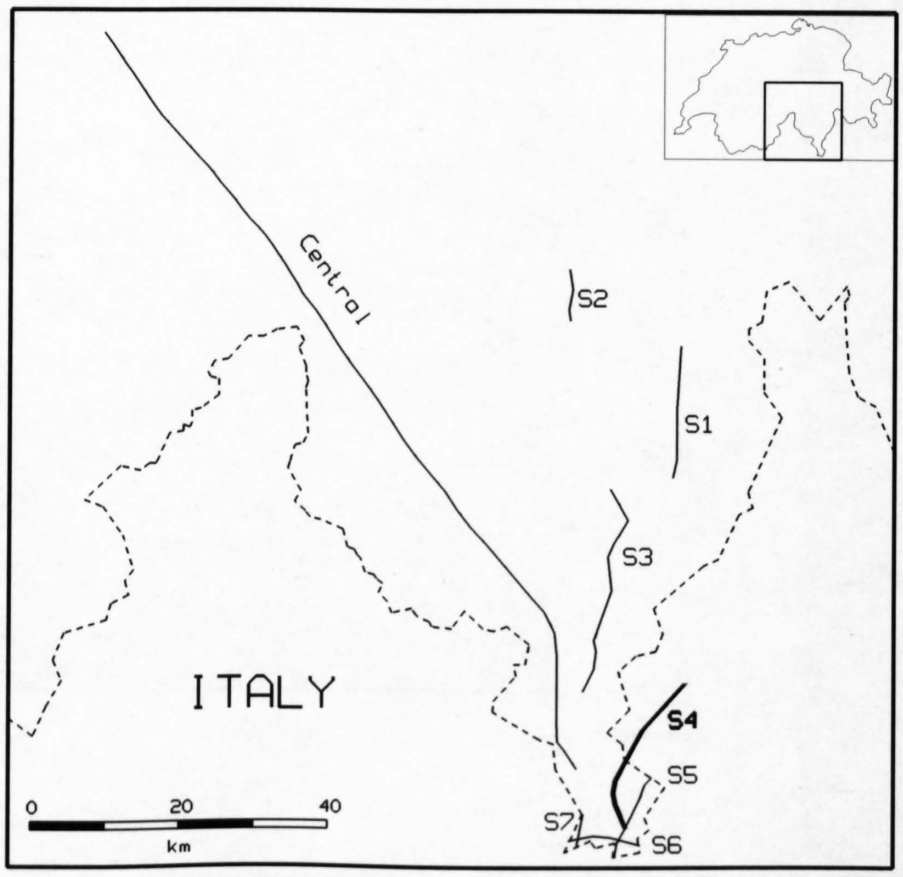

88-NF-D4 (S4) & CROP

N S NE S

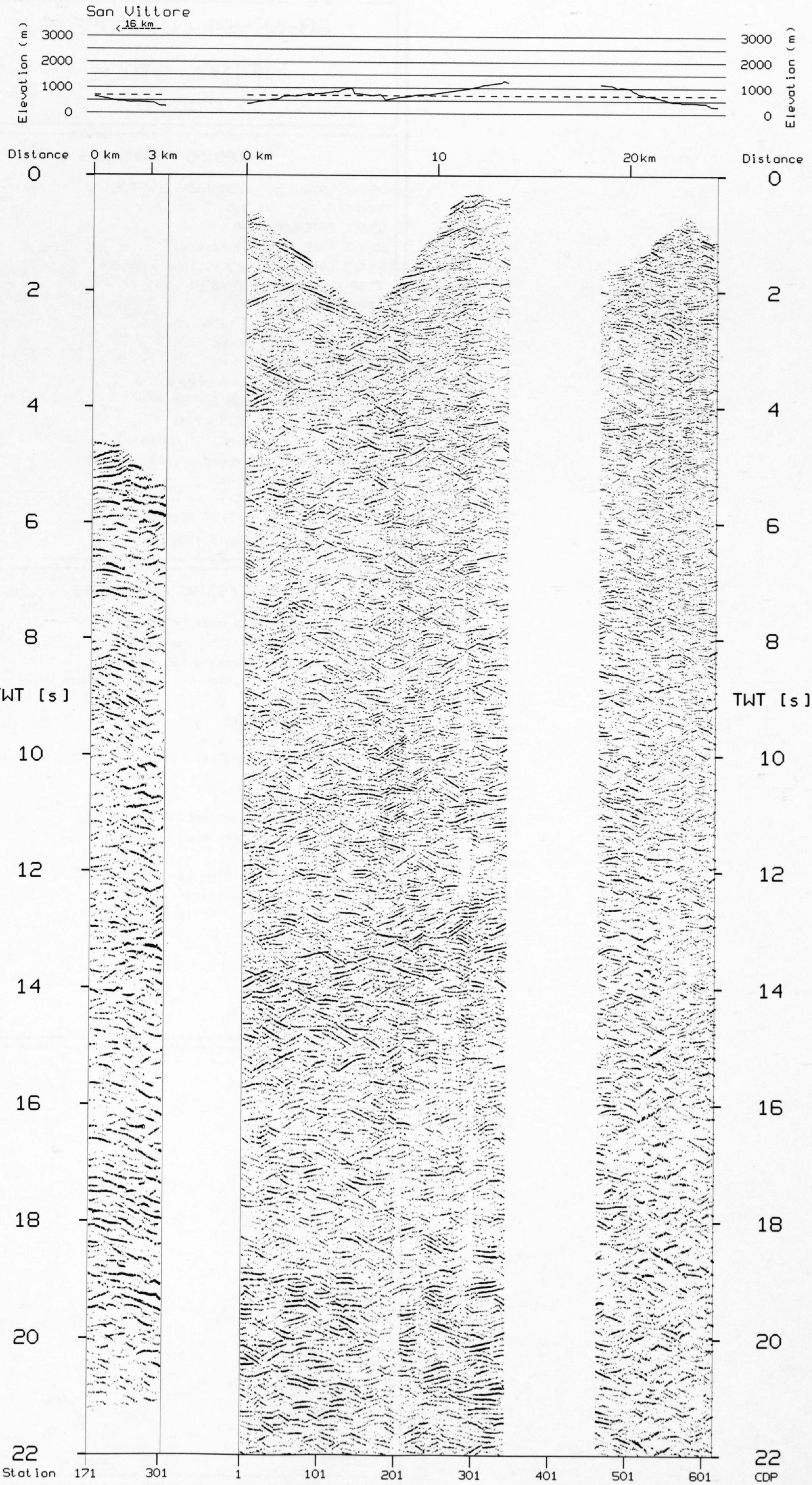

SWISS NATIONAL SCIENCE FOUNDATION

88-NF-S4 (VIBROSEIS)

FINAL STACK

1: 100'000

RECORDING PARAMETERS

SPREAD LAYOUT	7290-150-x-150-7290 m
CHANNELS	240
SOURCE INTERVAL	30 m
SOURCE TYPE	Vibroseis
SOURCE LAYOUT	6/3 Vibrators at 5 m
SWEEP FREQUENCY	10-48 Hz
SWEEP LENGTH	20 s
SWEEPS/VP	2 to 8
GROUP INTERVAL	60 m
GEOPHONE TYPE	10 Hz
GEOPHONE LAYOUT	24 spaced 2.5 m
INSTRUMENTATION	SERCEL 368
FIELD FILTERS	HC 88.8 Hz
COVERAGE	2 x 120 (nominal)
RECORDING MODE	summed and correlated
SAMPLING RATE	4 ms
RECORDING LENGTH	16 s
RECORDED BY	PRAKLA SEISMOS AG
DATE RECORDED	Sept. 1988

PROCESSING PARAMETERS

1. Demultiplex with gain recovery
2. Trace editing and resample to 8 ms
3. Crooked line geometry (15 m CDP)
4. Elevation correction to floating datum
5. CDP-Sort
6. Trace equalisation
7. Gapped deconvolution
8. Time variant bandpass filter
9. NMO-Correction
10. Mute application
11. Surface consistent residual statics
12. CDP consistent residual statics
13. CDP-Stack
14. Elevation correction to reference datum
15. Strong coherency filter
16. Trace mix (2-fold horizontal sum)

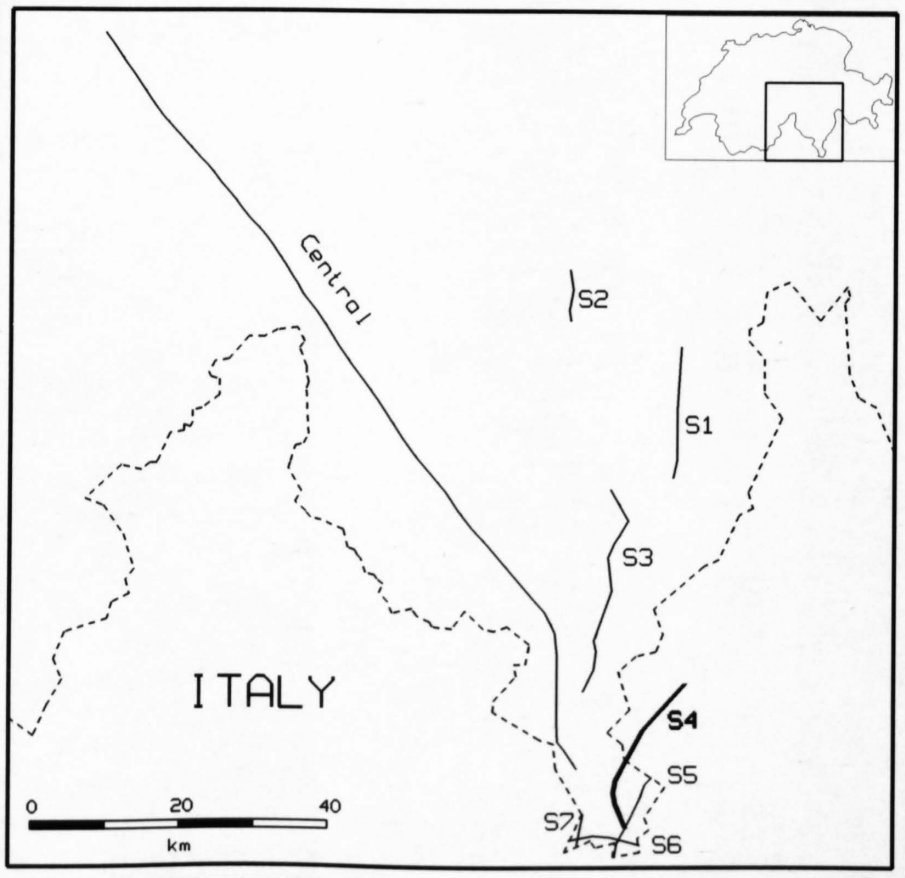

S4 (88-NF-V4)

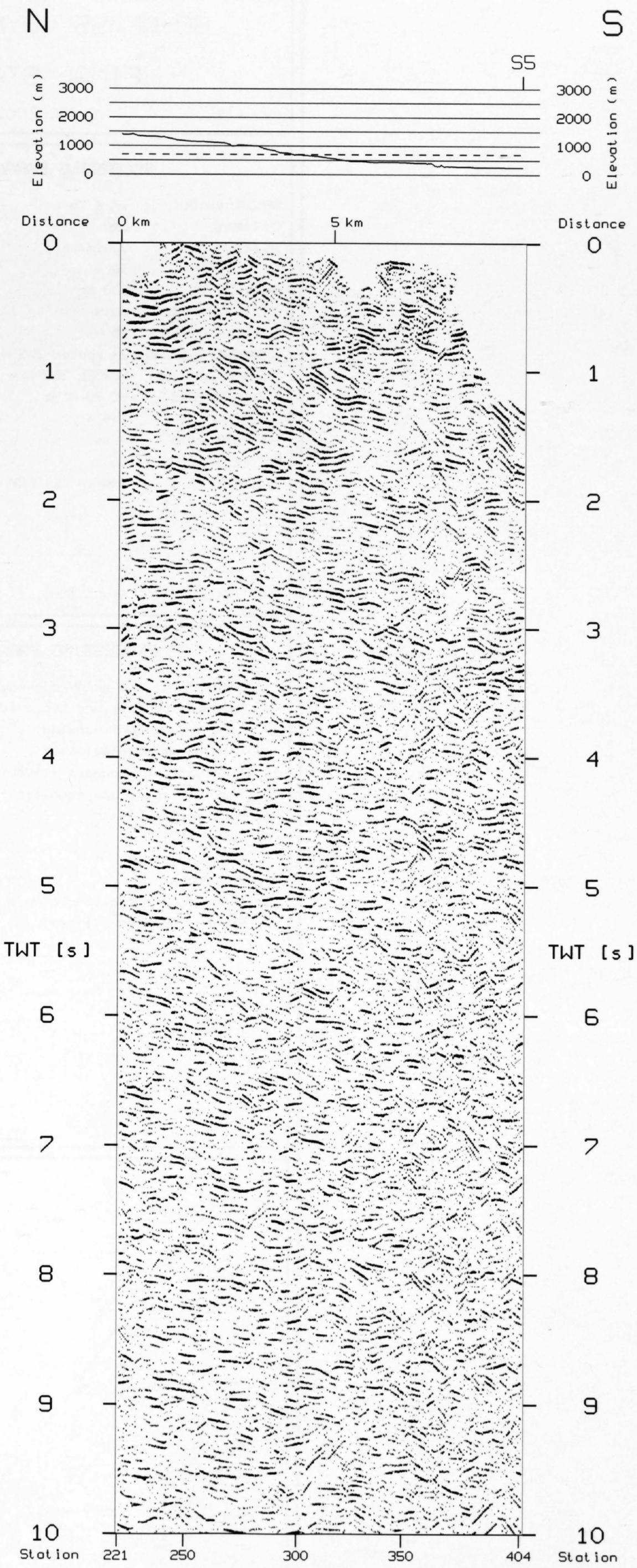
N
S
S5
Elevation (m)
3000
2000
1000
0
Distance
0 km
5 km
0
1
2
3
4
5
6
7
8
9
10
TWT [s]
Station
221
250
300
350
404

SWISS NATIONAL SCIENCE FOUNDATION

88-NF-S5 (DYNAMITE)

FINAL STACK

1: 200'000

RECORDING PARAMETERS

SPREAD LAYOUT	14.4 km
CHANNELS	240
SOURCE TYPE	Dynamite
SOURCE DEPTH	50 m
CHARGE SIZE	200 kg
GROUP INTERVAL	60 m
GEOPHONE TYPE	10 Hz
GEOPHONE PATTERN	24 spaced 2.5 m
INSTRUMENTATION	SERCEL 368
FIELD FILTERS	HC 88.8 Hz
COVERAGE	1 - 4
SAMPLING RATE	4 ms
RECORDING LENGTH	60 s
RECORDED BY	PRAKLA SEISMOS AG

DATE RECORDED Sept. 1988

PROCESSING PARAMETERS

1. Demultiplex and gain recovery
2. Resample to 8 ms and trace editing
3. Data independant scaling
4. Predictive deconvolution
5. Time variant bandpass filter
6. Time variant trace equalisation
7. Mute application
8. CDP-Sort
9. NMO-Correction
10. CDP-Stack
11. Elevation correction to reference datum
12. Strong coherency filter

S5 (88-NF-D5)

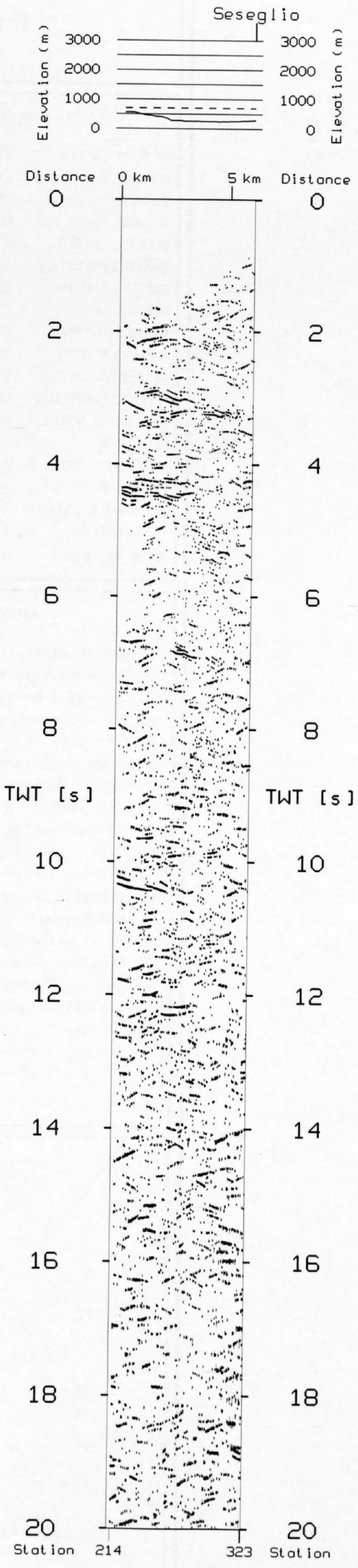
N
S
Seseglio
Elevation (m)
3000
2000
1000
0
Distance
0 km
5 km
0
2
4
6
8
TWT [s]
10
12
14
16
18
20
Station
214
323

SWISS NATIONAL SCIENCE FOUNDATION

88-NF-S5 (VIBROSEIS)

FINAL STACK

1: 100'000

RECORDING PARAMETERS

SPREAD LAYOUT	7290-150-x-150-7290 m
CHANNELS	240
SOURCE INTERVAL	30 m
SOURCE TYPE	Vibroseis
SOURCE LAYOUT	6/3 Vibrators at 5 m
SWEEP FREQUENCY	10-48 Hz
SWEEP LENGTH	60 s / 20 s
SWEEPS/VP	2 to 8
GROUP INTERVAL	60 m
GEOPHONE TYPE	10 Hz
GEOPHONE LAYOUT	24 spaced 2.5 m
INSTRUMENTATION	SERCEL 368
FIELD FILTERS	HC 88.8 Hz
COVERAGE	2 x 120 (nominal)
RECORDING MODE	summed and correlated
SAMPLING RATE	4 ms
RECORDING LENGTH	24 s / 16 s
RECORDED BY	PRAKLA SEISMOS AG
DATE RECORDED	Sept. 1988

PROCESSING PARAMETERS

1. Demultiplex with gain recovery
2. Trace editing and resample to 8 ms
3. Crooked line geometry (15 m CDP)
4. Elevation correction to floating datum
5. CDP-Sort
6. Trace equalisation
7. Gapped deconvolution
8. Time variant bandpass filter
9. NMO-Correction
10. Mute application
11. Initial surface consistent residual statics
12. Initial CDP consistent residual statics
13. NMO-Removal
14. Final velocity analysis and NMO-Correction
15. Final surface consistent residual statics
16. Final CDP consistent residual statics
17. Elevation correction to reference datum
18. CDP-Stack
19. Strong coherency filter
20. Trace mix (2-fold horizontal sum)

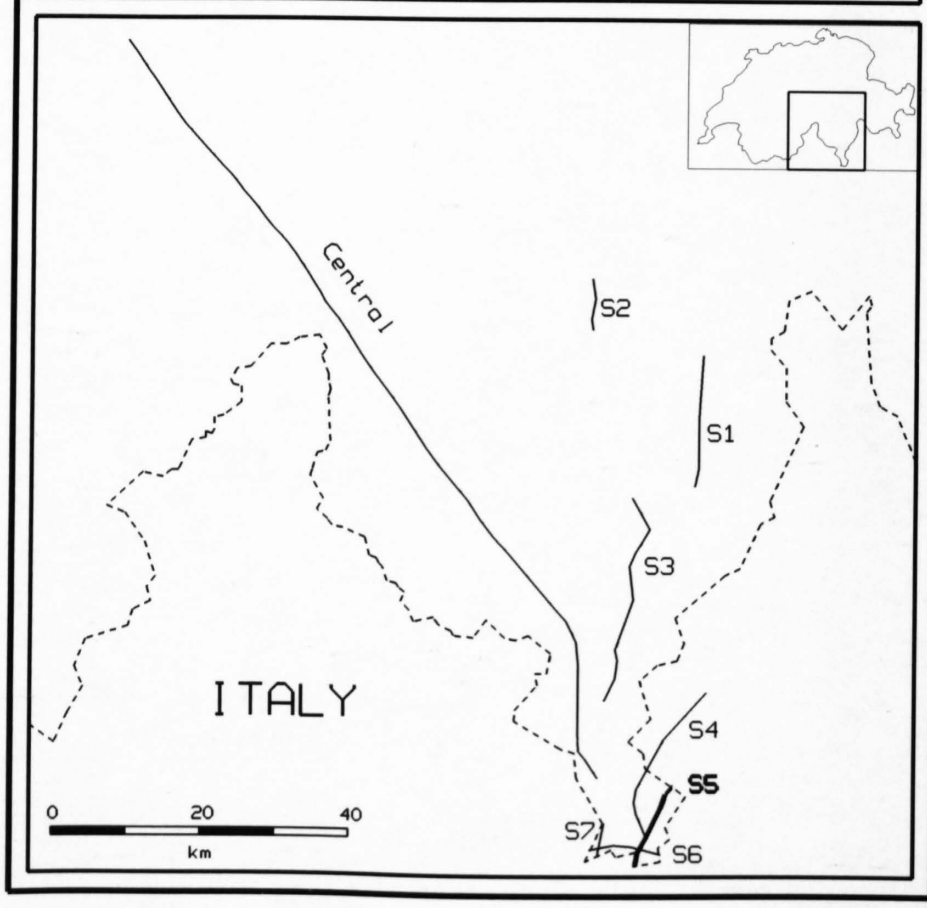

S5 (88-NF-V5)

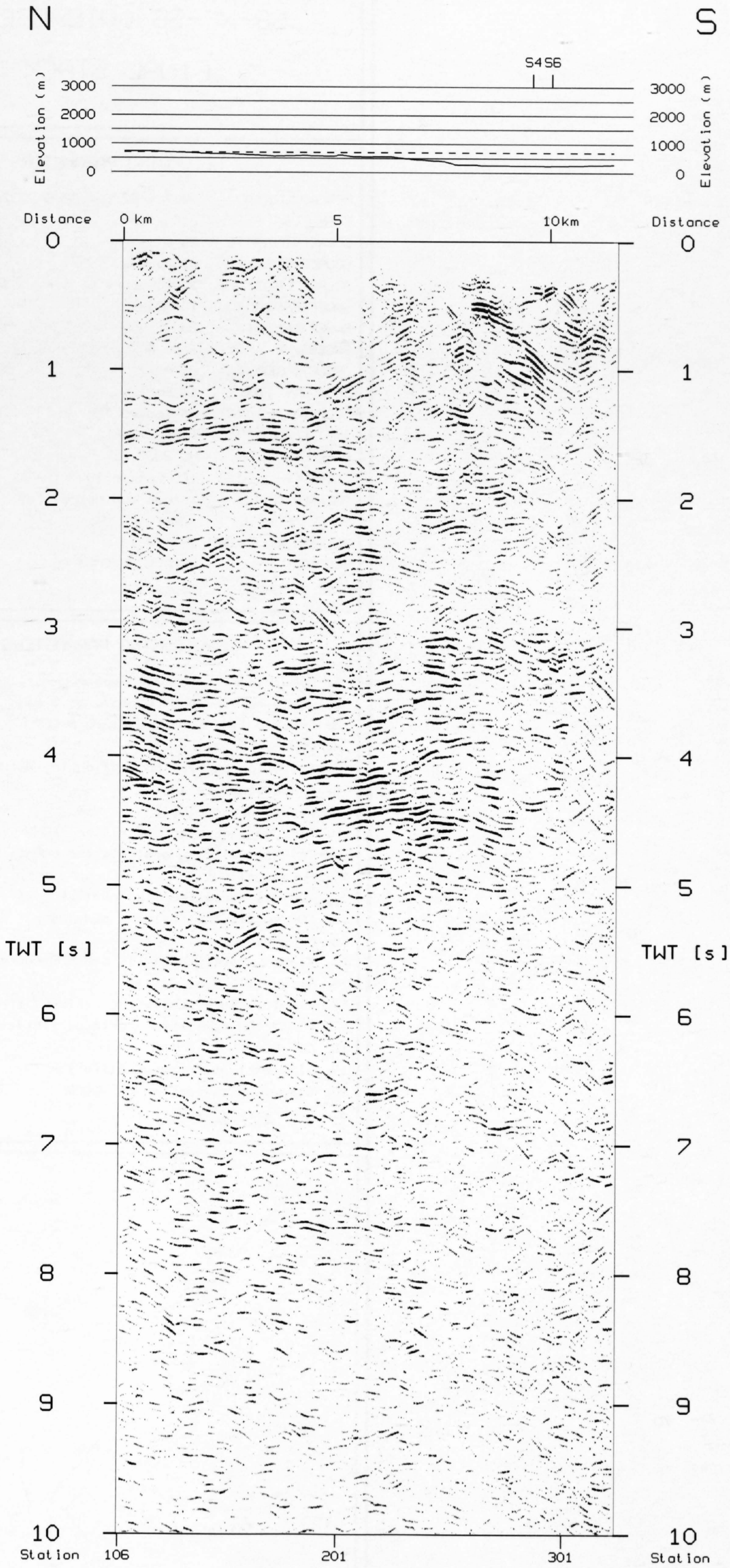
N
S
S4 S6
Elevation (m)
3000
2000
1000
0
Distance
0 km
5
10km
0
1
2
3
4
5
6
7
8
9
10
TWT [s]
Station
106
201
301

SWISS NATIONAL SCIENCE FOUNDATION

88-NF-S6 (VIBROSEIS)

FINAL STACK

1: 100'000

RECORDING PARAMETERS

SPREAD LAYOUT	3037.5-62.5-x-62.5-3037.5 m
CHANNELS	240
SOURCE INTERVAL	25 m
SOURCE TYPE	Vibroseis
SOURCE LAYOUT	3 Vibrators at 5 m
SWEEP FREQUENCY	10-60 Hz
SWEEP LENGTH	20 s
SWEEPS/VP	4 to 6
GROUP INTERVAL	25 m
GEOPHONE TYPE	10 Hz
GEOPHONE LAYOUT	24 spaced 1 m
INSTRUMENTATION	SERCEL 368
FIELD FILTERS	HC 88.8 Hz
COVERAGE	120 (nominal)
RECORDING MODE	summed and correlated
SAMPLING RATE	4 ms
RECORDING LENGTH	16 s / 14 s
RECORDED BY	PRAKLA SEISMOS AG
DATE RECORDED	Sept. 1988

PROCESSING PARAMETERS

1. Demultiplex with gain recovery
2. Trace editing and resample to 8 ms
3. Crooked line geometry (12.5 m CDP)
4. CDP-Sort
5. Elevation correction to floating datum
6. Trace equalisation
7. Gapped deconvolution
8. Time variant bandpass filter
9. Initial velocity analysis and NMO-Correction
10. Mute application
11. Surface consistent residual statics
12. CDP consistent residual statics
13. NMO-Removal
14. Final velocity analysis and NMO-Correction
15. Resampling 8 to 2 ms
16. Final surface consistent residual statics
17. Final CDP consistent residual statics
18. CDP-Stack
19. Time variant trace equalisation
20. Elevation correction to 700 m
21. Coherency filter

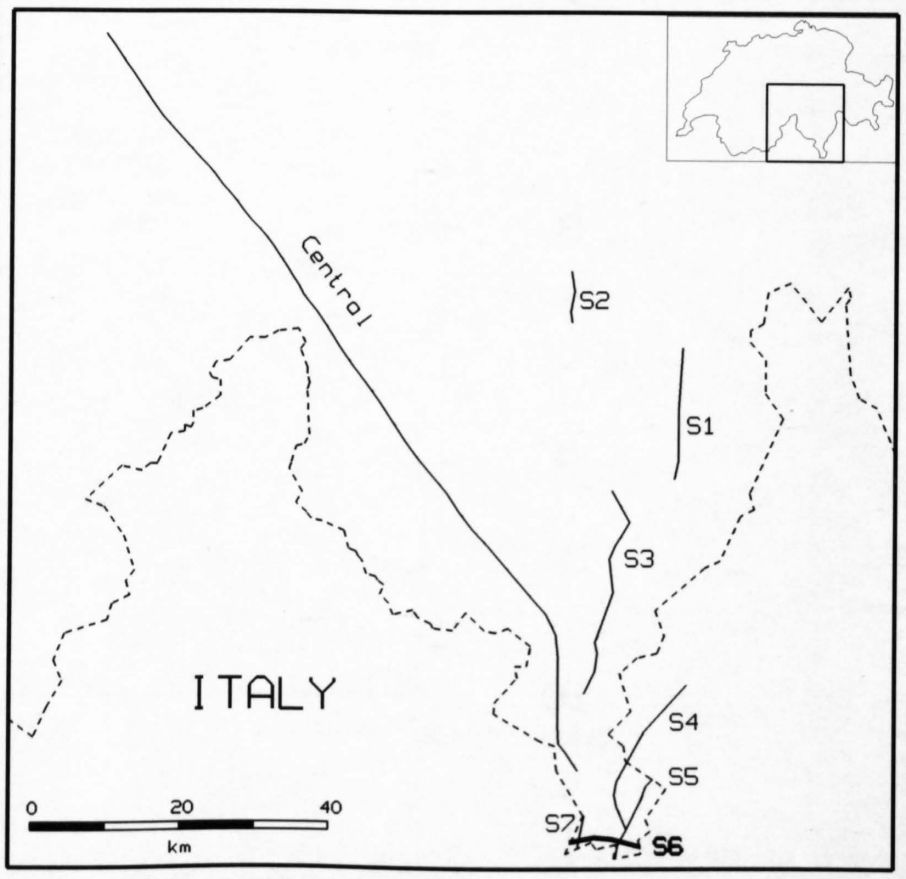

S6 (88-NF-V6)

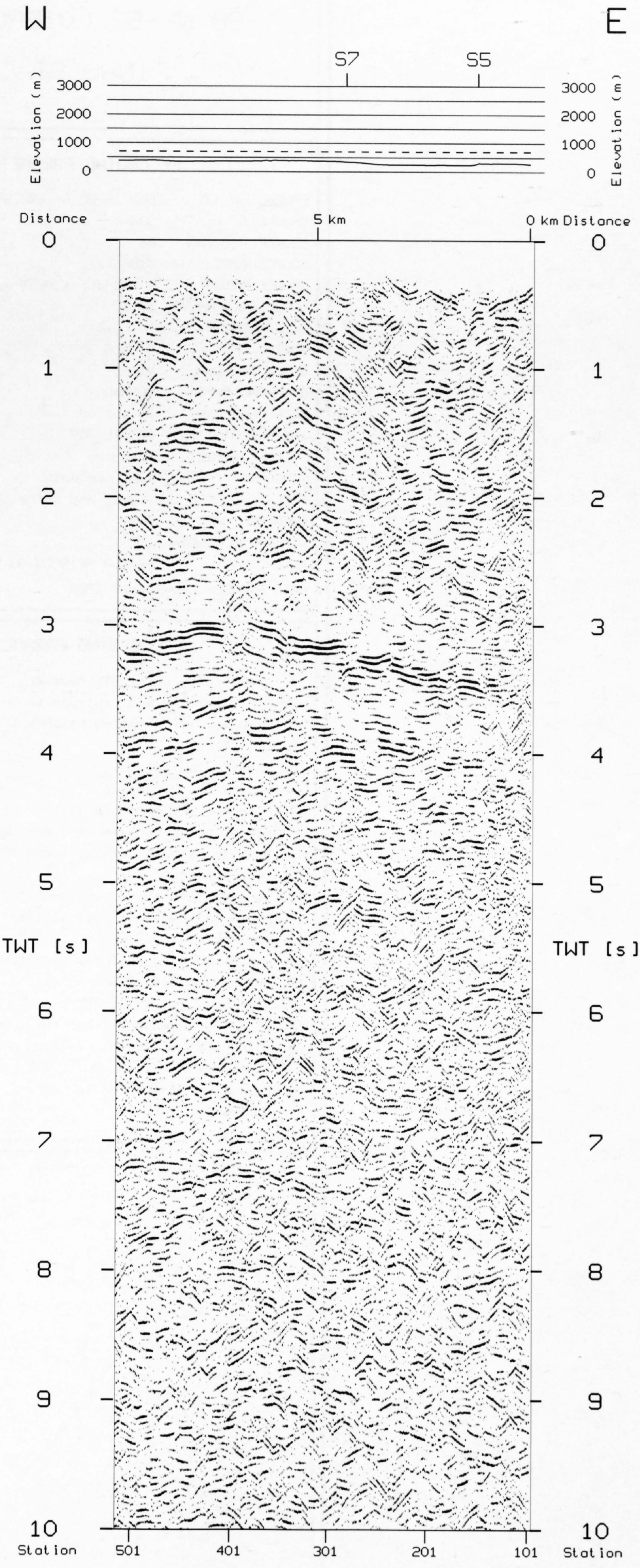
W
E
S7
S5
Elevation (m)
3000
2000
1000
0
Distance
5 km
0 km Distance
0
1
2
3
4
5
TWT [s]
6
7
8
9
10
Station
501
401
301
201
101

SWISS NATIONAL SCIENCE FOUNDATION

88-NF-S7 (VIBROSEIS)

FINAL STACK

1: 50'000

RECORDING PARAMETERS

SPREAD LAYOUT	3037.5-62.5-x-62.5-3037.5 m
CHANNELS	384
SOURCE INTERVAL	25 m
SOURCE TYPE	Vibroseis
SOURCE LAYOUT	3 Vibrators at 5 m
SWEEP FREQUENCY	10-60 Hz
SWEEP LENGTH	20 s
SWEEPS/VP	4 to 6
GROUP INTERVAL	25 m
GEOPHONE TYPE	10 Hz
GEOPHONE LAYOUT	24 spaced 1 m
INSTRUMENTATION	SERCEL 368
FIELD FILTERS	HC 89 Hz
COVERAGE	120 (nominal)
RECORDING MODE	summed and correlated
SAMPLING RATE	4 ms
RECORDING LENGTH	12 s
RECORDED BY	PRAKLA SEISMOS AG
DATE RECORDED	Sept. 1988

PROCESSING PARAMETERS

1. Demultiplex with gain recovery
2. Trace editing and resample to 8 ms
3. Crooked line geometry (12.5 m CDP)
4. CDP-Sort
5. Trace equalisation
6. Gapped deconvolution
7. Time variant bandpass filter
8. Elevation correction to floating datum
9. Initial velocity analysis and NMO-Correction
10. Mute application
11. Surface consistent residual statics
12. CDP consistent residual statics
13. NMO-Removal
14. Final velocity analysis and NMO-Correction
15. Resampling 8 to 2 ms
16. High pass filter 12/72 Hz
17. Final surface consistent residual statics
18. Final CDP consistent residual statics
19. CDP-Stack
20. Elevation correction to 700 m
21. Coherency filter

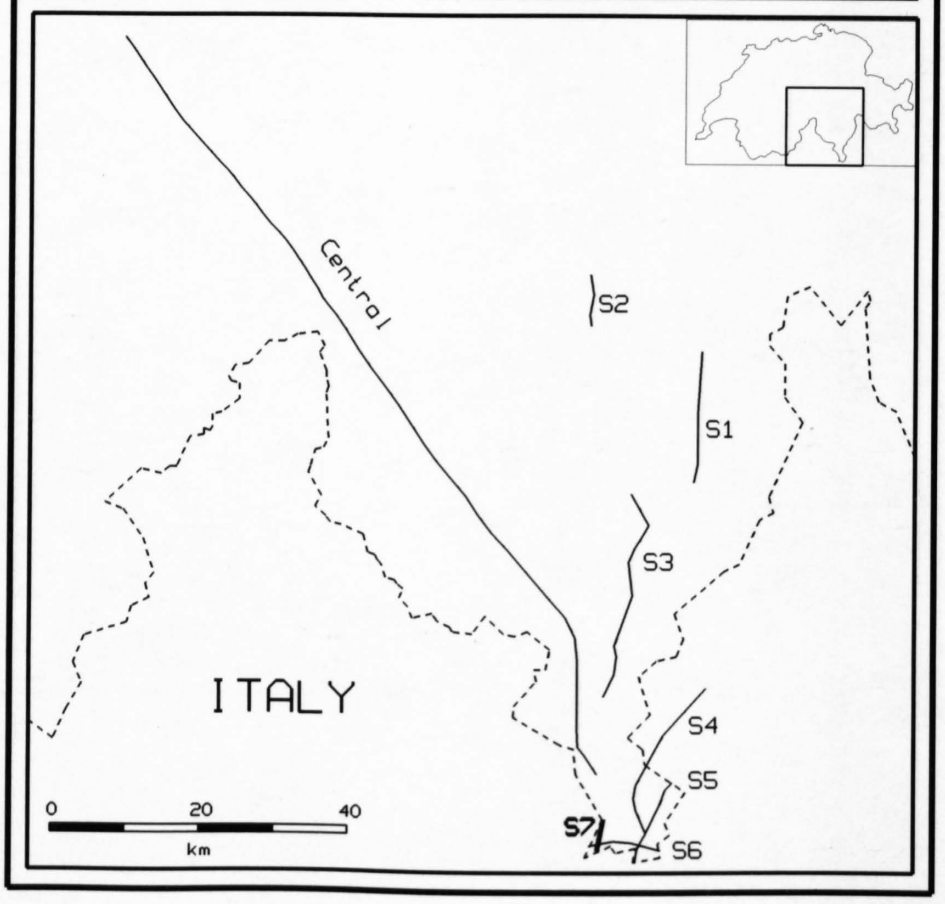

S7 (88-NF-V7)

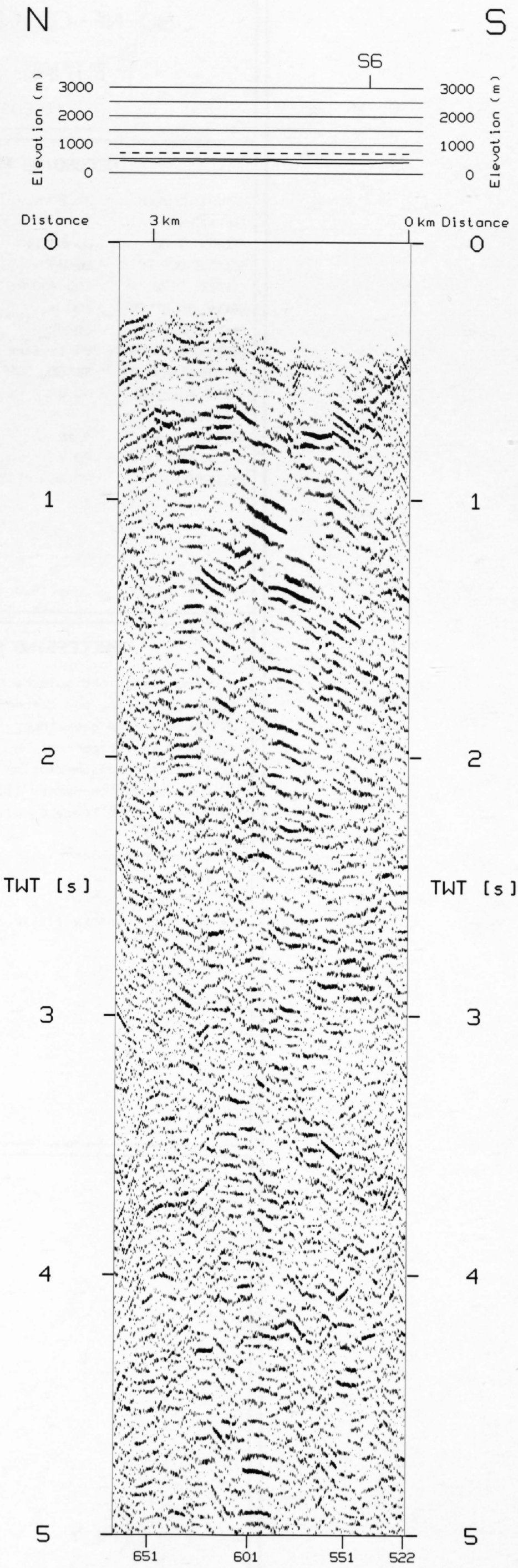
N
S
S6
Elevation (m)
3000
2000
1000
0
Distance
0
3 km
0 km Distance
1
2
TWT [s]
3
4
5
651
601
551
522

SWISS NATIONAL SCIENCE FOUNDATION

90-NF-C3 (DYNAMITE)

FINAL STACK

1: 200'000

RECORDING PARAMETERS

SPREAD LAYOUT	34.8 km
CHANNELS	360
SOURCE TYPE	Dynamite
SOURCE DEPTH	20-80 m
CHARGE SIZE	100-400 kg
GROUP INTERVAL	100 m
GEOPHONE TYPE	10 Hz
GEOPHONE PATTERN	24 in-line / 100 m
INSTRUMENTATION	SERCEL 368
FIELD FILTERS	HC 88.8 Hz
COVERAGE	1 - 4
SAMPLING RATE	4 ms
RECORDING LENGTH	60 s
RECORDED BY	PRAKLA SEISMOS AG
DATE RECORDED	June 1990

PROCESSING PARAMETERS

1. Demultiplex and gain recovery
2. Trace editing and resample to 8 ms
3. Crooked line geometry
4. Field static correction
5. Predictive deconvolution
6. Time variant bandpass filter
7. Time variant trace equalisation
8. CDP-Sort
9. Mute application
10. NMO-Correction
11. CDP-Stack
12. Strong coherency filter

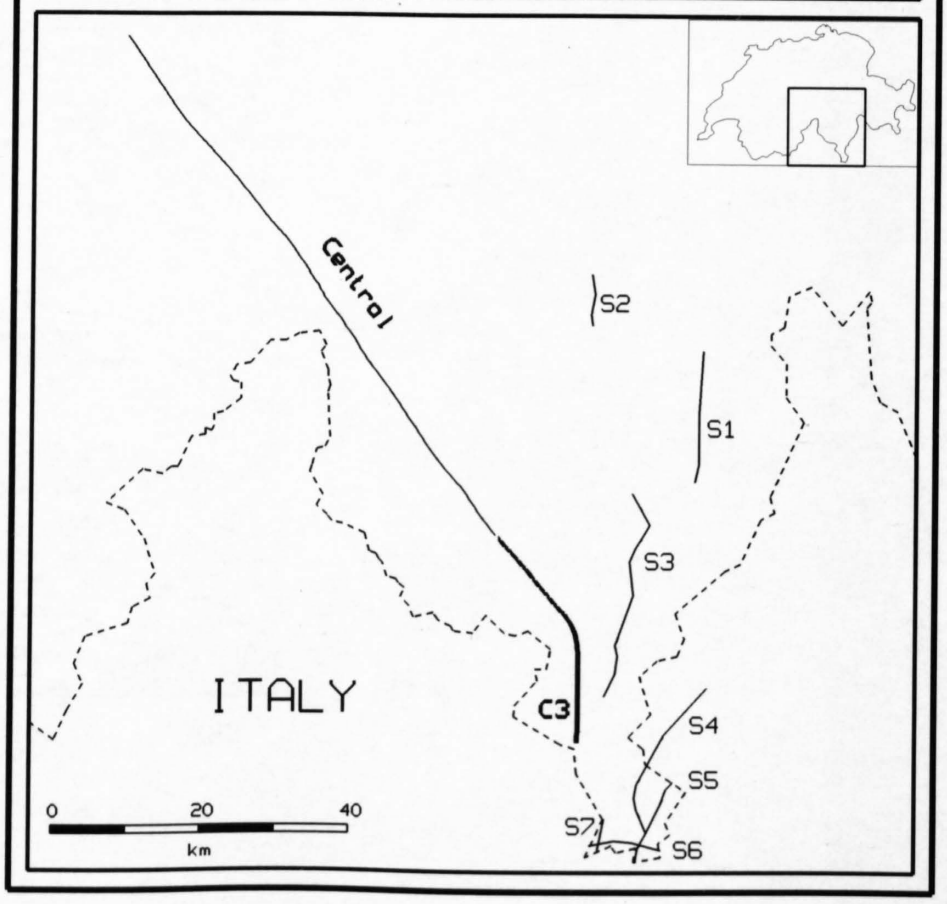

C3 (90-NF-D3)

NW

S

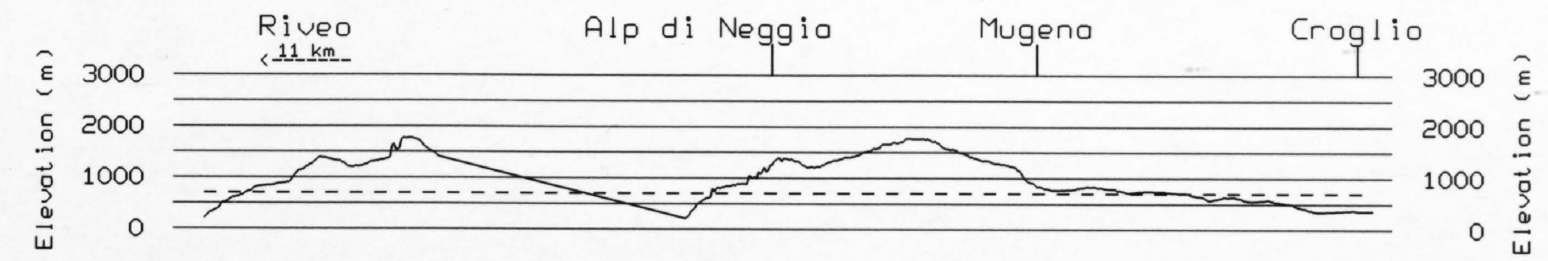

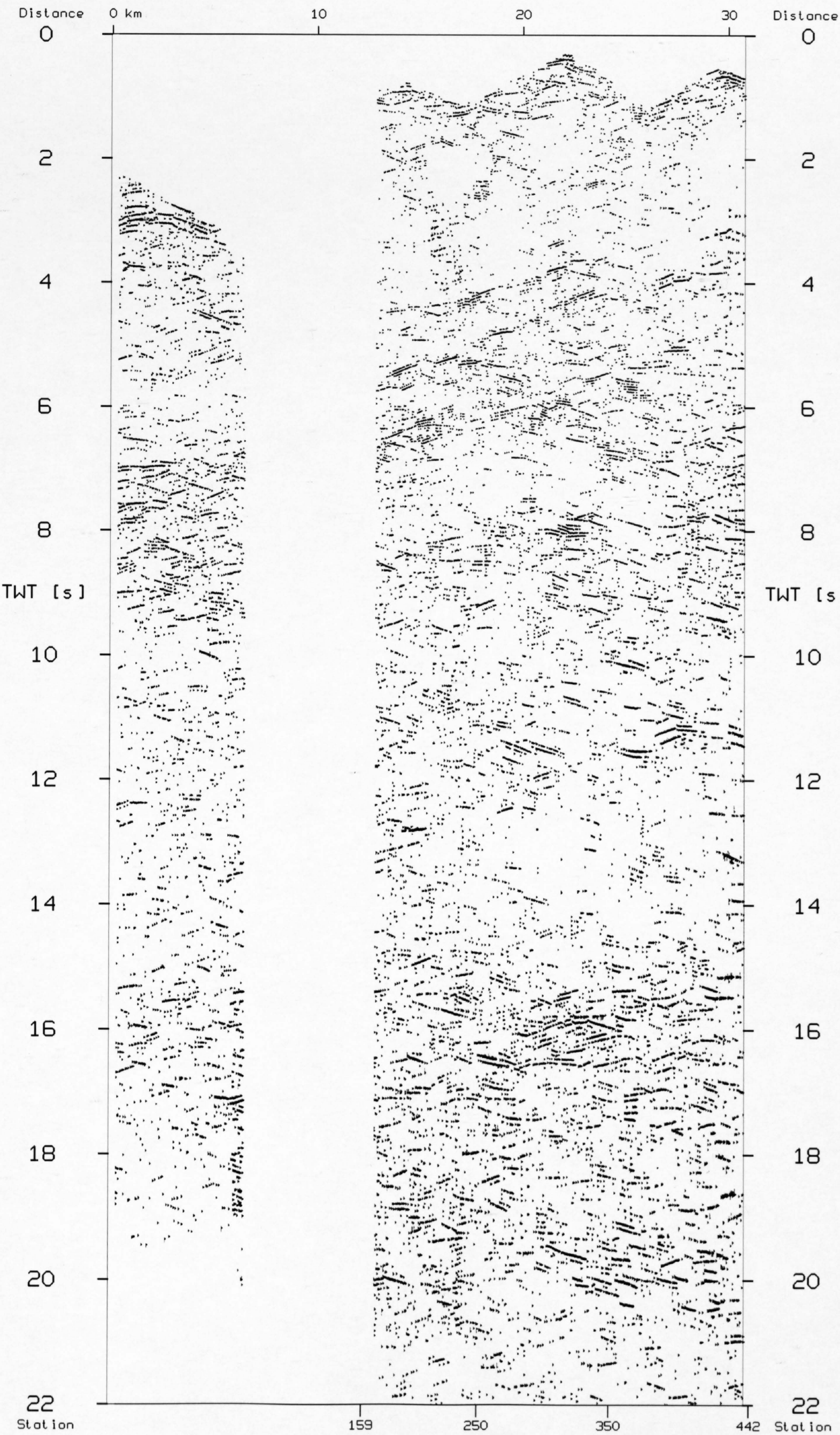

11 Geological interpretation of the seismic profiles of the Central Traverse (lines C1, C2 and C3-north)

O. A. Pfiffner & P. Heitzmann

Contents

11.1 Introduction

The Central Traverse was conceived as an addition to the neighboring Eastern and Western Traverses aiming at a 3 dimensional coverage of the crustal structure of the Swiss Alps. The Central Traverse crosses the Alps from the Subalpine Molasse through the Helvetic and Penninic nappes across the Insubric line into the Southern Alps (see Figure 11-1). The northernmost line C1 contains a short Vibroseis segment which was registered jointly with an industry line (TGK 1) that continues uninterruptedly across the Brünig Pass to the NE. Unfortunately the NRP 20 segment of this line turned out to be of rather poor quality. This shortcoming could be compensated by exchange with the indurstry line TGK 3 (see Figure 13.1-13), which was recorded parallel to the northern segment of line C1 in the valley 10–15 km to the east (Kleines Melchtal). The lines C1, C2 and C3 are thus essentially explosion seismic experiments with low coverage and large offsets and consequently of low resolution in the upper part of the crust. To the south line C3 joins the network of the southern traverse discussed in chapter 10.

Similar to the Eastern Traverse E1 (chapter 9) some of the geologic structures, namely in the Penninic nappes, crossed by the Central Traverse possess considerable dip across the seismic lines. Other structures, such as for example the Aar and Gotthard massifs are crossed more or less perpendicular to their strike. It is thus in some instances possible to establish a geometric tie between the exposed and seismically imaged structures.

Although **line C1** (Figure 11-1) traverses the Helvetic nappes in the north (Wildhorn and Axen nappes) virtually no seismic information was gained from this zone. The geologic cross section shown in Figure 11-6a is thus constructed on the basis of geologic surface data. A general discussion on the structure of the Helvetic nappes is given by Pfiffner 1993 (C1 being located about 5 km E of section D in Pfiffner 1993). The next unit covered by C1 to the south and beneath the Helvetic nappes is the Infrahelvetic complex consisting of the Aar massif – a basement uplift made up of Pre-Triassic basement rocks – and its Mesozoic-Tertiary sedimentary cover which was partly sheard off its original substratum. A more thorough discussion on the geologic structure of this complex is to be found in Chapter 13.1. To the south of the Aar massif a steeply dipping zone of Permo-Carboniferous and Mesozoic cover rocks marks the boundary to the neighboring Gotthard massif (Figure 11-1). Near shot point Oberwald located at the northern end of C2, a sliver of pre-Triassic basement rocks – the Goms "massif" – indicates imbrications at the base of the Gotthard massif.

Line C2 traverses the Gotthard massif and the Penninic basement nappes (Maggia and Antigorio) and the steep belt north of the Insubric Line which contains Penninic (Orselina, Mte Rosa) and Austroalpine (Sesia) nappes (Figure 11-1). In the Gotthard massif Late- to Post-Variscan granites intruded a polymetamorphic gneiss complex containing Caledonian and older rocks. A pervasive Alpine foliation is steeply dipping and even overturned to a northerly dip at the massif's southern end due to a late phase of local backfolding (see Marquer 1990). The Maggia nappe corresponds to a major transverse zone prohibiting direct correlation of the structures forming the Toce dome (or Simplon subdome) in the west and the Lepontine nappe pile (or Ticino subdome) in the east. The Maggia nappe consists essentially of pre-Triassic crystalline basement rocks with some occasional lenses or layers of carbonates of presumably Triassic age. To the west it overlies the Antigorio nappe, to the east it is in steep contact with the adjoining Simano nappe. Merle et al. (1989) interpreted this northern part of the Maggia nappe as a N-S trending synform that evolved as consequence of serial uplift of the Simplon and the Ticino subdomes. In such a scenario the Antigorio (Orsalia, Pioda di Crana and Mergoscia digitations) and Simano nappes would be part of one and the same complex. A different interpretation could be envisaged in which the Maggia transverse structure extends to greater depth and, consequently the Simano nappe is considered as a structurally separate unit from the Antigorio nappe. In this case, the two basement nappes would now lie in similar structural positions but could be thought of as having moved northward as independent blocks (see Probst 1980). In any case the Maggia nappe and foliation planes are sheared into an E–W strike towards the Insubric line (Klaper 1990), and the stretching lineations become successively steeper (Merle et al. 1989). Both features are related to back-thrusting along the Insubric Line. As discussed by Merle et al. (1989) radiometric data indicate that the eastern, Ticino subdome was uplifted mainly in Late Oligocene times (25–20 ma), whereas the western, Simplon subdome was mainly uplifted in Miocene times (15–10 ma). The Maggia transverse zone, which is followed by line C2, is located between these subdomes and possibly related to their mutual interference.

South of the Insubric Line, **line C3** crosses into crystalline basement of the Southern Alps, which consists of the Ivrea Zone and the Strona-Ceneri zone s. l. Line C3 bends sharply and only the NW branch, which forms a continuation of line C2, is dicussed here. The southern branch is treated in more detail in the context of the neighboring seismic lines of the Southern Traverse (Chapter 10). The Ivrea zone is made up of granulite and amphibolite grade paragneisses, and mafic rocks. It contains also lenses of peridotites and thin pegmatite dykes and marble layers (see Schmid 1993 for a review). The Ivrea zone pinches out to the NE such that where crossed by the central traverse its surficial width is only about 1.2 km at most. The Ivrea zone is thought to represent a lower crustal section which was exhumed in the course of Mesozoic extension and Alpine compression (Handy 1990).

The Strona-Ceneri zone s.l. consists of Ordovician pelitic and arenaceous metasediments (see Schmid 1993), some of them possibly being polymetamorphic prior to intrusion of the Ordovician granites. The Strona-Ceneri zone s.l. is intruded by metagranites of Ordovician age (466 ma, Boriani et al. 1982/83) and by Permian granites and basaltic dykes (285.275 Ma, Boriani et al. 1990). The contact between the Ivrea zone and the Strona-Ceneri zone is called Pogallo fault (see Schmid et al. 1987), a deep crustal fault re-

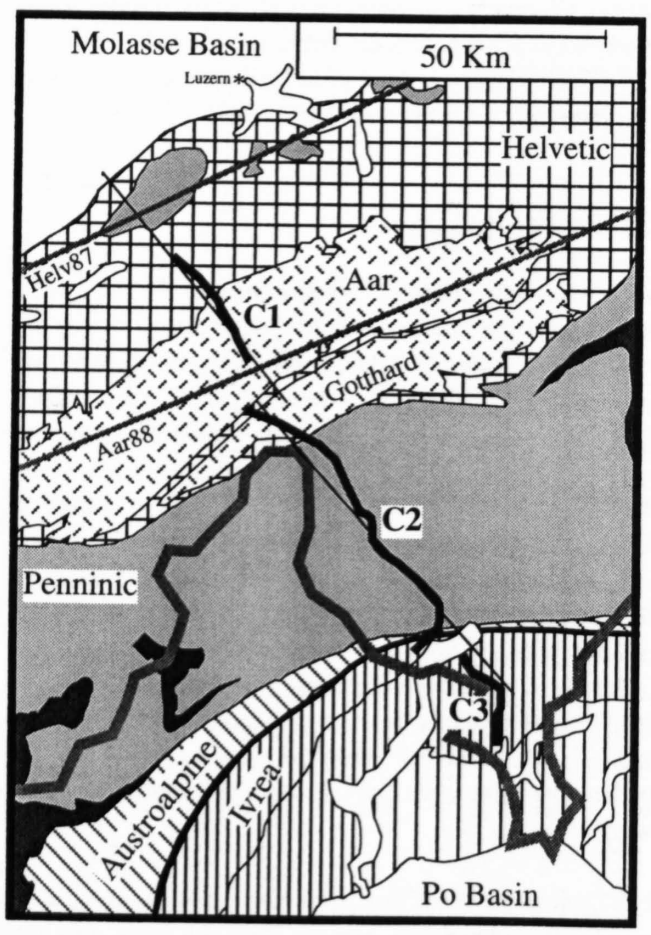

Figure 11-1
Simplified tectonic map of the area of the central traverse showing traces of reflection seismic lines C1, C2 and C3 (thick black lines), refraction seismic lines Helv 87 and AAR 88 (thick gray lines) and cross sections (thin lines).

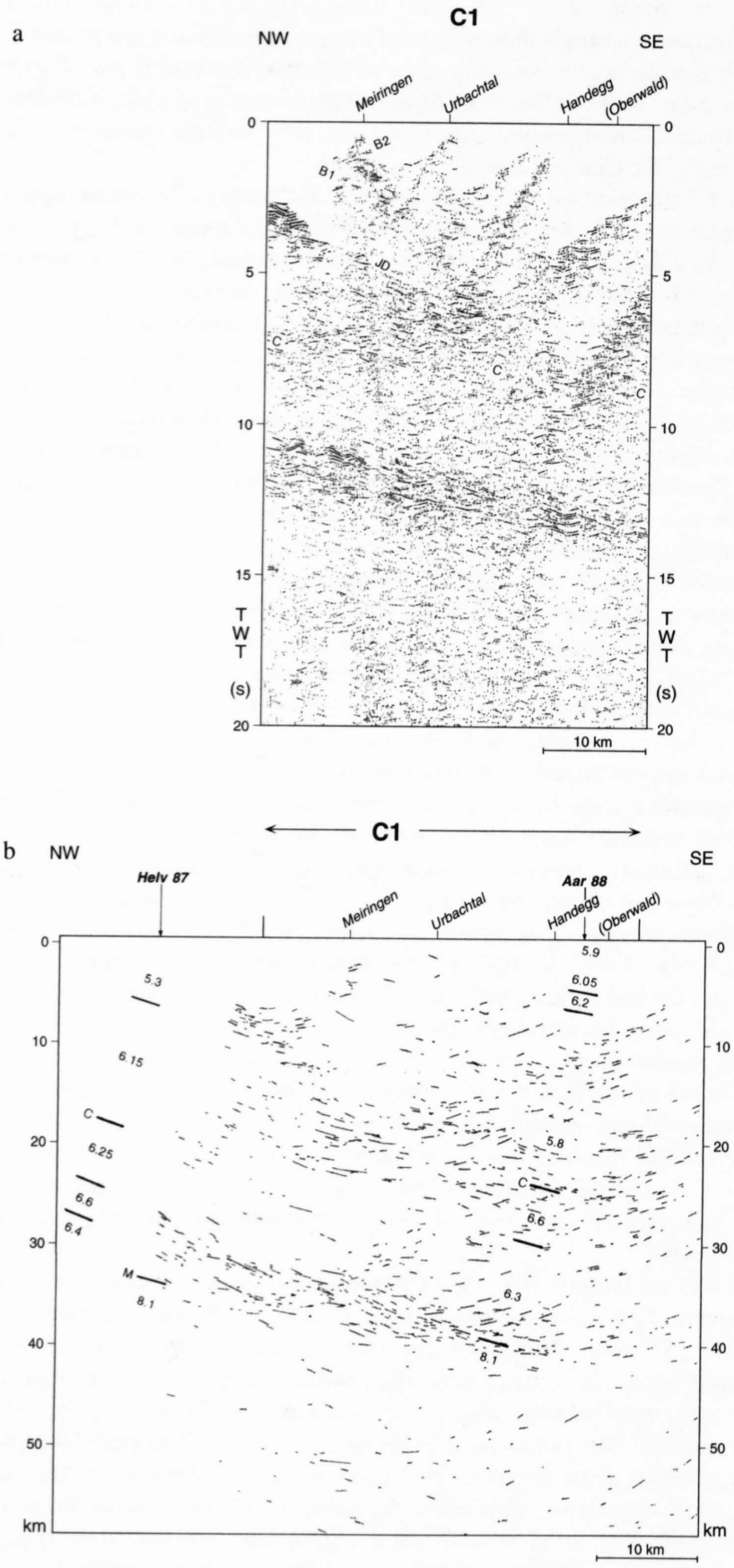

Figure 11-2
Seismic data of line C1.
a) Coherency-filtered, unmigrated explosion seismic data. B1: Mesozoic cover of foreland, B2: Mesozoic cover of Aar massif, JD: Jura detachment (?), C: Conrad discontinuity, M: Moho. Localities are shot points.
b) Depth-migrated explosion seismic data. Numbers are velocities derived from longitudinal refraction experiments Helv 87 (Maurer & Ansorge 1992) and AAR 88 (Baumann 1994), both in migrated position. C: Conrad discontinuity, M: Moho.

lated to Mesozoic extension. Mylonitic foliations related to the Insubric line are nearly vertical in the cross section of the central traverse. These mylonites form a belt of about 1 km thickness along the northern rim of the Southalpine basement. Within the main body of the Strona-Ceneri zone s. l. foliations also dip steeply, but they are of Paleozoic age. Alpine overprint resulted in a network of brittle faults (Schuhmacher 1990), of which line C3 crosses the NW dipping Gambarogno thrust. A more detailed discussion on the structure and evolution of the Southern Alps is given in Chapters 10 and 15.

11.2 Reflection seismic data

The seismic data are presented as final stack on Plate 11-1 (the southern end, line C3, is also discussed by Schumacher in Chapter 10 in the context of the Southern Alps).

Line C1 extends across the Helvetic nappes and the Aar massif and is discussed in chapter 13 in conjunction with the external basement massifs. Figure 11-2 shows computer-generated line drawings of the unmigrated and depth-migrated explosion data (from Valasek 1992). The shallow part of the section to 5 sTWT shows some discontinuous events only. Beneath shot point Meiringen SE-dipping reflections at 2 STWT (B1 in Figure 11-2a) and NW-dipping reflections at 1 sTWT can be recognized. The reflections at 3 to 4 sTWT at the NW end are first arrivals from shot point Flühli located 7.5 km to the NW of the NW end of the seismic section and will thus not be considered in the following. However, the reflections dipping to the SE located between 4 and 5 sTWT just N of shot point Meiringen (marked JD in Figure 11-2a) are possibly real. More coherent reflections (C) are visible in a S-dipping zone at depths between 6 and 10 sTWT. Finally, a well defined band of reflections (M) extends beneath a transparent zone across the entire line from 10–12 sTWT in the NW to 13–15 sTWT in the SE.

Line C2 covers the Penninic basement nappes. Additional seismic data from the Southern Alps and across the Insubric line were registered from shot Mugena located in Line C3 some 20 km SE of the Insubric line and included in this line. Several short, but distinct reflections can be recognized in the shallow part (An, BI, Ve, B4 and B3 at 1, 1.5, 2, 3.5 and 5 sTWT, respectively, between shot points San Carlo and Rivea). A particularly transparent zone extends across the entire section between 12 and 15 sTWT. Reflections above this transparent band are dipping both, to the SE and the NW (C and IL in Figure 11-3). A faint, SW-dipping reflection band (M) is visible at around 16 sTWT beneath shot point San Carlo, tapering off to the SE.

Line C3 crosses the crystalline basement of the Southern Alps. Seismic data from the Penninic nappes N of the Insubric line were also collected by shot Riveo, which is located on line C2 and some 20 km NW of the Insubric line. In the shallow part of the section coherent reflections occur at 3 sTWT near the NW end of the line. In the SE three NW dipping reflections are visible between 3 and 6 sTWT (SAT 1, SAT 2 and SAT 3 in Figure 11-4a). A relatively weak reflection band (Ve in Figure 11-4a) is seen at 2 sTWT beneath shot point Alpe di Neggia. Discontinuous reflections are located above a distinctly transparent band that extends across the entire section at a time interval between 10 and 15 sTWT. Finally, a band of reflections dipping slightly to the S reaches the southern end of C3 at around 20 sTWT.

11.3 Geological interpretation

The crustal structure of this Alpine transect is well known in the uppermost 1–2 km only. The deeper parts are much more difficult to assess by surface data and projection techniques. In the Penninic nappes extrapolation of surface data is rendered particularly difficult because the Central Traverse (line C2) follows the Maggia transverse zone quite closely. This transverse zone separates the Penninic nappe pile of the Toce dome in the west from the Penninic nappe pile of the Leventina area in the east. The structures of both these nappe piles are relatively well constrained, but the lateral correlation across the Maggia transverse zone in the subsurface ("beneath" the Maggia nappe) is problematic. An additional discussion of the structure of the Penninic nappes is given in conjunction with the Southern Traverse (Chapter 10).
The shallow structure and velocities were assessed by 2D ray tracing by Kuhn (1993). The deep crustal structure has been explored by refraction experiments (Lines Helv 87, see Maurer & Ansorge 1992 and AAR 88, see Baumann 1994), which run parallel to the general strike of the Alps and cross line C1 at its NW end.

Interpretation of the shallow structure of **line C1** is also discussed in Chapter 13. It is aided by the reflection data of two industry Vibroseis lines, one registered in the Kleines Melchtal 10–15 km farther east (line TGK 3), the other, TGK 1, being a continuation of line C1 over the Brünig pass. Reflections at 2.2-2.5 sTWT beneath shot point Meiringen (B1 in Figure 11-2), dipping to the SE originate from the autochthonous Mesozoic cover of the foreland.

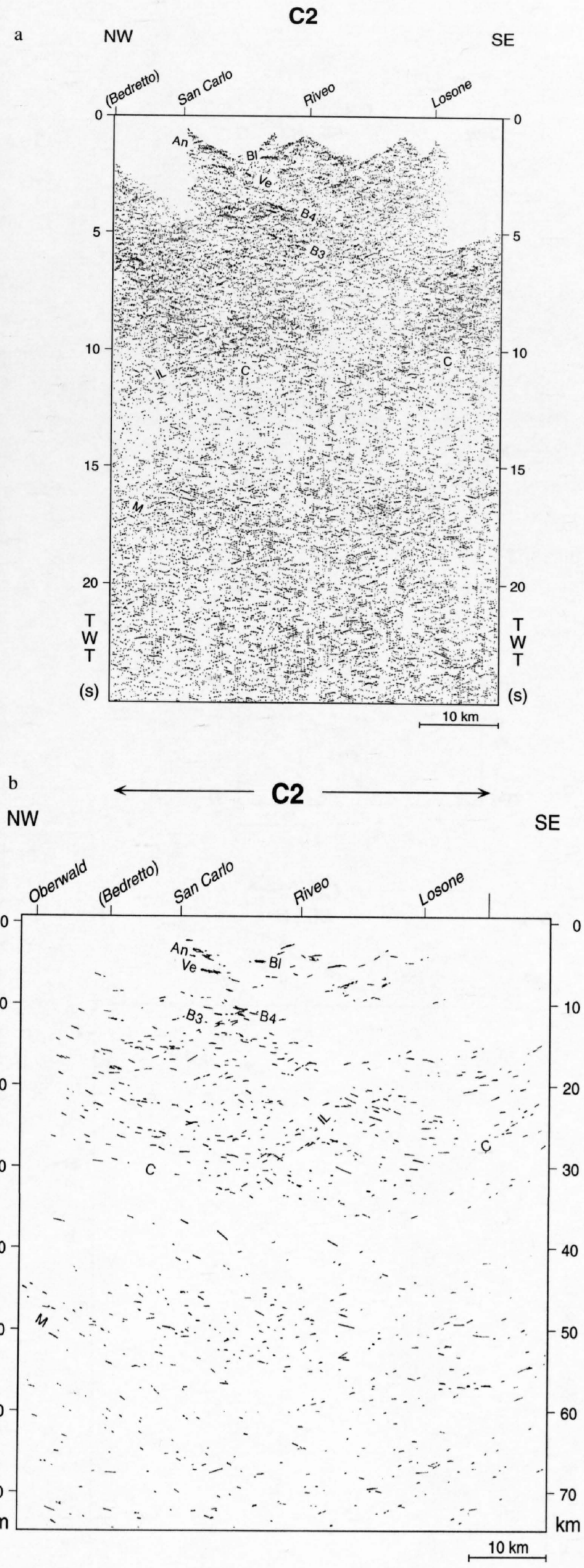

Figure 11-3
Seismic data of line C2.
a) Coherency-filtered, unmigrated explosion seismic data. B3: top Aar massif, B4: top Gotthard, Ve: top Verampio, An: base Antigorio, BI: top Bosco-Isorno, C: Conrad discontinuity, M: Moho, IL: Insubric Line. Localities are shot points.
b) Depth-migrated explosion seismic data. B3: top Aar massif, B4: top Gotthard, Ve: top Verampio, An: base Antigorio, BI: top Bosco-Isorno, C: Conrad discontinuity, M: Moho, IL: Insubric Line.

They can be followed half way to shot point Urbachtal. NW-dipping reflections at about 1–5 sTWT (B2 in Figure 11-2) line up southward with the Mesozoic cover of the Aar massif which breaks surface just north of shot point Urbachtal. The reflections JD (Figure 11-2) could originate from the fault zone related to the detachment of the Jura Mountains discussed in Chapter 8.
In the deeper part the limit between the transparent zone and the overlying reflective zone (C in Figure 11-2, at 8–10 sTWT or 20 km beneath shot point Meiringen) corresponds to the Conrad velocity discontinuity, which marks the limit between the upper and lower crust. According to the refraction experiment Helv 87 (Maurer & Ansorge 1992) the P-wave velocity increases at this interface from 6.15 to 6.35/6.25 km/s, whereas Valasek (1992) has used an increase from 6.1 to 6.5 km/s. The base of the reflection band, which is found at a depth of 12 sTWT or 35 km near the NW end of line C1, corresponds to the MOHO velocity discontinuity (from 6.4 to 8.1 km) marking the crust-mantle boundary as determined from the refraction experiment. The reflection band itself corresponds to a low-velocity layer within the lower crust with a velocity of 6.4 km/s as compared to 8.1 in the underlying mantle and 6.6 in the overlying lower crust. At the southern end of line C1 the refraction experiment AAR 88 (Baumann 1994) indicates a velocity increase from 5.8 to 6.6 km/s at a depth of around 25 km, and a low velocity laryer (6.3 km/s) between 32 and 43 km. Thus, the reflective band extending all the way across line C1 (and parts of C2) can be identified as a reflective lowermost crust, whereas the upper limit of the transparent zone represents the boundary between the upper and lower crust, the Conrad discontinuity.
The geologic profile shown in Figure 11-6a) was constructed based on the interpretations discussed above. The geometry and structure shown in the shallow part was obtained by extrapolation of geologic surface data, by the Vibroseis data (industry line TGK 3; see Figure 13.1-13), and using the information gained from the neighboring line C2 in the SE. The latter is particularly true for the shape of the contact between the Gotthard and Aar massifs, which is formed by a very steeply dipping (and even overturned) layer of Permo-Carboniferous and Mesozoic sediments (the so-called Urseren zone) that levels off southwards. In the deeper part the depth migrated seismic reflection data of line C1 were used to extrapolate the crustal structure gathered from the intersecting refraction lines Helv 87 (Maurer & Ansorge 1992) and AAR 88 (Baumann 1994) across the entire length of C1. The unit overlying the Gotthard massif beneath shot point Bedretto, the Lucomagno/Leventina unit, outcrops in the Leventina valley (located east of this transect) and pinches out going west. Thus in Figure 11-6a it forms a thin sliver only, and in the profile of Figure 11-6b, which is slightly farther west, it does not appear anymore at all and is replaced by the Verampio unit. This latter unit is observed at outcrop farther west in the Verampio inlier.

The interpretation of **line C2** is based on an analysis of the 3D geometry of the Penninic nappes in this transect. Similar to the Eastern Traverse the Penninic basement nappes are partly separated by thin, sometimes discontinuous layers of Mesozoic carbonates. The contacts between such carbonates and the crystalline basement rocks (mainly gneisses and schists) possess high impedance contrasts and are thus potential reflectors (see e. g. Sellami et al. 1990, Pfiffner et al. 1991, and Wagner et al., Chapter 6). The geometry of the various nappe contacts has been studied by Klaper (1990) by means of structure contour maps, integrating a wealth of regional data. Figure 11-5 is a compilation of the structure contour maps of the Penninic Antigorio and Simano nappes (after Klaper 1990) and the adjacent Gotthard and Aar massifs (from Pfiffner et al 1990a). The Aar and Gotthard massifs are elongate structural highs that parallel the Alpine strike. The Antigorio and Simano nappes on the other hand display an extremely irregular shape dure to intensive post-nappe folding. The two nappes are laterally juxtaposed along the Maggia transverse zone. This transverse structure is particularly well underlined by the top of the two basement nappes which form a V-shaped depression in a NNW–SSE direction. This "valley" is occupied by the Maggia basement nappe. This nappe's internal structure also reflects the transverse trend: strikes of the principal foliation and trends of stretching lineations closely follow the NNW–SSE orientation of the transverse "valley" (see Klaper 1990). One of the striking features of the Antigorio nappe is the Wandfluhhorn fold (W in Figure 11-5) which wraps the Antigorio nappe around the fold's core consisting of the Bosco-Isorno nappe (see also Merle et al. 1989). The upper limb of this fold (the so-called Pioda di Crana digitation) strikes NW–SE, i. e. parallel to line C2. Reflections from this limb should thus appear horizontal. Upon projection of this NE-dipping limb into the seismic section one obtains a nearly perfect match with a horizontal reflection located betweeen shot points Riveo and San Carlo at 1.6 s TWT (marked BI in Figure 11-3). Similarly the slightly SE-dipping reflection marked An at 1.5 s TWT beneath shot point San Carlo in Figure 11-3 closely matches the projected base of the Antigorio basement, which overlies Bündnerschiefer at this location (Probst 1980). The Antigorio nappe overlies the Verampio unit. The latter outcrops just beneath the circular high (3 km above sea level) that can be recognized in the western part of this nappe in Figure 11-5 (coord. 665/120)

and which corresponds to the heart of the Toce culmination. The top of the Verampio basement is approximatly 2 km beneath the top Antigorio, the contact between the two nappes being marked by a sedimentary layer. This contact zone projects northeastwards into line C2 to a depth of 2–2.5 s TWT (or about 5 km below sea level) beneath shot point San Carlo (Ve in Figure 11-3). Two deeper lying, S-dipping reflection groups, B3 and B4, appear at around 4 and 5 sTWT beneath shot point Riveo (Figure 11-3a). In the depth-migrated data (Figure 11-3b) only B4 remains as coherent reflection group, whereas reflections contributing to B3 are torn apart. B4 can be correlated to the southern extension of the top of the Gotthard massif with some confidence. The latter dips steeply near the surface. In the central part of the Gotthard it is even slightly overturned, as indicated by the +1km-contour in Figure 11-5, which is located to the N of contour +3km near shot point V. Bedretto. The deformation held responsable for this overturning, the so-called "back-folding", corresponds to a phase of horizontal N–S shortening and vertical extension. It reoriented the earlier foliation into a fan structure with the foliation in a subvertical orientation in the center, steeply S-dipping in the north, and N-dipping in the south (see Merz 1989, Marquer 1990). A second, crenulation type cleavage is associated with these "back-folds" (Etter 1986), whereas Marquer (1990) Merz (1989) described shear zones with "top to the SE" shear sense in the Gotthard basement. The wavelength and amplitude of these backfolds has been assessed by Etter (1986) and Marquer (1990). The amplitude of the backfold seems to be maximum in the area crossed by line C2, tapering off eastwards and westwards. In any case the basement top eventually continues deeper down with a southerly dip. It is interpreted to match with reflection group B4.

Reflection group B3 is tentatively correlated with the contact between Aar and Gotthard basement. At the surface this contact is subvertical and marked by a layer of Permo-Carboniferous and Mesozoic sediments (Urseren zone). How far down this sedimentary layer extends is open to discussion. The top of southernmost Aar massif (labeled B3 in line C2) and the Gotthard massif both represent the crystalline substratum of the Helvetic nappes. The latter have a minimum length of 20 km in the retrodeformed stage when considering only the block outcropping between shot points Urbachtal and Flühli. Their eroded southern continuation above the Aar massif would add at least another 20 km. Thus a minimum of 40 km of crystalline basement is needed as substratum for the Helvetic nappes. The repartition of these 40 km between the Aar and Gotthard basement blocks (and possibly the Verampio and Simano units) is difficult to assess (see Pfiffner 1985 for a more detailed discussion). A solution with 20 km of Aar massif basement, capped by remnants of Triassic carbonates, extending from shotpoint Oberwald southwards is at least plausible. This would bring the potential reflector, i. e. the basement-carbonate interface, to a position beneath shot point San Carlo. To explain the reflection package B3 beneath shot points San Carlo and Riveo, about 30 km of Aar massif basement would be needed. In such a solution the southern subsurface extension of the Aar massif would account as crystalline basement for most of the Helvetic nappes in this transect. In comparison with the eastern and central traverses this solution is rather unlikely. An alternative model would be to explain the reflections B3 beneath San Carlo and Riveo to stem from a mylonite zone forming the downward extension of the the thrust fault putting the Gotthard massif onto the Aar massif. Considering displacements (Pfiffner 1985) of a basal thrust putting the Gotthard massif onto the Aar-massif, thereby shearing off a sedimentary layer of initially 20 km length, a southward extension of that basal thrust within the crystalline basement would likely reach as far as Riveo and be associated with a mylonite zone, which could in turn explain reflection group B3.

The transparent zone beneath C in Figure 11-3 lines up with the similar transparent zone in the neigboring line C1. There the upper limit of this zone was correlated with the Conrad discontinuity, an interpretation that is followed in line C2. Similarly, the lower limit of the reflection band (M in Figure 11-3) visible at the northern end of line C2 is identified as the Moho. In contrast to line C1, the lowermost crust thins and loses its reflective character rapidly going to the SE. The curst/mantle boundary as shown in the geologic profile of Figure 11-6b is based on the velocity data used for migration by Valasek (1992).

Line C2 crosses the Insubric Line near shot point Losone. This major fault zone is very steeply dipping where it breaks surface. The rather vague NW-dipping reflections IL at 25 – 30 km beneath Riveo (Figure 11-3b) could well originate from a mylonite zone associated with an Insubric Line levelling off at this mid-crustal level (see also chapter 10). The shape of the Insubric Line as shown in the geologic profile of Figure 11-6b is based on this tentative interpretation. It will be noted that the Insubric Line at this depth coincides with the top of a wedge of lower Adriatic crust. Inspection of the transparent zone beneath the Conrad discontinuity (C in Figure 11-3) reveals that the latter tends to rise near the SE end of line C2. This trend continues in the neighboring line C3.

The interpretation of **line C3** is only briefly commented on here. A more detailed discussion is given by Schumacher in Chapter 10. The Southalpine

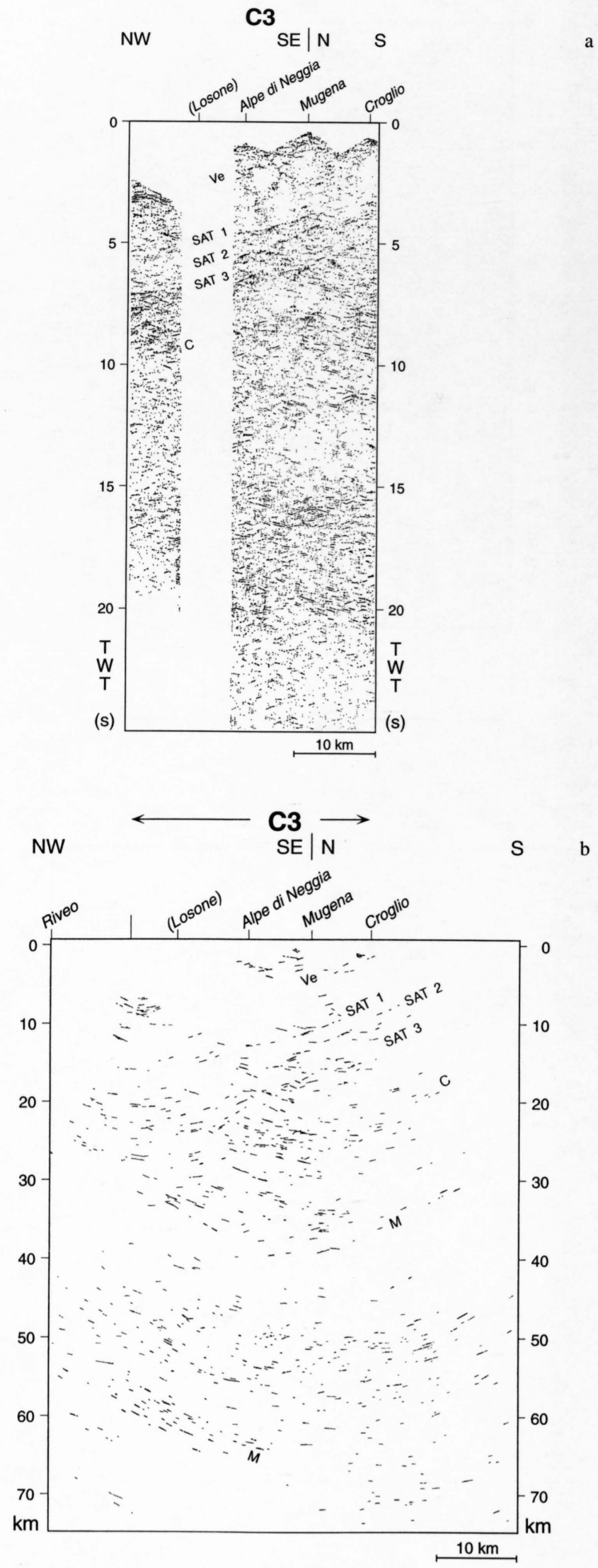

Figure 11-4
Seismic data of line C3.
a) Coherency-filtered, unmigrated explosion seismic data. C: Conrad, Vd: Veddasca thrust, SAT 1, 2, 3: Southalpine thrust 1, 2, 3. Localities are shot points.
b) Depth-migrated explosion seismic data. C: Conrad, Ve: Veddasca thrust, SAT 1, 2, 3: Southalpine thrust 1, 2, 3, M: Moho. Localities are shot points.

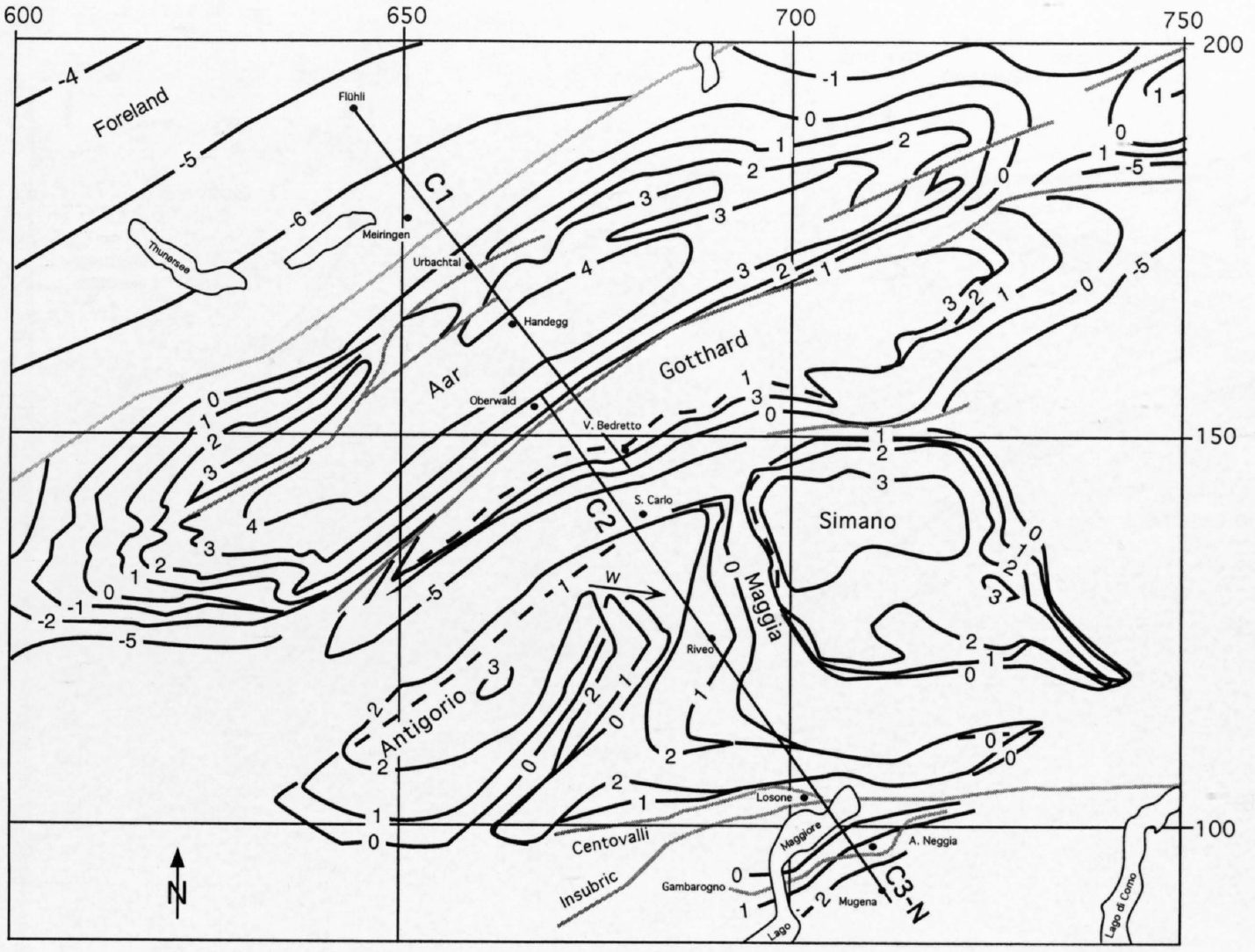

Figure 11-5
Structure contour map of the top of the major basement units in the transect of the Central Traverse. Dots are shot points (with locality names). Thin black lines are traces of the geologic profile of Figure 11-6. Gray lines are major thrust faults. Numbers are km above/ below sea level. Horizontal and vertical coordinates are km of Swiss National grid net.

crystalline basement crossed by the NW part of line C3 is cut by various faults (Schumacher 1990 and Chapter 10) of differing ages, orientations and types. The uppermost structure, the Gambarogno thrust (see Figure 11-5) is too shallow to be imaged by this seismic survey. Reflection band Ve (Figure 11-4) would break surface SE of shot point Mugena and could match the Veddasca thrust fault. The deeper reflections SAT 1, SAT 2 and SAT 3 are tentatively interpreted to represent N- or NW-dipping Alpine thrust faults putting basement onto basement similar to the ones observed and interferred in the area east of Lago di Como (Schönborn 1992). Whether or not a correlation between units I, II and III as defined by Schönborn (1992) and the Southalpine thrust faults SAT 1, SAT 2 and SAT 3 as identified in line C3 exists, is left open. Schumacher discusses SAT 1 (I) and SAT 2 (J) in chapter 10 in terms of two thrust faults converging eastwards, but which can be related to reflections on line S3 located some 10 km to the east of line C3.
In the deeper part of the section the Adriatic Conrad discontinuity (C in Figure 11-4) is positioned according to the velocity model used by Valasek (1992) beneath shot point Alpe di Neggia, but is prolonged to the SE up-dip parallel to the migrated reflections. It corresponds to a velocity increase from 6.1 to 6.5 km/s. The Adriatic crust/mantle boundary (M in Figure 11-4) is also positioned according to the velocity discontinuity (6.5 to 7.9 km/s). Inspection of Figure 11-4 reveals that beneath shot points Alpe di Neggia and Mugena a NW-dipping Adriatic Moho at a depth of 40 km clearly overlies a SE-dipping European Moho positioned at a depth of 65 km. This represents clear evidence for a wedge of Adriatic mantle and lower crust thrust northward on a SE-dipping thrust fault over Eurpean mantle and lower crust. The wedge is bounded at its top in the frontal part by a NW-dipping thrust fault (reflections IL in Figure 11-3) which steepens up-dip and breaks surface as Insubric Line. A different interpretation concerning noteably the depth and orientation of the Conrad discontinuity and the crust-mantle boundary is presented by Marchant & Stampfli in Chapter 24.

11.4 Discussion

The Central Traverse displays all the features and structures of the continent-continent collision between the European and Adriatic plates. To the north (lines C1 and C2) northvergent thrusting resulted in a stack of upper crustal, crystalline basement nappes. The Mesozoic cover of these units was sheared off in an early stage of the deformational history and has been largely removed by erosion in this transect. Similarly, southvergent thrusting within the Southern Alps (line C3) produced a stack of crystalline basement units involving both, the upper crust (Strona Ceneri zone) and the lower crust (Ivrea zone).

The seismic data support the idea of a doubly vergent compressional orogen, similar to the model by Willet et al. (1993). In particular these data suggest the presence of an Adriatic wedge of lower crust and lithosperic mantle which was forced into the European crust. The lower European crust was overridden (or subducted). Given the greater thickness of the European lower crust just beneath the tip of the wedge as compared to the northern end of the central traverse (see Figure 11-7) it seems that the subducted lower crust was internally shortend and thickened in this process. This is underlined by the fact that this lower crust represents the thinned margin of the European plate (substratum of the Gotthard and the Penninic basement units). This margin was extended and thinned in Jurassic and Cretaceous times and the lower crust was thus propably thinner than the one in the foreland to the north prior to Alpine compression. Deformation in the hanging wall of the wedge led to the formation of a low-taper pro-wedge (Aar, Gotthard, Verampio and Antigorio in Figure 11-7) and a high-taper retro-wedge. The latter comprises the crustal flakes of the Southern Alps (line C3) as well as the rear end of the Penninic nappes, which were up-thrusted along the steeply N-dipping Insubric Line. Ductile folding accompanied this up-thrusting in the area just north of the Insubric Line. Ductile deformation produced steeply N-dipping foliations and stretching lineations along the Insubric Line. Fission track data suggest an episode of rapid cooling and associated uplift of the northern block in the time span 25 – 20 Ma (Hurford et al. 1989). It has to be stressed here, however, that significant horizontal movements occurred as well along the Insubric Line in post-Oligocene times. These strike-slip movements can be seen in the framework of sideways escape of the Lepontine dome in response to indentation (Schmid et al. 1989).
The ductile deformation of the northern block is more or less coeval with the Bregaglia intrusion situated farther east (see Chapter 22). This intrusion is likely to have some remnants of a connection to the Adriatic mantle from petrological arguments (von Blanckenburg 1990). The white lenses straddling the Insubric Line and the base of the Adriatic wedge in Figure 11-7 could represent equivalents of this intrusion in the central transect. At the very same position, i. e. between the Monte Rosa and the Sesia basement one would also expect remnants of the Alpine suture in the form of ophiolitic lenses of the Piemont ocean. It has to be said, though, that at the moment no geophysical evidence for the presence (or absence) of such lenses exists.

Acknowledgements

This chapter benefitted from critical review and discussion by J. Ansorge, M. Baumann, L. Hitz, E. Klaper and P. Lehner. Thanks go to I. Blaser, S. Sahli, W. Schaad and R. Zurbriggen for technical assistance.

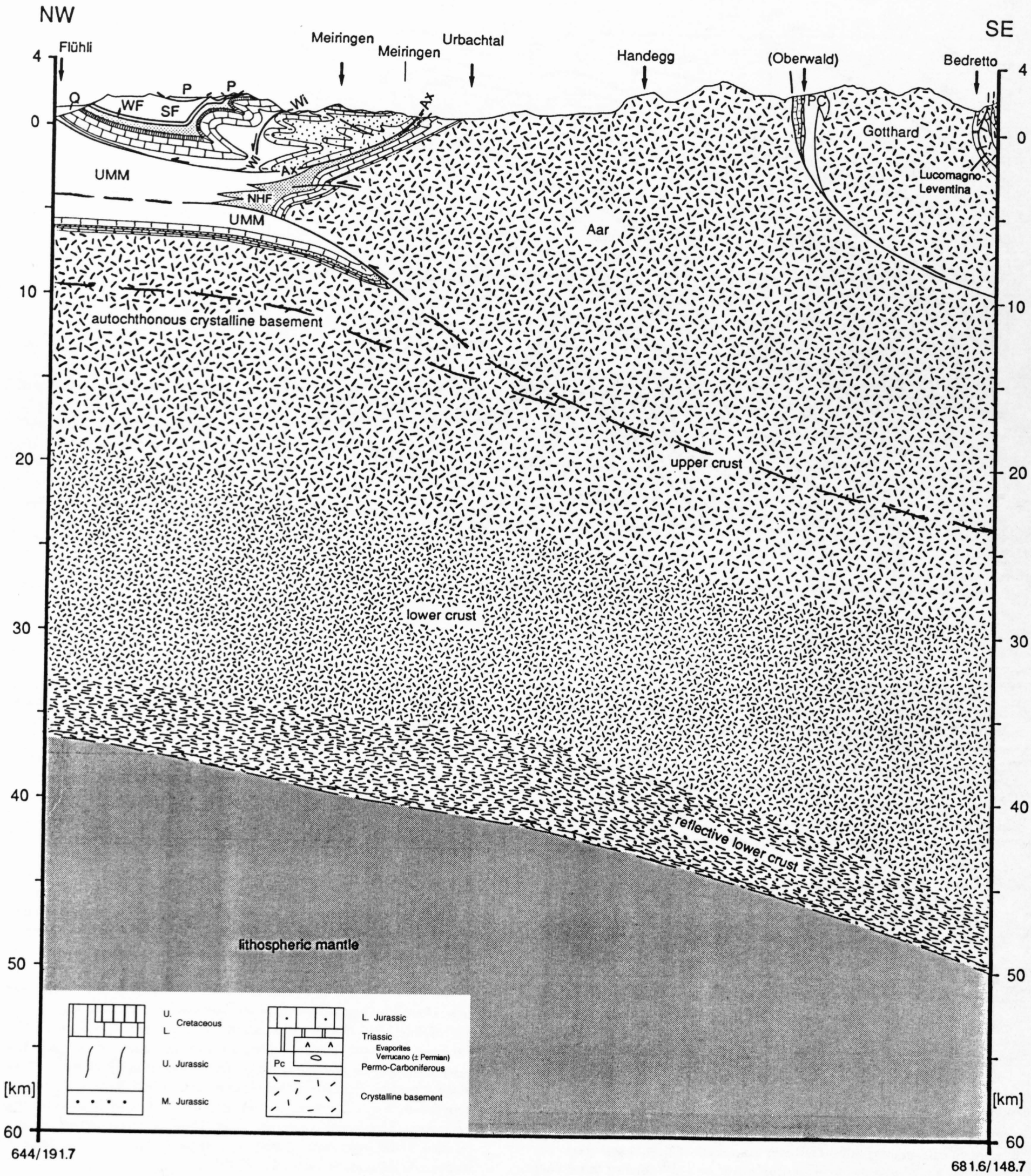

Figure 11-6a

Geologic profile of Central Traverse based on interpretation of seismic data. Trace is given in Figure 11-5. Section is parallel to seismic line C1. The Aar massif is thrust northward onto the autochthonous foreland. The top of the Aar / base of the Gotthard are subvertical at the surface, levelling off going southward. P: Penninic nappes, SF: Schlieren Flysch, WF: Wildflysch, UMM: Subalpine, Lower Marine Molasse, NHF: North-Helvetic Flysch, Ax, Wi: Axen, Wildhorn thrust.

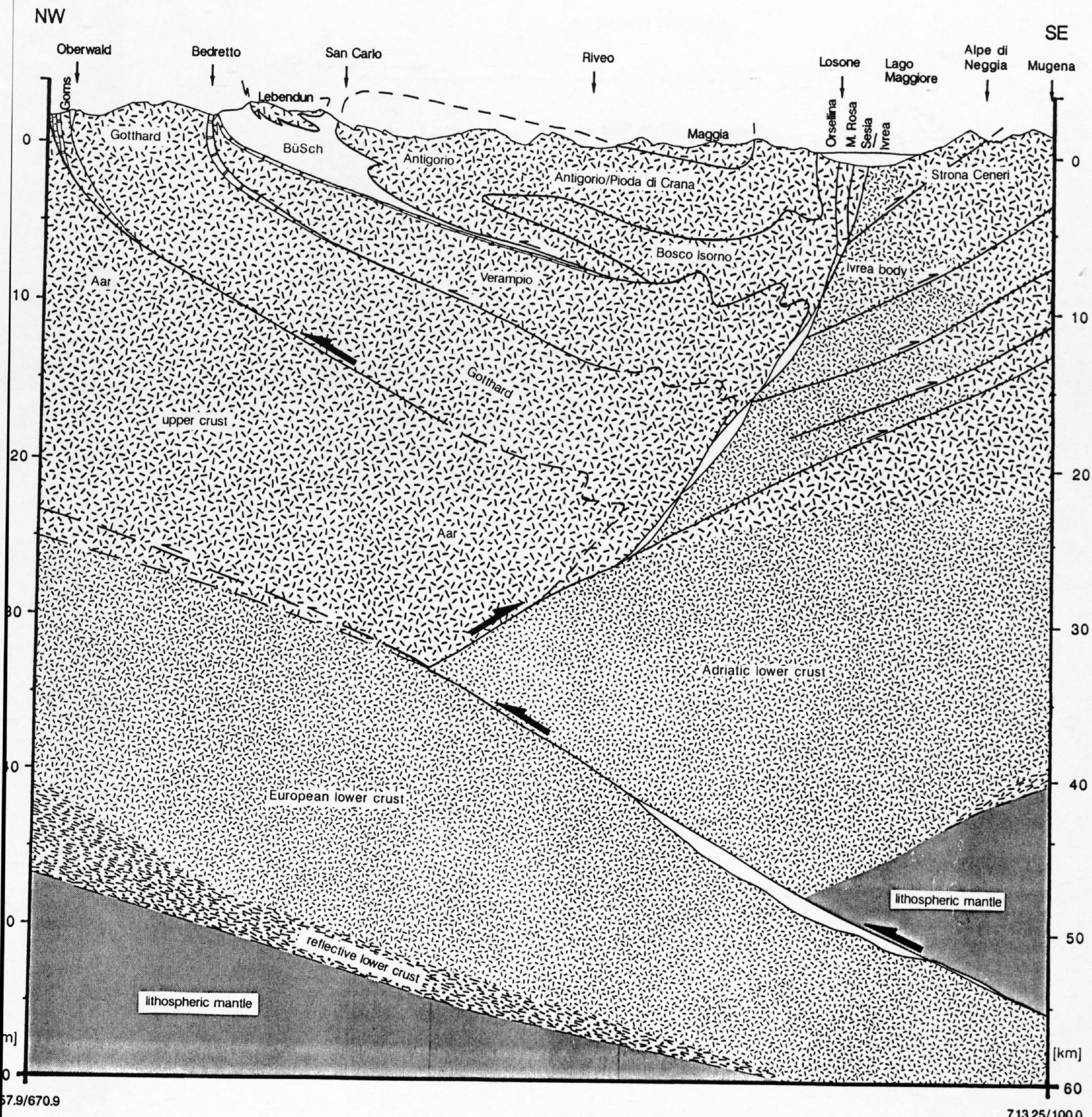

Figure 11-6 b

Geologic profile of Central Traverse based on interpretation of seismic data. Trace is given in Figure 11-5. Section is parallel to seismic lines C2 and NW part of C3. The Penninic basement nappes (Verampio, Antigorio, Maggia) were stacked in a northerly direction, the Southalpine crystalline thrust sheets in a southerly direction. A wedge of Adriatic lower crust and lithospheric mantle was forced into the European crust, splitting it apart and overriding the European lower crust. White areas along Insubric Line at the N limit of the Ivrea body are equivalents of Bregaglia intrusion and/or lenses of ophiolitic rocks from the Piemont oceanic suture. BüSch: Penninic Bündnerschiefer.

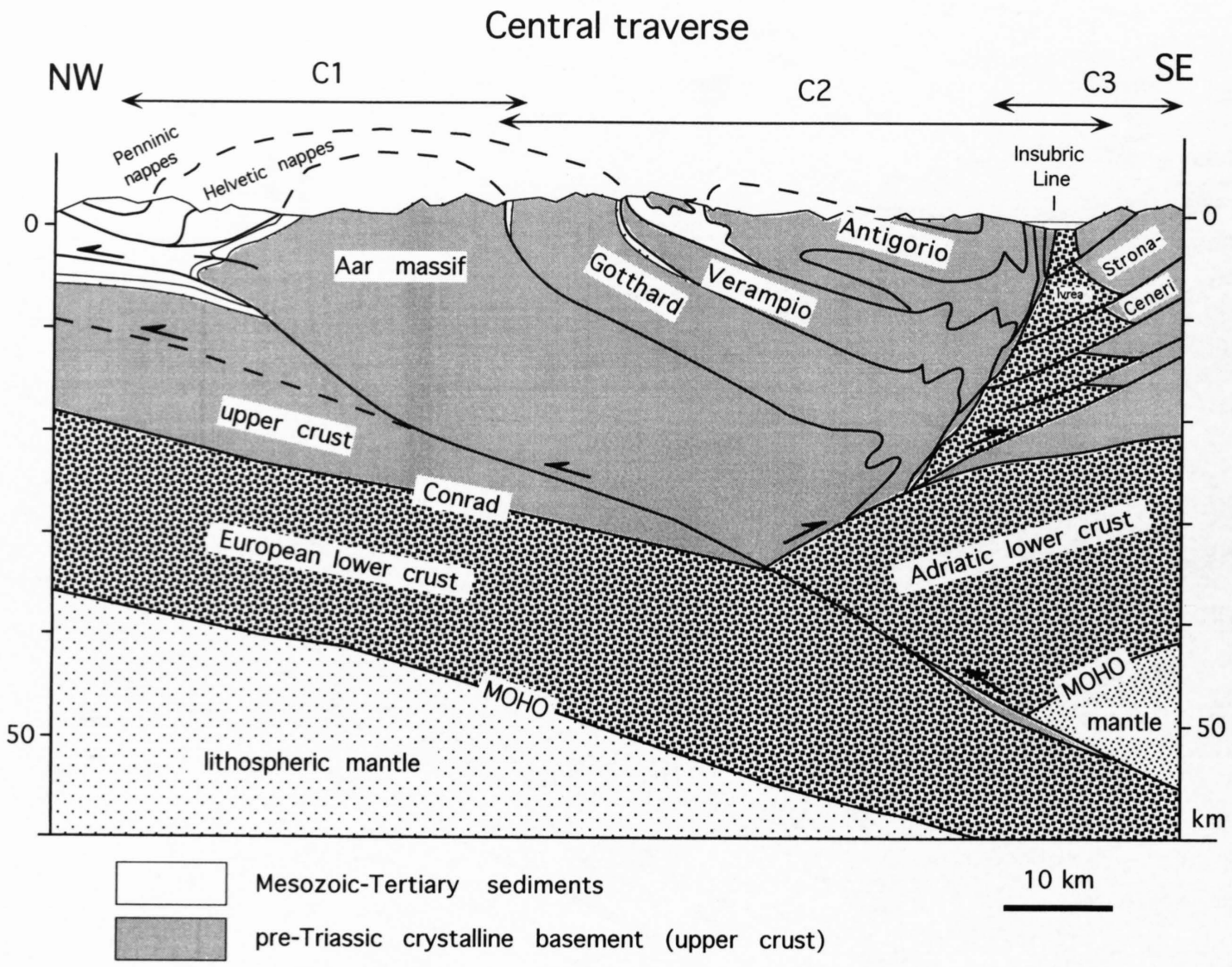

Figure 11-7
Geologic profile along the Central Traverse constrained by seismic data from lines C1, C2 and C3.

Plate 11-1

SWISS NATIONAL SCIENCE FOUNDATION

90-NF-CENTRAL (DYNAMITE)

FINAL STACK

1: 200'000

RECORDING PARAMETERS

SPREAD LAYOUT	34.8 km
CHANNELS	360
SOURCE TYPE	Dynamite
SOURCE DEPTH	20-80 m
CHARGE SIZE	100-400 kg
GROUP INTERVAL	100 m
GEOPHONE TYPE	10 Hz
GEOPHONE PATTERN	24 in-line / 100 m
INSTRUMENTATION	SERCEL 368
FIELD FILTERS	HC 88.8 Hz
COVERAGE	1 - 4
SAMPLING RATE	4 ms
RECORDING LENGTH	60 s
RECORDED BY	PRAKLA SEISMOS AG
DATE RECORDED	June 1990

PROCESSING PARAMETERS

1. Demultiplex and gain recovery
2. Trace editing and resample to 8 ms
3. Crooked line geometry
4. Field static correction
5. Predictive deconvolution
6. Time variant bandpass filter
7. Time variant trace equalisation
8. CDP-Sort
9. Mute application
10. NMO-Correction
11. CDP-Stack
12. Strong coherency filter
13. Combination of several lines

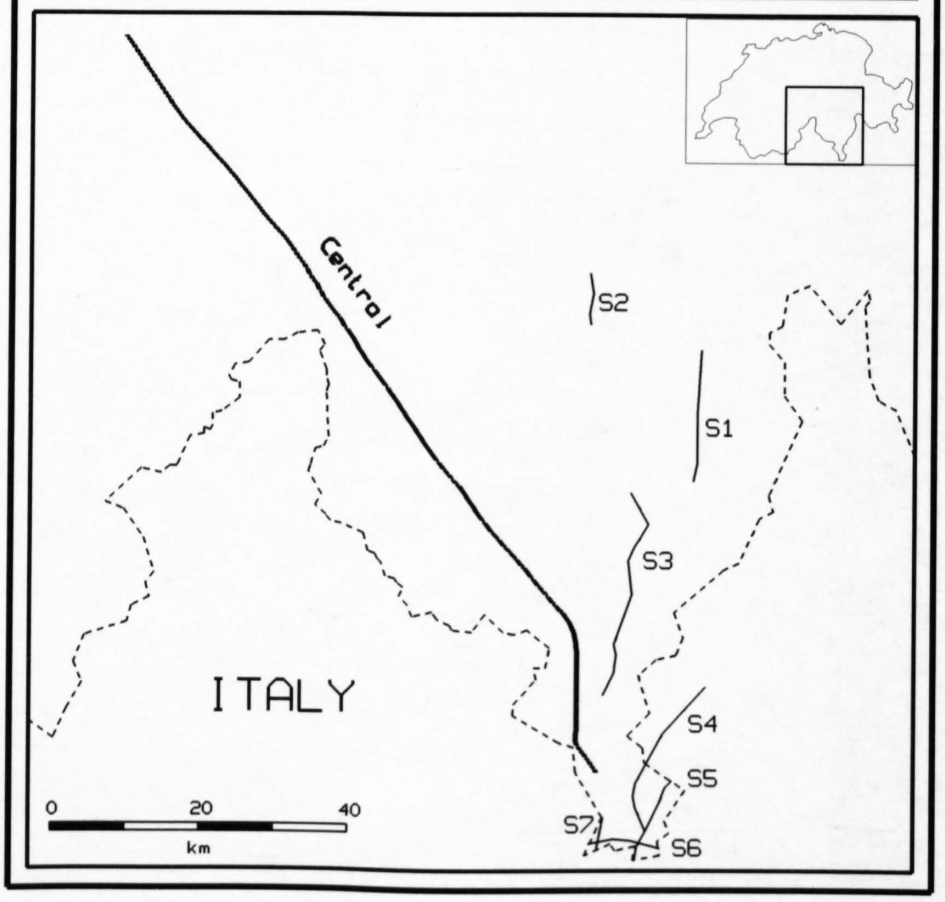

Plate 11-1

C1 C2 C3

NW SE

Meiringen Urbachtal Handegg Oberwald Bedretto San Carlo Bignasco Riveo Gordevio Losone Magadino Mugena Croglio

Elevation (m) 3000 2000 1000 0

Distance 0 km 10 20 30 40 50 60 70 80 90 100 110km

TWT [s] 0 2 4 6 8 10 12 14 16 18 20 22

CDP 1 100 200 300 400 500 600 700 800 900 1000 1100 1200 1300 1400 1500 1600 1700 1800 1900 2000 2100 2200 2300

12 Geological interpretation of the seismic profiles through Western Switzerland: Rawil (W1), Val d'Anniviers (W2), Mattertal (W3), Zmutt-Zermatt-Findelen (W4) and Val de Bagnes (W5)

A. Steck, J.-L. Epard, A. Escher, P. Lehner, R. Marchant & H. Masson

Contents

12.1 Introduction

The Central Alps are one of the best studied mountain belts of the world. In the middle of the last century, Hans Gerlach (1869) produced a geological map of the Penninic Alps between the Bergell area and the Mont Blanc Massif. In 1901, during the construction of the Simplon railway tunnel, Hans Schardt (1903) discovered and described the nappe structures of the Penninic region. Ten years later, Emile Argand (1911) devised a method to construct geological cross sections of the Penninic zone of the Central Alps down to a depth of more than 20 km. Since this time several generations of geologists have worked in this region. The deep seismic survey of the NRP 20 program is the first reflection seismic study that has been undertaken in this region of the Central Alps. The NRP 20 Western Traverse consists of five deep-seismic lines (W1–W5; for location, see Figure 12-1) as well as a few seismic profiles from the petroleum industry (W6, discussed by Pfiffner et al. in Chapter 13.1 and W7–W10

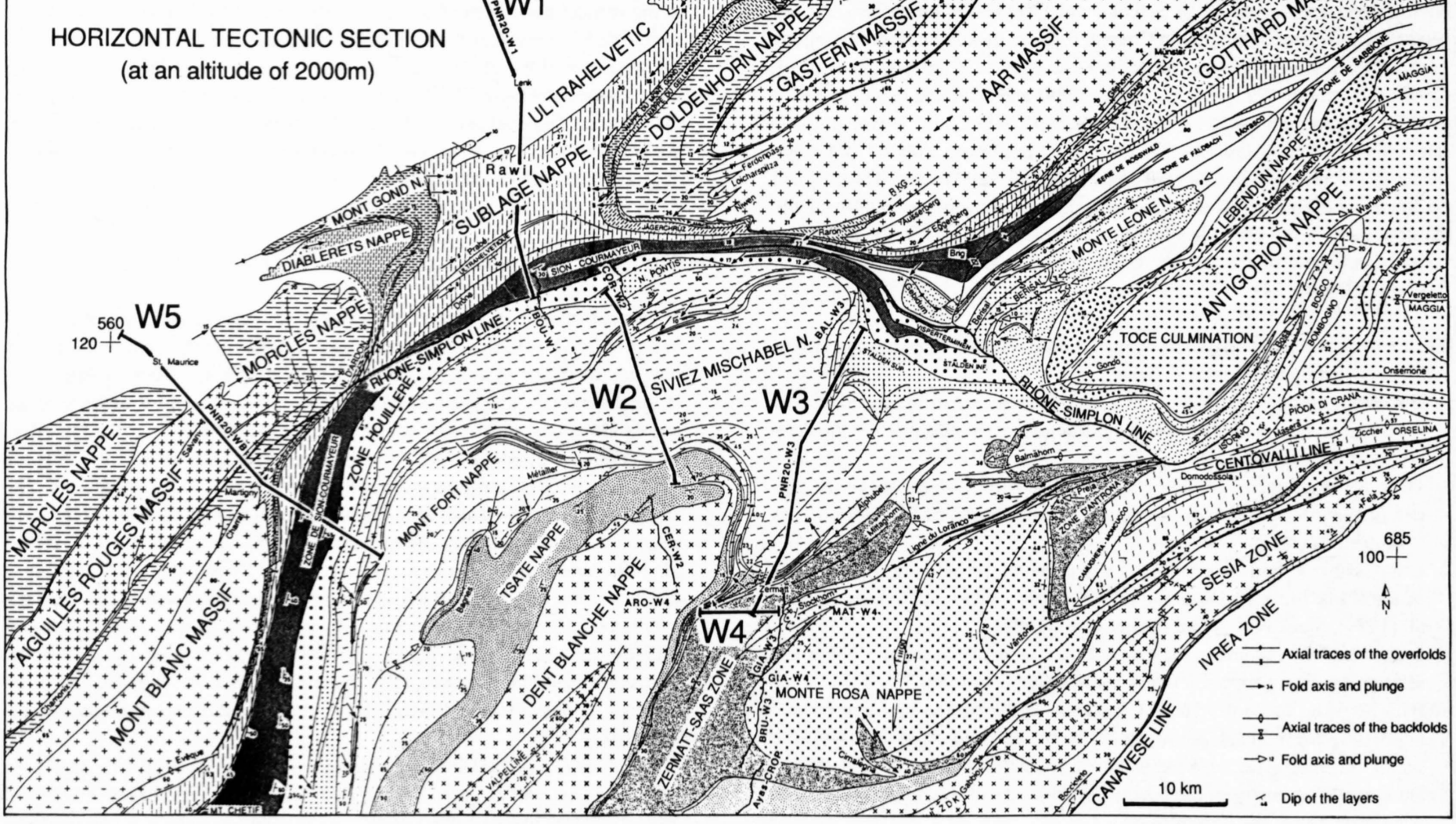

Figure 12-1
Horizontal tectonic section of the Central Alps of Western Switzerland with location of the seismic profiles W1–W5.

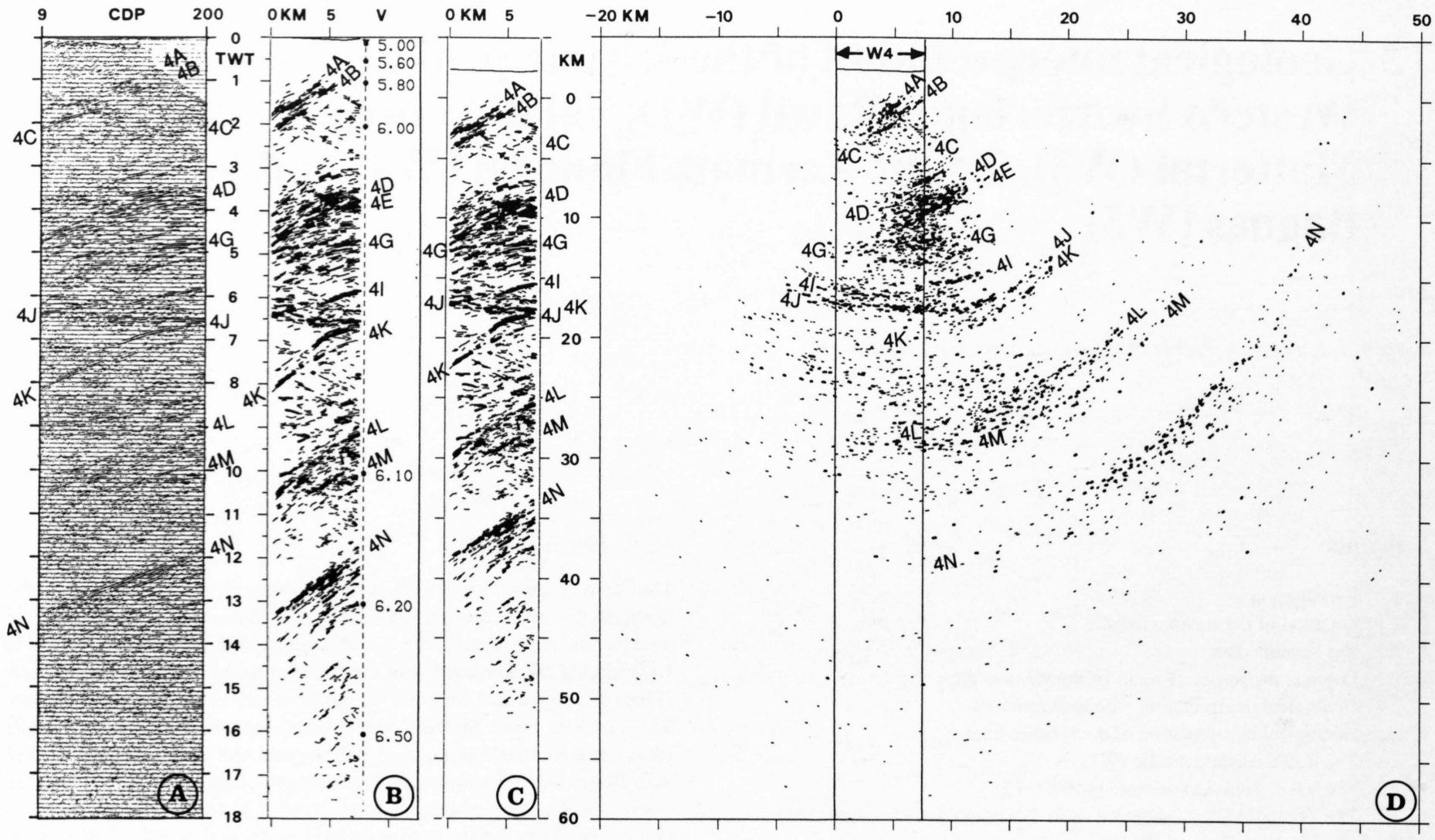

Figure 12-2
Geometric depth migration of the W4-vibroseis-line using the CIGOGNE program; A: initial stacked section; B: digitized stacked section with the depth-velocity function (V = averaged velocity in km/s); C: depth converted stacked section; D: geometrically depth migrated section.

by Pfiffner et al. in Chapter 8). Several publications, describing the NRP 20 program as a whole, mention some general aspects of the Western Traverse (Finckh et al. 1987; Frei et al. 1989, 1990, 1992; Heitzmann et al. 1991). Information on acquisition and processing, as well as some preliminary interpretations, can be found in publications from Du Bois et al. (1990a, 1990b), Valasek et al. (1990), Valasek (1992), Levato et al. (1993, 1994) and Green et al. (1993). Laboratory velocity measurements on rock samples from the survey area were carried out by Sellami et al. (1993), Sellami (1993), and are reported by Wagner & Sellami in Chapter 6. More detailed interpretations, as well as seismic and gravity modelling are presented in Marchant et al. (1993), Marchant (1993), Levato et al. (1994) and Klingelé (Chapter 13.2). Additional information can be found in the NFP 20 Bulletins as well as Pfiffner et al. (Chapters 8 and 13.1). In particular, an extensive review of the geology and tectonics in the area covered by the NRP 20 Western Traverse can be found in Escher et al. (Chapter 16). The geodynamic evolution of the Western Alps is presented in Stampfli & Marchant (Chapter 17) and lithospheric-scale interpretations along the Western Traverse in Marchant & Stampfli (Chapter 24).

The main questions to be solved by the seismic survey in the Central Alps of western Switzerland are the following:

- What type of geological structures may be detected in the metamorphic rocks of the Alps and what types of structural style characterize the deep zones of the Alps?
- What is the geometry of the crystalline basement – Mesozoic cover contact of the external massifs below the Helvetic nappes of the Rawil Pass axial depression?
- Is it possible to find the continuation at depth of the SE-verging backfolds of the Mont Blanc and Aar massifs described on the outcrop by Steck et al. (1979), Steck (1987) and Escher et al. (1987)?
- Is it possible to recognize the Lower Penninic nappe structures below the Higher Penninic nappe stack of the Valpelline depression?
- Are the main late Alpine fault structures, as the Rhone-Simplon normal and strike-slip fault and the Insubric line (Canavese inverse fault), visible on the seismic sections? What is their geometry at depth?
- What is the geometry of the Moho-discontinuity of the SE-dipping European plate below the Central Alps?

12.1.1 Location of the seismic lines

The locations of the seismic lines, shown in Figure 12-1 were constrained by geographic, technical and geological boundary conditions. The four seismic lines W1, W2, W3 and W5 follow roads in Alpine valleys oriented at approximately 90 degrees to the regional strike direction. Therefore, the dip of the main planar structures (at least those related to the nappe system) lies roughly in the vertical plane defined by the W1, W2, W3 and W5 seismic lines. However, line W4 intersects the geological structures at a low angle and crosses the seismic line W3 at Zermatt. This configuration yields information in the third dimension (Figure 12-1) and additional 3-D information is also gained thanks to the substantial axial dip that affects the surveyed area; for instance, the near surface structures along the northern part of the W3-line will appear several km deeper on the W2-line.

12.1.2 The seismic data

Numerous seismic displays were consulted for the interpretation of the W1-W5 profiles. The Vibroseis data revealed a much higher resolution for deciphering the nappe system, while the dynamite data had a better penetration at greater depths. The stacked sections were used in part for examining the amplitude of the reflections (thus for the identification of the potential reflectors) and in particular the true amplitude processing of part of the W1-line (Levato et al. 1994) helped in detecting the origin of some reflections. The stacked section served also for comparison with synthetic seismograms produced by normal-incidence ray-tracing modelling (Marchant 1993; Levato et al. 1994) and for displaying seismic attributes (Marchant 1993). The most useful seismic attribute turned out to be the instantaneous phase that enhances considerably the continuity of weak reflections. Conventional migration (by wave-equation) yielded good results for the long lines (e. g., W3) but was inadequate for the very short lines (e. g., W4), as they tended to be smeared with migration artifacts. This is why geometric depth-migration was extensively used.

All the depth-migrated line-drawing shown in this chapter were produced using the Cigogne program (Sénéchal 1989, 1991; Sénéchal & Thouvenot 1991), which is based on the principle of the common tangent of two spherical wave-fronts. Figure 12-2 illustrates the various steps of this migration process applied to the W4 line. On the basis of a stacked section (Figure 12-2A), a man-

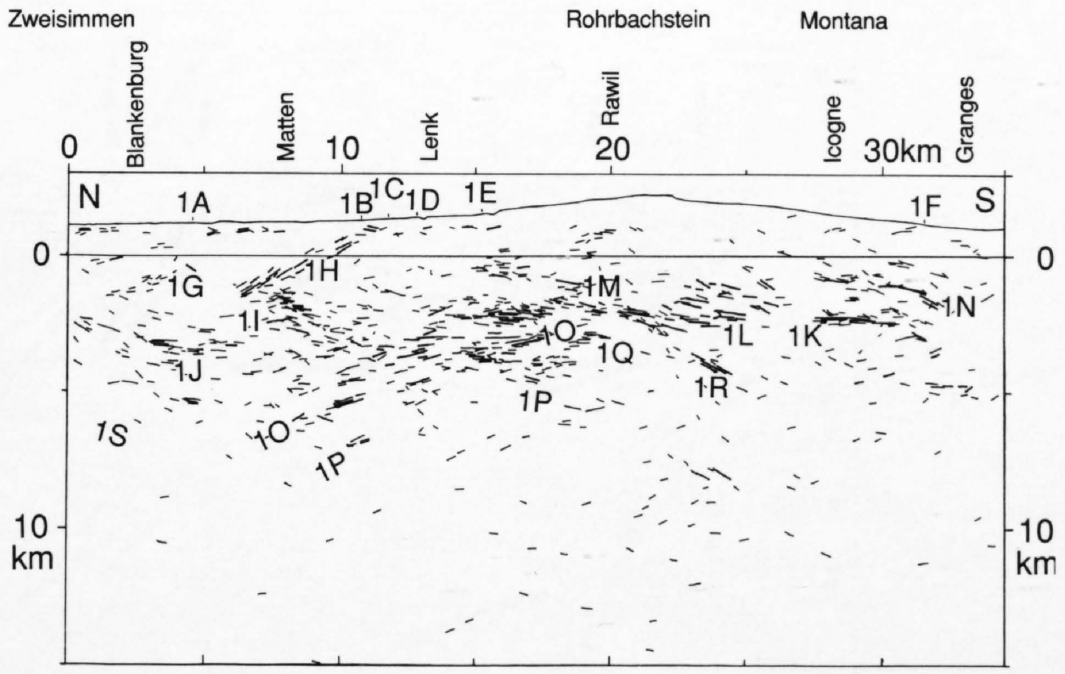

Figure 12-3
Geometric depth migration of the W1-vibroseis-line.

ual line drawing is performed, allowing for a differentiation of the amplitude of the reflections (in Figure 12-2, thin lines = low to medium amplitude reflections; thick lines = high amplitude reflections). These reflections are then digitized into small individual segments (of 5–10 CDPs) and converted to depth according to a velocity function that can vary horizontally and vertically (Figure 12-2B-C). Finally each segment is migrated (Figure 12-2D).
This depth-migrated section of the W4 line is a striking example of the effects of migrating deep dipping reflections: some of the reflections were moved over distances of more than 40 km! The overall reflection pattern changed also drastically: the stacked section (Figure 12-2A) shows many strongly west-dipping reflections and few sub-horizontal ones that produce several "unconformity" patterns; once migrated (Figure 12-2D), these "unconformities" disappear in favor of much more continuous reflections with a listric shape. These "unconformities" are a half bow-tie pattern, a pattern typical of a synformal structure.
As a 2-D seismic line records events from a whole volume of rocks, the possibility of sideswipes (or lateral arrivals) in an area as complex as the Western Alps is quite high. However, for the following reasons the effect of sideswipes could be well constrained in this study:
- Surface geology projections allow the interpreter to predict the lateral dip of the structures relatively to the seismic line.
- Intersecting lines (such as W3 & W4) help to define the true dip of the reflections.
- Along some of the lines, pseudo-3D processing was applied (Du Bois et al.1990a) to produce small stacked sections perpendicular to the seismic line that give a direct image of the lateral dip of the reflections.

12.1.3 Physical properties of rocks of the Western Alps

Specific weights and P-wave velocities of rocks and the acoustic impedance (AI) are the most important physical properties that constrain the interpretation of potential seismic reflectors. These physical values have been determined by laboratory measurements on rocks sampled along the seismic lines and others typical for the upper crust, the lower crust and the upper mantle (Wagner et al., Chapter 6).
From laboratory measurements of seismic velocities of rock samples from the Alps (Sellami et al. 1990 and 1993, and pers. comm.) the expected reflection coefficients (RC) of the various rock-interfaces can be calculated. According to these measurements, important RC values are to be expected at the contact between the following rock types (occurring along the profiles):
Gneiss/dolomite, gneiss/marble, gneiss/serpentinite, gneiss/metagabbro, gneiss/amphibolite, schist/dolomite, schist/marble, gneiss/eclogite, gneiss/peridotite, anhydrite/gneiss and anhydrite/schist.
Gneiss/schist, gneiss/quartzite, anhydrite/marble or dolomite rock interfaces give low RC values. Surprisingly, the parameters for the mylonites are roughly the same as their undeformed protoliths.

12.1.4 Geological interpretation – general remarks

The geological interpretation of the seismic lines is based on
1) the construction by extrapolation and lateral projection of surface geology on a depth-migrated line-drawing and
2) the comparison and correlation of seismic reflections with lithological limits characterized by an important reflection coefficient, calculated from the laboratory measurements by Sellami (Wagner et al., Chapter 6).

The Alps, with their abundant outcrop and detailed surface geology, makes the geometric projection of geological surface data on the seismic sections the most important tool for the geological interpretation. Due to the complexity of the polyphased deformation, these projections are not purely cylindrical; they must be considered as a somewhat adapted cylindrism done along curved axial directions (Escher et al. 1987). In the Rawil Pass – Valpelline axial depression in the Helvetic and Penninic zones of western Switzerland, three dimensional reconstruction of deep structures attain a depth of 10 to 20 km (Escher et al., 1987). These constructions are largely based on a new (1:100 000) tectonic map, corresponding to the 4 sheets "Col du Pillon", "Oberwallis", "Val de Bagnes" and "Monte Rosa" (Steck et al., in prep.). A horizontal geological section at a level of 2000m (Figure 12-1 and Steck et al., 1989) has been constructed, and structural measurements have been compiled (Steck, 1990). From these data, vertical sections were constructed, parallel and perpendicular to the seismic lines as well as structure-contour maps of seismically relevant geological boundaries. The knowledge of the kinematics of the Alps, especially the time relationship between major geological structures as nappe structures, folds, faults and shearzones is very important for the understanding of the geometry of the deep structures of the mountain belt.

12.2 Geological interpretation of the seismic lines

12.2.1 The Rawil seismic profile (W1)

J.-L. Epard, P. Lehner, L. Levato, H. Masson, A. Steck & P. Zwahlen

Introduction

The W1-line starts to the N in the Prealps at Zweisimmen (Laubegg, Simme Nappe), crosses the Ultrahelvetic and Helvetic nappes and ends at Granges (Sion-Courmayeur zone) in the Rhone Valley to the S. The following surface-intersection points of geological boundaries can be placed on the seismic profile (Figures 12-2, 12-3 and 12-4): (**1A**) the roof of the Niesen nappe, CDP 123, (**1B**) the base of the Niesen nappe, CDP 280, (**1C**) the base of the Infra Niesen unit, CDP 302, (**1D**) the tectonic window of Lenk (Cretaceous and Tertiary of the Wildhorn nappe, (**1E**) top Cretaceous of the Wildhorn nappe and (**1F**) the Penninic front (Sion-Courmayeur zone).

Main reflections and their geological interpretation

Stacked sections of the explosion and vibroseis data sets are shown in Plates 12-1 and 12-2. The reflections observable in the subsurface are labelled in Figures 12-3 and 12-4a and will be discussed for individual tectonic unites separately.

The Prealps
- Reflection (**1G**) is related to a zone of conglomerates in the "transparent" flysch sediments of the Niesen nappe. We use in our interpretation of the seismic lines the term of *reflection* for a bundle of reflections. The quality of the reflections observed on the sections of the Alps are not the same of reflections on seismograms of horizontal sedimentary rocks (e. g., Swiss Molasse basin).

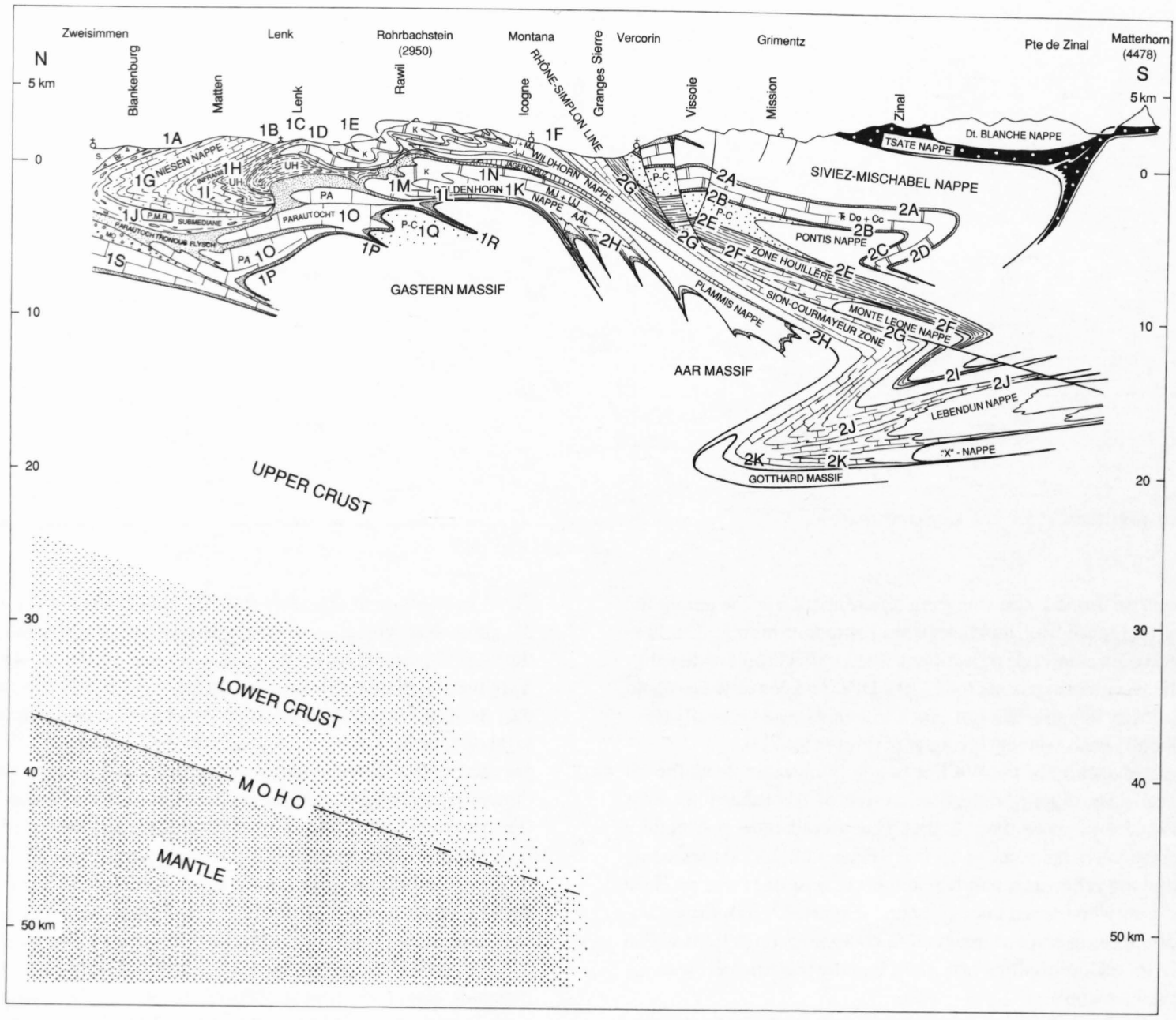

Figure 12-4a and b
Geological interpretation of the W1- and W2-vibroseis-lines. Labels are observed reflections (see Figures 12-3 and 12-5).

- The Infra-Niesen zone **(1H)** is characterized by alternations of Triassic dolomites, gypsum and anhydrite with Middle Jurassic "Aalenian" blackshales or Flysch series. This type of contact is a strong seismic reflection.
- The south dipping reflections **(1I)** are correlated with the folded Niesen and Infra-Niesen units.
- The interpretation of reflection **(1J)** is difficult. It may represent large lenses in the Submédiane zone or, more likely, a wedge of limestones and dolomites of the Préalpes Médianes Rigides.

The Helvetics

- Lateral geometric projections of surface geology suggest that the strong reflections **(1K)**, **(1L)** and **(1M)** have to be related to structures in the Morcles-Doldenhorn nappe. Potential reflectors in this nappe are the contacts between shales and limestones. The reflection **(1K)** is attributed to the interface separating the "Aalenian" shales and the Dogger limestones of the normal limb of the fold-nappe. The group of reflections **(1L)** may be related to the Berriasian marls/Malm limestones contact (this interpretation) or with other contacts in the Dogger. The reflections **(1M)** may be attributed to repetitions of Cretaceous marls and limestones by folding in the front of the Morcles-Doldenhorn nappe. The reflection **(1N)** below Icogne is correlated with the roof of the Doldenhorn nappe.

The Pre-Triassic basement massifs (Gastern and Aiguilles–Rouges massifs) and their cover sediments:
The external basement massifs, composed mostly of gneisses and granites, are seismically transparent. Their autochthonous sedimentary cover with Triassic to Tertiary sediments is composed of an alternation of quartzites, dolomites, limestones and shales. On the crest of the Gastern–Aiguilles–Rouges basement this sedimentary sequence has a variable thickness ranging from a few meters to about 50 meters. It becomes thicker to the North. No reflections have been observed on this major stratigraphic boundary. It is possible that the different lithologic units that compose this sedimentary cover are not thick enough to be imaged on the seismic line or that the reflected signals from these thin units are absorbed or weakened by interference phenomena (Sellami, 1993). We attribute the very poor and discontinuous reflections in the northern part of the section to a thicker autochthonous sedimentary cover. To the South, the top of the basement has been drawn considering an extrapolated reasonable thickness for the Morcles–Doldenhorn nappe.
Below the Rawil Pass, at 1.7 s, weak reflections above the transparent basement may correspond to flysch sediments or to an alternation of shales and conglomerates of a Permo-Carboniferous graben, similar to the Permo-Carboniferous structure from the Aiguilles-Rouges massif (Pilloud, 1991).
The strong reflections **(1O)** are undoubtedly generated by sedimentary series with good reflectivity contrasts. We correlate them with minor thrust-sheets or -folds of the parautochthonous cover of the Gastern and Aiguilles–Rouges massifs. The volume of these parautochthonous sediments is much larger than that deduced from outcrops to the North of the Gastern and Aiguilles-Rouges massifs. This may be explained by the presence of a wider sedimentary basin located at the extremities of the two massifs in their en échelon position (Figures 12-1 and 12-15). The weak and discontinuous reflections **(1P)** may be caused by the autochthonous cover of the Gastern massif. The zone **(1Q)** below the Rawil Pass is characterized by weak, short and discontinuous reflections. These weak reflections may be interpreted as an alternation of conglomerates and schists of a Permo-Carboniferous through. The straight and south dipping reflection **(1R)** may be produced by a deep-rooted sedimentary syncline in the Gastern basement.
The reflection **(1S)** at the top of the basement below the Niesen nappe is not visible. The indicated position of this limit is derived from observations from seismic line W7 (Pfiffner et al., Chapter 8).

Finally we conclude that the interface between the gneiss basement and the sedimentary cover is folded and not faulted, as represented on Pfiffner's interpretation of the W 7 line (Pfiffner et al., Chapter 13.1). Detailed geological maps show clearly that this limit outcrops around the Gastern, Aar, Aiguilles-Rouges, and Mont-Blanc massifs. It is mainly folded and only exceptionally faulted. Moreover, it is obvious that the deformation becomes more ductile with depth and higher temperatures (Steck, 1984, 1987, Escher et al. 1993). Therefore, there is no geologic reasons to draw a faulted cover-basement boundary. The cross section we propose shows broad basement anticlines separated by narrow synclines of Mesozoic sediments. Ramsay (1967, p. 383) was the first to suggest a rheological reason for this particular geometry. He compared the geometry of the folded external massifs with buckling folds formed at the limit of two materials with a contrasting viscosity.

12.2.2 The Val d'Anniviers seismic profile (W2)

R. Marchant, A. Escher, P. Lehner, M. Marthaler, A. Steck & P. Viredaz

Introduction

The W2 seismic line follows the Val d'Anniviers road from Chippis in the Rhone Valley up to Zinal (Figure 12-1). The line is situated in the Penninic nappes and crosses from N to S: the Pontis gneisses and their Permo-Mesozoic cover (quartzites, dolomites, gypsum and anhydrite), the basement gneisses of the Siviez-Mischabel nappe and their Permo-Triassic cover (quartzites and dolomites) and ends in the calcschists and prasinites (metabasites) of the Combin zone (Figure 12-4).

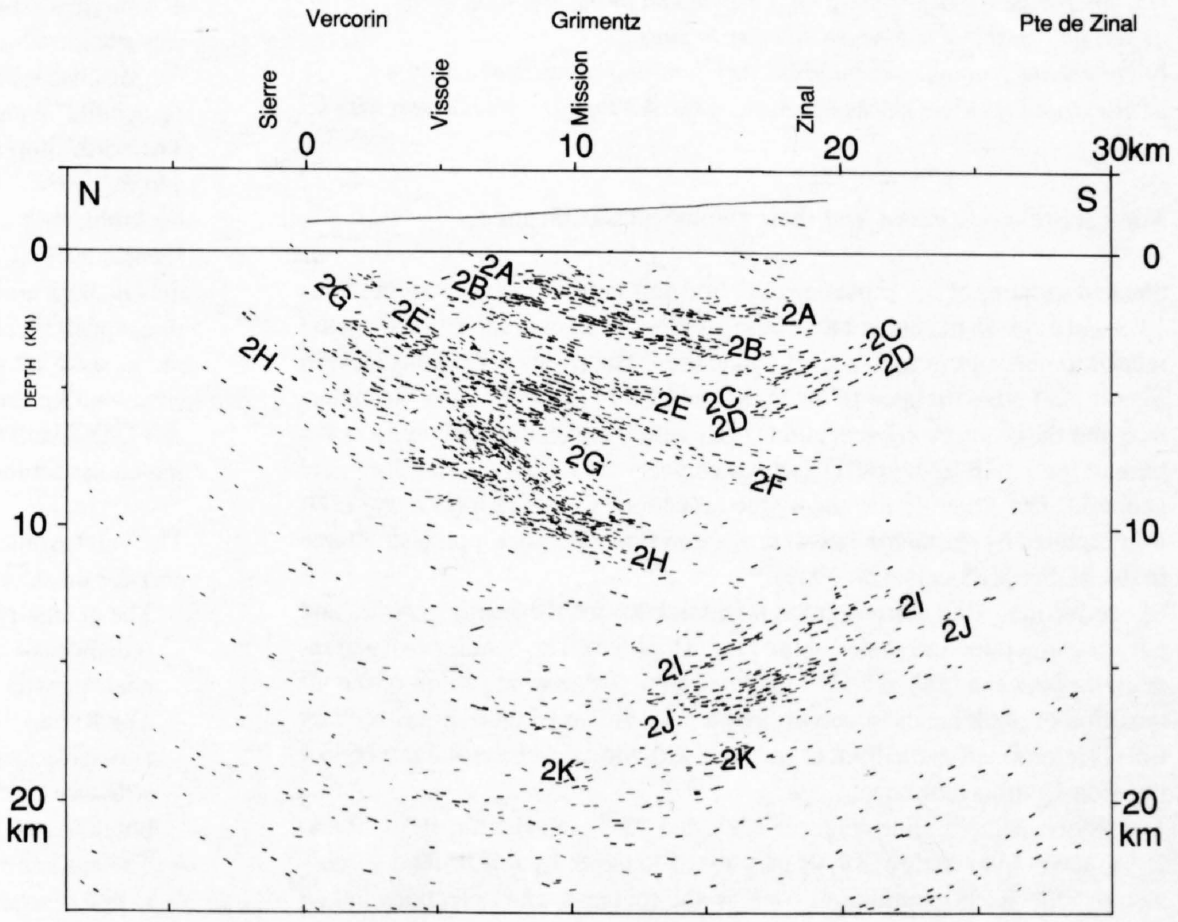

Figure 12-5
Geometric depth migration of the W2-vibroseis-line.

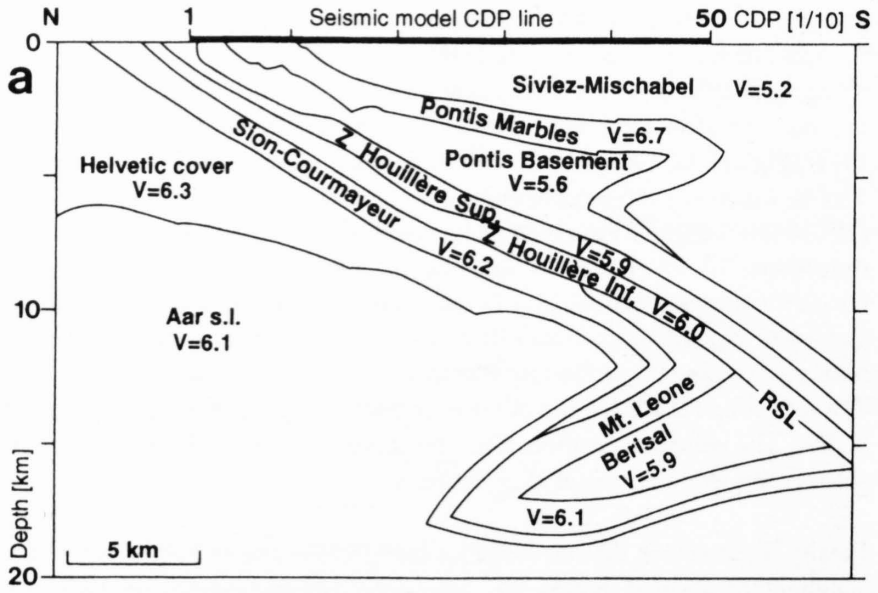

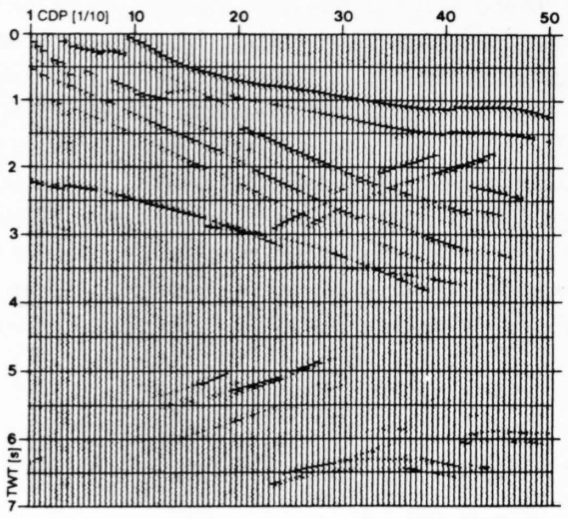

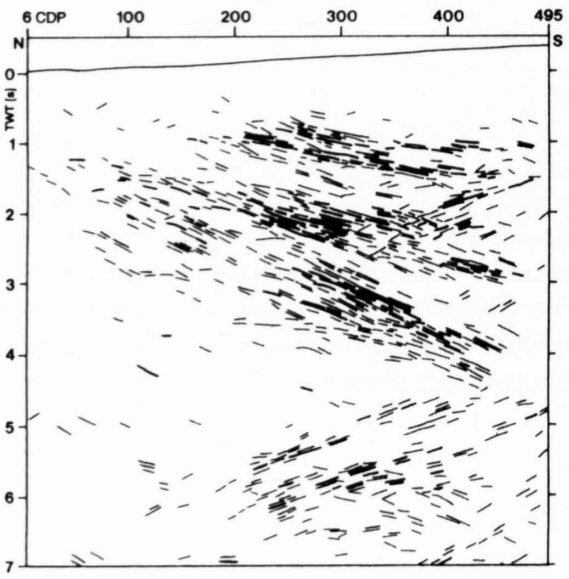

Figure 12-6
Normal incidence ray-tracing on a 2-D model of the W2-line.
a: seismic model; V = P-wave velocity in km/s.
b: convolved synthetic seismogram with addition of random noise.
c: line drawing of the stacked section of the W2 line for comparison with b.

Main seismic reflections and their geological significance

Stacked sections of the explosion and vibroseis data sets are shown in Plates 12-3 and 12-4. In the upper part of the profile, the seismic reflections may be related to outcrops of lithological boundaries. The strong reflections **(2A)** in Figure 12-4 are correlated to the gneiss and quartzites/Pontis marbles interface and the other strong reflections **(2B)** with the gneiss/marble limit at the base of the Pontis gneisses. These two contacts are folded by the Mischabel backfold. The structure formed by the reflections **(2A)**, **(2B)**, **(2C)** and **(2D)** is interpreted by geometric lateral projection from the outcropping structures in the Mattertal (Steck et al. 1989).
The reflections **(2E)** correspond to the limit between the Pontis gneisses and the conglomerates and shales of the Zone Houillère. The bundle of strong reflections between **(2E)** and **(2F)** may represent the seismic pattern of the alternation of thick bands of conglomerates and shales of the Zone Houillère. (2F) is interpreted as the limit of this unit with the calcschists and marbles of the Sion-Courmayeur zone.
The Rhone–Simplon line (Figures 12-1, and 12-4, and Bearth, 1956, Steck, 1984, 1987, Mancktelow, 1990) was traced to depth by following a succession of reflector discontinuities (onlaps and toplaps). The reflections linked to this fault **(2G)** are not particularly strong as its mylonite reflectivity is weak and as this fault juxtaposes rocks with similar seismic properties. Furthermore because of its southward dip, it will not be imaged on the southern end of the seismic line. Above this fault, the rather transparent zone on the southern end of the section is interpreted as the basement gneiss of the zone Houillère.
The contact between the sedimentary Helvetic cover nappes and the gneisses of the Aar massif was determined by the transition from a reflective zone to a more transparent one. Projections of the nearby outcrops of the Aar massif helped to specify the shape of this contact. When followed to depth, the south-dipping reflections linked to this contact **(2H)** are interrupted at a depth of 11 km below Mission (CDP 310). One then observes a broad set (about 6 km thick) of north-dipping reflections **(2I)** and **(2J)** down to a depth of about 18 km. These north-dipping reflectors are interpreted as corresponding to the N-dipping flank of the Berisal synformal structure. Surface geology of the Simplon region clearly shows this backfold with very constant SW to WSW plunging fold axes, which by geometric projection cross our seismic profile (W2). Similar structures are the SE-verging Glishorn anticline and the S-verging Mischabel backfold (Figures 12-1, 12-4 and 12-7 and Escher et al. 1987, Steck et al. 1979, Steck 1984 and Steck et al. 1989). Moreover, we know that with higher temperatures the rock viscosity decreases. For this reason the folds observed in the outcrop become even more isoclinal with depth. Crosscutting faults are very unlikely in the ductile root zone of the Alps as demonstrated by the deep structures of the Lepontine Gneiss dome. Exceptions are more brittle late orogenic structures as the Insubric and Rhone – Simplon faults. The interpretation proposed here corresponds to the best fit with the geometric projection of the surface geology exposed in the Aar Massif, Simplon and Lepontine area of the Central Alps (Figure 12-1).
To test the plausibility of such a large-scale backfold, 2-D seismic modelling was performed along the W2-line (Marchant 1993). The pseudo-3D study from Du Bois et al. (1990a) has revealed that the lateral dips average around 10° to the West along this profile. This is in perfect agreement with values based on surface geology, and as these lateral dips are approximately constant over the whole section, there is no need to use 3-D modelling along this line. This average lateral dip of 10° implies a depth correction of less than 2% to compare the seismic model with a true vertical cross-section, and therefore it can be considered as negligible. The 2-D seismic model shown here (Figure 12-6a) is based on a preliminary interpretation of the W2 line (Marchant 1993). The P-wave velocities used for the modelling were chosen on the basis of laboratory measurements carried out by Sellami et al. (1990, 1993) and Sellami (1993 & pers. communication) carried out on rocks of similar lithologies. The synthetic seismogram (Figure 12-6b) was produced by performing normal-incidence ray-tracing (zero-offset approximation) and convoluted with a 10–45 Hz Klauder wavelet to imitate the acquisition and processing parameters; random noise was finally added for the display of the synthetic section.

When compared with the original stacked section (Figure 12-6c), the synthetic section looks very similar, except for the northern end of the line, where the reflectivity of the stacked section is poor. This is probably partly due to the rough topography (the line was shot along a cliff) and to the dense dextral fault system (Sartori 1993) which affects the lower part of the Val d'Anniviers (south of Sierre in Figure 12-4). This kind of flower-structure was not introduced in the seismic model. Near the southern end of the line, the Mischabel backfold, which affects the Pontis marbles, produces a typical "crocodile" pattern matching perfectly the reflections of the stacked section. The north-dipping reflections of the synthetic section situated between 4.5 and 6s below CDP 200 correspond to the overturned limb of the Glishorn backfold; they are perfectly parallel to the north-dipping reflections on the stacked section, but slightly offset to the North, indicating that the hinge of the Glishorn antiform is probably situated a bit further south than on the seismic model. Finally, the reflections below 5.5s on the southern half of the synthetic section, which correspond to the Berisal synform, match well the cross-cutting pattern of reflections observed on the stacked section. Thus, this 2-D seismic modelling confirms the possibility of large-scale backfolding on the southern side of the External massifs.

The Val d'Anniviers seismic survey produces the following main results concerning the deep structures of the Alps:
- The geometry and south-western continuation of the Aar massif backfold (Glishorn backfold, Figure 12-7 and Steck et al. 1979, Steck 1984) have been shown.
- The Rhone-Simplon line (Figure 12-1 and Steck 1984, Steck et al. 1989) is detected as two reflector bundles, representing obliquely crosscutting structures, characterized by onlaps and toplaps of the transected nappe boundaries.
- The base of the Siviez-Mischabel backfold and the geometry of the Pontis nappe (Escher et al. 1987) are determined.

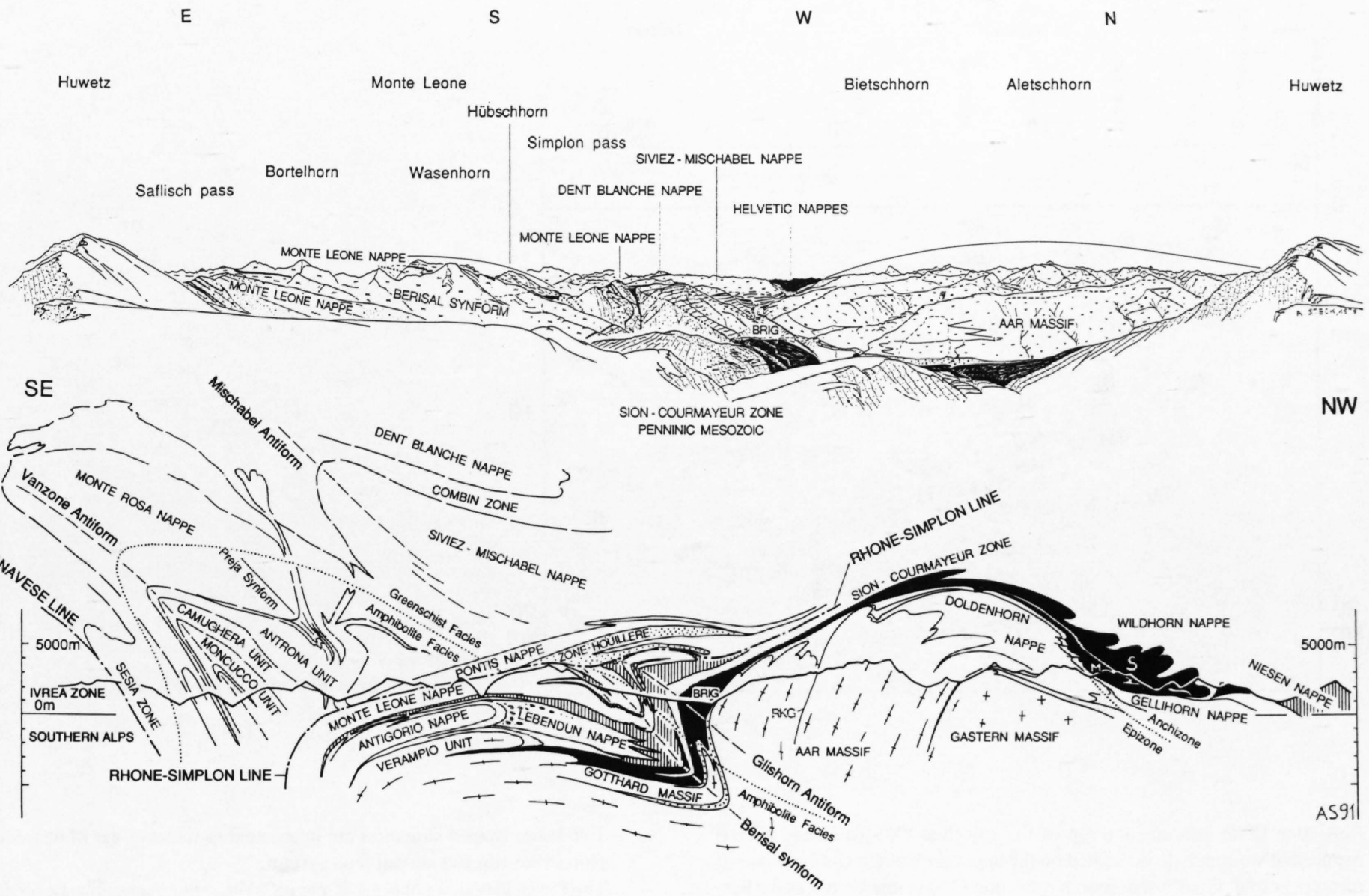

Figure 12-7
Panoramic view from Folluhorn, E of Rosswald and Brig and tectonic section of the Simplon transect of the Central Alps.

12.2.3 The Zermatt Valley (Mattertal or St. Niklaustal) seismic line (W3)

R. Marchant, A. Colombi, P. Lehner, A. Escher & A. Steck

Introduction

The W3-seismic line follows the main road of the Mattertal. It starts at Neubrück, 2 km N of Stalden and ends at Zermatt (Figure 12-1). This profile images the whole pile of Penninic nappes, as it roughly extends from the Penninic front to the Austroalpine thrust. The line crosses from N to S the metagraywackes of the Zone Houillère (Stalden inferieur unit), the basement gneisses and their Permo-Triassic sedimentary cover of the Pontis nappe (Stalden supérieur unit), and the basement gneisses of the Siviez-Mischabel nappe. It cuts the hinge of the Mischabel backfold and reaches the Zermatt-Saas Fee zone. The latter is composed mainly of serpentinites, metabasites and metagabbros, often with preserved eclogitic parageneses. The interpretation of this line is facilitated by the detailed knowledge of the structure and kinematics of geology exposed to the east of the seismic line in the Simplon area and the Lepontine Gneiss dome (Figure 12-1, Figure 16-2 by Escher et al. 1987 and Steck & Hunziker 1994).

Main reflections and their geological significance

Stacked sections of the explosion and vibroseis data sets are shown in Plates 12-5 and 12-6. The **(3A)** reflection in Figure 12-8 is correlated with the lower limb of the Pontis gneiss backfold, corresponding to a gneiss and quartzite/Triassic dolomite contact. The horizontal **(3B)** reflection is very strong. It probably represents the contact of the Siviez-Mischabel basement gneisses of the lower limb of the Mischabel backfold with eclogites of the Combin zone. The large reflection coefficient characterizing the gneiss/eclogite contact may explain the very strong amplitude of this reflection.
The reflection **(3C)** and the zone below it shows the same seismic facies as the conglomerates and shales of the Zone Houillère on the seismic profile of the Val d'Anniviers (W2) farther to the W (reflection **2E**). The identification of the top of this unit is confirmed by its surface intersection at Stalden. It is still a mystery, why the contact between gneisses and shales and conglomerates is a good reflector.
The north-dipping reflections **(3D – 3F)** are related to the Monte Rosa nappe and its underlying units. The top of the Monte Rosa nappe is too close to the surface here to yield any good reflectors and its frontal part is probably too steep to be imaged on the seismic section. Nevertheless one can approximately locate these contacts on the seismic line from surface projections. The bottom of this nappe is in contact with the Antrona ophiolitic unit and provokes a strong northward dipping reflection **(3E)**. The Monte Rosa nappe (mainly orthogneisses) is very transparent on the seismic section with the exception of a strip of a few reflections **(3D)**. These fit in well with the position of the Furgg zone, which nearly divides the Monte Rosa nappe in two. The frontal part of the Antrona unit is very hard to identify on the seismic section. Its outcrop structure is so complex that it is impossible to project it accurately down to depth. The limits of this unit are drawn around areas showing strong reflectivity, which could correspond to the limits of this ophiolitic unit (eclogites) with its surrounding gneissic units. On the southern end of the section at a depth of around 10 km, a few north dipping reflections **(3F)** stop short at the Rhone–Simplon line. They can be correlated with the Camughera and Moncucco zones, which in the field show a similar relationship in the Domodossola area: they are truncated by the Rhone–Simplon line.
A continuous succession of reflector discontinuities, with onlaps and toplaps **(3G)** is interpreted as the trace of the discordant Rhone–Simplon line. This major Miocene fault shows a similar structural relationship with its surrounding rocks in outcrop between the Simplon Pass and Domodossola. Reflections **(3H)** and **(3I)** limit the Berisal syncline.
The next good reflections **(3J)** correspond to the basal gneiss/marble contact of the Monte Leone nappe. The seismically transparent zone between the reflections **(3J)** and **(3L)** is interpreted as the orthogneiss zone of the Antigorio fold-nappe, surrounded by the Mesozoic marbles of the Teggiolo zone. The bundle of strong reflections between **(3K)** and **(3M)** may correspond to the alternations of schists and marbles of the Sion-Courmayeur zone.

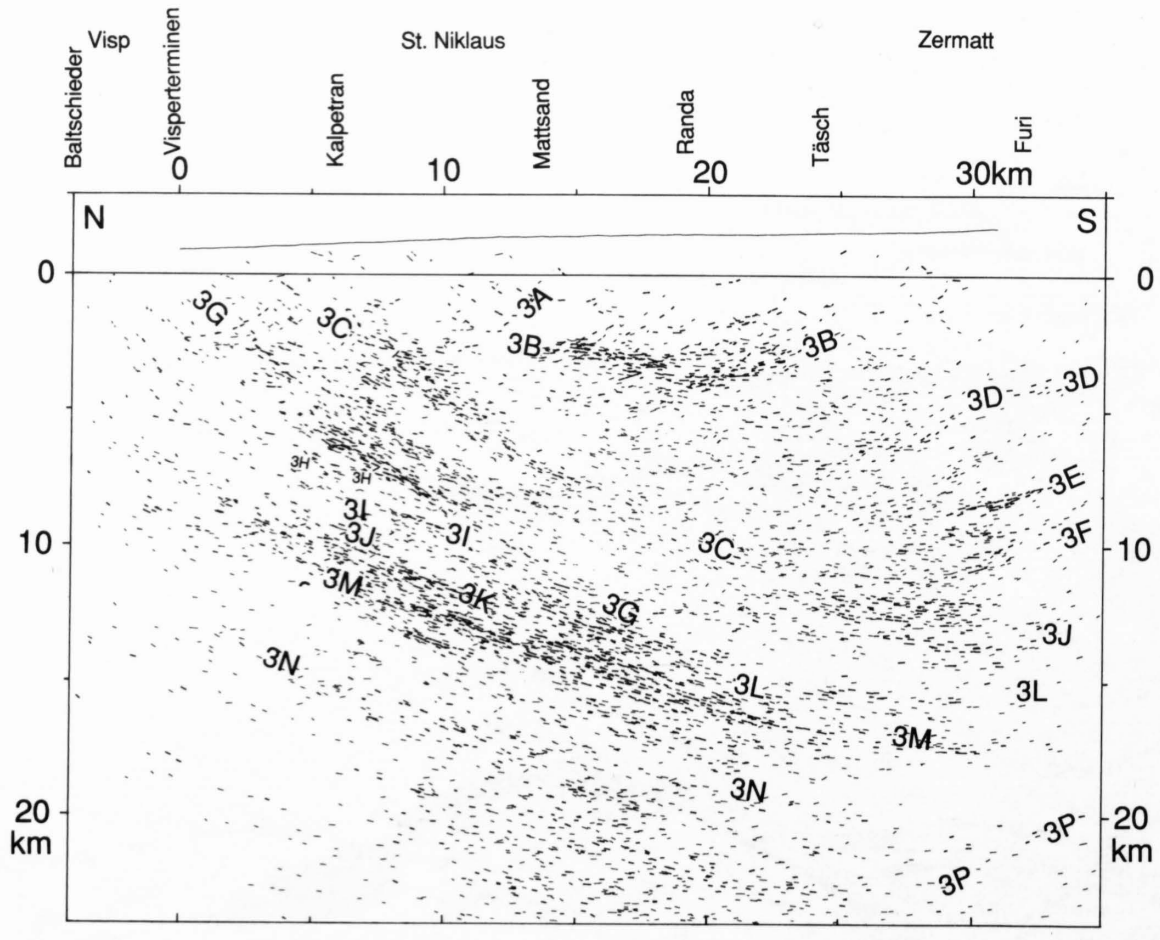

Figure 12-8
Geometric depth migration of the W3-vibroseis-line.

Reflection **(3M)** indicates the top of the so-called "X"-(basement gneiss) nappe, that we conclude is situated on the upper limb of the Gotthard massif recumbent fold. Finally, the smooth reflection **(3N)** is interpreted as the basment-marble contact on top of the Gotthard massif.

The main results of the Mattertal seismic line are the following:

- The interface of the lower limb of the Siviez-Mischabel gneiss backfold with the eclogites of the Zermatt–Saas zone is detected as a very strong reflector bundle ("bright spot").
- Two listric shaped structures are interpreted as faults of the Rhone–Simplon strike-slip and normal fault system.
- The lower Penninic nappes ("X-nappe", Verampio, Antigorio, Lebendun and Monte Leone nappes), outcropping to the E of the Simplon Pass, are recognized as a set of parallel reflector bundles situated at a depth of 10 to 17 km below the Mattertal.

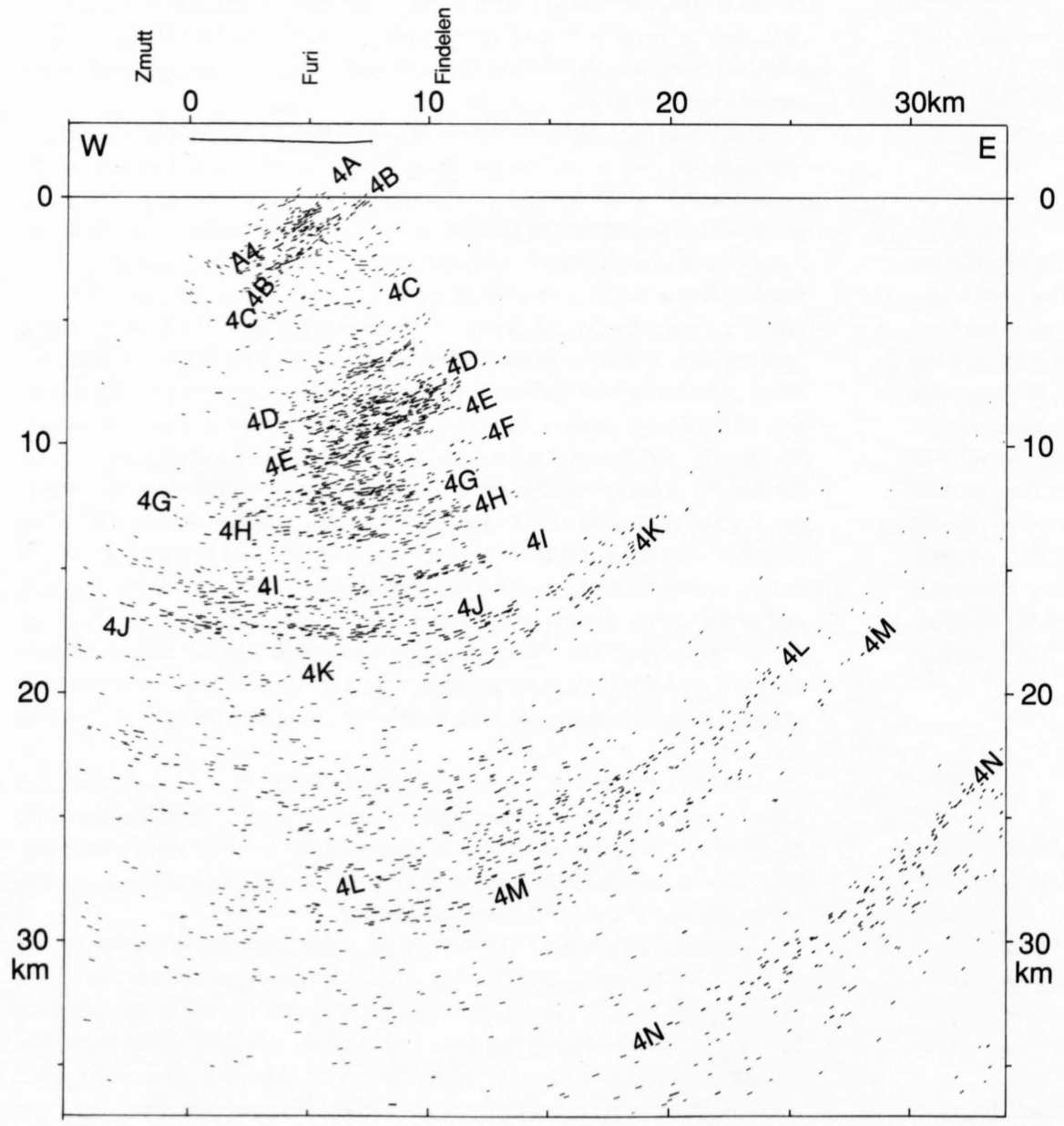

Figure 12-10
Geometric depth migration of the W4-vibroseis-line.

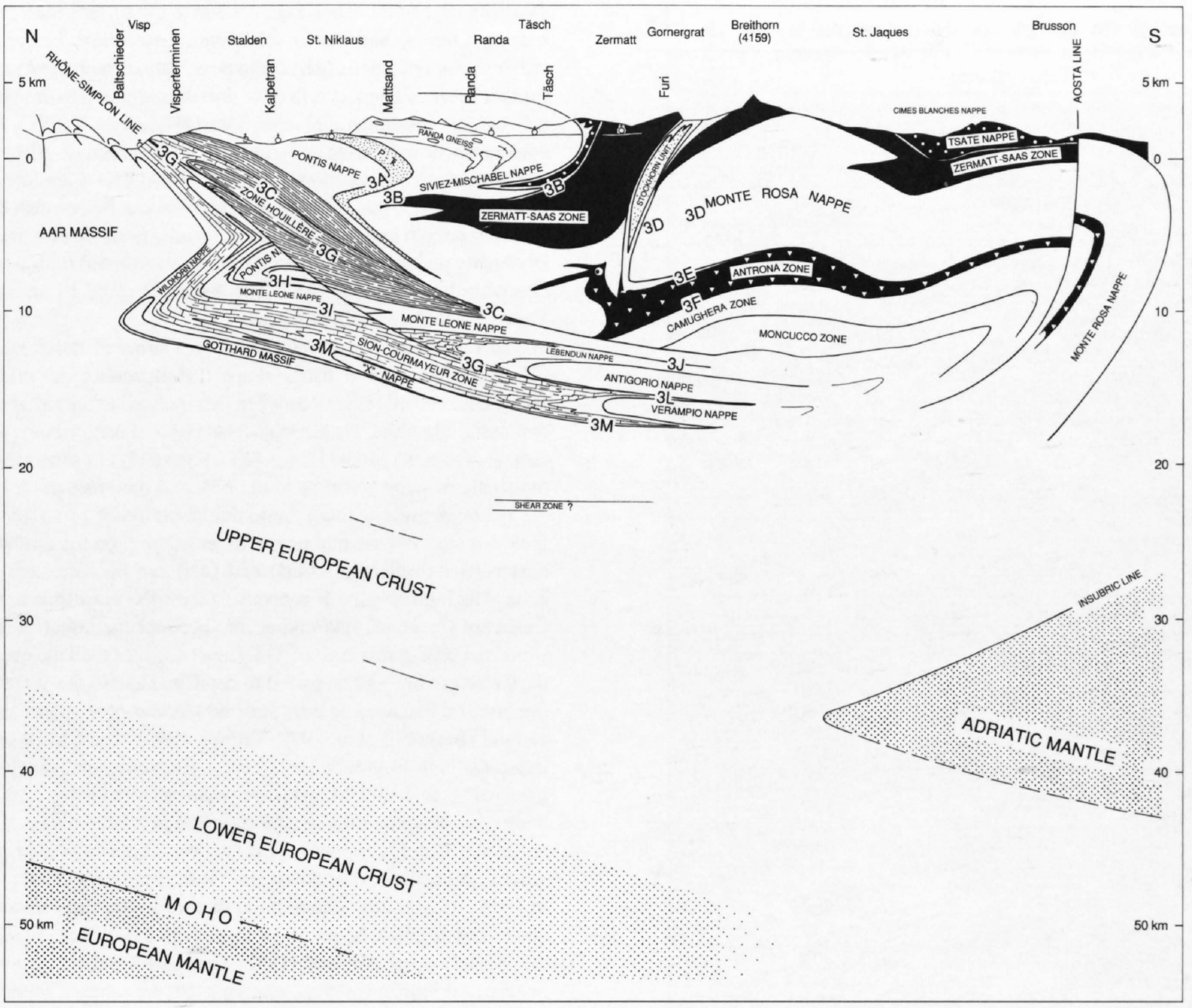

a

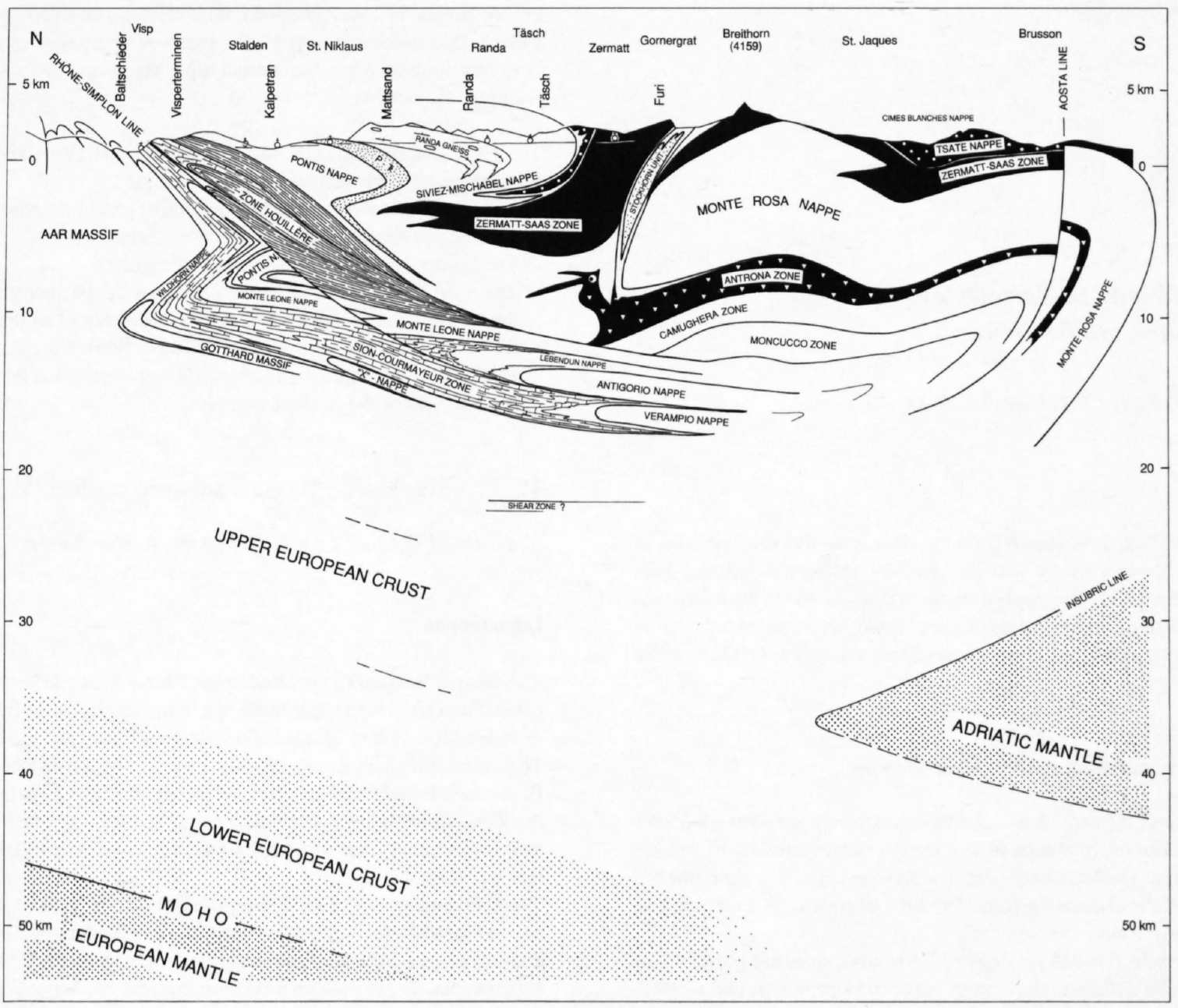

b

Figure 12-9a and b
Geological interpretation of the W3-vibroseis-line. Labels are observed seismic reflections (see Figure 12-8).

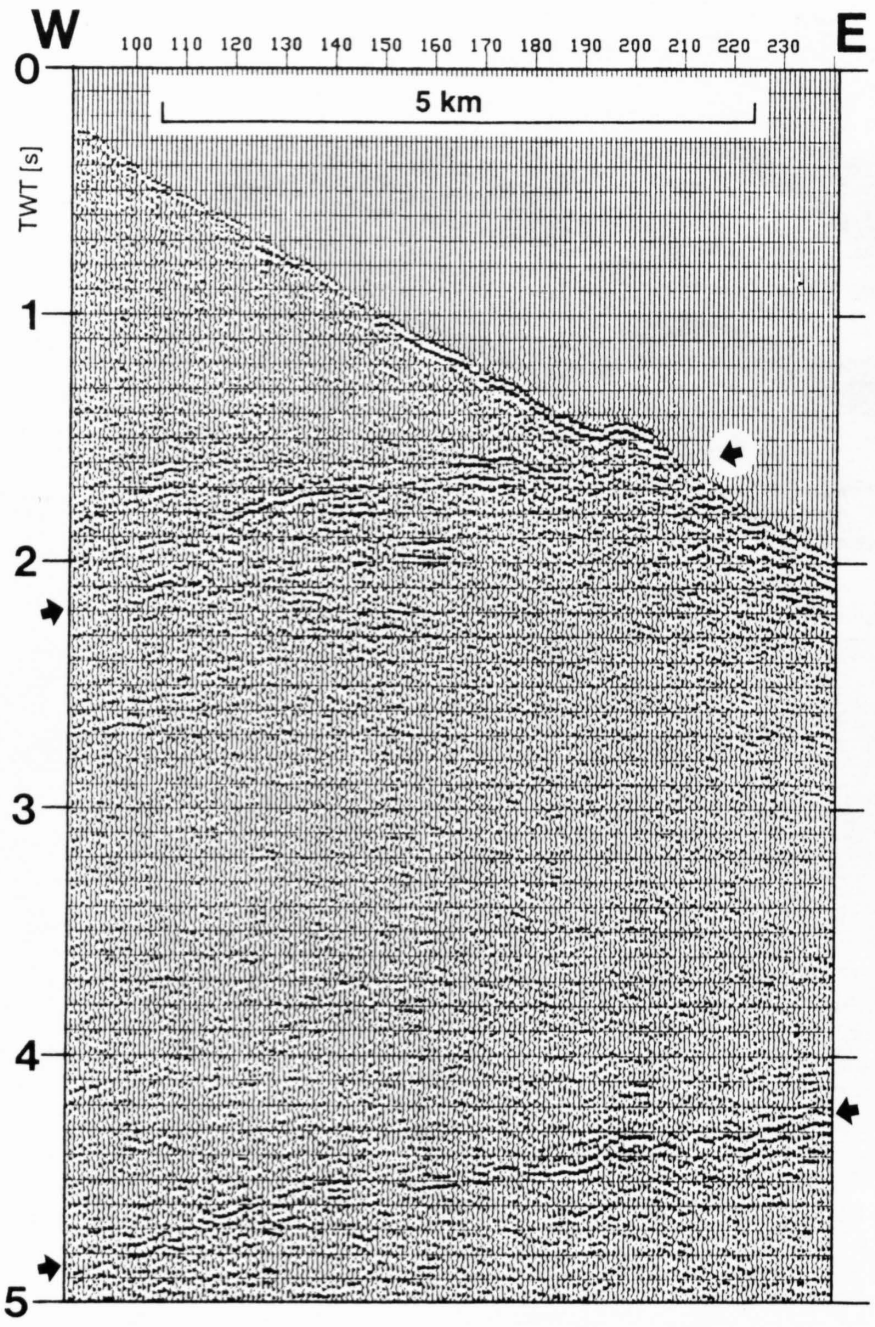

Figure 12-12
W4-dynamite-seismic-line.

12.2.4 The Findelen-Zermatt-Zmutt seismic profile (W4)

R. Marchant, A. Escher, P. Lehner & A. Steck

Introduction

This very short line, less than 8 km long, intersects the southern end of line W3, just above Zermatt and lies entirely inside the Zermatt–Saas Fee zone (Figure 12-1). The stacked section (Plate 12-8) shows a few sub-horizontal reflections and many that have a strong westward dip. Some of these, once migrated (Figure 12-10), were displaced well over 30 km to the east!

Main reflections and their geological significance

Stacked sections of the explosion and vibroseis data sets are shown in Plates 12-7 and 12-8. The interpretation of this section (see Figures 12-10 and 12-11) shows that many reflections are due to sideswipes: this very short line has recorded reflections originating from a volume of rock with a surface area wider than 30 by 50 km.
The first strong reflection **(4A)** in Figure 12-10 corresponds to a projected intersection with the surface to the contact between serpentinites and metabasites of the Zermatt–Saas Fee zone and the underlying marbles on the top of the Stockhorn unit. Two strong reflection strips (**4B** and **4D**) delimit a rather transparent zone, which appears even more clearly on the Zmutt dynamite shot (Figure 12-12). When extrapolated to the surface these reflections coincide with the top and base of the Monte Rosa nappe. Under this unit, many rather strong reflections **(4E)** could be correlated with the Antrona ophiolites. Further down, a few less reflective horizons, dipping to the West **(4F)**, terminate against sub-horizontal reflections **(4G)**. As on line W3, this kind of unconformity is interpreted as being caused by the Rhone–Simplon line. Under this fault, a similar seismo-facies (**4H**, **4I** and **4K**) as on line W3 is found at the same depth. Therefore, these reflections can be correlated with the Antigorio, Verampio and "X"- nappes. It is quite possible that the latter is folded isoclinally underneath the Strahlhorn, its overturned limb would then correlate with the reflections **(4K)**. This backfold could be an equivalent of the Vanzone anticline farther to the S.
To the East under the Monte Moro, two strips of rather strong reflections **(4L** and **4M)** show a listric shape that flattening out under the seismic line. These curved reflections when extrapolated to the surface, coincide with two ophiolitic units, the Zermatt-Saas Fee and Antrona zones, wrapping the radical part of the Monte Rosa nappe. Figure 12-11a shows that in this region the southern steep belt dips to the NW and therefore the former reflections are lateral arrivals with an angle that could reach up to 25° relative to the E-W oriented W4 seismic line. Further to the E on the migrated section, the area between reflections **(4M)** and **(4N)** can be correlated with the Sesia zone. The high-amplitude reflective zone (4N) corresponds perfectly to the Canavese (Insubric) line taking into account the effect of lateral dips (towards the NW in this region). On deeper sections than the one analyzed here, the Canavese line can be traced to depth and shows the same listric shape as the Insubric line does on deep seismic sections of southern and central Switzerland (Bernoulli et al. 1990, Valasek 1992). The Canavese line shows an unusually high amplitude for reflectors situated at such depths on a Vibroseis line. This is probably because they emanate from the top of the Ivrea mantle-body (gneiss – granulitic amphibolite and peridotite interface), which would produce a very high-amplitude reflection. This fact is also corroborated by gravity modelling (Berckheimer 1968; Marchant 1993; Marchant and Stampfli, chapter 24), which shows that some very high-density material (eg. upper-mantle) must be present very near to the surface. In his 3-D model of the Western Alps, Valasek (1992) proposes for this region a huge wedge made of Adriatic lower crust, implying that the Adriatic Moho plunges northward below the Insubric line. Such an interpretation is in total contradiction with the data from the Ecors-Crop Alp deep-seismic profile that ends in the Po plain, near the prolongation of the NRP 20 Western Traverse. Along this Franco-Italian line, the Adriatic Moho is clearly seen stepping up towards the surface, thus making impossible the presence of a wedge of Adriatic lower-crust indenting deep into the internal Alps (Marchant 1993 and Marchant and Stampfli, chapter 24).

The E–W oriented seismic line through Zermatt (W4) gives information about the nappe structures in a third dimension:
- This line shows the geometry of the frontal part of the Monte Rosa nappe, situated at a depth of 4 to 10 km below Zermatt.
- The Lower Penninic nappes are also recognized.
- The most important result is the finding of the geometry and location of the NW-dipping roots of the Antrona and Zermatt–Saas ophiolitic nappes, the Monte Rosa and Sesia nappes and the Insubric Line (Canavese reverse fault). This latter structure corresponds to the upper and frontal limit of the mantle rocks of the Adriatic indenter.

12.2.5 The Val de Bagnes seismic profile (W5)

A. Escher, M. Burri, P. Lehner, H. Masson, R. Marchant & A. Steck

Introduction

The seismic W5-profile, situated in the Rhone Valley between Vionnaz and Charrat and covering farther to the South the whole Val de Bagnes, cuts successively from NW to SE the following main geological units:
The internal Prealpine nappes, the external Aiguilles-Rouges and Mont Blanc massifs and their Helvetic cover rocks, the Sion–Courmayeur zone and the Zone Houillère, the Penninic Pontis, Siviez–Mischabel and Mont Fort nappes, and finally the Tsate ophiolitic nappe and its overlying Dt Blanche nappe (Figure 12-1).
The main importance of the W5-profile is that it intersects entirely the external massifs and thus may give an answer to two fundamental problems: 1) the geometry of the basement/cover interface underneath the Prealpine and Helvetic nappes, 2) the structural relation between the Mont Blanc massif and the Penninic nappes.

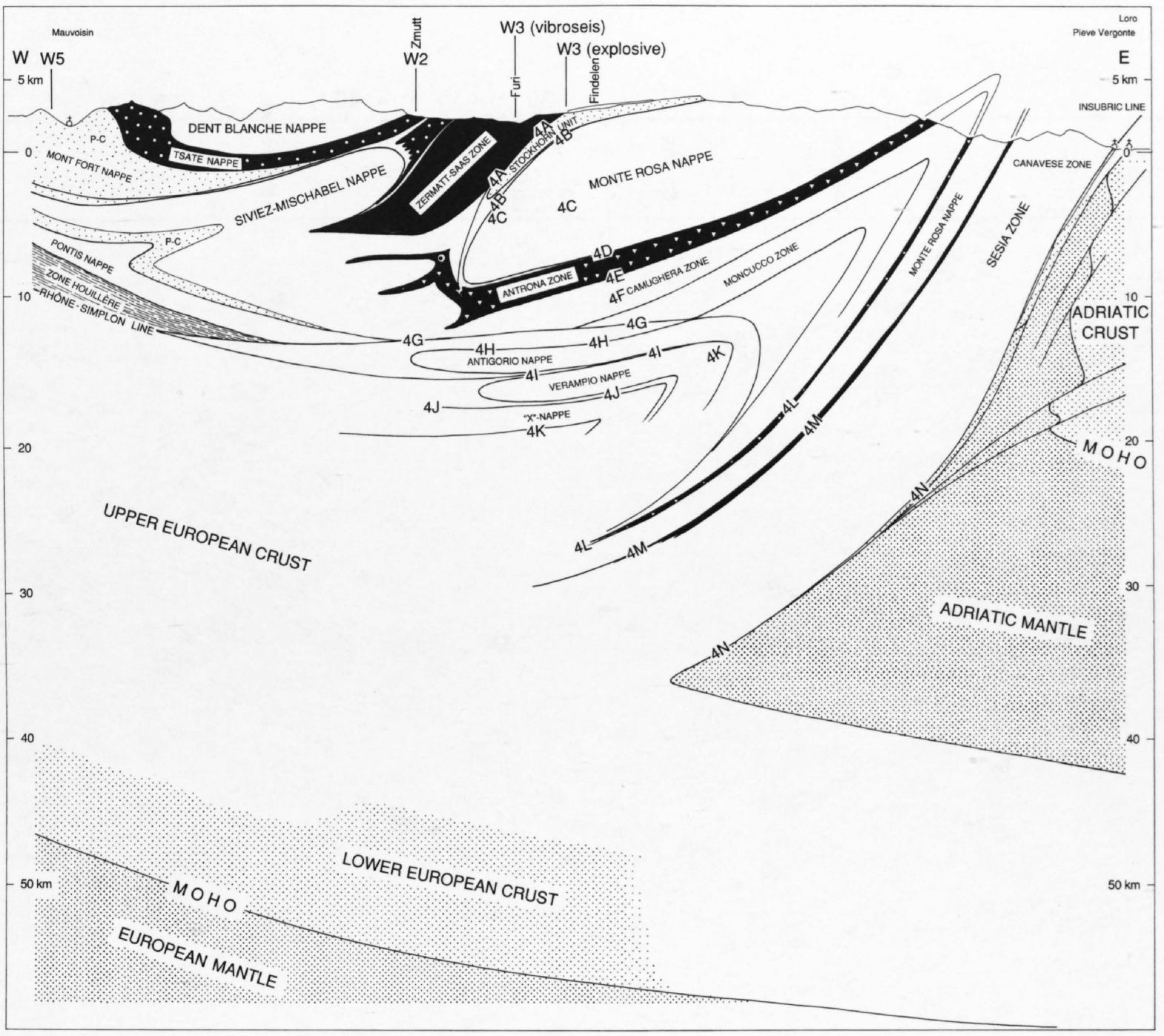

a

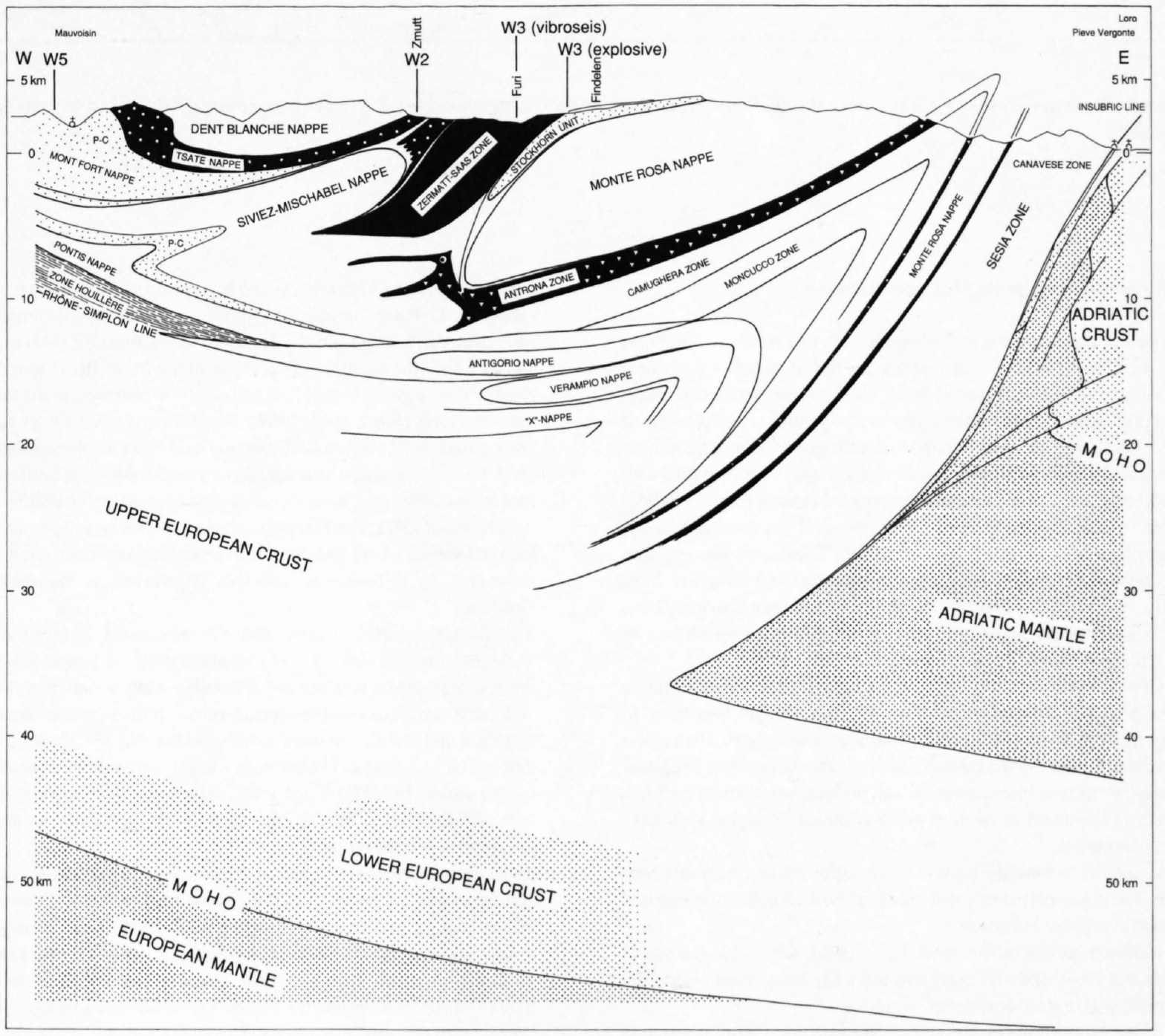

b

Figure 12-11a and b
Geological interpretation of the W4-seismic-line. Labels are observed seismic reflections (see Figure 12-10).

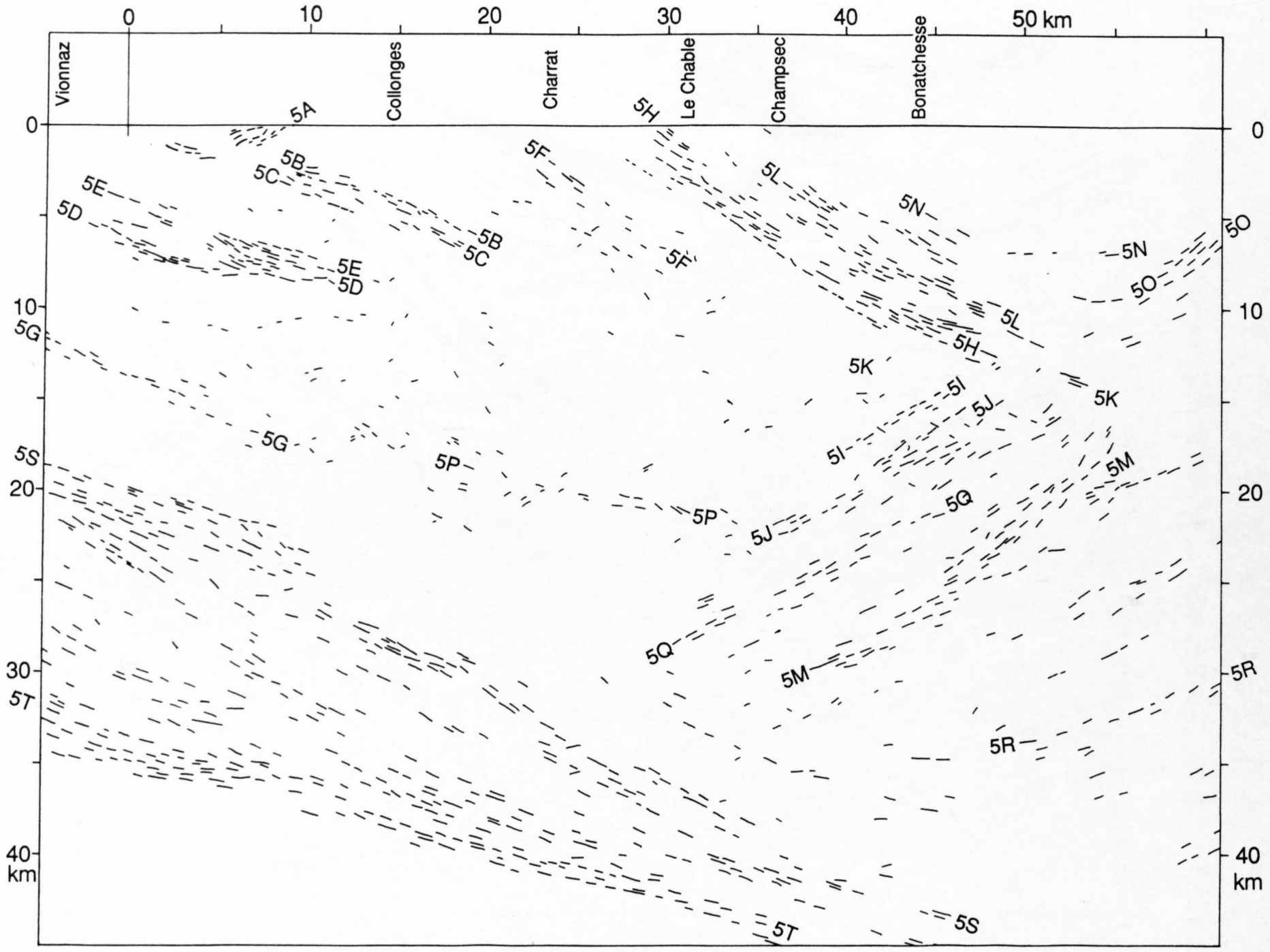

Figure 12-13
Geometric depth migration of the W5-seismic-line. This line drawing is a compilation of depth-migrated sections based on several stacked sections (vibroseis and dynamite data).

Main reflections and their geological significance

Stacked sections of the explosion and vibroseis data sets are shown in Plates 12-9 and 12-10. The basement area underneath the Monthey – Aiguilles-Rouges region contains several well-defined south dipping reflection packages that may correspond to Mesozoic sedimentary synclines similar to that of the Chamonix zone. They can be followed to depths of 8–10 km. The following reflections can be distinguished in this zone (see Figures 12-13 and 12-14):
(5A-B-C-D-E) probably correspond to the contacts between Permo-Carboniferous basement (gneisses, schists or quartzites) and the overlying anhydrites, massive limestones and marbles of middle Triassic to Jurassic age. These reflections thus represent the contact zone separating basement from cover. Locally, in the internal part of the synclines, they may also have been caused by the interfaces separating the massive Cretaceous limestones or marbles from their overlying Tertiary flysch.
The **(5A-B-C)** stack thus probably represents a sedimentary cover syncline separating the Aiguilles-Rouges massif from the Infra-Rouges basement. In the same way the **(5D-E)** bundle of reflections may show the existence of a synclinal structure separating the Infra-Rouges basement from another lower part of the crust. Both structures correlate well with known surface geology. Their existence is important in relation to the complex Prealpine structures and the Jura deformation.
(5F) appears logically to form the curved continuation of the Chamonix syncline at depth. The upper part of this structure is almost vertically dipping and therefore gives no seismic reflection.
(5G) forms a discontinuous reflection at 12 to 15 km depth. Its geological significance is not clear. It could represent a ductile shear zone inside the gneiss basement, with a well-developed foliation.
The SE part of the Mont Blanc massif and its Helvetic cover displays several well defined reflections down to 24 km depth.

(5H) and **(5I)** probably correspond to a group of successive interfaces separating the Helvetic Jurassic limestones, marbles and evaporites from basement and interlayered schists. Their dip varies from SE **(5H)** to NW **(5I)** and shows nicely the backfolding at depth in the Mont Blanc massif. The hinge zone of this large scale backfold can partly be observed in the field, in the upper Val Ferret (Steck et al. 1989). Its geometric position on the W5-profile corresponds well with an ENE dipping axis from its observed position in the field. Because of steep to vertical dips, no reflections can be seen from the actual hinge zone and it is therefore represented by a shallow SE-dipping "white zone" **(5K)**. The Helvetic cover rocks can be followed to depth in the **(5J)** reflections where they appear as a syncline separated from the other **(5I)** sediments by a basement anticline (equivalent to the Mont Chetif or Gotthard).
The Sion–Courmayeur zone and the associated Zone Houllière, (S of Vollèges) are both characterized by alternations of pelitic schists with calcschists, limestones, marbles and dolomites. They should therefore give good and numerous reflections of seismic waves. It thus appears logical to assume that their continuation at depth corresponds to the **(5L)** bundle of reflections that can be followed to 14 km depth. Their continuations at depth, after being folded around the **(5K)** hinge zone, may eventually correspond to the wide area of reflections **(5M)**, visible down to 30 km. At this depth however, the interpretation becomes very unreliable.
The Pontis, Siviez–Mischabel and Mont Fort nappes along the W5-profile consist mainly of gneiss anticlines separated by Permo-Carboniferous conglomerates, quartzites and micaschists. All these rocks possess interfaces of low RC values. This explains the absence of good reflections in the SW part of the profile down to 10 km depth. The only thin reflection that can be seen here **(5N)**, could represent the Permo-Carboniferous sequence separating the Pontis from the overlying Siviez–Mischabel nappe.
The clearly visible bundle of NW dipping reflections **(5O)** at the outer SE

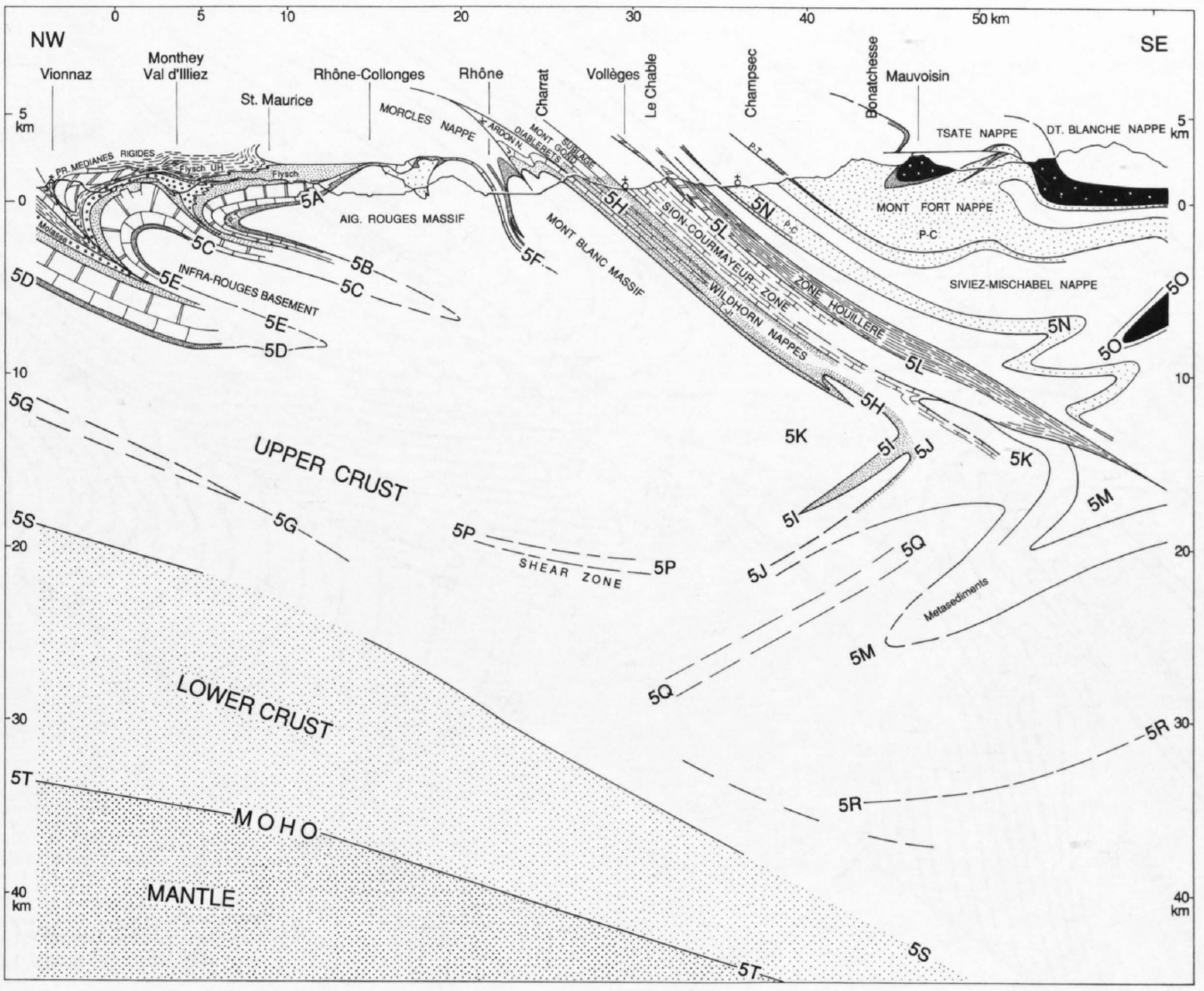

a

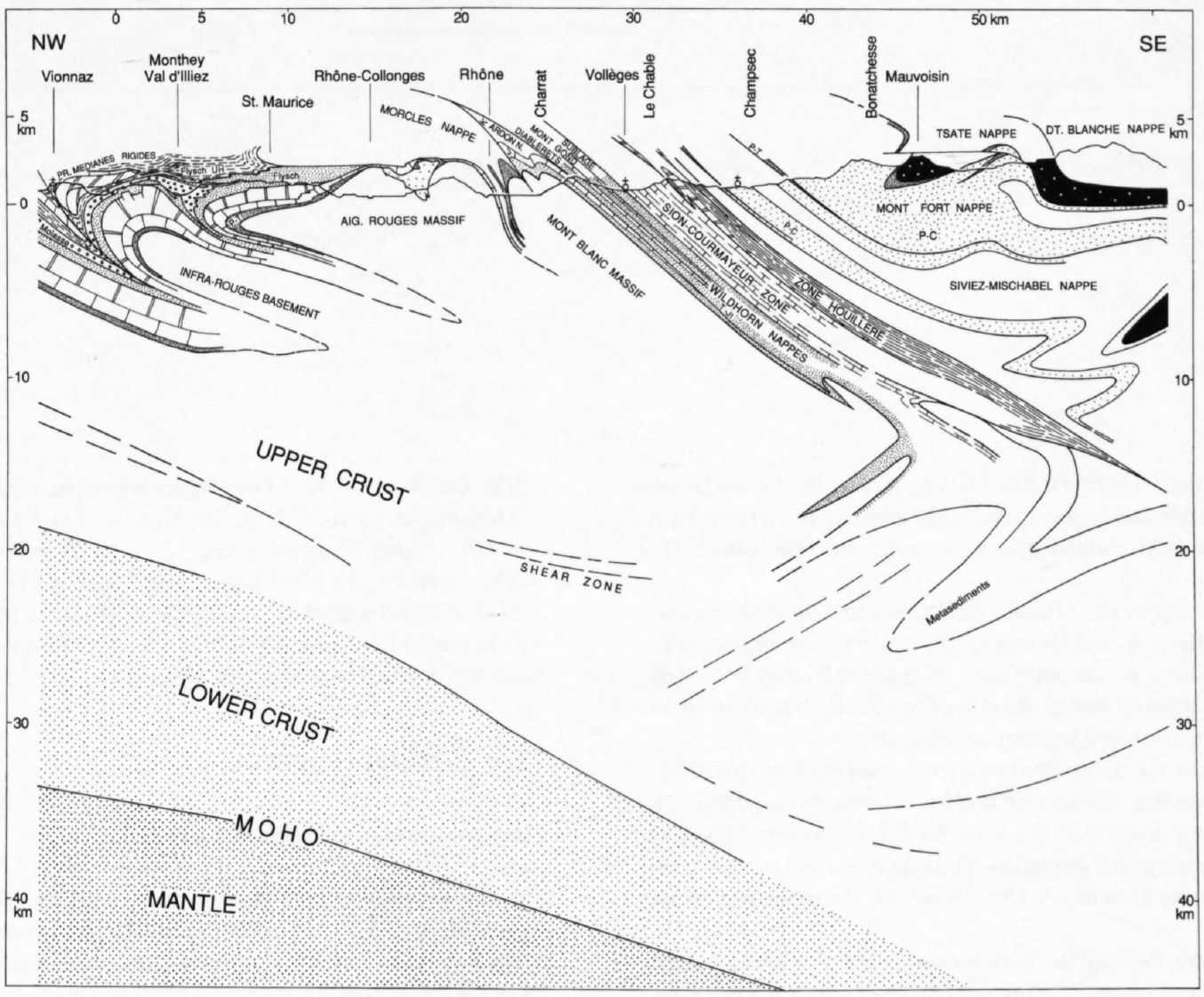

b

Figure 12-14 a and b
Geological interpretation of the W5-vibroseis-line. Labels are observed reflections (see Figure 12-13).

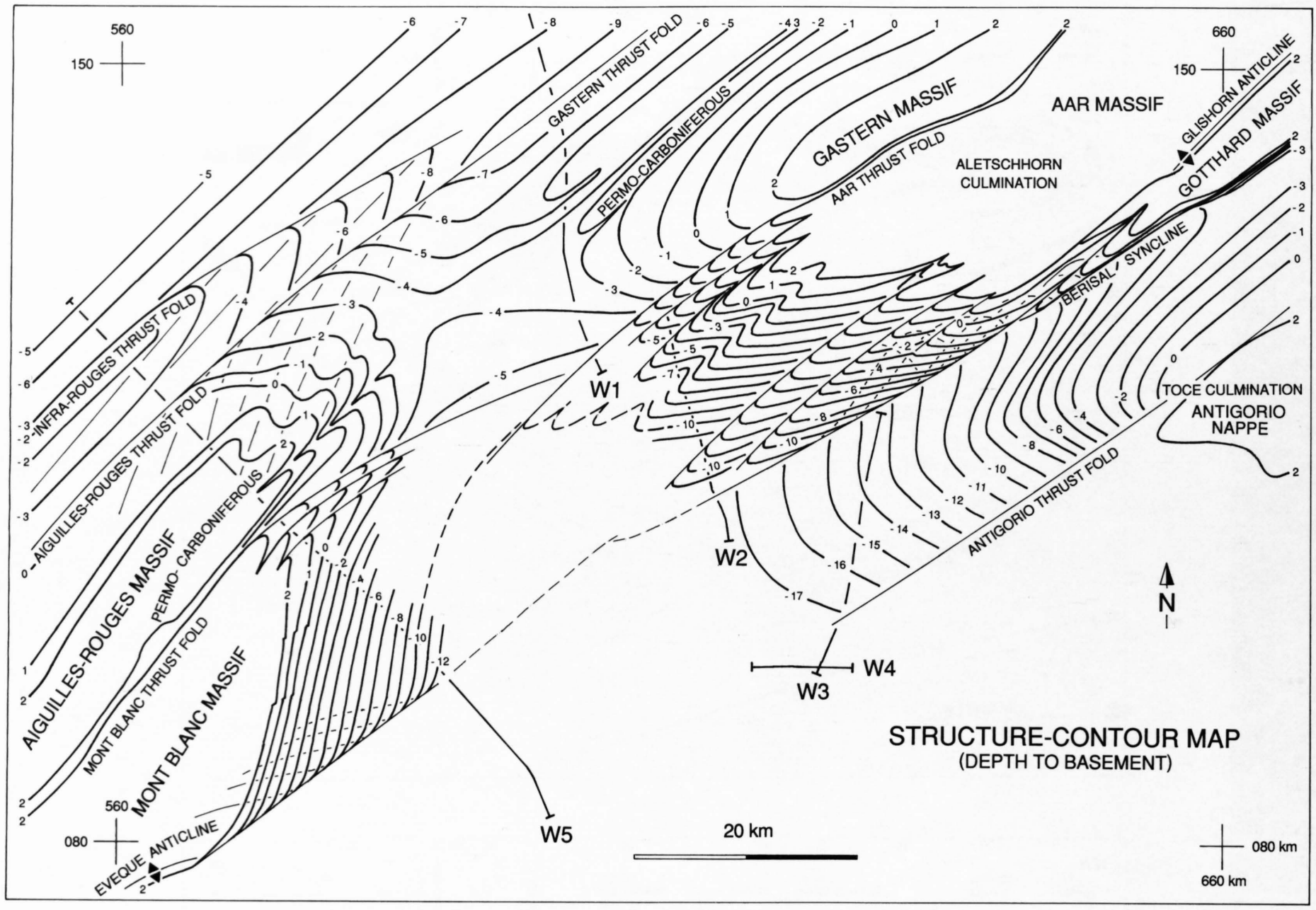

Figure 12-15
Structural-contour map of the external massifs Aiguilles-Rouges, Mont Blanc, Gastern and Aar.

limit of the profile, at depths between 5 and 10 km, is probably caused by the presence of basic to ultrabasic rocks equivalent to those of the Zermatt-Saas Fee ophiolite unit. The NW oriented dips are caused by the Mischabel backfold.

In the lower part of the upper crust from 20 to 30 km depth, several approximately continuous reflections can be observed throughout the profile: **(5P)** may have no real meaning, on the other hand **(5Q)** and **(5R)** may be caused by an intense axial-surface foliation developed inside the basement rocks during backfolding, or to internal lithological contacts.

The interface separating the upper European crust from the lower crust appears very clearly on the W5 seismic profile **(5S)**. It can be followed from 18 to 45 km depth. Directly underneath the Aiguilles-Rouges massif it displays a discontinuity and a change in orientation. This could be a shear zone associated with the ductile backfolding that locally refolds the upper part of the lower crust.

The Moho discontinuity, forming the limit between the lower crust, and the European mantle also appears very clearly as a bundle of reflections **(5T)** varying in width from 5 to 2 km and in depth from 32 to 45 km from NW to SE. Inside the European lower crust many good reflections are visible. Their meaning is still unclear. However, if one compares this unit with the Adriatic lower crust, outcropping in the Ivrea zone, it seems logical to assume that most reflections represent here interfaces between granulitic amphibolites and gneisses. The total width of this lower crust varies considerably, from 15 km in the NW to approximately 8 km in the SE. The interpretation proposed by Valasek (1992), showing a huge wedge of Adriatic lower crust (its top corresponding to the N-dipping reflections **(5J)**, is considered irrelevant for the same reasons as mentioned previously for the W4-line.

The most important results of the Val de Bagnes (W5) seismic survey are the following:

- The discovery of the Infra-Rouges basement separated by synclines of Mesozoic cover rocks from the Aiguilles-Rouges massif thrust-fold and the SE-dipping European crust,
- The existence of a Mont Blanc massif backfold (Evêque backfold, Steck et al. 1989) at a depth of 12 km below the Lac of Mauvoisin.

An alternative interpretation of line W5 (as well as the crossing line W6) is discussed by Pfiffner et al. in Chapter 13.1.

12.3 General conclusions

The external massifs' NW boundary

The external (NW) part of the W1- and W5-profiles clearly reveal the existence at depth of at least 2 major cover-sediment synclines separated by anticlinal basement units. These synclinal structures are probably similar to the Chamonix zone and to the Aar massif cover synclines observed in outcrops, though seemingly less deformed. This means that the external Alpine basement (Aiguilles-Rouges, Infra Rouges, Gastern) overlain by the Prealpine and Helvetic nappes was drastically shortened by folding and thrusting. This was previously suspected but could never have been proven without the present seismic reflection survey. The basement shortening may be partly responsible for the translation of the Molasse and Jura cover rocks towards the NW and simultaneously the folding and thrusting inside the Jura belt and, to a lesser degree within the Molasse basin.

One of the synclinal zones revealed by the W5-section is situated just NW of the Infra Rouges basement. Its existence was postulated by Badoux (1962). It corresponds near the surface to a major thrust separating the internal from the external part of the Prealps. This thrust finally explains the relations between the Simme, Gets and Brèche nappes.

The external massifs' SE boundary and the Lower Penninic nappes

The internal (SE) part of the seismic profile W5, as well as the external W2- and W3-lines yield evidence for the existence of an important hinge zone at 10 to 15 km depth related to a large scale backfold affecting basement and cover rocks belonging to the Helvetic and lower Penninic domains. These NW dipping reflection lines have all been migrated and can best be explained by representing the continuation at depth of the backfolded Helvetic and lower Penninic cover rocks. Surface outcrops along and on both sides of the sections confirm this interpretation. Therefore, little doubt remains about the large-scale backfolding of the internal Aar, Gotthard and Mont Blanc massifs (Figures 12-1, 12-4, 12-9 and 12-14, Steck et al. 1979, 1989, Steck, 1984, 1987, Escher et al. 1987).

The Rhone-Simplon line

The Rhone-Simplon line, a late extensional and dextral fault (Figure 12-1 and Steck, 1984, 1987, Steck et al. 1989), may be traced to depth by following a succession of reflection discontinuities (onlaps and toplaps). The related mylonitic zone shows only weak reflections.

The Insubric line (Canavese line) and the Adriatic indenter

On Line W4, the limit between the Alpine metamorphic gneisses of the Sesia zone and the peridotitic upper mantle rocks of the Ivrea zone is well defined by a strong reflection with a listric shape, corresponding to the Canavese line (a branch of the Insubric line). This strong reflection corresponds to the front of the Adriatic indenter formed by more rigid mantle rocks. This rigid Adriatic indenter, already postulated by Argand (1916), is now confirmed by the reflection seismic survey.

The Moho discontinuity and the lower crust

The Moho discontinuity appears clearly underneath many parts of the dynamite seismic sections, its depth varying from 30 km in the NW to 50 km in the SE part of the profiles. It is generally overlain by a well layered lower crust of 15 km (NW) to 6 km (SW) thickness. The origin of the numerous seismic reflections inside this lower crust is still unclear. However, comparing this unit with the Adriatic lower crust, outcropping in the Ivrea zone, it seems logical to assume that most reflections represent interfaces between amphibolites and granulitc gneisses.

Plates 12-1 to 12-11

SWISS NATIONAL SCIENCE FOUNDATION

87-NF-W1 (DYNAMITE)

FINAL STACK

1: 200'000

RECORDING PARAMETERS

SPREAD LAYOUT	19.2 km
CHANNELS	240
SOURCE TYPE	Dynamite
SOURCE DEPTH	15-60 m
CHARGE SIZE	50-150 kg
GROUP INTERVAL	80 m
GEOPHONE TYPE	10 Hz
GEOPHONE PATTERN	18 spaced 5 m
INSTRUMENTATION	SERCEL 348
FIELD FILTERS	LC 8 Hz / HC 62.5 Hz
COVERAGE	120 (nominal)
SAMPLING RATE	4 ms
RECORDING LENGTH	60 s
RECORDED BY	CGG
DATE RECORDED	Sept. 1987

PROCESSING PARAMETERS

1. Demultiplex and gain recovery
2. Trace editing and resample to 8 ms
3. F/K-Filter
4. Predictive deconvolution
5. Crooked line geometry (20 m CDPs)
6. CDP-Sort
7. Field static corrections
8. NMO-Correction
9. CDP-Stack
10. Time variant bandpass filter
11. Time variant trace equalisation
12. Time variant bandpass filter
13. Strong coherency filter

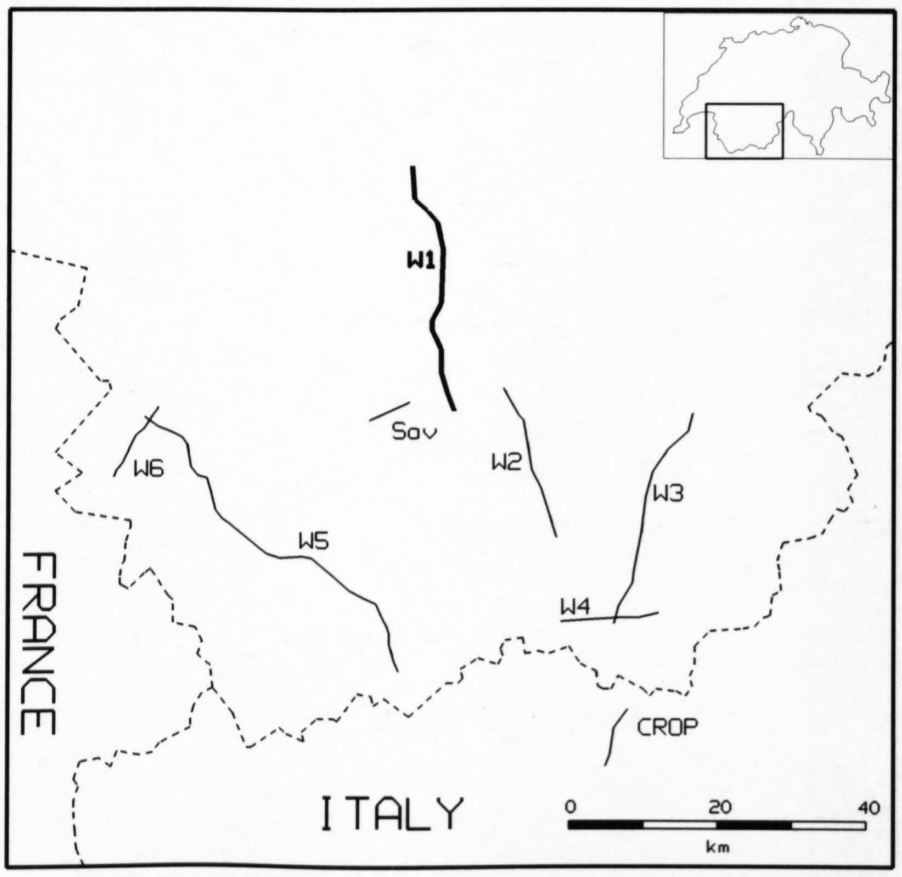

W1 (87-NF-D1)

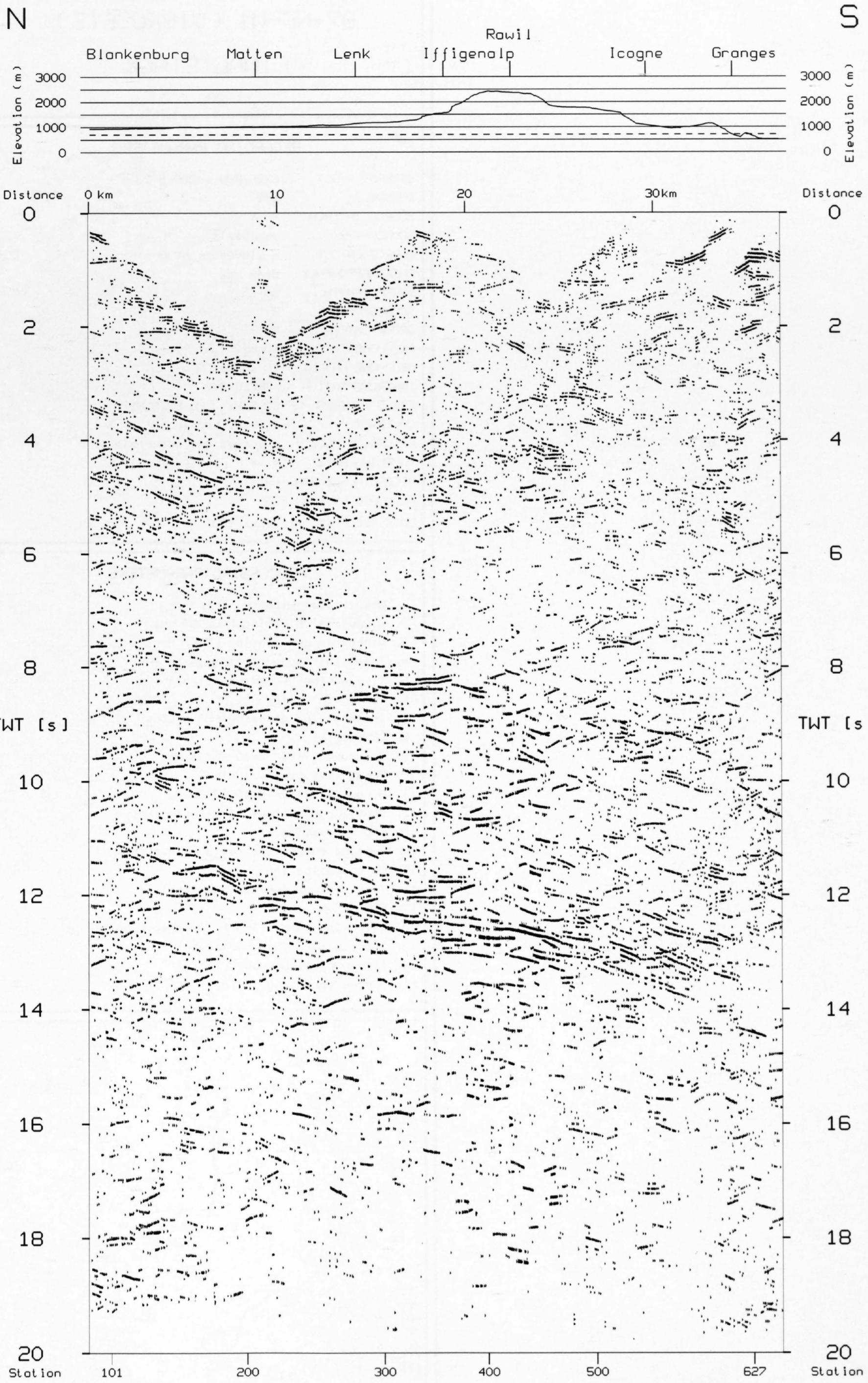
N
S
Rawil
Blankenburg
Matten
Lenk
Iffigenalp
Icogne
Granges
Elevation (m)
3000
2000
1000
0
Distance
0 km
10
20
30km
0
2
4
6
8
TWT [s]
10
12
14
16
18
20
Station
101
200
300
400
500
627

SWISS NATIONAL SCIENCE FOUNDATION

87-NF-W1 (VIBROSEIS)

FINAL STACK

1: 200'000

RECORDING PARAMETERS

SPREAD LAYOUT	9720-200-x-200-9720 m
CHANNELS	240
SOURCE INTERVAL	40 m
SOURCE TYPE	Vibroseis
SOURCE LAYOUT	6 Vibrators at 5 m
SWEEP FREQUENCY	9-49 Hz
SWEEP LENGTH	60 s
SWEEPS/VP	2
GROUP INTERVAL	80 m
GEOPHONE TYPE	10 Hz
GEOPHONE LAYOUT	18 spaced 5 m
INSTRUMENTATION	SERCEL 348
FIELD FILTERS	LC 8 Hz / Hc 62.5 Hz
COVERAGE	2 x 120 (nominal)
RECORDING MODE	unsummed and uncorrelated
SAMPLING RATE	4 ms
RECORDING LENGTH	64 s
RECORDED BY	CGG
DATE RECORDED	Sept. 1987

PROCESSING PARAMETERS

1. Demultiplex with gain recovery
2. Vibroseis whitening (AGC 500 ms)
3. Vibroseis correlation (Min. Phase)
4. Trace editing and resample to 8 ms
5. Time variant trace equalisation
6. Vertical summing
7. Crooked line geometry (20 m CDPs)
8. CDP-Sort
9. Bandpass filter 6/10-48/54 Hz
10. Predictive deconvolution
11. Bandpass filter 6/10-44/52 Hz
12. Static corrections to floating datum
13. NMO-Correction
14. Surface consistent residual statics
15. Mute application
16. Time variant correlation statics
17. CDP-Stack
18. Elevation correction to reference datum
19. Trace mix (2-fold horizontal sum)
20. Time variant bandpass filter
21. Strong coherency filter

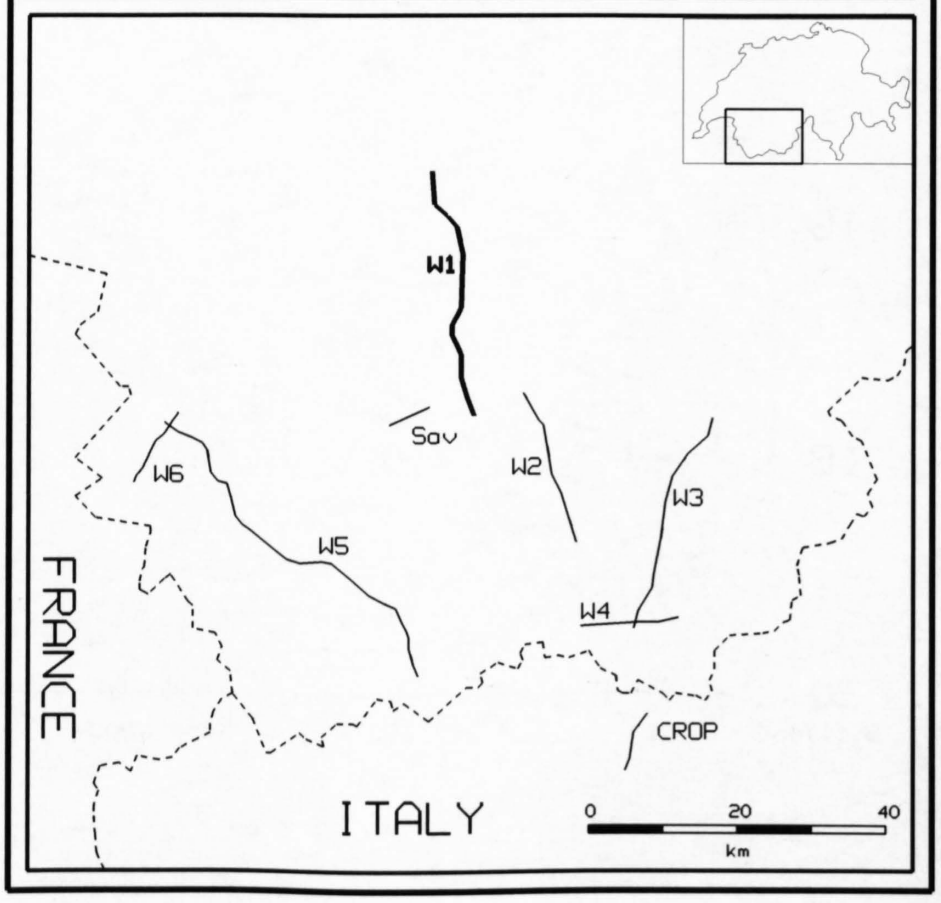

W1 (87-NF-V1)

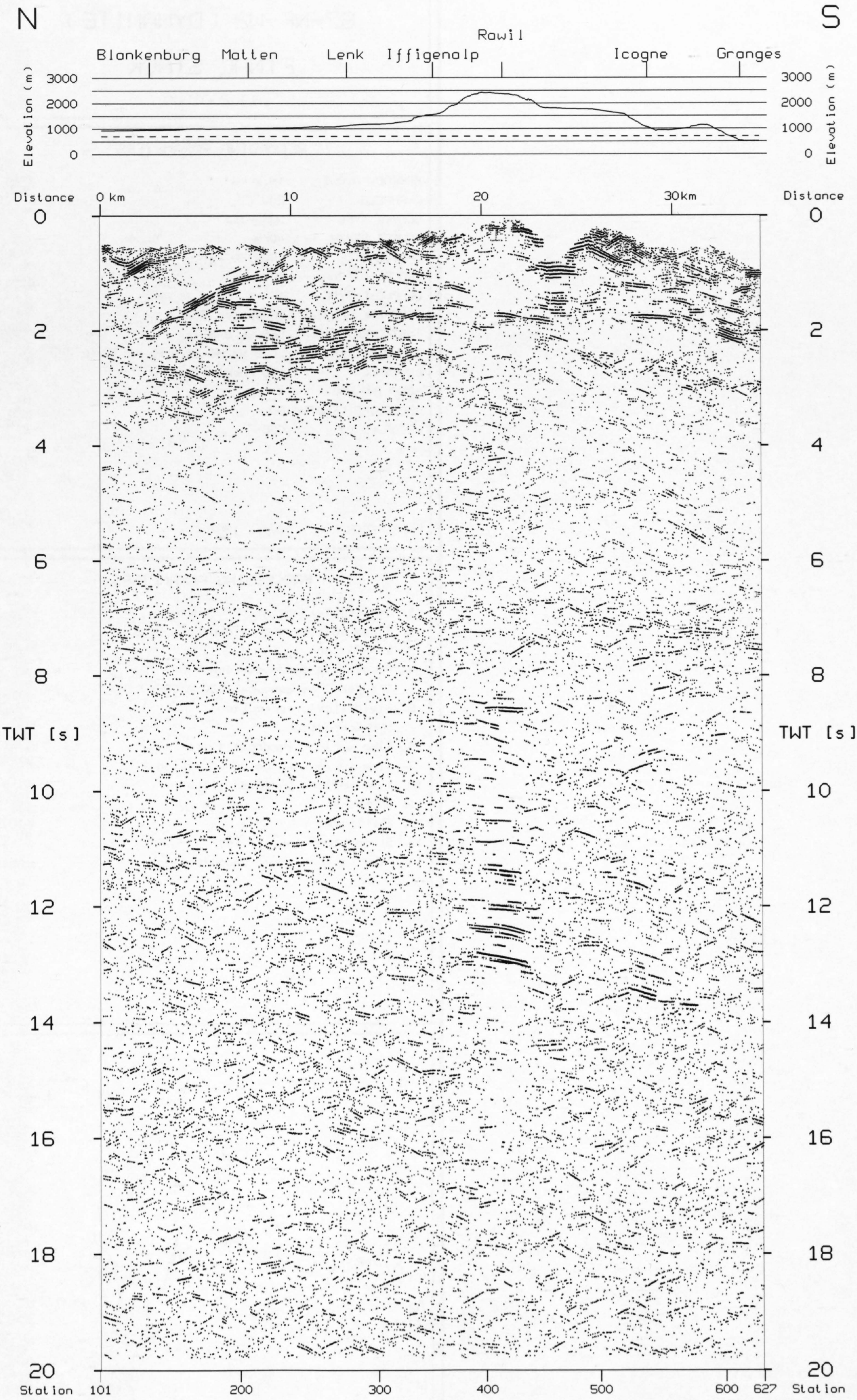
N
S
Rawil
Blankenburg
Matten
Lenk
Iffigenalp
Icogne
Granges
Elevation (m)
3000
2000
1000
0
Distance
0 km
10
20
30km
0
2
4
6
8
TWT [s]
10
12
14
16
18
20
Station
101
200
300
400
500
600
627

SWISS NATIONAL SCIENCE FOUNDATION

87-NF-W2 (DYNAMITE)

FINAL STACK

1: 200'000

RECORDING PARAMETERS

SPREAD LAYOUT	19.2 km
CHANNELS	240
SOURCE TYPE	Dynamite
SOURCE DEPTH	40 m
CHARGE SIZE	100-150 kg
GROUP INTERVAL	80 m
GEOPHONE TYPE	10 Hz
GEOPHONE PATTERN	18 spaced 5 m
INSTRUMENTATION	SERCEL 348
FIELD FILTERS	LC 8 Hz/HC 62.5 Hz/NT 50 Hz
COVERAGE	120 (nominal)
SAMPLING RATE	4 ms
RECORDING LENGTH	60 s
RECORDED BY	CGG
DATE RECORDED	Sept. 1987

PROCESSING PARAMETERS

1. Demultiplex and gain recovery
2. Trace editing and resample to 8 ms
3. F/K-Filter
4. Predictive deconvolution
5. Crooked line geometry (20 m CDPs)
6. Field static corrections
7. NMO-Correction
8. Time variant bandpass filter
9. Time variant trace equalisation
10. Time variant bandpass filter
11. CDP-Sort
12. CDP-Stack
13. Strong coherency filter
14. Time variant trace equalisation

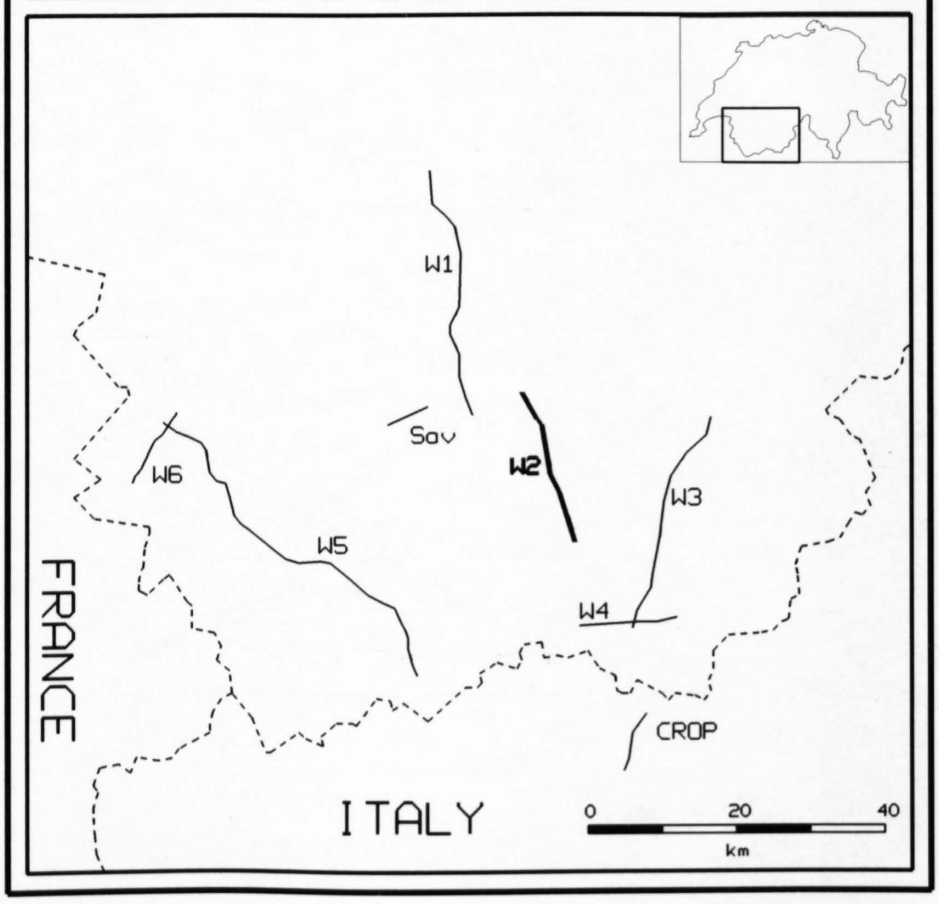

W2 (87-NF-D2)

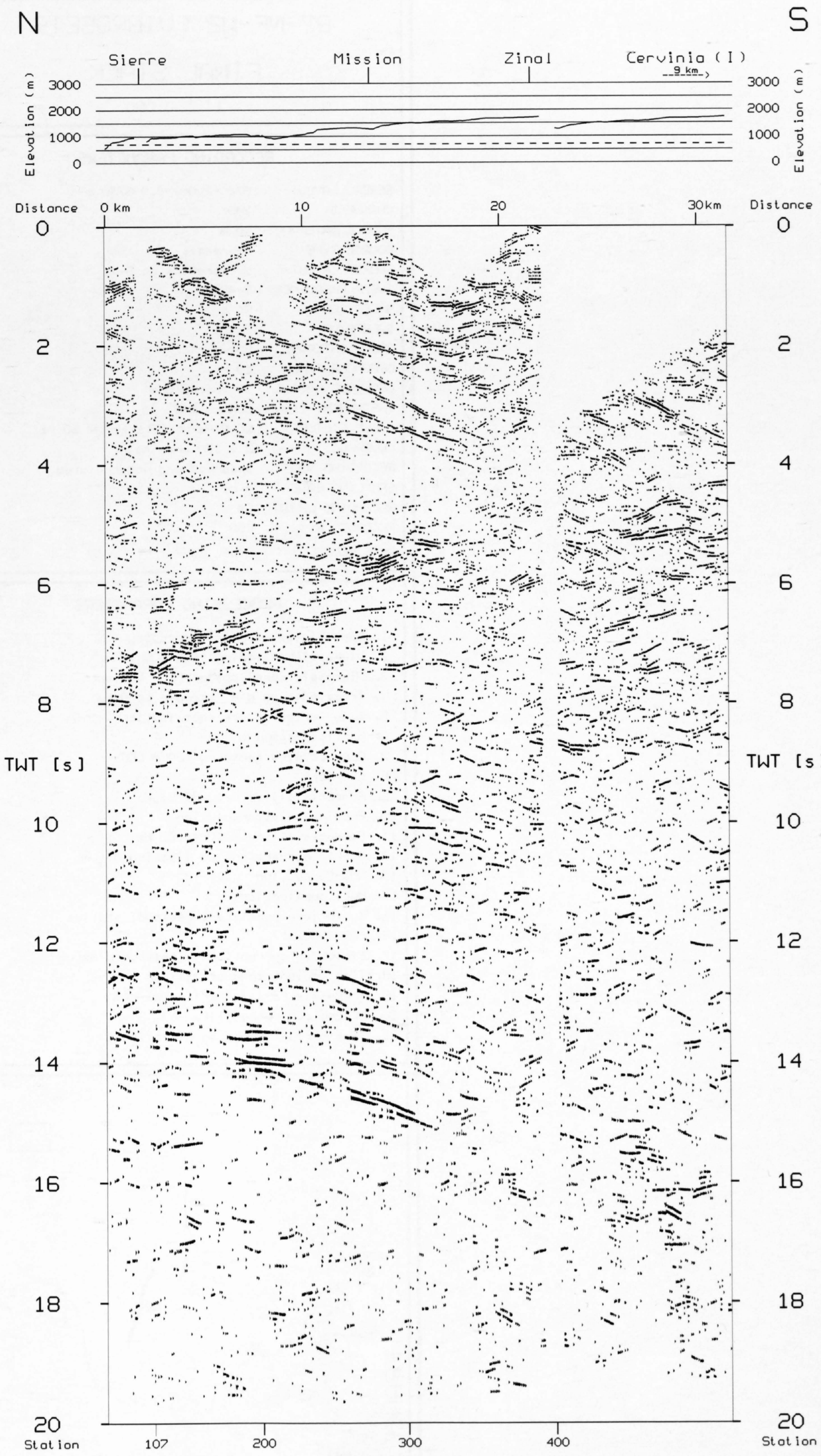
N
S
Sierre
Mission
Zinal
Cervinia (I)
9 km
Elevation (m)
3000
2000
1000
0
Distance
0 km
10
20
30km
TWT [s]
0
2
4
6
8
10
12
14
16
18
20
Station
107
200
300
400

SWISS NATIONAL SCIENCE FOUNDATION

87-NF-W2 (VIBROSEIS)

FINAL STACK

1: 200'000

RECORDING PARAMETERS

SPREAD LAYOUT	9720-200-x-200-9720 m
CHANNELS	240
SOURCE INTERVAL	40 m
SOURCE TYPE	Vibroseis
SOURCE LAYOUT	6 Vibrators at 5 m
SWEEP FREQUENCY	9-49 Hz
SWEEP LENGTH	60 s
SWEEPS/VP	2
GROUP INTERVAL	80 m
GEOPHONE TYPE	10 Hz
GEOPHONE LAYOUT	18 spaced 5 m
INSTRUMENTATION	SERCEL 348
FIELD FILTERS	LC 8 Hz/HC 62.5 Hz/NT 50 Hz
COVERAGE	2 x 120 (nominal)
RECORDING MODE	unsummed and uncorrelated
SAMPLING RATE	4 ms
RECORDING LENGTH	64 s
RECORDED BY	CGG
DATE RECORDED	Sept. 1987

PROCESSING PARAMETERS

1. Demultiplex with gain recovery
2. Vibroseis whitening (AGC 500 ms)
3. Vibroseis correlation (Min. Phase)
4. Trace editing and resample to 8 ms
5. Time variant trace equalisation
6. Vertical summing
7. Crooked line geometry (20 m CDPs)
8. CDP-Sort
9. Bandpass filter 6/10-48/54 Hz
10. Predictive deconvolution
11. Bandpass filter 6/10-44/52 Hz
12. Static corrections to floating datum
13. NMO-Correction
14. Mute application
15. Subsurface consistent residual statics
16. CDP-Stack
17. Elevation correction to reference datum
18. Time variant bandpass filter
19. Trace mix (2-fold horizontal sum)
20. Strong coherency filter
21. Time variant trace equalisation

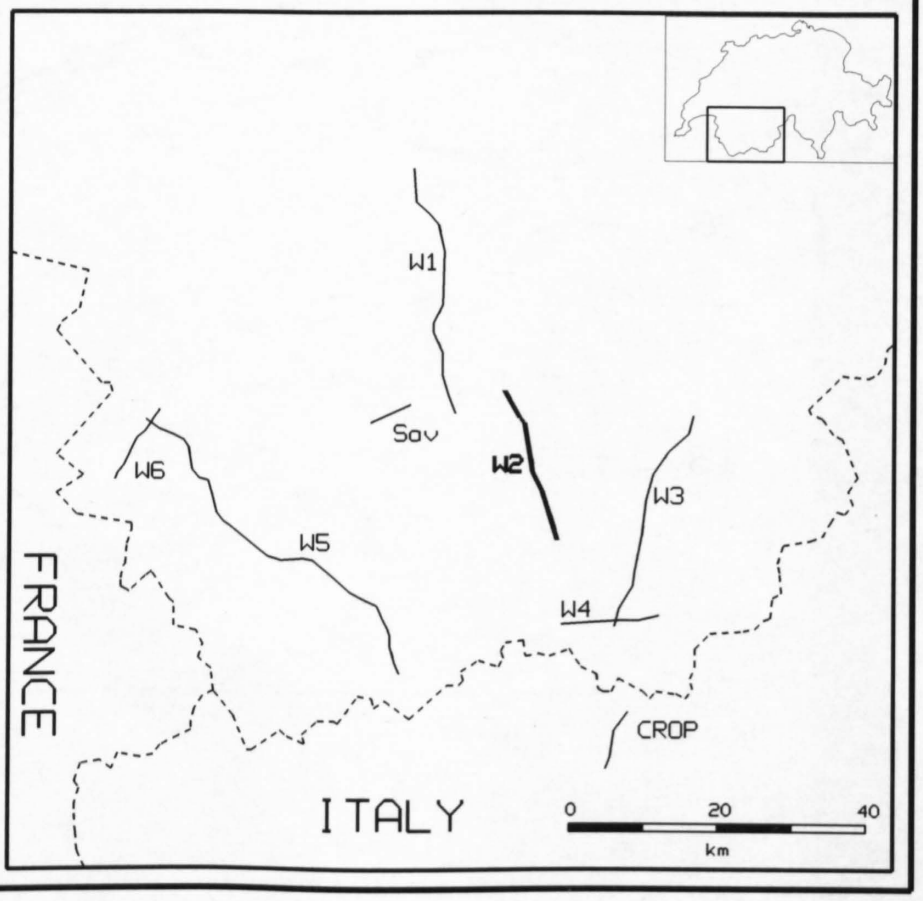

W2 (87-NF-V2)

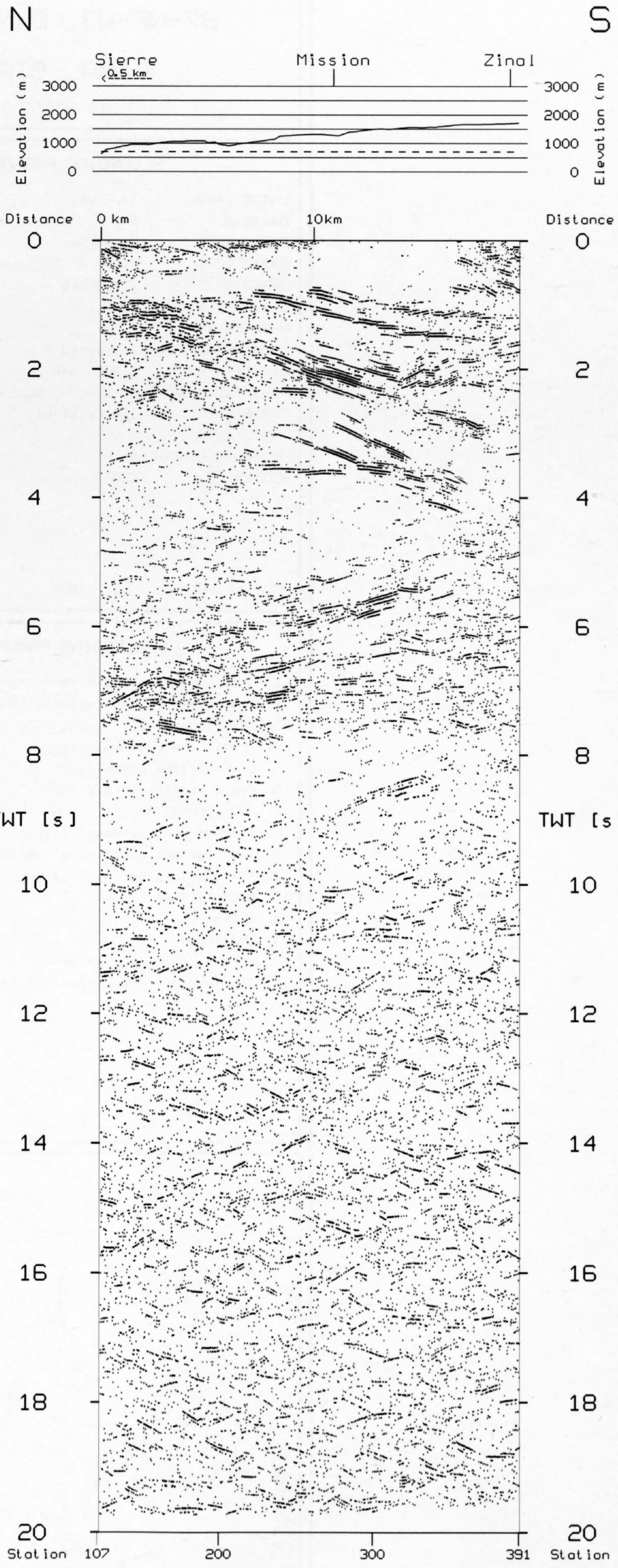
N
S
Sierre
0.5 km
Mission
Zinal
Elevation (m)
3000
2000
1000
0
Distance
0 km
10km
0
2
4
6
8
TWT [s]
10
12
14
16
18
20
Station
107
200
300
391

SWISS NATIONAL SCIENCE FOUNDATION

87-NF-W3 (DYNAMITE)

FINAL STACK

1: 200'000

RECORDING PARAMETERS

SPREAD LAYOUT	19.2 km
CHANNELS	240
SOURCE TYPE	Dynamite
SOURCE DEPTH	20-50 m
CHARGE SIZE	75-150 kg
GROUP INTERVAL	80 m
GEOPHONE TYPE	10 Hz
GEOPHONE PATTERN	18 spaced 5 m
INSTRUMENTATION	SERCEL 348
FIELD FILTERS	LC 8 Hz/HC 62.5 Hz/NT 50 Hz
COVERAGE	120 (nominal)
SAMPLING RATE	4 ms
RECORDING LENGTH	60 s
RECORDED BY	CGG
DATE RECORDED	Sept. 1987

PROCESSING PARAMETERS

1. Demultiplex and gain recovery
2. Trace editing and resample to 8 ms
3. F/K-Filter
4. Predictive deconvolution
5. Crooked line geometry
6. Field static corrections
7. NMO-Correction
8. Time variant bandpass filter
9. Time variant trace equalisation
10. Time variant bandpass filter
11. Notch filter
12. CDP-Sort
13. CDP-Stack
14. Strong coherency filter
15. Time variant trace equalisation

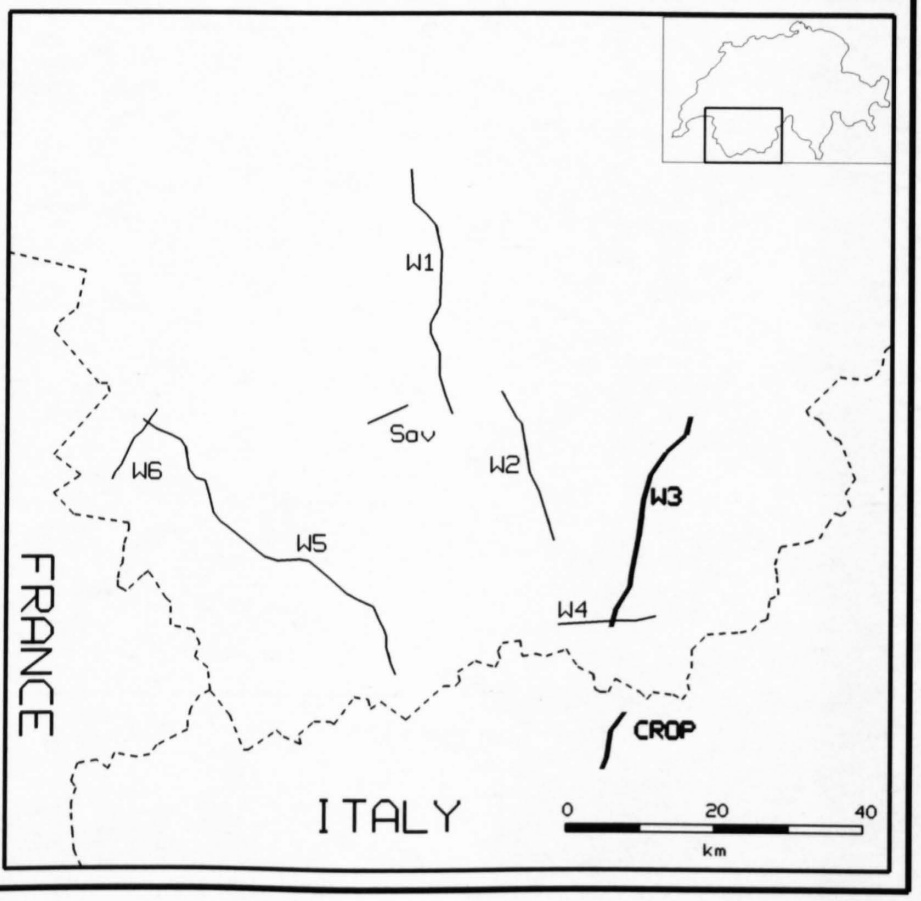

W3 (87-NF-D3 & 87CROP (CR3))

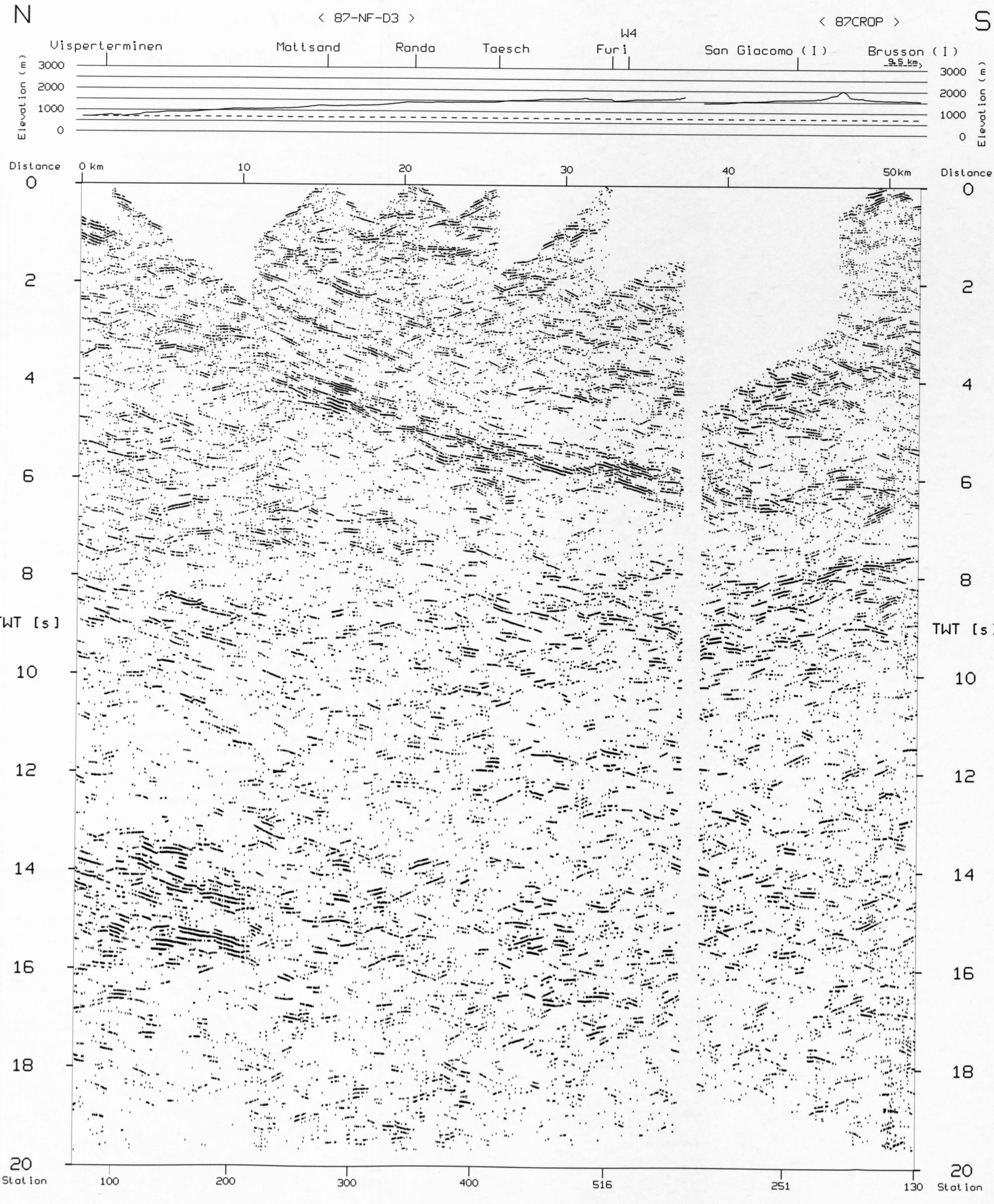

SWISS NATIONAL SCIENCE FOUNDATION

87-NF-W3 (VIBROSEIS)

FINAL STACK

1: 200'000

RECORDING PARAMETERS

SPREAD LAYOUT	9720-200-x-200-9720 m
CHANNELS	240
SOURCE INTERVAL	40 m
SOURCE TYPE	Vibroseis
SOURCE LAYOUT	6 Vibrators at 5 m
SWEEP FREQUENCY	9-39 Hz
SWEEP LENGTH	60 s
SWEEPS/VP	2
GROUP INTERVAL	80 m
GEOPHONE TYPE	10 Hz
GEOPHONE LAYOUT	18 spaced 5 m
INSTRUMENTATION	SERCEL 348
FIELD FILTERS	LC 8 Hz/HC 62.5 Hz/NT 50 Hz
COVERAGE	2 x 120 (nominal)
RECORDING MODE	unsummed and uncorrelated
SAMPLING RATE	4 ms
RECORDING LENGTH	64 s
RECORDED BY	CGG
DATE RECORDED	Sept. 1987

PROCESSING PARAMETERS

1. Demultiplex with gain recovery
2. Vibroseis whitening (AGC 500 ms)
3. Vibroseis corr. (Min. Phase) + vertical stack
4. Trace editing and resample to 8 ms
5. Time variant trace equalisation
6. Vertical summing
7. Crooked line geometry (20 m CDPs)
8. CDP-Sort
9. Static corrections to floating datum
10. NMO-Correction
11. Subsurface consistent residual statics
12. Mute application
13. CDP-Stack
14. Elevation correction to reference datum
15. Trace mix (2-fold horizontal sum)
16. Time variant bandpass filter
17. Strong coherency filter
18. Time variant trace equalisation

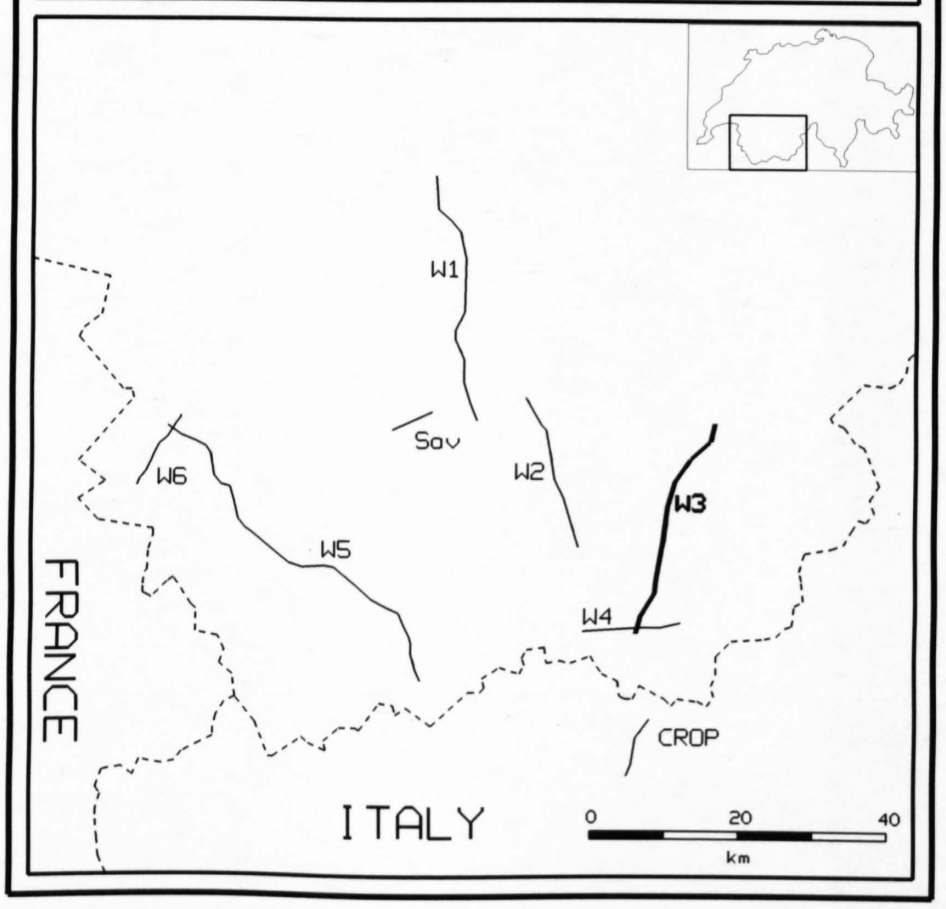

W3 (87-NF-V3)

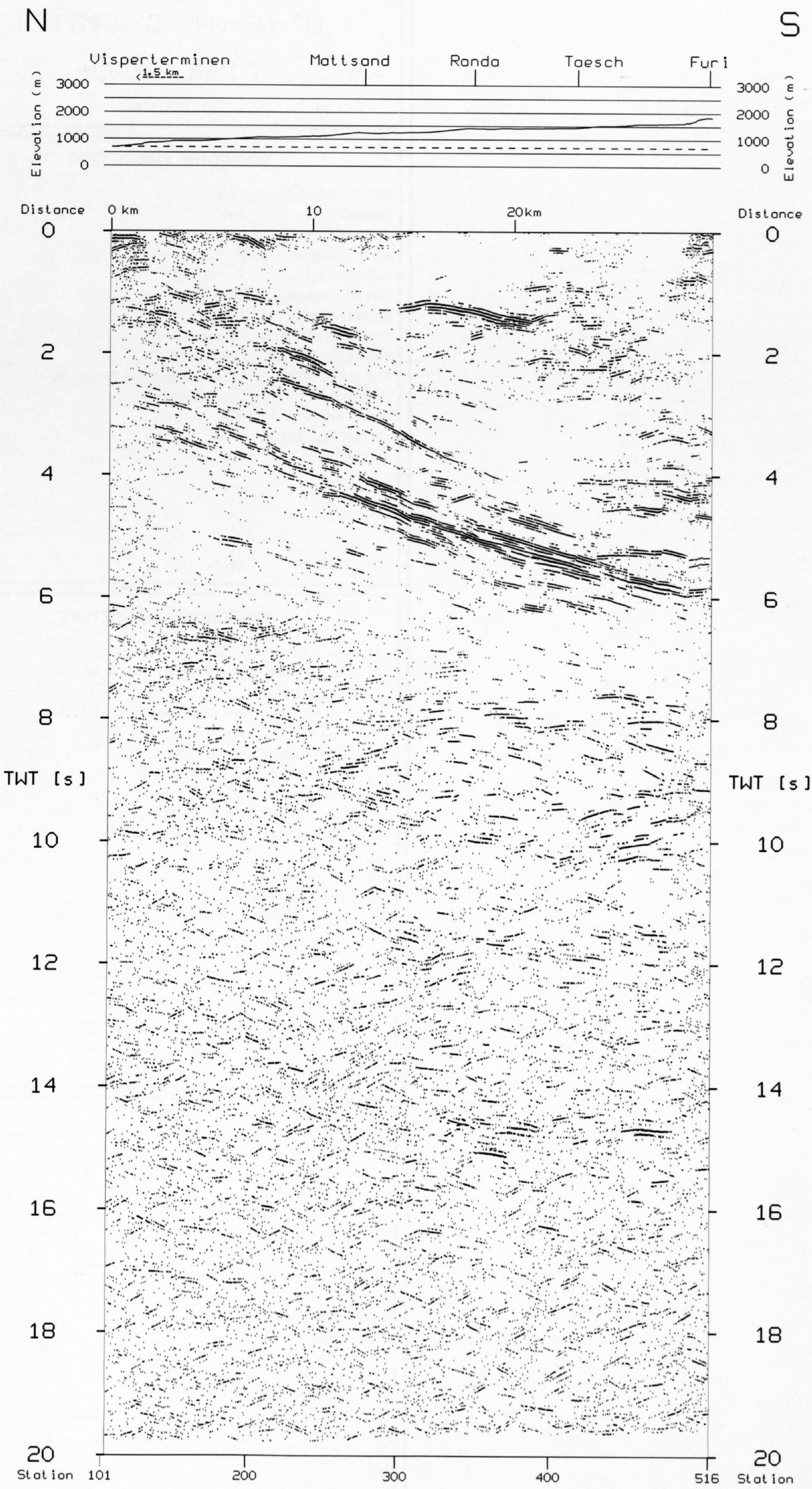
N
S
Visperterminen
1.5 km
Mattsand
Randa
Toesch
Furi
Elevation (m)
3000
2000
1000
0
Distance
0 km
10
20km
TWT [s]
0
2
4
6
8
10
12
14
16
18
20
Station
101
200
300
400
516

SWISS NATIONAL SCIENCE FOUNDATION

87-NF-W4 (DYNAMITE)

FINAL STACK

1: 200'000

RECORDING PARAMETERS

SPREAD LAYOUT	19.2 km
CHANNELS	240
SOURCE TYPE	Dynamite
SOURCE DEPTH	20-50 m
CHARGE SIZE	75-150 kg
GROUP INTERVAL	80 m
GEOPHONE TYPE	10 Hz
GEOPHONE PATTERN	18 spaced 5 m
INSTRUMENTATION	SERCEL 348
FIELD FILTERS	LC 8 Hz/HC 62.5 Hz/NT 50 Hz
COVERAGE	120 (nominal)
SAMPLING RATE	4 ms
RECORDING LENGTH	60 s
RECORDED BY	CGG
DATE RECORDED	Sept. 1987

PROCESSING PARAMETERS

1. Demultiplex and gain recovery
2. Trace editing and resample to 8 ms
3. F/K-Filter
4. Predictive deconvolution 160 / 20 ms
5. Crooked line geometry
6. Field static corrections
7. NMO-Correction
8. Time variant bandpass filter
9. Time variant trace equalisation
10. Time variant bandpass filter
11. CDP-Sort
12. CDP-Stack
13. Strong coherency filter
14. Time variant trace equalisation

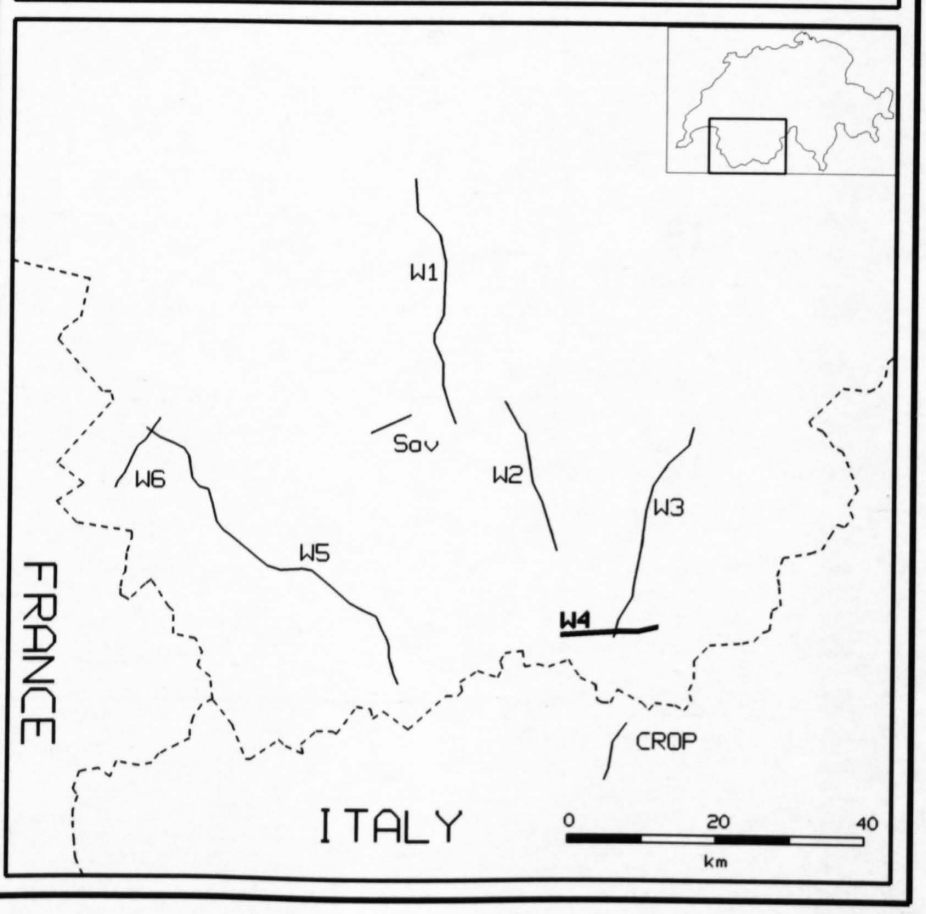

W4 (87-NF-D4)

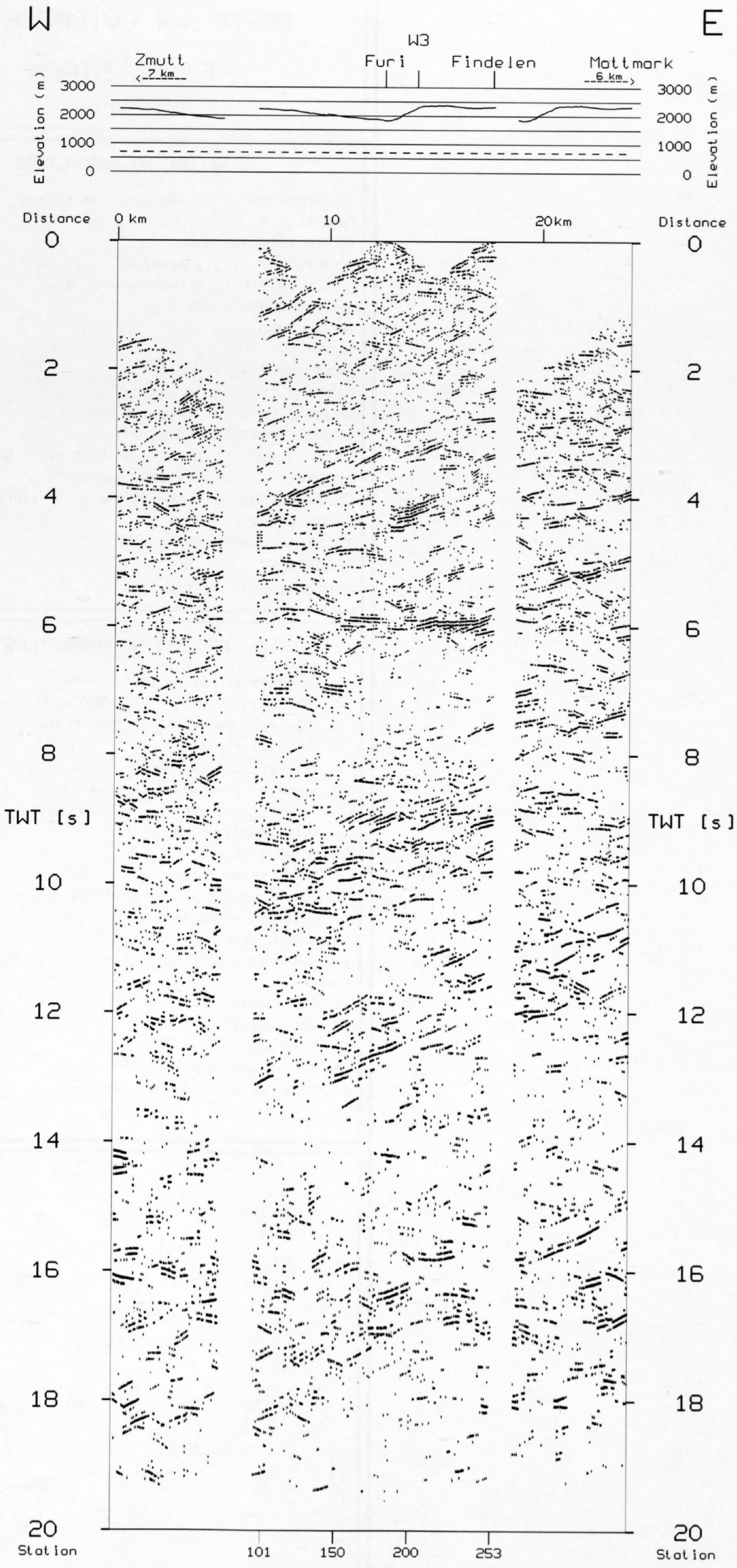
W
E
W3
Zmutt
2 km
Furi
Findelen
Mattmark
6 km
Elevation (m)
3000
2000
1000
0
Distance
0 km
10
20km
0
2
4
6
8
TWT [s]
10
12
14
16
18
20
Station
101
150
200
253

SWISS NATIONAL SCIENCE FOUNDATION

87-NF-W4 (VIBROSEIS)

FINAL STACK

1: 200'000

RECORDING PARAMETERS

SPREAD LAYOUT	9720-200-x-200-9720 m
CHANNELS	240
SOURCE INTERVAL	40 m
SOURCE TYPE	Vibroseis
SOURCE LAYOUT	6 Vibrators at 5 m
SWEEP FREQUENCY	9-39 Hz
SWEEP LENGTH	60 s
SWEEPS/VP	2
GROUP INTERVAL	80 m
GEOPHONE TYPE	10 Hz
GEOPHONE LAYOUT	18 spaced 5 m
INSTRUMENTATION	SERCEL 348
FIELD FILTERS	LC 8 Hz/HC 62.5 Hz/NT 50 Hz
COVERAGE	2 x 120 (nominal)
RECORDING MODE	unsummed and uncorrelated
SAMPLING RATE	4 ms
RECORDING LENGTH	64 s
RECORDED BY	CGG
DATE RECORDED	Sept. 1987

PROCESSING PARAMETERS

1. Demultiplex with gain recovery
2. Vibroseis whitening (AGC 500 ms)
3. Vibroseis correlation (Min. Phase)
4. Vertical stack
5. Crooked line geometry
6. Sperical divergence compensation
7. Time variant zero-phase deconvolution with equalization
8. Notch filter
9. First break mutes
10. Elevation static corrections: datum 2100 m
11. Velocity analysis
12. Normal move out
13. Residual static corrections (surf.cons.)
14. Stack
15. Datum shift to 700 m
17. Bandpass filter
18. Resample to 8 ms
19. Strong coherency filter
20. Time variant trace equalisation

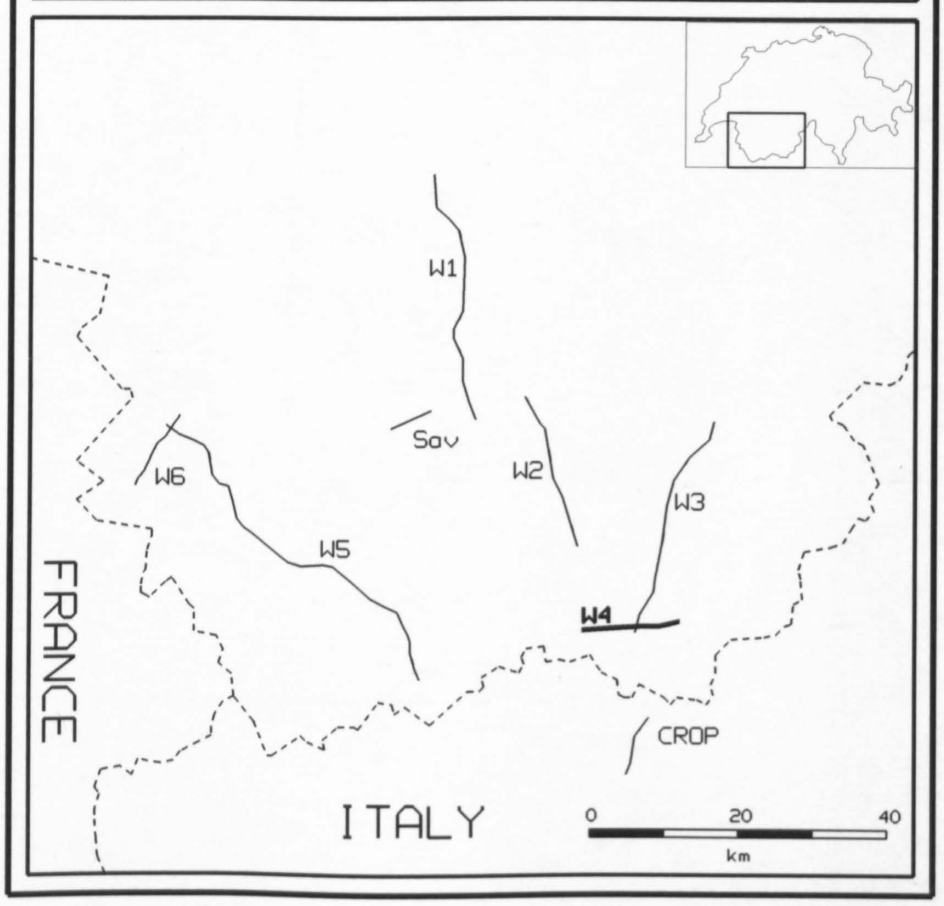

W4 (87-NF-V4)

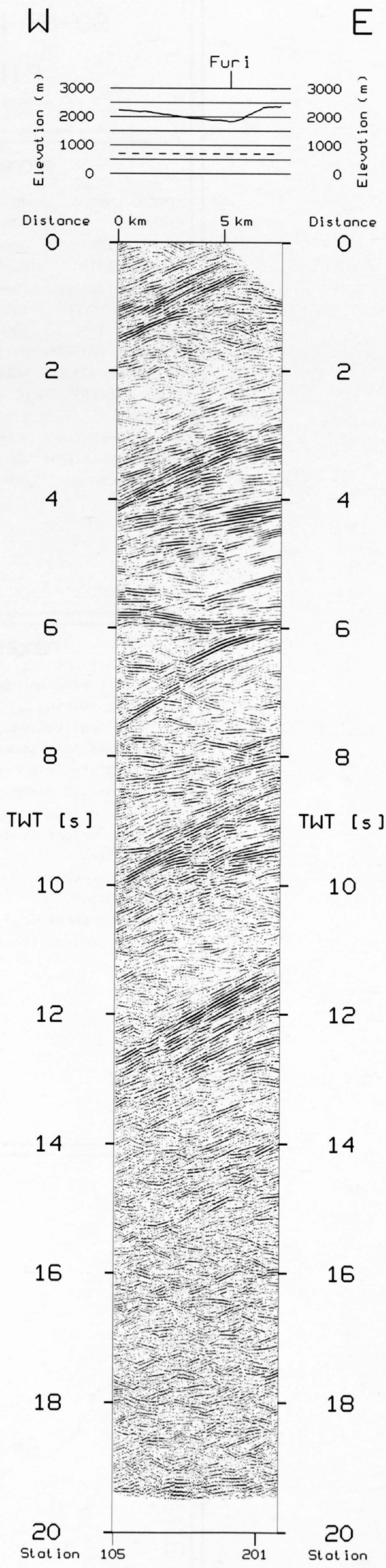
W
E
Furi
Elevation (m)
3000
2000
1000
0
Distance
0 km
5 km
0
2
4
6
8
TWT [s]
10
12
14
16
18
20
Station
105
201

SWISS NATIONAL SCIENCE FOUNDATION

90-NF-W5 (DYNAMITE)

FINAL STACK

1: 200'000

RECORDING PARAMETERS

SPREAD LAYOUT	48 km
CHANNELS	480
SOURCE TYPE	Dynamite
SOURCE DEPTH	20-90 m
CHARGE SIZE	25-430 kg
GROUP INTERVAL	100 m
GEOPHONE TYPE	10 Hz
GEOPHONE PATTERN	24 in-line / 100 m
INSTRUMENTATION	SERCEL 368
FIELD FILTERS	HC 89 Hz
COVERAGE	1 - 4
SAMPLING RATE	4 ms
RECORDING LENGTH	32 s
RECORDED BY	PRAKLA SEISMOS AG
DATE RECORDED	Oct. 1990

PROCESSING PARAMETERS

1. Demultiplex and gain recovery
2. Trace editing
3. Mute application
4. Crooked line geometry
5. Field static corrections
6. Predictive deconvolution
7. Time variant bandpass filter
8. Time variant trace equalisation
9. CDP-Sort
10. NMO-Correction
11. CDP-Stack
12. Strong coherency filter
13. Time variant trace equalisation

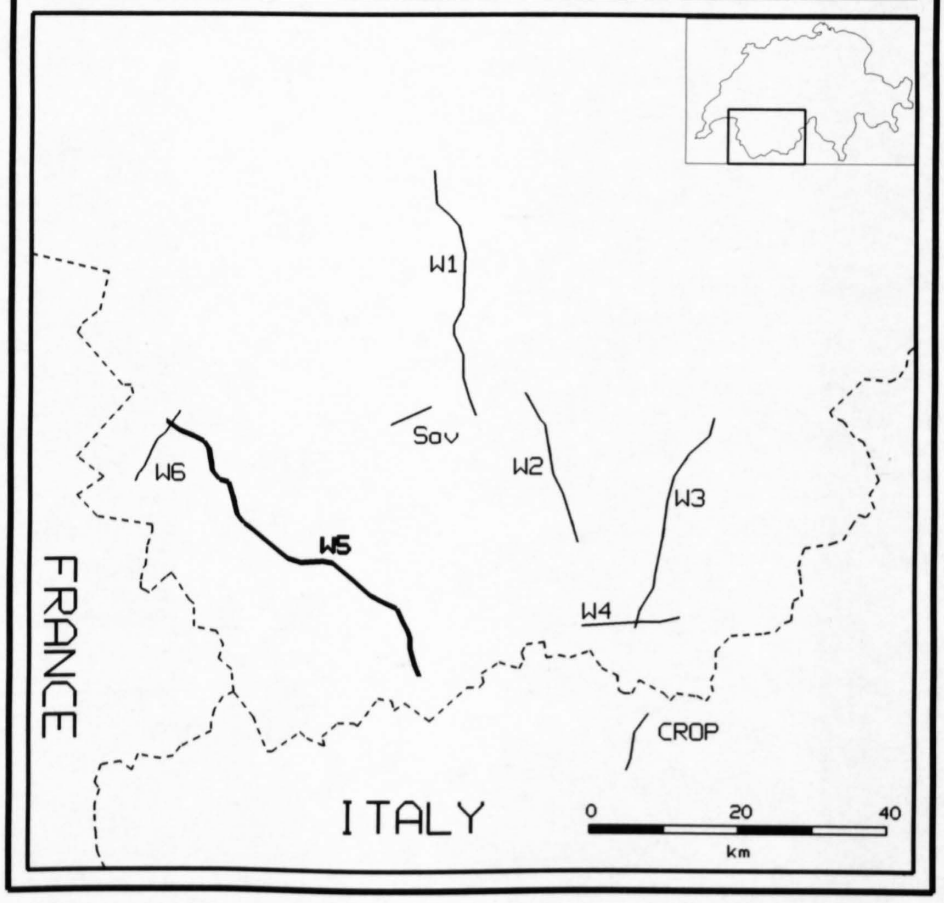

W5 (90-NF-D6)

NW

SE

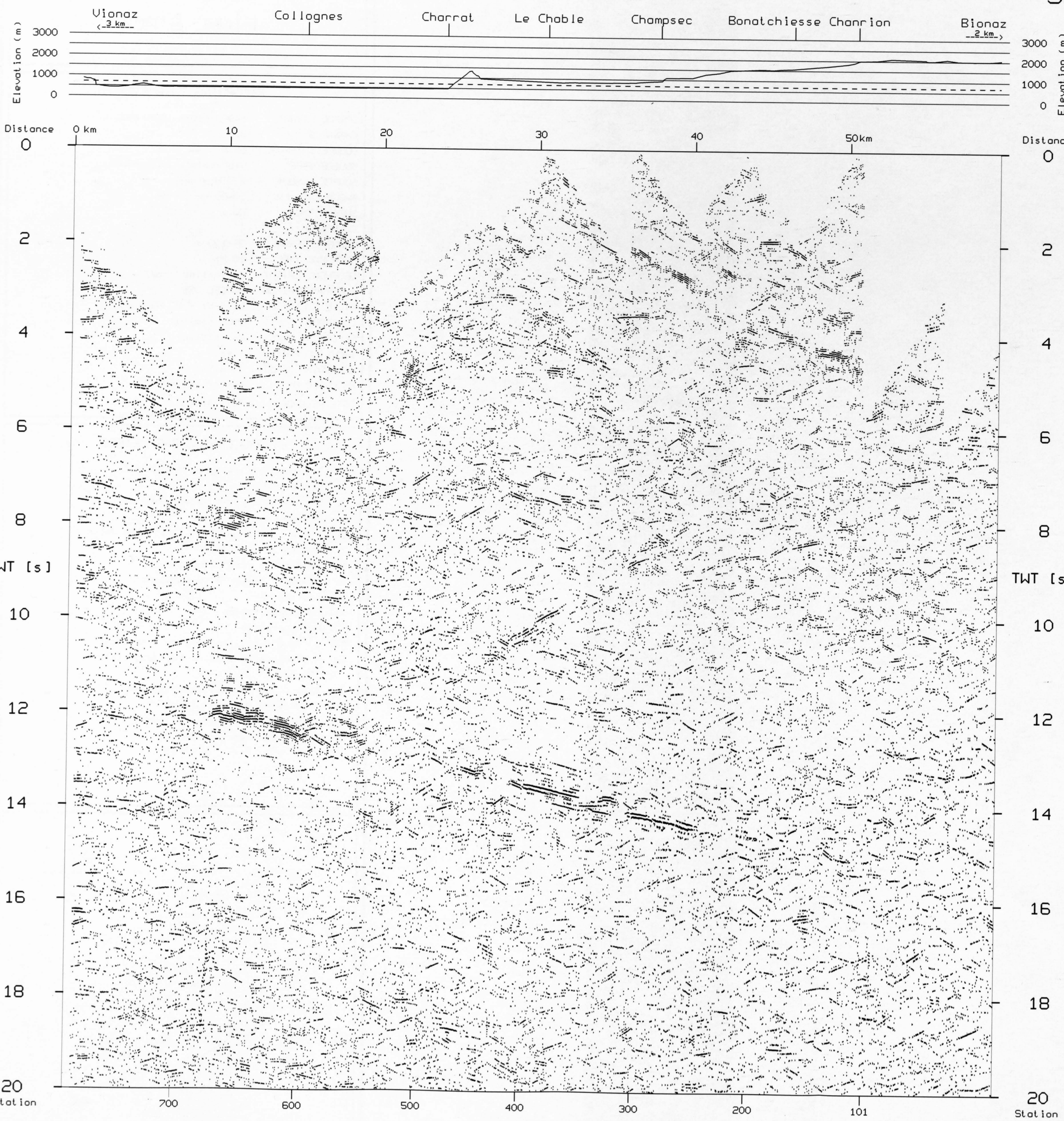

SWISS NATIONAL SCIENCE FOUNDATION

90-NF-W5 (VIBROSEIS)

FINAL STACK

1: 100'000

RECORDING PARAMETERS

SPREAD LAYOUT	14900-150-x-150-14900 m
CHANNELS	300
SOURCE INTERVAL	50 m
SOURCE TYPE	Vibroseis
SOURCE LAYOUT	5 Vibrators
SWEEP FREQUENCY	10-80 Hz
SWEEP LENGTH	60 s
SWEEPS/VP	1
GROUP INTERVAL	30/100 m
GEOPHONE TYPE	10 Hz
GEOPHONE LAYOUT	24 in-line / 100 m
INSTRUMENTATION	SERCEL 368
FIELD FILTERS	LC 8 Hz / HC 88.8 Hz
COVERAGE	300 (nominal)
RECORDING MODE	correlated
SAMPLING RATE	4 ms
RECORDING LENGTH	15 s
RECORDED BY	PRAKLA SEISMOS AG
DATE RECORDED	Oct. 1990

PROCESSING PARAMETERS

1. Reformatting and gain recovery
2. Trace editing
3. Line geometry and survey data assignment
5. CDP-Sort
6. Elevation correction to floating datum
7. Static correction
8. Predictive deconvolution
9. Bandpass filter 6/10-75/85 Hz
10. Scaling
11. Mute application
12. NMO-Correction
13. Surface consistent residual statics
14. Subsurface consistent residual statics
15. CDP-Stack
16. Time variant trace equalisation
17. Predictive deconvolution
18. Time variant bandpass filter
19. Strong coherency filter

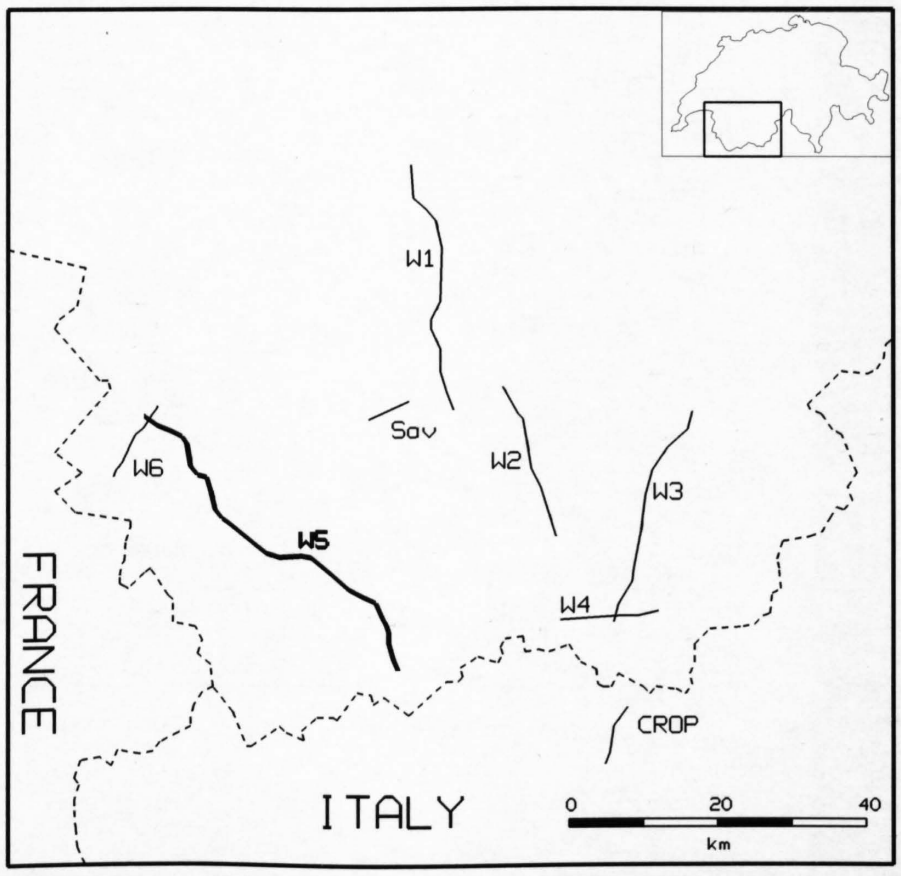

W5 (90-NF-V5)

NW

SE

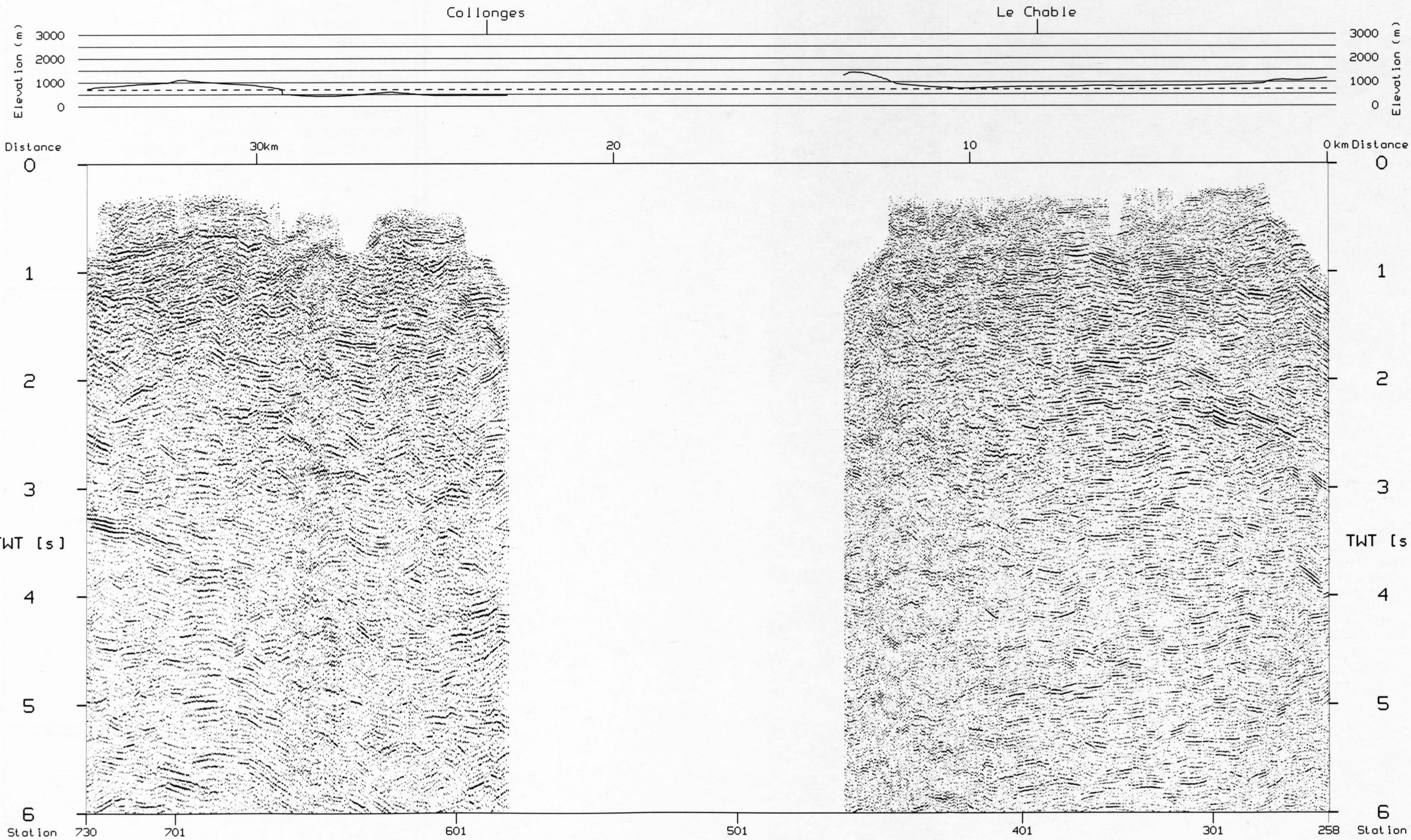

SWISS NATIONAL SCIENCE FOUNDATION

87-NF-W6 (VIBROSEIS)

(Petrosvibri Exchange line PSBR 8429)

FINAL STACK

1: 100'000

RECORDING PARAMETERS

SPREAD LAYOUT	2360-x-2360 m
CHANNELS	120
SOURCE INTERVAL	40 m
SOURCE TYPE	Vibroseis
SOURCE LAYOUT	3 Vibrators
SWEEP FREQUENCY	18-82 Hz
SWEEP LENGTH	12 s
SWEEPS/VP	8
GROUP INTERVAL	40 m
GEOPHONE TYPE	SM 4-10 Hz
GEOPHONE LAYOUT	24 in line
INSTRUMENTATION	SERCEL 348
FIELD FILTERS	LC 12.5 Hz / Hc 125 Hz
COVERAGE	60 (nominal)
RECORDING MODE	correlated
SAMPLING RATE	2 ms
RECORDING LENGTH	4 s
RECORDED BY	PRAKLA SEISMOS AG
DATE RECORDED	Oct. 1984

PROCESSING PARAMETERS

1. Demultiplex with gain recovery
2. Line geometry and survey data assignment
3. Elevation corrections to floating datum
4. CDP-Sort
5. Application of residual statics from PRAKLA
6. Time variant trace equalisation
7. Notch filter 16.67 + 50 Hz
8. Spectral balancing
9. Mute application
10. NMO-Correction
11. Surface consistent residual static corrections
12. Subsurface consistent res. static corrections
13. CDP-Stack
14. Bandpass filter 14/24-64/82 Hz
15. Coherency filter
16. Bandpass filter 14/20-45/57 Hz
17. Spiking deconvolution
18. Bandpass filter 14/20-45/57 Hz
19. Elevation correction to datum (700 m)

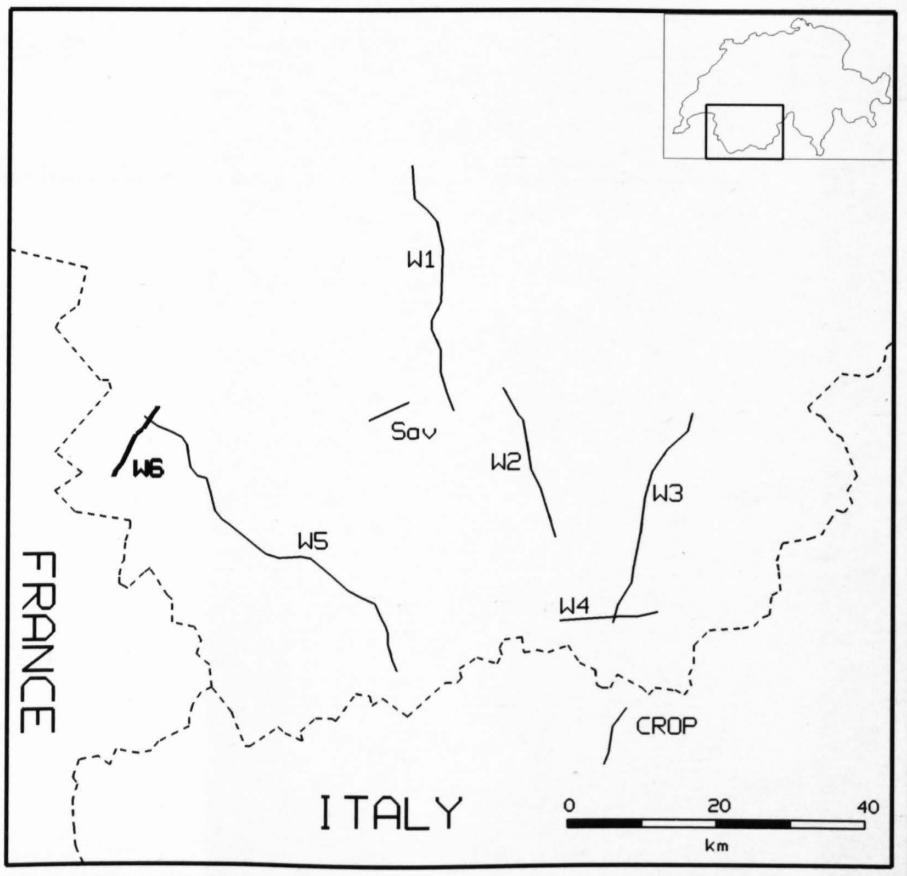

Plate 12-11

W6 (PSBR8429)

NE SW